

AD-A052 267

KANSAS STATE UNIV MANHATTAN DEPT OF PHYSICS  
INFRARED STUDIES OF WATER AND HYDRATED MATERIALS. (U)  
MAR 78 D WILLIAMS

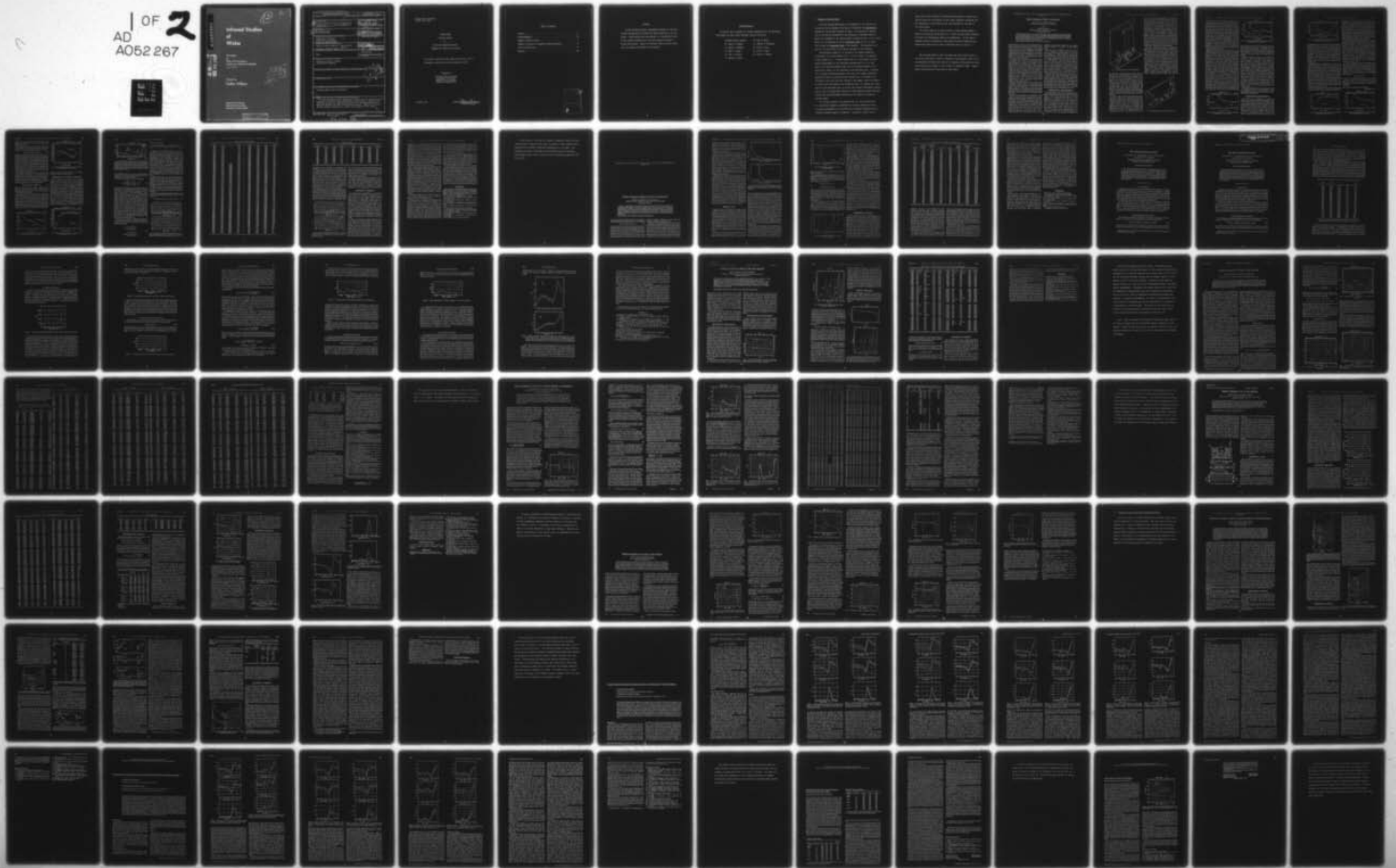
F/G 7/2

N00014-67-A-0403-0001

NL

UNCLASSIFIED

1 OF 2  
AD  
A052 267



AD A 052267

12 2

# Infrared Studies of Water

Final Report  
on  
Office of Naval Research  
Contract No. N00014-67-A-0403-001  
Period: 1968-1978

AD No. [ ]  
DDC FILE COPY

DDC  
APR 6 1978  
F

Prepared by  
Dudley Williams

Department of Physics  
Kansas State University  
Manhattan, Kansas 66506

This document has been approved  
for public release and sale; its  
distribution is unlimited.

REPORT DOCUMENTATION PAGE		READ INSTRUCTIONS BEFORE COMPLETING FORM
1. REPORT NUMBER	2. GOVT ACCESSION NO.	3. RECIPIENT'S CATALOG NUMBER
4. TITLE (and Subtitle) <b>6</b> Infrared Studies of Water and Hydrated Materials		5. TYPE OF REPORT & PERIOD COVERED <b>9</b> Final <sup>rept.</sup> 1967-1978
7. AUTHOR(s) <b>40</b> Dudley/Williams		6. PERFORMING ORG. REPORT NUMBER G1136
9. PERFORMING ORGANIZATION NAME AND ADDRESS Department of Physics Kansas State University Manhattan, Kansas 66506		8. CONTRACT OR GRANT NUMBER(s) Contract No. <b>15</b> N00014-67-A-0403-0001
11. CONTROLLING OFFICE NAME AND ADDRESS Office of Naval Research: Physics Branch Arlington, Virginia 22217 Code 421		10. PROGRAM ELEMENT, PROJECT, TASK AREA & WORK UNIT NUMBERS
14. MONITORING AGENCY NAME & ADDRESS (if different from Controlling Office) Same		12. REPORT DATE <b>11</b> 31 March 1978
		13. NUMBER OF PAGES 126 <b>12</b> 132P.
		15. SECURITY CLASS. (of Report) Unclassified
		15a. DECLASSIFICATION/DOWNGRADING SCHEDULE
16. DISTRIBUTION STATEMENT (of this Report) Approved for public release; distribution unlimited		
17. DISTRIBUTION STATEMENT (of the abstract entered in Block 20, if different from Report)		
18. SUPPLEMENTARY NOTES		
19. KEY WORDS (Continue on reverse side if necessary and identify by block number) Infrared; Water; Optical Constants		
20. ABSTRACT (Continue on reverse side if necessary and identify by block number) We have developed several experimental methods for the quantitative determination of absorption band intensities in the infrared. These methods have been applied in a quantitative study of the infrared properties of water and aqueous solutions of strong electrolytes. Copies of the major journal articles reporting our results are included in this report.		

DD FORM 1473  
1 JAN 73EDITION OF 1 NOV 65 IS OBSOLETE  
S/N 0102-014-6601

Unclassified

SECURITY CLASSIFICATION OF THIS PAGE (When Data Entered)

403 521 JOB

Kansas State University  
Project No. G1136

FINAL REPORT  
Infrared Studies  
of

Water and Hydrated Materials

CONTRACT NO. N00014-67-A-0403-001

This report covers work done under this contract and its  
predecessor contract, which was initiated in 1968.

Prepared by

Professor Dudley Williams  
Department of Physics  
Kansas State University  
Manhattan, Kansas 66506

31 March 1978

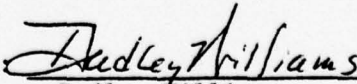
Signed   
Dudley Williams

TABLE OF CONTENTS

Abstract . . . . . 11  
Acknowledgements . . . . . 111  
Summary of Work on Water . . . . . 1  
Summary of Results on Inorganic Hydrated Materials . . . . . 61  
List of Publications . . . . . 97  
Appendix . . . . . 100

ACCESSION for	
NTIS	W Re Section <input checked="" type="checkbox"/>
DDC	Buff Section <input type="checkbox"/>
UNANNOUNCED	<input type="checkbox"/>
DISSEMINATION _____	
DISTRIBUTION/AVALIABILITY CODES	
SPECIAL	
A	

#### ABSTRACT

We have developed several experimental methods for the quantitative determination of absorption band intensities in the infrared. These methods have been applied in a quantitative study of the infrared properties of water and aqueous solutions of strong electrolytes. Copies of the major journal articles reporting our results are included in this report.

#### ACKNOWLEDGEMENTS

We should like to express our sincere appreciation to the following individuals who have played important roles in this work:

Professor Basil Curnutte

Dr. Harry D. Downing

Dr. David A. Draegert

Dr. Kent F. Palmer

Dr. Lary W. Pinkley

Dr. Marvin R. Querry

Dr. Paul E. Rhine

Dr. Charles W. Robertson

Dr. Alvin N. Rusk

Dr. Joel W. Schaaf

Dr. Prochy P. Sethna

## I. Summary of Work on Water

The major program undertaken at the beginning of the work was involved with the development of methods of determining the quantitative features of the infrared spectrum of water. The quantitative description of the optical properties of any substance in condensed states is given by a statement of its complex index of refraction  $\hat{N}(\nu) = n(\nu) + ik(\nu)$ , where  $n(\nu)$  is sometimes called the refractive index and  $k(\nu)$  is similarly called the absorption index of the material. The quantities  $n(\nu)$  and  $k(\nu)$  are also known as the optical constants of the substance.

The absorption index  $k(\nu)$  is related to the Lambert absorption coefficient  $\alpha(\nu)$  by the equation  $k(\nu) = \alpha(\nu)/4\pi\nu$ , where  $\nu$  is expressed in wave numbers  $\text{cm}^{-1}$ . It would appear that  $\alpha(\nu)$  could easily be determined by measurement of the fractional transmittance  $T(\nu)$  of a thin layer of the absorbing material and use of the relation Lambert  $T(\nu) = \exp[-\alpha(\nu)x]$ , where  $x$  is the thickness of the absorbing layer. Actually, for a strongly absorbing substance like water, this simple exponential expression cannot be employed without extreme care (1) because of reflections at the front and back surfaces of the sample, which are usually in contact with the windows of an absorption cell; (2) because the thickness  $x$  of the absorbing layer is so thin that optical interference effects set in; and (3) because small amounts of stray radiation produce spurious effects that become extremely important at the centers of strong absorption bands.

In the early stages of the present work, Dr. Marvin Querry and Dr. Alvin Rusk attempted to determine the optical constants of water by careful measurement of the reflection of polarized radiation at two carefully measured angles of incidence. Although Dr. Querry in his



later work at the University of Missouri has been able to obtain satisfactory results by this method, we were never completely satisfied with the efficiency of the polarizers that were available at the time of our initial work.

In a later stage of our work on water, we made precise measurements of the spectral reflectance  $R(\nu)$  of water at near-normal incidence, for which case polarization effects are unimportant. On the basis of measured spectral reflectance at near-normal incidence Kramers-Kronig phase-shift analysis can be used to determine both  $n(\nu)$  and  $k(\nu)$ .

The following paper by Rusk, Williams, and Querry gives values of the optical constants of water as determined from measured values of  $R(\nu)$  at near-normal incidence and values of the spectral reflectance of polarized radiation at an angle in the vicinity of Brewster's angle. Experimental uncertainties are discussed in some detail.

## Optical Constants of Water in the Infrared\*

ALVIN N. RUSK AND DUDLEY WILLIAMS  
*Kansas State University, Manhattan, Kansas 66502*

AND

MARVIN R. QUERRY  
*University of Missouri, Kansas City, Missouri 64110*  
(Received 2 January 1971)

The infrared reflectance of water in the region 5000–300  $\text{cm}^{-1}$  has been measured at near-normal incidence and at an incidence angle of 53°. On the basis of the measured values of spectral reflectance and the existing data on spectral transmittance, we have obtained values for the real and imaginary parts of the refractive index of water. The resulting values, which are presented in both graphical and tabular form, are compared with recent determinations by other investigators.

INDEX HEADINGS: Refractive index; Water; Infrared; Reflectance.

On the basis of a critical survey of the existing literature, Irvine and Pollack<sup>1</sup> pointed out the lack of reliable values for the real  $n_r$  and imaginary  $n_i$  parts of the refractive index of water in the infrared. A knowledge of these quantities is of great importance to an understanding of the earth's heat balance and to the effective application of Mie theory to calculations of the transmission of infrared radiant flux through fog and cloud layers in the earth's atmosphere.

In principle, the value of  $n_i$  can be determined from the relation  $n_i = k\lambda/4\pi$ , where  $k$  is the Lambert absorption coefficient for radiation of wavelength  $\lambda$  and is based on laboratory measurements of spectral transmittance  $T = (1 - \rho) \exp(-kx)$ , where  $x$  is the thickness of the water layer and  $\rho$  is the fraction of the incident radiant flux that is reflected at the cell windows. In practice, the necessity of providing extremely thin but accurately measured absorbing layers makes the determination of  $n_i$  very difficult at the centers of strong absorption bands. Determination of  $n_i$  from transmission studies in much of the infrared is further complicated by the lack of transparent, insoluble cell windows of high optical quality.

However, in spectral regions where  $n_i$  is known from transmission measurements, the corresponding values of  $n_r$  can be determined from  $n_i$  and from measured values of spectral reflectance. At the time of the Irvine-Pollack survey,<sup>1</sup> no detailed experimental studies of reflectance had been reported for nearly two decades. Since that time several pertinent investigations have been made.

Pontier and Dechambenoy<sup>2</sup> have published a table of optical constants based on transmission measurements in the spectral range 10 000–250  $\text{cm}^{-1}$  and measurements of the reflectance of polarized radiant flux at incidence angles of 50° and 60° in the spectral range 10 000–360  $\text{cm}^{-1}$ . Querry, Curnutte, and Williams<sup>3</sup> have measured the spectral reflectance of polarized radiant flux for incidence angles of 70° and 75° in the spectral range 5000–400  $\text{cm}^{-1}$ ; these authors used their reflectance measurements to determine both  $n_r$  and  $n_i$  in spectral regions of strong absorption and their own

reflectance measurements, along with the Irvine-Pollack<sup>1</sup> values of  $n_i$ , to obtain  $n_r$  in other spectral ranges.

Still more recently, Zolotarev *et al.*<sup>4</sup> have used a variety of techniques to obtain values of  $n_i$  and  $n_r$  at selected points in the spectral range between the visible and radiofrequency regions. Their experimental work included transmission measurements in the 5000–250- $\text{cm}^{-1}$  region, attenuated total reflection measurements in the 5000–1000- $\text{cm}^{-1}$  region, and reflection measurements at an incidence angle of 12° between 5000 and 200  $\text{cm}^{-1}$ . They used their own results, along with those of several other investigators, to compute values of  $n_i$  and  $n_r$  by means of Kramers-Kronig methods; although their calculations involve a hypothetical ultraviolet band centered at 100 000  $\text{cm}^{-1}$ , they assert that the choice of parameters for this "model band" does not influence the calculated values of  $n_r$  in the infrared.

Although there is now fair agreement of the optical constants  $n_i$  and  $n_r$  reported by different investigators, certain discrepancies still remain. The present work was undertaken with the purpose of resolving some of the remaining disagreements and of obtaining more detailed information in the 5000–300- $\text{cm}^{-1}$  region. Our major purpose was to obtain reliable experimental data that would permit calculations of  $n_r$  and  $n_i$  by methods not involving the use of band models of any kind.

### EXPERIMENTAL MEASUREMENTS

The reflectometers employed in the present study are shown schematically in Figs. 1 and 2. Radiant flux from Globar A is directed by mirrors B and C to the water sample or to a reference-mirror surface at D; the reflected flux is directed by mirrors E and F to the spectrometer entrance slit at G. In the reflectometer used for near-normal incidence, which is shown in Fig. 1, converging mirror C was masked in such a way that the maximum incidence angle in the cone of radiant flux reaching D was 7° and the angle of incidence for the central ray was approximately 4°; for this arrangement the Cauchy relation giving reflectance in terms of  $n_r$  and  $n_i$  can be used with confidence. In

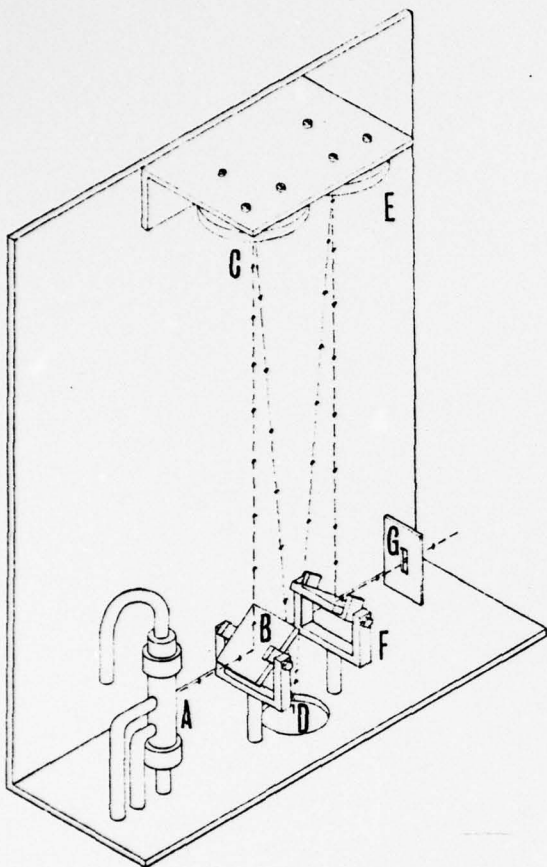


FIG. 1. Reflectometer used for near-normal incidence.

the reflectometer used for oblique incidence, which is shown in Fig. 2, converging mirror C was equipped with a slotted mask. For the slotted mask used in most of the work, all radiant flux reaching D had incidence angles in the range  $53.0^\circ \pm 0.8^\circ$ ; however, for the lowest-frequency region covered, we sometimes widened the slot in order to increase the radiant flux reaching the spectrometer; and with this arrangement, the incidence angles were in the range  $53.0 \pm 1.5^\circ$ . The geometry of the oblique-incidence reflectometer permitted the insertion of a polarizer in the beam between F and G; the polarizer consisted of six AgCl plates oriented at Brewster's angle with respect to the beam direction.

In earlier studies, Pontier and Dechambenoy<sup>2</sup> determined water reflectance by comparing the radiant flux reflected by water with the flux reflected by a high-quality front-surface mirror, which was assumed to be a perfect reflector. Querry *et al.*<sup>3</sup> made absolute measurements of water reflectance by repositioning two plane mirrors in their reflectometer; although direct measurement of absolute reflectance is desirable, the difficulties of achieving exact repositioning of mirrors introduced more scatter in the resulting data than in

those of Pontier and Dechambenoy. In the present study, we first obtained values of nominal reflectance  $R_N$  by comparing the reflectance of water with that of an aluminized reference mirror. Then, by means of an auxiliary reflectometer, we made absolute measurements of the mirror reflectance  $\mu$ ; from these two measurements, we obtained the water reflectance  $R$  from the product  $\mu R_N$ . For normal incidence, values of  $\mu_0$  for the reference mirror ranged from 0.950 at  $5000 \text{ cm}^{-1}$  to 0.975 in the low-frequency region; for an incidence angle of  $53^\circ$ , values of  $\mu_\theta$  were somewhat higher. For both incidence angles, the probable error in  $\mu$  was approximately 1%; checks of  $\mu$  were made from time to time in the course of the investigation. We used a cathetometer to match the vertical positions of water and mirror surfaces at D in Figs. 1 and 2 and employed an auxiliary laser beam to ensure that the surface of the reference mirror was horizontal.

We used a Perkin-Elmer model 112 single-beam spectrometer employing a Reeder thermocouple with a CsBr window as a detector; we used LiF, CaF<sub>2</sub>, NaCl, and CsBr prisms in various spectral regions. The spectrometer was used in its double-pass mode with an internal radiation chopper. Because water reflectance for most of the infrared is small compared with that of the reference mirror, the voltages produced at the thermocouple by radiant flux from the water sample are much smaller than the voltages obtained with the reference mirror. In their measurements, Pontier and Dechambenoy<sup>2</sup> relied on amplifier linearity and made use of amplifier-gain steps in comparing amplified signals. In the present work, we used the scheme employed by Querry *et al.*<sup>3</sup> and Zolotarev *et al.*<sup>4</sup> and placed a rapidly rotating calibrated sector wheel in front of the spectrometer entrance slit when the

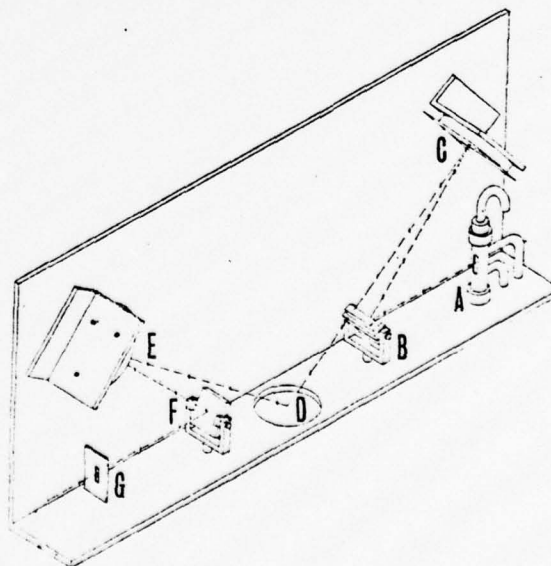


FIG. 2. Reflectometer used for an incidence angle of  $53^\circ$ .

reference mirror was in position, so that the flux reaching the detector from the reference mirror was not greatly different from that reaching the detector from the water surface when the sector wheel had been removed. Without change of amplifier gain controls, the two output signals were compared by noting recorder-chart deflections from a zero position recorded when a shutter interrupted the beam leaving the source. Because the rotating sector wheel was somewhat warmer than its surroundings, the shutter-zero trace with the wheel running was displaced from its normal chart position; therefore it was necessary to run one shutter-zero trace for the reference-mirror measurements and a second shutter-zero trace for water measurements. An opaque metal shutter was used in the 5000-800-cm<sup>-1</sup> region and, in order to minimize the effects of possible stray radiation, a glass shutter was employed at lower frequencies.

Because Brewster's angle for water is near 53°, the radiant flux reflected by the water surface at this angle is nearly completely polarized; its electric vector  $E_H$  is parallel to the horizontal water surface and is also horizontal in the path through the spectrometer. Because the beam reflected by the metallic surface of the reference mirror is largely unpolarized, it might be thought that the reflectance  $R_H$  for horizontal polarization could be determined directly from the recorder tracings for water and reference-mirror reflections. However, initially unpolarized flux entering the spectrometer is partially polarized by the time it reaches the detector, chiefly as a result of preferential reflection of vertically polarized radiant flux by the prism surfaces. Therefore, it was necessary to determine the discrimination factor of the spectrometer. We did this in an auxiliary arrangement by placing a 12-plate AgCl polarizer in front of the entrance slit and comparing chart deflections obtained with  $V$ -polarized flux with those obtained with an equal flux having  $H$  polarization. Assuming negligible leakage of undesired flux through the 12-plate polarizer, we obtained the spectrometer discrimination factor  $\alpha$  from the relation  $D_V = \alpha D_H$ , where  $D_V$  and  $D_H$  are chart deflections when equal quantities of  $V$ -polarized and  $H$ -polarized flux

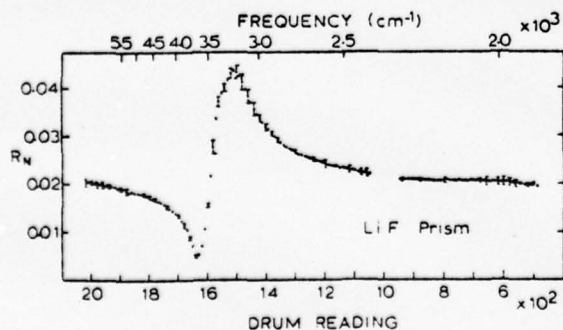


FIG. 3. Nominal spectral reflectance at near-normal incidence as determined with a LiF prism.

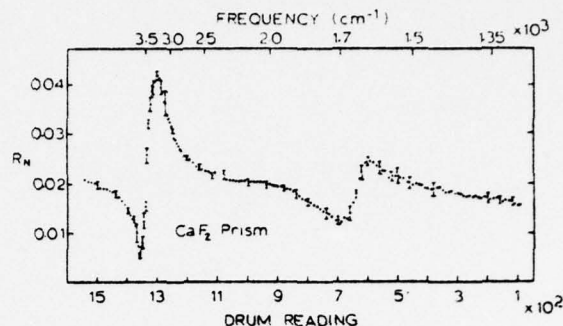


FIG. 4. Nominal spectral reflectance at near-normal incidence as determined with a CaF<sub>2</sub> prism.

pass through the entrance slit. The measured values of  $\alpha$  are a function of frequency and depend upon the prism used in the spectrometer; the largest values of  $\alpha$  were obtained with the LiF prism and the lowest with the CsBr prism, as would be expected if preferential reflection at the prism faces is the dominant effect involved.

In spectral regions for which  $n_r \gg n_i$ , the radiant flux reflected by water at an incidence angle of 53° has nearly complete  $H$  polarization. This condition is realized throughout most of the near infrared except in the vicinity of strong absorption bands. We made measurements of reflectance without the use of polarizers throughout the entire spectral range covered in the investigation and, in regions of large  $n_i$ , also made measurements with the 6-plate AgCl polarizer in the beam. When a polarizer is employed, the effects of leakage of undesired flux must be considered. Although Pontier and Dechambeno<sup>2</sup> assumed zero leakage for their 6-plate polarizer, Query<sup>3</sup> showed that leakage  $\lambda$  through such a polarizer can be as great as 0.1. With the 6-plate polarizer used in the present study,  $\lambda$  was considerably less than 0.1 for frequencies greater than 400 cm<sup>-1</sup>. The discrimination characteristics of our spectrometer serve to reduce still further the effects of  $V$ -polarized flux.

The distilled deionized water samples employed were at a temperature of 25°C. Care was taken to avoid contamination of the free surfaces during the course of the reflection measurements.

## REFLECTANCE MEASUREMENTS

The results of our measurements of nominal reflectance at near-normal incidence are shown in Figs. 3-6 for each prism used in the study. Each point shown in these plots represents the mean of at least four sets of independent measurements; the probable errors are given by the error bars at various points in the plots. The uncertainty is somewhat larger in spectral regions where spectral reflectance is changing rapidly and we attribute the increased uncertainty in  $R_N$  to slight failures to reproduce prism settings on successive runs.

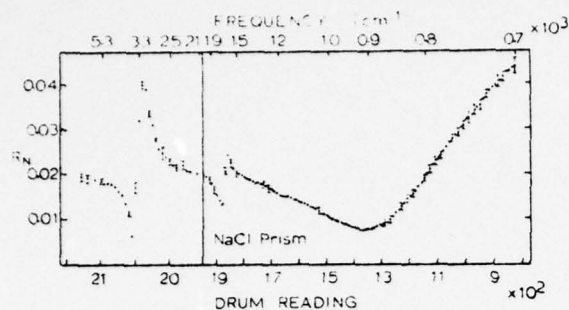


Fig. 5. Nominal spectral reflectance at near-normal incidence as determined with a NaCl prism.

The probable errors are quite small in most spectral regions but become larger in the low-frequency region in which we used the CsBr prism; these increased uncertainties are due in part to the low emissive power of the source and in part to the reduction of flux produced by the pure rotational lines of water vapor in the atmospheric path through the reflectometer and spectrometer. It was impossible to obtain reliable data in the vicinity of the strong  $\nu_3$  band of atmospheric carbon dioxide; however, inspection of Fig. 3 indicates that reliable values of  $R_N$  can be obtained in this region by interpolation.

Nominal-reflectance measurements of water for an incidence angle  $\theta = 53^\circ$  are summarized in the plots of Figs. 7-10; the general features of these curves are similar to those noted in Figs. 3-6. We maintained the same schedule of slit widths for corresponding nominal reflectance spectra shown in these two sets of figures. Because of the slotted mask on mirror C, the radiant flux in the oblique-incidence measurements was smaller than that available for the normal-incidence measurements, and it was necessary to use higher amplifier-gain settings in obtaining the results shown in Figs. 7-10. However, the scatter of the data points shown in the two sets of figures is approximately the same; this result is attributable, at least in part, to the increased water reflectance for oblique incidence.

The data shown in Figs. 3-10 were obtained without the use of a polarizer in the reflectometer. Because the

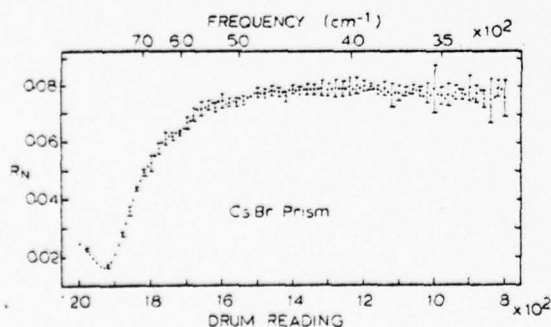


Fig. 6. Nominal spectral reflectance at near-normal incidence as determined with a CsBr prism.

assumption that the reflection of V-polarized flux is negligible is of doubtful validity in spectral regions where  $n_r$  is significantly different from 1.3 and where  $n_i$  is larger, we also measured the nominal reflectance  $R_N'$  for H-polarized flux in the vicinity of absorption bands. The results were essentially similar to those shown in Figs. 7-10; however, the nominal reflectance  $R_N'$  was, of course, numerically different from the values of  $R_N$  in Figs. 7-10. Because the use of AgCl polarizing plates involves a significant loss of radiant flux, the scatter of points in plots of  $R_N'$  is somewhat greater than the corresponding scatter in Figs. 7-10.

The measured values of fractional spectral reflectance  $R_0$  are summarized in the lower curve in Fig. 11 and represent the product of mirror reflectance  $\mu_0$  and  $R_N$  as given in Figs. 3-6. There are slight differences between the values of  $R_0$  as determined by the CaF<sub>2</sub> and NaCl prisms in the vicinity of 1600 cm<sup>-1</sup> and by the NaCl and CsBr prisms in the vicinity of 900 cm<sup>-1</sup>. The uncertainty of spectral reflectance at normal incidence is given by the expression  $\delta R_0 = [(R_N \delta \mu_0)^2 + (\mu_0 \delta R_N)^2]^{1/2}$ , where  $\delta \mu_0$  and  $\delta R_N$  are the probable errors of  $\mu_0$  and  $R_N$ , respectively. Except at low frequencies, the uncertainties  $\delta R_0$  were too small to plot in Fig. 11 but were tabulated for use in subsequent computations of  $n_r$  and  $n_i$ .

Our later computations involved expressions for these optical constants in terms of  $R_0$  and  $R_{\theta H}$ , where  $R_{\theta H}$  is the spectral reflectance for H-polarized flux at incidence angle  $\theta = 53^\circ$ . On the assumption that at this angle the water reflectance for V-polarized flux is negligible and that the reflectance  $\mu_0$  of the metallic reference mirror is the same for H- and V-polarized flux, we obtain

$$R_{\theta H} = \mu_0(1 + \alpha)R_N, \quad (1)$$

where  $R_N$  is the measured nominal reflectance plotted in Figs. 7-10 and  $\alpha$  is the discrimination factor of the spectrometer. Because  $\mu_0$ ,  $\alpha$ , and  $R_N$  were measured independently, the uncertainty  $\delta R_{\theta H}$  is given by the expression

$$\delta R_{\theta H} = \{ [R_N(1 + \alpha)\delta \mu_0]^2 + [\mu_0(1 + \alpha)\delta R_N]^2 + (\mu_0 R_N \delta \alpha)^2 \}^{1/2}, \quad (2)$$

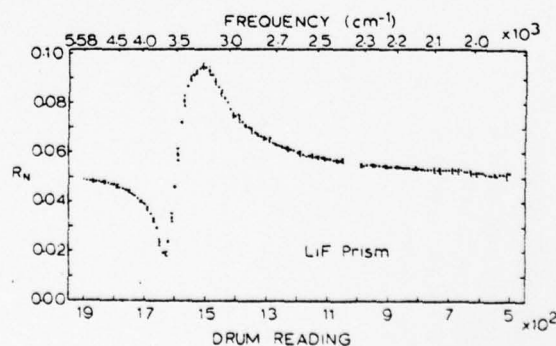


Fig. 7. Nominal spectral reflectance at an incidence angle of 53° as determined with a LiF prism.

where  $\delta R_N$ ,  $\delta\mu_\theta$ , and  $\delta\alpha$  are the probable errors. The results obtained for  $R_{\theta H}$  are given by points in the upper curve of Fig. 11.

Also shown in Fig. 11 are points based on measurements in which the polarizer was employed. With the polarizer set to transmit *H*-polarized flux, we obtain

$$R_{\theta H} = \mu_\theta(1 + \lambda\alpha)R_N' - R_{\theta V}\lambda\alpha, \quad (3)$$

where  $R_N'$  is the nominal water reflectance as determined with the polarizer in the beam,  $\lambda$  is the leakage factor of the polarizer, and  $R_{\theta V}$  is the water reflectance for *V*-polarized flux. On the assumption that  $\lambda < 0.1$ , the last term in Eq. (3) can be safely neglected because  $\alpha < 0.5$  for all prisms and independent tests with the polarizer set to pass *V*-polarized flux showed that  $R_{\theta V}$  was too small for measurement. In computing the values of  $R_{\theta H}$  plotted in Fig. 11, we also assumed that the product  $\lambda\alpha$  was small compared with unity and used the expression  $R_{\theta H} = \mu_\theta R_N'$ .

The proper computation of the uncertainty  $\delta R_{\theta H}$  should include consideration of the uncertainties of all quantities in Eq. (3). However, since the uncertainty  $\delta\lambda$  is difficult to establish, because the measured uncertainty  $\delta\alpha$  involves the assumption that  $\lambda=0$  for a 12-plate polarizer, and since  $R_{\theta V}$  is itself too small for accurate measurement, we used the expression

$$\delta R_{\theta H} = [(R_N'\delta\mu_\theta)^2 + (\mu_\theta\delta R_N')^2]^{1/2}. \quad (4)$$

Although this expression probably underestimates  $\delta R_{\theta H}$ , the computed values of this quantity are in general larger than those given by Eq. (2) and become very large at low frequencies.

As indicated in Fig. 11 the values of  $R_{\theta H}$  determined from  $R_N$  and  $R_N'$  agree to within  $\pm 5\%$  of their mean values in all spectral regions except for frequencies below  $700 \text{ cm}^{-1}$ . Because the spectral transmittance of AgCl decreases for the lowest frequencies studied, the uncertainties of the plotted  $R_{\theta H}$  values in this region are large. Since the refractive index of AgCl decreases rapidly with decreasing frequency in this spectral region and the AgCl plates are no longer oriented at Brewster's

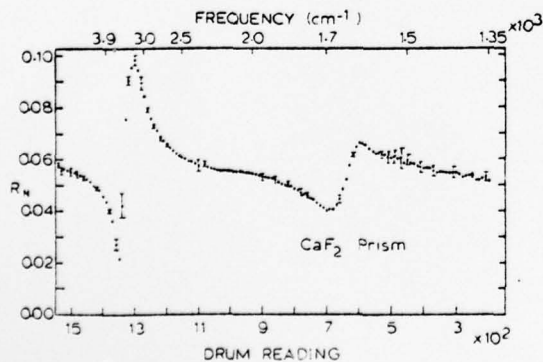


Fig. 8. Nominal spectral reflectance at an incidence angle of  $53^\circ$  as determined with a  $\text{CaF}_2$  prism.

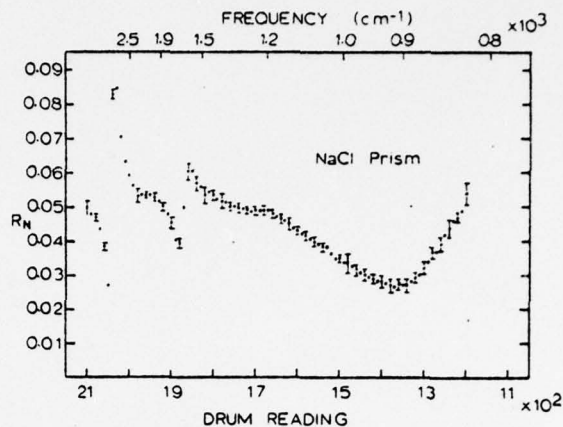


Fig. 9. Nominal spectral reflectance at an incidence angle of  $53^\circ$  as determined with an NaCl prism.

angle, our neglect of the term  $\lambda\alpha$  in Eq. (3) is open to question in the low-frequency region.

### COMPUTATION OF OPTICAL CONSTANTS

Because reflection measurements can, in general, provide accurate values of  $n_r$  but can give reliable values of  $n_i$  only for large values of this quantity:<sup>5</sup> (a) We first used our measured values of  $R_0$  together with values of  $n_i$  based on transmission studies to obtain one set of  $n_r$  values. (b) Then we used a computer program to obtain both  $n_r$  and  $n_i$  from our measured values of  $R_0$  and  $R_{\theta H}$ . (c) We next obtained a set of weighted-mean values of  $n_r$ , based on plots of this quantity as given by the earlier steps; these best values of  $n_r$  are our final tabulated values. (d) Using the final values of  $n_r$ , and our measured values of  $R_0$ , we obtained a set of  $n_i$  values. (e) Our final tabulated values of  $n_i$  are based on our computed values in regions of strong absorption and on transmittance studies in regions of weak absorption. As a consistency check of

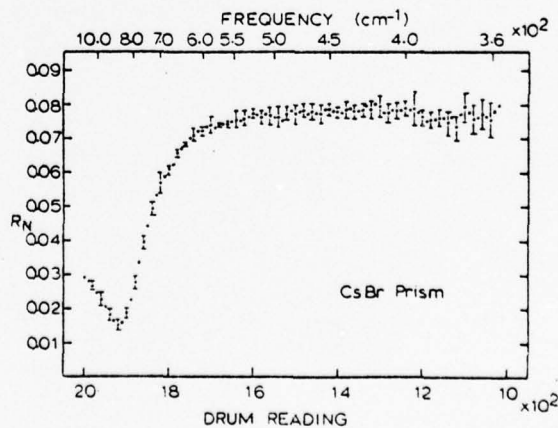


Fig. 10. Nominal spectral reflectance at an incidence angle of  $53^\circ$  as determined with a CsBr prism.

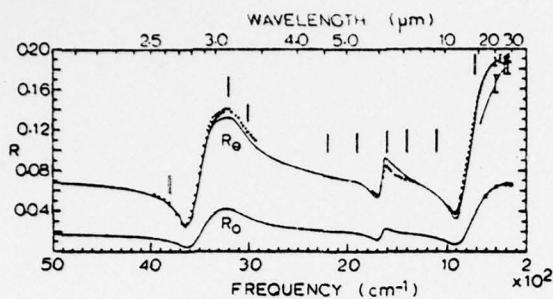


FIG. 11. The reflection spectrum of water in the infrared for  $R_0$  and  $R_{90}$ . Spectral slit widths, indicated by the vertical bars, are noted for various spectral regions. Uncertainty bars are placed on the solid curves in regions where they are sufficiently large to be observable on the plots. The points shown near the  $R_{90}$  curve represent data obtained with a polarizer in the beam. The light curve for  $R_{90}$  in the 300–600- $\text{cm}^{-1}$  region represents data taken with an inefficient polarizer.

the tabulated values of  $n_r$  and  $n_i$ , we used them to compute values of  $R_0$  and  $R_{90}$  for comparison with our measured values of these quantities.

In step (a) we obtained  $n_r$  from the expression

$$n_r = \frac{(1+R_0)}{(1-R_0)} + \left[ \frac{4R_0}{(1-R_0)^2} - n_i^2 \right]^{1/2} \quad (5)$$

obtained from the Cauchy relation. The values of  $n_i$  are based on the transmittance measurements of Plyler and Griff<sup>6</sup> in the 4000–1400- $\text{cm}^{-1}$  range, on those of Plyler and Acquisti<sup>7</sup> in the 1400–1000- $\text{cm}^{-1}$  range, and on those of Draeger *et al.*<sup>8</sup> in the 1200–300- $\text{cm}^{-1}$  range; at frequencies higher than 4000  $\text{cm}^{-1}$   $n_i$  is negligible, compared with the other quantities in Eq. (5). Plyler and his associates used  $\text{CaF}_2$  absorption cells in the 4000–1000- $\text{cm}^{-1}$  region and KRS-5 cells in the 1000–250- $\text{cm}^{-1}$  region; probably as a result of the use of non-uniform layers, their results for frequencies less than 1000  $\text{cm}^{-1}$  gave complex values of  $n_r$  when substituted along with our values of  $R_0$  in Eq. (5). The results of Draeger *et al.* were obtained with water samples in  $\text{AgCl}$  and polyethylene cells, which like KRS-5 cells, are not entirely satisfactory for the purpose; although their values for  $n_i$  had uncertainties as large as 25%, their results were compatible with  $R_0$  and gave real values of  $n_r$  when used in Eq. (5).

The values of  $n_r$  obtained in step (b) were based on a computer program leading to a consistent set of values of  $n_r > 1$  and  $n_i \geq 0$  that were compatible with measured values of  $R_0$  and  $R_{90}$

$$R_0 = \frac{(n_r - 1)^2 + n_i^2}{(n_r + 1)^2 + n_i^2} \quad (6)$$

$$R_{90} = \frac{(Q - \cos\theta)^2 + P^2}{(Q + \cos\theta)^2 + P^2}$$

where  $P = n_r n_i$ ,  $Q$ , and

$$Q = \left[ \frac{n_r^2 - n_i^2 - \sin^2\theta + (n_r^2 - n_i^2 - \sin^2\theta + 4n_r^2 n_i^2)^{1/2}}{2} \right] \quad (7)$$

In step (c) we plotted the values of  $n_{ra}$  and  $n_{rb}$  obtained in steps (a) and (b) as functions of frequency and drew a smooth curve through the plotted series. The agreement between the curves for  $n_{ra}$  and  $n_{rb}$  was nearly perfect in the 5000–3000- $\text{cm}^{-1}$  range; in the 3300–2800- $\text{cm}^{-1}$  region, the curves were within  $\pm 2\%$  of their unweighted mean; agreement between the two curves was excellent in the 2800–850- $\text{cm}^{-1}$  range. Between 850 and 650  $\text{cm}^{-1}$ , the agreement was poorest; in this region  $n_{ra}$  and  $n_{rb}$  differed from their unweighted mean by as much as 8%, with  $n_{rb} > n_{ra}$ . Between 650 and 450  $\text{cm}^{-1}$ , there was fair agreement between the  $n_{ra}$  and  $n_{rb}$  curves, but between 450 and 330  $\text{cm}^{-1}$  the curves again diverged, so that they were separated from their unweighted mean by as much as 3%, with  $n_{ra} > n_{rb}$ .

Inspection of the plots of  $n_{ra}$  and  $n_{rb}$  as functions of frequency indicated that the scatter of individual  $n_{rb}$  values from the smooth curve was approximately twice as great as the corresponding scatter for  $n_{ra}$  points. Therefore, in completing step (c), we arbitrarily selected the weighted mean  $(2n_{ra} + n_{rb})/3$  as the best value of  $n_r$ , where  $n_{ra}$  and  $n_{rb}$  are the values of these quantities read from the smooth curves. These best values of  $n_r$  are plotted in the lower panel of Fig. 12 and are listed in Table I.

In step (d), we substituted our best values of  $n_r$  along with the measured values of  $R_0$  in the Cauchy equation to obtain

$$n_i = \left\{ [(n_r + 1)^2 R_0 - (n_r - 1)^2] / (1 - R_0) \right\}^{1/2} \quad (8)$$

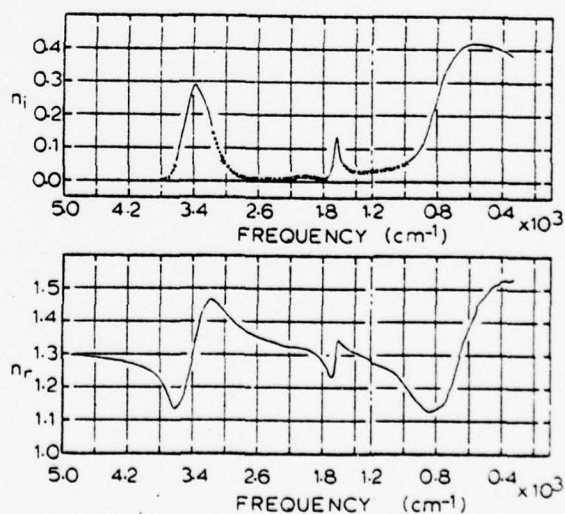


FIG. 12. The optical constants of water obtained in the present study. The crosses on the curve for  $n_i$  are based on transmission measurements. Estimates of uncertainties are given in the text.

TABLE I. Optical constants of water.

$\nu$ in $\text{cm}^{-1}$	$n_r$	$n_i$	$\lambda$ in $\mu\text{m}$	$\nu$ in $\text{cm}^{-1}$	$n_r$	$n_i$	$\lambda$ in $\mu\text{m}$
5000	1.300	...	2.00	2440	1.343	0.006	4.10
4920	1.299	...	2.03	2400	1.339	0.006	4.17
4840	1.297	...	2.07	2360	1.336	0.006	4.24
4760	1.296	...	2.10	2320	1.334	0.007	4.31
4680	1.294	...	2.14	2280	1.330	0.008	4.39
4600	1.292	...	2.17	2240	1.329	0.009	4.46
4520	1.290	...	2.21	2200	1.327	0.011	4.54
4440	1.286	...	2.25	2180	1.326	0.012	4.59
4360	1.283	...	2.29	2160	1.324	0.014	4.63
4280	1.280	...	2.34	2140	1.324	0.015	4.67
4200	1.275	...	2.38	2120	1.324	0.015	4.72
4160	1.273	...	2.40	2100	1.323	0.015	4.76
4120	1.271	...	2.43	2080	1.323	0.015	4.80
4080	1.267	...	2.45	2060	1.322	0.015	4.85
4040	1.264	...	2.47	2040	1.321	0.015	4.90
4000	1.260	0.003	2.50	2020	1.320	0.015	4.95
3960	1.255	0.003	2.52	2000	1.319	0.015	5.00
3920	1.249	0.003	2.55	1980	1.318	0.015	5.05
3880	1.241	0.003	2.58	1960	1.316	0.014	5.10
3840	1.232	0.004	2.60	1940	1.314	0.013	5.15
3800	1.220	0.004	2.63	1920	1.312	0.012	5.21
3780	1.215	0.004	2.65	1900	1.308	0.010	5.26
3760	1.206	0.005	2.66	1880	1.305	0.009	5.32
3740	1.200	0.005	2.67	1860	1.302	0.008	5.38
3720	1.186	0.009	2.69	1840	1.294	0.008	5.43
3700	1.174	0.015	2.70	1820	1.288	0.008	5.50
3680	1.160	0.021	2.72	1800	1.280	0.008	5.56
3660	1.146	0.032	2.73	1780	1.270	0.009	5.62
3640	1.135	0.045	2.75	1760	1.262	0.009	5.68
3620	1.136	0.067	2.76	1740	1.253	0.023	5.75
3600	1.140	0.083	2.78	1720	1.240	0.026	5.81
3580	1.145	0.104	2.79	1700	1.234	0.047	5.88
3560	1.150	0.126	2.81	1680	1.235	0.072	5.95
3540	1.159	0.148	2.82	1660	1.257	0.114	6.02
3520	1.175	0.173	2.84	1640	1.302	0.139	6.10
3500	1.190	0.199	2.86	1620	1.338	0.120	6.17
3480	1.207	0.225	2.87	1600	1.350	0.077	6.25
3460	1.227	0.247	2.89	1580	1.345	0.064	6.33
3441	1.245	0.270	2.91	1560	1.338	0.054	6.41
3420	1.274	0.281	2.92	1540	1.333	0.046	6.49
3400	1.297	0.290	2.94	1520	1.325	0.042	6.58
3380	1.320	0.291	2.96	1500	1.323	0.038	6.67
3360	1.345	0.284	2.97	1480	1.320	0.033	6.76
3340	1.367	0.278	2.99	1460	1.316	0.033	6.85
3320	1.385	0.269	3.01	1440	1.314	0.032	6.94
3300	1.405	0.258	3.03	1420	1.312	0.030	7.04
3280	1.420	0.248	3.05	1400	1.310	0.029	7.14
3260	1.436	0.234	3.07	1380	1.308	0.029	7.25
3240	1.447	0.222	3.09	1360	1.306	0.029	7.35
3220	1.457	0.209	3.11	1340	1.303	0.029	7.46
3200	1.465	0.194	3.12	1320	1.301	0.029	7.57
3180	1.468	0.162	3.14	1300	1.298	0.029	7.69
3160	1.465	0.143	3.16	1280	1.296	0.030	7.81
3140	1.464	0.124	3.18	1260	1.293	0.030	7.94
3120	1.460	0.112	3.20	1240	1.290	0.031	8.06
3100	1.455	0.098	3.23	1220	1.286	0.031	8.20
3080	1.450	0.086	3.25	1200	1.282	0.032	8.33
3060	1.445	0.075	3.27	1180	1.275	0.032	8.47
3040	1.440	0.065	3.29	1160	1.272	0.034	8.62
3020	1.432	0.054	3.31	1140	1.269	0.036	8.77
3000	1.426	0.048	3.33	1120	1.264	0.037	8.93
2960	1.415	0.035	3.38	1100	1.258	0.038	9.09
2920	1.407	0.025	3.42	1080	1.254	0.042	9.26
2880	1.397	0.017	3.47	1060	1.246	0.045	9.43
2840	1.389	0.013	3.52	1040	1.238	0.047	9.61
2800	1.383	0.009	3.57	1020	1.222	0.058	9.80
2760	1.376	0.007	3.62	1000	1.216	0.054	10.0
2720	1.370	0.006	3.67	980	1.200	0.067	10.2
2680	1.366	0.006	3.73	960	1.187	0.075	10.4
2640	1.361	0.005	3.79	940	1.175	0.079	10.6
2600	1.356	0.005	3.85	920	1.164	0.091	10.9
2560	1.353	0.005	3.91	900	1.150	0.110	11.1
2520	1.349	0.005	3.97	880	1.142	0.132	11.4
2480	1.345	0.005	4.03	860	1.134	0.160	11.6



TABLE I (continued)

$\nu$ in $\text{cm}^{-1}$	$n_r$	$n_i$	$\lambda$ in $\mu\text{m}$	$\nu$ in $\text{cm}^{-1}$	$n_r$	$n_i$	$\lambda$ in $\mu\text{m}$
840	1.130	0.193	11.9	560	1.435	0.416	17.9
820	1.132	0.228	12.2	540	1.459	0.415	18.5
800	1.137	0.261	12.5	520	1.469	0.415	19.2
780	1.142	0.295	12.8	500	1.476	0.413	20.0
760	1.150	0.324	13.2	480	1.494	0.411	20.8
740	1.168	0.343	13.5	460	1.509	0.408	21.7
720	1.190	0.364	13.9	440	1.518	0.405	22.7
700	1.225	0.378	14.3	420	1.523	0.402	23.8
680	1.260	0.392	14.7	400	1.527	0.397	25.0
660	1.300	0.398	15.1	380	1.527	0.392	26.3
640	1.330	0.407	15.6	360	1.528	0.387	27.8
620	1.348	0.402	16.1	340	1.531	0.383	29.4
600	1.353	0.415	16.7	330	1.535	0.380	30.3
580	1.393	0.416	17.2				

Computation of the uncertainty of  $n_i$  associated with uncertainties of  $R_0$  and  $n_r$  shows that the uncertainty of  $n_i$  is inversely proportional to  $n_i$  and thus  $\delta n_i$  becomes unacceptably large for small values of  $n_i$ . Therefore, in our final tabulation of  $n_i$ , we used values of this quantity based on transmittance measurements in all cases for which  $n_i < 0.05$ . We also adopted  $n_i$  values based on transmittance in the region 3200–3000  $\text{cm}^{-1}$ , where the values of  $n_i$  given by Eq. (8) are in the range 0.05–0.15 but have uncertainties greater than the uncertainties of the values of  $n_i$  based on transmittance measurements. Our best values of  $n_i$  are plotted in the upper panel of Fig. 12 and are listed in Table I.

The determinations of  $n_i$  by reflection methods complement determinations based on transmittance studies, from which it is difficult to determine large values of  $n_i$  at the centers of strong absorption bands. However, we note that our values of  $n_i$  are in excellent agreement with those obtained by Plyler and Griff<sup>6</sup> in their careful studies of the 1640- and 3400- $\text{cm}^{-1}$  absorption bands.

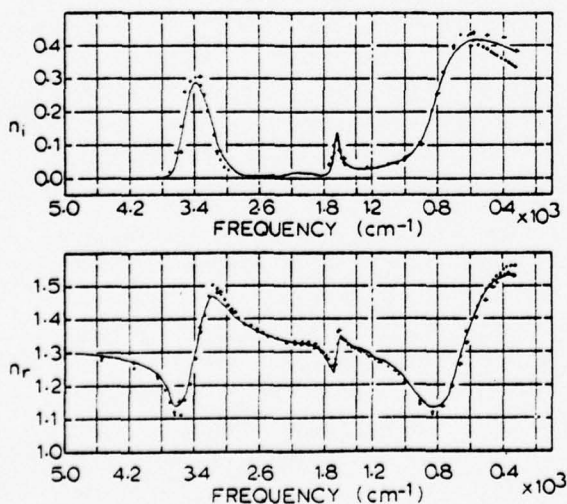


FIG. 13. Comparison of present values of  $n_r$  and  $n_i$ , given by the solid curves, are compared with the results of Pontier and Dechambenoy given by crosses and with those of Zolotarev *et al.*, given by solid circles.

We note also that our present value of the maximum value of  $n_i$  at 3400  $\text{cm}^{-1}$  is nearly 70% greater than some of the values cited by Irvine and Pollack on the basis of their survey.<sup>1</sup> Values of  $n_i$  in the 1000–300- $\text{cm}^{-1}$  region cannot be determined with precision from existing transmittance data.

When the values of the optical constants in Table I were used to calculate values of  $R_0$  and  $R_{\theta H}$ , the calculated values of these quantities agreed with the measured values well within the limits of experimental error. Agreement between the observed and calculated values serves essentially as a check of the internal consistency of our measurements and computations.

#### DISCUSSION OF RESULTS

In estimating the uncertainties in the tabulated values of the optical constants, it is necessary to consider not only the scatter of the original reflectance measurements but also possible systematic instrumental errors of various kinds. Detailed analysis of the data leads to the following uncertainties in  $n_r$ :  $\pm 1\%$  in the 5000–3700- $\text{cm}^{-1}$  region,  $\pm 2\%$  in the 3700–2900- $\text{cm}^{-1}$  region,  $\pm 1.5\%$  between 2900 and 900  $\text{cm}^{-1}$ , and  $\pm 2\%$  in the 900–330- $\text{cm}^{-1}$  region. In the case of  $n_i$  values based on reflectance data, we estimate an uncertainty of  $\pm 7\%$  in the peak value at 3400  $\text{cm}^{-1}$ ,  $\pm 10\%$  in the peak value at 1640  $\text{cm}^{-1}$ , and  $\pm 5\%$  in the 600- $\text{cm}^{-1}$  region. Because the smaller  $n_i$  values are based on measurements of published transmittance curves, the tabulated values are accurate to perhaps  $\pm 10\%$ .

In Fig. 13 we compare the results obtained in other recent studies with the present results, which are given by the solid curves. In the case of  $n_r$ , the values obtained by Pontier and Dechambenoy<sup>2</sup> are in excellent agreement with the present results over the entire range between 5000 and 900  $\text{cm}^{-1}$ ; the maximum deviations, which occur near 3134 and 910  $\text{cm}^{-1}$ , fall well within the limits of uncertainty stated in the two investigations. Between 900 and 330  $\text{cm}^{-1}$ , the  $n_r$  values listed by Pontier and Dechambenoy are consistently lower than the present values but there is some over-

lapping when the estimated uncertainties are considered. The  $n_r$  values of Zolotarev *et al.*<sup>4</sup> are consistently lower than the present values between 5000 and 3300  $\text{cm}^{-1}$  and consistently higher than the present results between 3300 and 2500  $\text{cm}^{-1}$ ; there is good agreement between our values and the Zolotarev results between 2500 and 900  $\text{cm}^{-1}$ . The Zolotarev values are lower than ours near 800  $\text{cm}^{-1}$ , are in excellent agreement with ours between 700 and 450  $\text{cm}^{-1}$ , and become progressively greater than ours for frequencies less than 450  $\text{cm}^{-1}$ . Zolotarev *et al.* placed special emphasis on their low extreme of 1.11 for  $n_r$  near 3500  $\text{cm}^{-1}$  and their high extreme of 1.50 near 3170  $\text{cm}^{-1}$ ; the present study did not confirm these extreme values.

For  $n_i$ , there is good agreement between maximum values for the absorption bands at 3400 and 1640  $\text{cm}^{-1}$ . However, there seems to be some disagreement regarding the shape of the 3400- $\text{cm}^{-1}$  band; this band, as defined by the four values listed by Pontier and Dechambenoy, appears to be somewhat narrower than the band shown by the solid curve in Fig. 13; this band, as mapped by Zolotarev, has the same width as that noted in the present study but seems to be shifted slightly toward higher frequencies. For the band in the vicinity of 600  $\text{cm}^{-1}$  Zolotarev *et al.* report a rather sharp peak at 665  $\text{cm}^{-1}$  followed by rapidly decreasing values of  $n_i$  at lower frequencies. Pontier and Dechambenoy report the maximum value of  $n_i$  at the same frequency as the maximum obtained in our study and obtain a general band shape similar to that we obtained.

At the lowest frequencies, the Pontier values of  $n_i$  are in general slightly higher than ours and the Zolotarev values are considerably lower.

Although the recent studies have provided values of optical constants that are sufficiently accurate for use in Mie-theory calculations and for calculations of emissivity, further improvements of accuracy are desirable. Pending the development of improved optical attenuators or amplifier-detector systems of improved linearity, it appears unlikely that  $\delta R_0/R_0$  can be made appreciably less than 0.01; however, even with this limitation, the ratio  $\delta n_r/n_r$  could be reduced to values smaller than our present value of 0.01 in the high-frequency region, where  $n_i$  is less than 0.01. The value of  $\delta n_r/n_r$  in other spectral regions is now limited by the

value of  $\delta n_i/n_i$  obtained in transmittance measurements. Dr. C. Robertson of our laboratory is using an absorption cell of novel design to obtain values of  $n_i$  that are more precise than those listed in Table I; his results can, in turn, be used with our present values of  $R_0$  to provide more precise values of  $n_r$ .

In view of the necessity for using polarizers and in view of the influence of  $\Delta\theta$ , for oblique angles of incidence  $\delta R_{\theta H}/R_{\theta H}$  is greater than  $\delta R_0/R_0$ . However, if improved polarizers can be developed, it is possible that more accurate values of the optical constants can be obtained from reflection measurements at some of the special angles suggested by Humphrey-Owens.<sup>5</sup>

We close by noting that several computer techniques have been developed for obtaining  $n_r$  and  $n_i$  from measurements of  $R_0$  alone. Spitzer *et al.*<sup>9,10</sup> have successfully used the so-called dispersion analysis, which involves the assumption of band models, to obtain the optical constants of quartz. Gottlieb<sup>11</sup> has successfully used Kramers-Kronig relations to obtain the optical constants for LiF from  $R_0$  measurements. Although, in the present study, we have not used these techniques, it is possible to use our  $R_0$  values in such computations and to use our  $R_{\theta H}$  values to test the validity of the validity of the computed values of the optical constants.

#### REFERENCES

- \* Paper presented at the Annual Meeting of the Optical Society, Hollywood, Florida, October 1970 [J. Opt. Soc. Am. 60, 1569A (1970)]. Supported in part by the Office of Naval Research through a contract with Kansas State University and by the Missouri Water Resources Research Center (OWRR) through a grant to the University of Missouri, K.C.
- <sup>1</sup> W. M. Irvine and J. B. Pollack, *Icarus* 8, 324 (1968).
- <sup>2</sup> L. Pontier and C. Dechambenoy, *Ann. Geophys.* 21, 462 (1965); 22, 633 (1966).
- <sup>3</sup> M. R. Querry, B. Curnutte, and D. Williams, *J. Opt. Soc. Am.* 59, 1299 (1969).
- <sup>4</sup> V. M. Zolotarev, B. A. Mikhailov, L. I. Aperovich, and S. I. Popov, *Opt. Spektrosk.* 27, 790 (1969). [*Opt. Spectrosc.* 27, 430 (1969)].
- <sup>5</sup> S. P. F. Humphrey-Owens, *Proc. Roy. Soc. (London)* 77, 949 (1968).
- <sup>6</sup> E. K. Plyler and N. Griff, *Appl. Opt.* 4, 1663 (1965).
- <sup>7</sup> E. K. Plyler and N. Acquista, *J. Opt. Soc. Am.* 44, 505 (1954).
- <sup>8</sup> D. A. Draeger, N. W. B. Stone, B. Curnutte, and D. Williams, *J. Opt. Soc. Am.* 56, 64 (1966).
- <sup>9</sup> W. G. Spitzer, D. A. Kleinman, and D. Walsh, *Phys. Rev.* 113, 127 (1959).
- <sup>10</sup> W. G. Spitzer, D. A. Kleinman, and C. J. Frosch, *Phys. Rev.* 113, 133 (1959).
- <sup>11</sup> M. Gottlieb, *J. Opt. Soc. Am.* 50, 343 (1960).

At this stage of the work Dr. Charles W. Robertson joined our group and developed a wedge-cell that made it possible to make accurate determinations of the Lambert absorption coefficient  $\alpha(\nu)$  of water. The technique involved is described in the following paper by Robertson and Williams, which lists  $\alpha(\nu)$  and  $k(\nu)$  for the spectral range  $4300 \text{ cm}^{-1}$  to  $300 \text{ cm}^{-1}$ .

## Lambert Absorption Coefficients of Water in the Infrared\*

CHARLES W. ROBERTSON AND DUDLEY WILLIAMS

*Department of Physics, Kansas State University, Manhattan, Kansas 66502*

(Received 23 April 1971)

By use of a wedge-shaped cell providing an absorbing layer tapering in thickness from less than one wavelength of visible light at one end to approximately  $20\ \mu\text{m}$  at the other end, we have measured the Lambert absorption coefficient for water in the spectral region between  $4000$  and  $288\ \text{cm}^{-1}$ . After proper initial alignment of the cell windows had been established by the observation of interference fringes in the visible, we measured film thicknesses at various positions along the wedge by interferometric methods, employing convenient wavelengths in the infrared. We present the results of the study in graphical and tabular form.

INDEX HEADINGS: Water; Infrared; Absorption; Spectrophotometry.

The fractional spectral transmittance  $T(\nu)$  of a liquid in an absorption cell of thickness  $z$  is given by the expression

$$T(\nu) = (1-R)(1-A)e^{-\alpha(\nu)z}, \quad (1)$$

where  $R$  is the fraction of the radiant flux reflected at the cell windows,  $A$  is the fraction absorbed by the cell windows, and  $\alpha(\nu)$  is the Lambert absorption coefficient of the liquid. In their survey of the existing literature dealing with the optical properties of water in the infrared, Irvine and Pollack<sup>1</sup> pointed out some of the practical difficulties in obtaining accurate values of the

Lambert absorption coefficient of water from conventional transmittance measurements.

In regions of strong absorption, the required values of  $z < 10\ \mu\text{m}$  are so small that it is difficult to form uniform water films of accurately measured thickness between plates of the available nonsoluble optical materials that are transparent in the infrared. Uncertainties of absorbing-film thickness thus limit the precision with which  $\alpha(\nu)$  can be determined in spectral regions of strong absorption. Stray flux from other spectral regions can also lead to serious overestimation of  $T(\nu)$  near the

centers of strong absorption bands and thus lead to additional uncertainties of the resulting values of  $\alpha(\nu)$ . In view of these difficulties, absorption coefficients at the centers of strong bands can be determined more reliably from reflection measurements than from typical transmittance measurements.

There are also experimental difficulties in  $\alpha(\nu)$  determinations in spectral regions of low absorption, where reflection techniques cannot be readily applied. Irvine and Pollack<sup>1</sup> noted that many investigators have assumed that the factor  $(1-R)(1-I)$  in Eq. (1) represents the fractional transmittance of the empty cell. Such an assumption is incorrect because the presence of the water changes the reflectance of the inner surfaces of the cell windows; use of  $(1-R)(1-I)$  as the transmittance of the empty cell introduces serious errors when measured values of  $T(\nu)$  are close to unity and thus introduces corresponding large errors of  $\alpha(\nu)$  in spectral regions of low absorption, unless large cell thicknesses  $z$  are employed.

One method of avoiding the problems imposed by the uncertainties of the reflectance correction is that employed by Dracert *et al.*<sup>2</sup> in their far-infrared study of water absorption; these authors measured nominal spectral transmittance for water films of different thickness  $z$  and obtained  $\alpha(\nu)$  from the slope of a semilog plot of measured  $T(\nu)$  vs  $z$ . An equivalent technique was used in the near infrared by Pontier and Dechambenois,<sup>3</sup> who used two cell thickness  $z_1$  and  $z_2$  and determined  $\alpha(\nu)$  from the ratio of transmittances:  $T_2(\nu)/T_1(\nu) = e^{-\alpha(z_2-z_1)}$ ; in taking the ratio, they eliminated the factor  $(1-R)(1-I)$  from Eq. (1). These authors report an uncertainty of  $\alpha(\nu)$  amounting to only a few percent in spectral regions of weak absorption but increasing to 15%-20% near most band centers and to 50% at the center of the strong band at  $3400\text{ cm}^{-1}$ . This general method is thus limited by the difficulties in establishing and measuring small differences of film thickness  $z$ .

### PRESENT WORK

The present study is essentially an extension of earlier methods<sup>2,3</sup> in which we employed an absorption cell providing a wide range of thicknesses  $z$  which can be measured by interferometric methods. The cell windows were rectangular plates of width  $X=50\text{ mm}$  and height  $Y=25\text{ mm}$ . The windows were in optical contact at  $x=0$  and were separated by a  $20\text{-}\mu\text{m}$  spacer at  $x=X$  and therefore provided a water film ranging in thickness  $z$  from less than  $1\text{ }\mu\text{m}$  at  $x=0$  to  $20\text{ }\mu\text{m}$  at  $x=X$ . In the initial assembly of the cell, the windows were aligned to give straight interference fringes parallel to the  $y$  axis when viewed in light from a He-Ne laser; thus, at a given value of  $x$ , cell thickness  $z$  showed little variation with  $y$ .

The empty cell was placed in a holder that could be moved laterally along ways parallel to the  $x$  axis. One spherical mirror produced an image of a Nernst glower

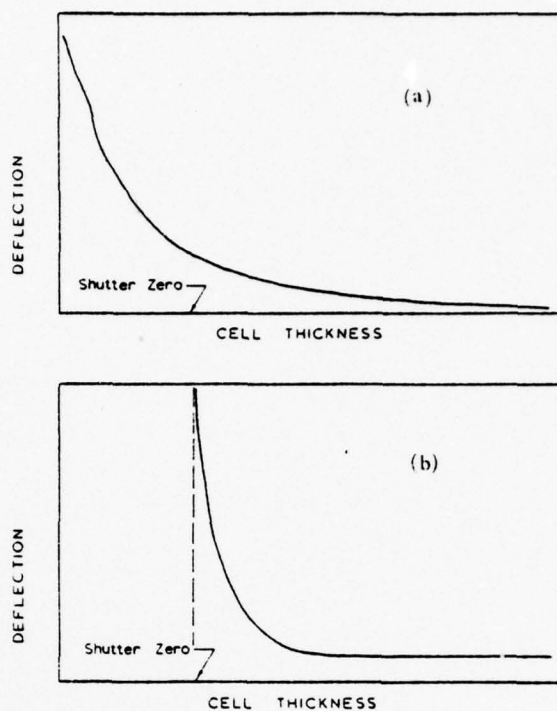


FIG. 1. (a) Typical chart record, giving deflection as a function of cell thickness. (b) Chart record for the  $3400\text{-cm}^{-1}$  region, in which deflections do not extrapolate to shutter zero for large cell thickness.

at the cell position and a second spherical mirror directed radiation transmitted by the cell to the entrance slit of the spectrograph. The effective width of the convergent beam traversing the cell was thus established by the width of the entrance slit of the spectrograph and was never greater than  $\Delta x=0.62\text{ mm}$ . With the spectrograph set for a convenient wavelength in the infrared, the cell holder, driven by a synchronous motor, was moved laterally in the  $x$  direction through the beam and interference fringes were observed on the recorder chart. From the spacing of the observed interference fringes, variations of thickness  $z$  as a function of  $x$  could be determined accurately in terms of the selected infrared wavelength. Lateral positions  $x$  of a pointer attached to the movable cell holder were noted from a small engraved scale attached to the ways. Thus, motion of the cell holder through a distance  $x-x_1$  along the ways produced a corresponding variation  $z-z_1$  in cell thickness at the position of the Nernst-glower image.

With water in the absorption cell, the spectrograph was set to pass a selected spectral frequency. The cell was moved slowly along the ways with the recorder running; the display on the recorder chart thus gives a record of deflection  $D$ , proportional to transmitted flux  $I$ , as a function of cell position  $x$ , proportional to cell thickness  $z$ . The deflections  $D$  were, in general, measured

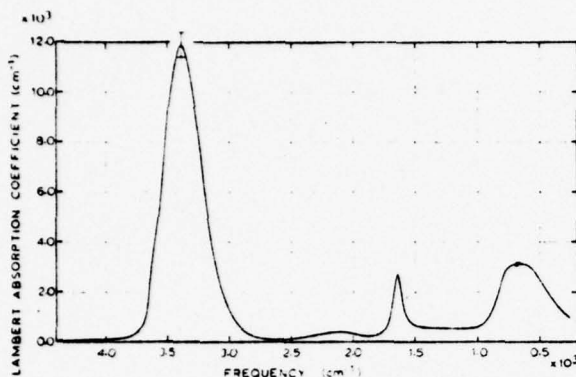


Fig. 2. Lambert absorption coefficients for regions of strong absorption.

from a shutter-zero trace recorded with an opaque shutter in the beam.

Typical recorder traces are shown in Fig. 1(a). If we select a given deflection  $D_1$  corresponding to some cell thickness  $z_1$ , we may determine the Lambert absorption coefficient  $\alpha(\nu)$  by taking the ratio of the deflection  $D$  at any larger value of  $z$  to  $D_1$

$$D/D_1 = I/I_1 = e^{-\alpha(\nu)(z-z_1)}$$

or

$$\alpha(\nu) = Ln(I/I_1)/(z-z_1), \quad (2)$$

where  $(z-z_1)$  is known from interferometric measurements of the empty cell. In practice,  $\alpha(\nu)$  was based on average values given by Eq. (2) for observed values of  $(I/I_1)$  obtained at numerous values of  $(z-z_1)$  as in the work of Draeger *et al.*<sup>2</sup> rather than on a single pair of values of  $I_1$  and  $I$  as in the study of Pontier and Dechambenoy.<sup>3</sup>

In spectral regions of extremely strong absorption, where very high amplifier gains were needed, we noted that a recorder plot of  $D$  as a function of  $z$  like that shown in Fig. 1(b) did not extrapolate to shutter zero as  $z$  becomes large. We attribute this to a slight amount of stray radiant flux from other spectral regions. In this

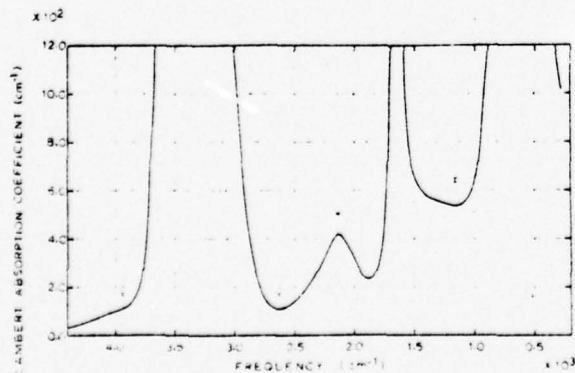


Fig. 3. Lambert absorption coefficients for regions of weak absorption.

situation, which was encountered only near  $3400 \text{ cm}^{-1}$ , we measured chart deflections from the extrapolated value of  $D$  rather than from the shutter zero level established with an opaque shutter in the beam from the source. Failure to identify and eliminate stray flux may account in part for difficulties encountered in the  $3400\text{-cm}^{-1}$  region by earlier investigators.

The absorption cells used in the  $4000\text{-}1000\text{-cm}^{-1}$  range were equipped with  $\text{CaF}_2$  windows of high optical quality. We observed no interference fringes when these cells contained water. The cells used in the  $1000\text{-}300\text{-cm}^{-1}$  region were equipped with selected KRS-5 plates. Because of the high refractive index of KRS-5 relative to water, interference fringes could be observed for water-filled cells in spectral regions where  $\alpha(\nu)$  is small; we made appropriate corrections for this effect in computing  $\alpha(\nu)$  from the recorder tracings.

The water was held in the cells by means of neoprene strips pressed against the edges of the plates when the cells were initially fabricated. We used freshly distilled de-ionized water in order to avoid the formation of air bubbles and made numerous checks of cell thickness  $z$  vs  $x$  in the course of the study.

We employed a Perkin-Elmer Model 112 spectrometer equipped with a Reeder thermocouple and used  $\text{LiF}$ ,  $\text{CaF}_2$ ,  $\text{NaCl}$ , and  $\text{CsBr}$  prisms in appropriate spectral regions. In all regions, the spectral slit width was small as compared with the spectral features being studied.

We note that, although Eqs. (1) and (2) apply strictly to parallel beams traversing an absorption cell, we actually employed a nonparallel beam. In the convergent beam entering the cell, the extreme rays made an angle  $\theta = 8^\circ$  with the central ray; this results in a maximum spread of absorption path lengths  $\Delta z = z_0/\cos\theta - z_0 = 0.01z_0$ . In view of the fact that the interferometric  $z$  measurements were made with the cell *in situ* and thus provide an average value of  $z$ , we have ignored the variations of  $z$  imposed by the nonparallel beam. Similarly, we have ignored the spread  $\Delta z$  imposed by the finite width  $\Delta x$  of the glower image at the position of the absorbing layer.

## EXPERIMENTAL RESULTS

In the course of the work we determined  $\alpha(\nu)$  at approximately 300 frequencies in the  $4500\text{-}300\text{-cm}^{-1}$  region and made approximately three independent determinations at each of these frequencies. The results of the study are summarized in Figs. 2 and 3, in which we present  $\alpha(\nu)$  vs  $\nu$  by smooth curves that were drawn through plots of the individual  $\alpha(\nu)$  values. The length of the uncertainty bars shown in the figures represent the scatter of individual  $\alpha(\nu)$  values and were determined from the averages of probable errors in each region.

Figure 2 gives a plot of  $\alpha(\nu)$  vs  $\nu$ , which shows the major absorption bands. The maximum value of  $\alpha(\nu)$  at the center of the  $3400\text{-cm}^{-1}$  absorption band is  $11\,900$  per centimeter, with an uncertainty of  $\pm 500$  per

TABLE I. Absorption coefficients of water in the infrared.

Frequency cm <sup>-1</sup>	Lambert absorption coefficient cm <sup>-1</sup>	Imaginary part of refractive index <i>n<sub>i</sub></i>	Wavelength μm	Frequency cm <sup>-1</sup>	Lambert absorption coefficient cm <sup>-1</sup>	Imaginary part of refractive index <i>n<sub>i</sub></i>	Wavelength μm
4300	46	0.0009	2.326	1650	2670	0.1288	6.061
4200	62	0.0012	2.381	1640	2738	0.1329	6.098
4100	81	0.0016	2.439	1630	2566	0.1253	6.135
4000	100	0.0020	2.500	1620	2139	0.1051	6.173
3900	118	0.0024	2.564	1610	1760	0.0870	6.211
3800	192	0.0040	2.632	1600	1465	0.0729	6.250
3700	762	0.0164	2.703	1580	1025	0.0516	6.329
3650	2270	0.0495	2.740	1550	806	0.0414	6.452
3600	4070	0.0900	2.778	1500	667	0.0354	6.667
3550	6020	0.1349	2.817	1400	584	0.0332	7.143
3500	8750	0.1989	2.857	1300	559	0.0342	7.692
3450	10 850	0.2503	2.899	1200	541	0.0359	8.333
3420	11 600	0.2699	2.924	1100	542	0.0392	9.091
3400	11 850	0.2774	2.941	1050	566	0.0429	9.524
3380	11 870	0.2795	2.959	1000	631	0.0502	10.000
3350	11 880	0.2822	2.985	980	673	0.0546	10.204
3300	10 000	0.2411	3.030	960	745	0.0618	10.417
3250	8270	0.2025	3.077	940	832	0.0704	10.638
3200	6010	0.1495	3.125	920	970	0.0839	10.870
3150	4320	0.1091	3.175	900	1112	0.0983	11.111
3100	2840	0.0729	3.226	880	1294	0.1170	11.364
3050	1840	0.0480	3.279	860	1557	0.1441	11.628
3000	1120	0.0297	3.333	840	1890	0.1790	11.905
2950	780	0.0210	3.390	820	2210	0.2145	12.195
2900	503	0.0138	3.448	800	2600	0.2586	12.500
2800	220	0.0063	3.571	780	2825	0.2882	12.821
2700	123	0.0036	3.704	760	2980	0.3120	13.158
2650	112	0.0034	3.774	725	3090	0.3392	13.793
2600	115	0.0035	3.846	700	3115	0.3541	14.286
2500	146	0.0046	4.000	675	3125	0.3684	14.815
2400	197	0.0065	4.167	650	3130	0.3832	15.385
2300	268	0.0093	4.348	625	3120	0.3973	16.000
2200	376	0.0136	4.545	600	3080	0.4085	16.667
2160	412	0.0152	4.630	575	2990	0.4138	17.391
2140	419	0.0156	4.673	550	2780	0.4022	18.182
2120	418	0.0157	4.717	525	2600	0.3941	19.048
2100	410	0.0155	4.762	500	2415	0.3844	20.000
2000	317	0.0126	5.000	475	2240	0.3753	21.053
1900	237	0.0099	5.263	450	2050	0.3625	22.222
1850	242	0.0104	5.405	425	1880	0.3520	23.529
1800	289	0.0128	5.556	400	1700	0.3382	25.000
1750	451	0.0205	5.714	375	1530	0.3247	26.667
1700	1200	0.0562	5.882	350	1335	0.3035	28.571
1680	1840	0.0872	5.952	325	1200	0.2938	30.769
1660	2430	0.1165	6.024	300	1100	0.2918	33.333

centimeter; this value is to be compared with 11 940 ± 830 per centimeter based on recent reflectance measurements.<sup>4</sup> It represents a marked improvement over the transmittance measurements of Pontier and Dechambenois,<sup>3</sup> whose peak value at 3400 cm<sup>-1</sup> had an uncertainty of 50%. The peak values of  $\alpha(\nu)$  near 1640 and 650 cm<sup>-1</sup> are in good agreement with the corresponding values obtained in recent reflectance studies.<sup>4-6</sup> This agreement between the present values and those based on reflectance studies is gratifying; we attribute it to our improved methods of determining the incremental thickness ( $z-z_1$ ) of the absorbing layers and to improvements in identifying and correcting for stray flux at the centers of absorption bands.

We note that the strong band with maximum at 3400 cm<sup>-1</sup> is not a simple band. The observed change of slope near 3700 cm<sup>-1</sup> is real and is established by eight indi-

vidual  $\alpha(\nu)$  determinations in this region; the asymmetrical wing extending toward lower frequencies is also well established by the data. The 3400-cm<sup>-1</sup> band is usually attributed to the  $\nu_1$ ,  $\nu_3$ , and  $2\nu_2$  bands of the H<sub>2</sub>O monomeric unit in the liquid structure. The flat top and asymmetric shape of the band at 650 cm<sup>-1</sup> also suggest a complex structure; this band is usually attributed to librational modes  $\nu_L$  of H<sub>2</sub>O monomers in the water lattice and two of these modes would be expected to be strongly infrared active.

Figure 3 gives a plot of  $\alpha(\nu)$  vs  $\nu$  with the  $\alpha(\nu)$  scale expanded by a factor of 10 as compared with the plot in Fig. 2. We note that in regions of small  $\alpha(\nu)$  the scatter of individual determinations is small even on this expanded scale. These uncertainties of  $\alpha(\nu)$  are considerably smaller than the uncertainties of  $\alpha(\nu)$  as determined from reflectance measurements alone. Some of

the recent reflectance studies have been augmented by transmittance data in regions where  $\alpha(\nu)$  is low; because these were not reported in detail,<sup>3,5</sup> it is not possible to make detailed comparisons with these studies; other sets of optical data<sup>1,4</sup> make use of  $\alpha(\nu)$  values obtained from published transmittance curves, in which even careful measurements of small-scale plots in the journals may introduce errors as large as  $\pm 10\%$ .

The peak frequency of the associational water band appears at  $2135\text{ cm}^{-1}$ . This band is usually interpreted as a combination band  $\nu_z = \nu_2 + \nu_L$ , where  $\nu_L$  is a librational mode; the required frequency of the librational mode is  $485\text{ cm}^{-1}$  and there is no absorption peak at this frequency in Fig. 2. However, the present results are in fair agreement with the suggested<sup>6</sup> assignment  $\nu_z = \nu_2 + \nu_L - \nu_T$ , where  $\nu_T$  is the hindered translation band<sup>2</sup> near  $175\text{ cm}^{-1}$ ; with this assignment  $\nu_z = (1640 + 650 - 175)\text{ cm}^{-1} = 2115\text{ cm}^{-1}$  as compared with the observed value of  $2130\text{ cm}^{-1}$ . However, the earlier assignment cannot be excluded because the requisite librational mode  $\nu_L = 485\text{ cm}^{-1}$  may be inactive in the infrared but may contribute to the observed Raman bands in this region.<sup>7</sup>

Because Irvine and Pollack<sup>1</sup> have stressed the importance of the publication of tabulated values of the optical constants obtained in quantitative studies of water, we are including an abbreviated listing of our results in Table I. In this table, we list our values of  $\alpha(\nu)$  along with the corresponding value of the imaginary part of the refractive index  $n_i = \lambda\alpha/4\pi$ ; interpolations between listed values can be made with the aid of Figs. 1 and 2.

Since reflectance is not strongly influenced by  $n_i$  in spectral regions of weak absorption, the values of  $n_i$  in Table I are more accurate than  $n_i$  values based on reflectance measurements alone in all cases in which  $n_i < 0.10$ . As noted earlier, the present results are in gratifyingly good agreement with those obtained by reflectance measurements near the absorption peaks at  $3400$ ,  $1640$ , and  $650\text{ cm}^{-1}$ . At frequencies below  $500\text{ cm}^{-1}$ , the  $n_i$  values listed in Table I become progressively lower than those based on reflectance

studies<sup>1,3,4</sup> and are approximately 25% lower at  $300\text{ cm}^{-1}$ . This divergence could be due in part to stray radiant flux in the present study, although checks of shutter-zero levels with opaque shutters and glass shutters failed to reveal it. Another possibility is that the polarizers used in the reflectance studies, consisting of stacks of AgCl plates, become inefficient in the low-frequency region where the transmittance and the refractive index of AgCl are decreasing. Some support for this suggestion is given by a Kramers-Kronig analysis of the normal-incidence reflectance measurements of Rusk *et al.*,<sup>4</sup> for which no polarizer was used: preliminary Kramers-Kronig results give values of  $n_i$  in excellent agreement with their published values in all spectral regions above  $500\text{ cm}^{-1}$  but considerably below the published values at the lowest frequencies.

Determinations of the Lambert absorption coefficient of water by the type of cell developed in the present work can be extended from  $300$  to  $250\text{ cm}^{-1}$  with selected KRS-5 windows and from  $200\text{ cm}^{-1}$  to the extreme infrared with quartz windows. The only readily available window material for use in the gap between  $250$  and  $200\text{ cm}^{-1}$  is polyethylene, a material not normally adaptable for use in a cell of the type we have used. Fortunately,  $n_i$  is sufficiently high in the far infrared to be measured accurately by the application of Kramers-Kronig techniques to normal-incidence reflectance measurements.

#### REFERENCES

- \* Supported in part by the Office of Naval Research.
- <sup>1</sup> W. M. Irvine and J. B. Pollack, *Icarus* 8, 324 (1968).
- <sup>2</sup> D. A. Draeger, N. W. B. Stone, B. Curnutte, and D. Williams, *J. Opt. Soc. Am.* 56, 64 (1966).
- <sup>3</sup> L. Pontier and C. Dechambenois, *Ann. Geophys.* 21, 462 (1965); 22, 633 (1966).
- <sup>4</sup> A. N. Rusk, D. Williams, and M. R. Querry, *J. Opt. Soc. Am.* 61, 395 (1971).
- <sup>5</sup> V. M. Zolotarev, B. A. Mikhailov, L. I. Aperovich, and S. I. Popov, *Opt. Spektrosk.* 27, 790 (1969) [*Opt. Spectrosc.* 27, 430 (1969)].
- <sup>6</sup> D. Williams, *Nature* 210, 194 (1966).
- <sup>7</sup> G. Walrafen, *J. Chem. Phys.* 40, 3249 (1964).



## The infra-red spectrum of water†

by CHARLES W. ROBERTSON, BASIL CURNUTTE  
and DUDLEY WILLIAMS

Department of Physics, Kansas State University,  
Manhattan, Kansas 66506, U.S.A.

(Received 15 September 1972)

The Lambert absorption coefficient of water has been measured in the far infra-red spectral region 800 to 50  $\text{cm}^{-1}$ . The results, along with earlier measurements in the near infra-red, provide values of the imaginary part  $k$  of the refractive index over the spectral range 4400 to 50  $\text{cm}^{-1}$ . Kramers-Kronig techniques have been used to obtain values of the corresponding real part  $n$  of the refractive index over this spectral range. The values of these constants provide a complete quantitative description of the optical properties of water in the infra-red.

### 1. INTRODUCTION

Although the infra-red spectrum of water has been the subject of numerous investigations dating from the early days of infra-red spectroscopy, a critical survey by Irvine and Pollack [1] revealed many inconsistencies in published results and emphasized the desirability of further quantitative studies of transmission and reflection with the purpose of obtaining more precise values of the real  $n$  and imaginary  $k$  parts of the refractive index in the infra-red. Several such quantitative studies have recently been reported [2-6].

In the present study we have measured the Lambert absorption coefficient  $\alpha(\bar{\nu})$  in the range 800 to 50  $\text{cm}^{-1}$  in the far infra-red. The results, along with those reported earlier [6], provide values of  $k$  in the spectral region 4400 to 50  $\text{cm}^{-1}$ . We have applied Kramers-Kronig techniques to obtain values of  $n$  from our measured values of  $\alpha(\bar{\nu})$ . The resulting values of  $k$  and  $n$  provide a quantitative description of the optical properties of water in the infra-red.

### 2. FAR INFRA-RED MEASUREMENTS

In the absence of multiple reflections, the spectral transmittance  $T(\bar{\nu})$  of a liquid in an absorption cell of thickness  $Z$  is given by the expression

$$T(\bar{\nu}) = [1 - \mathfrak{R}(\bar{\nu})][1 - \mathfrak{A}(\bar{\nu})] \exp[-\alpha(\bar{\nu})Z], \quad (2.1)$$

where  $\mathfrak{R}(\bar{\nu})$  is the fraction of the radiant flux reflected at the inner and outer surfaces of the windows,  $\mathfrak{A}(\bar{\nu})$  is the fraction absorbed by the cell windows, and

† Supported in part by the Office of Naval Research, U.S.A., and in part by the Kansas Agricultural Experiment Station.

## The infra-red spectrum of water†

by CHARLES W. ROBERTSON, BASIL CURNUTTE  
and DUDLEY WILLIAMS

Department of Physics, Kansas State University,  
Manhattan, Kansas 66506, U.S.A.

(Received 15 September 1972)

The Lambert absorption coefficient of water has been measured in the far infra-red spectral region 800 to 50  $\text{cm}^{-1}$ . The results, along with earlier measurements in the near infra-red, provide values of the imaginary part  $k$  of the refractive index over the spectral range 4400 to 50  $\text{cm}^{-1}$ . Kramers-Kronig techniques have been used to obtain values of the corresponding real part  $n$  of the refractive index over this spectral range. The values of these constants provide a complete quantitative description of the optical properties of water in the infra-red.

### 1. INTRODUCTION

Although the infra-red spectrum of water has been the subject of numerous investigations dating from the early days of infra-red spectroscopy, a critical survey by Irvine and Pollack [1] revealed many inconsistencies in published results and emphasized the desirability of further quantitative studies of transmission and reflection with the purpose of obtaining more precise values of the real  $n$  and imaginary  $k$  parts of the refractive index in the infra-red. Several such quantitative studies have recently been reported [2-6].

In the present study we have measured the Lambert absorption coefficient  $\alpha(\bar{\nu})$  in the range 800 to 50  $\text{cm}^{-1}$  in the far infra-red. The results, along with those reported earlier [6], provide values of  $k$  in the spectral region 4400 to 50  $\text{cm}^{-1}$ . We have applied Kramers-Kronig techniques to obtain values of  $n$  from our measured values of  $\alpha(\bar{\nu})$ . The resulting values of  $k$  and  $n$  provide a quantitative description of the optical properties of water in the infra-red.

### 2. FAR INFRA-RED MEASUREMENTS

In the absence of multiple reflections, the spectral transmittance  $T(\bar{\nu})$  of a liquid in an absorption cell of thickness  $Z$  is given by the expression

$$T(\bar{\nu}) = [1 - \mathfrak{R}(\bar{\nu})][1 - \mathfrak{A}(\bar{\nu})] \exp[-\alpha(\bar{\nu})Z], \quad (2.1)$$

where  $\mathfrak{R}(\bar{\nu})$  is the fraction of the radiant flux reflected at the inner and outer surfaces of the windows,  $\mathfrak{A}(\bar{\nu})$  is the fraction absorbed by the cell windows, and

† Supported in part by the Office of Naval Research, U.S.A., and in part by the Kansas Agricultural Experiment Station.

$\alpha(\bar{\nu})$  is the Lambert absorption coefficient of the liquid. In much of the infra-red region, the values of  $Z < 10 \mu\text{m}$  required for measurement of the transmittance of water are so small that the preparation of uniform layers of accurately measured thickness presents serious difficulties; uncertainties in absorbing-film thickness thus limit the precision with which  $\alpha(\bar{\nu})$  can be determined. Stray radiant flux from other spectral regions can also lead to serious overestimation of  $T(\bar{\nu})$  near the centres of strong absorption bands.

In our earlier study [6] we described a technique for avoiding these difficulties. By using a wedge-shaped absorbing layer with thickness  $Z$  ranging from less than one visible wavelength at one end to approximately  $20 \mu\text{m}$  at the other end, we were able to measure  $T(\bar{\nu})$  for various values of  $Z$ ; the alignment of the cell windows and the measurement of  $Z$  involved the use of interferometric techniques. By taking ratios of the transmittance  $T(\bar{\nu})$  for various values of  $Z$  we were able to obtain values of  $\alpha(\bar{\nu})$  without measuring the reflection  $\mathfrak{R}(\bar{\nu})$  and absorption  $\mathfrak{A}(\bar{\nu})$  factors of the cell windows; the detection of and correction for stray flux at the centres of strong bands could also be accomplished.

$\bar{\nu}$ $\text{cm}^{-1}$	$\alpha$ $\text{cm}^{-1}$	$k$	$n$	$\lambda$ $\mu\text{m}$
800	2620	0.260	1.12	12.5
760	3040	0.318	1.15	13.2
720	3230	0.357	1.19	13.9
680	3310	0.387	1.23	14.7
640	3290	0.409	1.27	15.6
600	3200	0.425	1.32	16.7
570	3080	0.430	1.35	17.6
560	3020	0.429	1.37	17.8
520	2780	0.425	1.41	19.3
480	2490	0.413	1.45	20.8
440	2210	0.400	1.48	22.7
400	1930	0.385	1.50	25.0
360	1660	0.366	1.52	27.8
320	1430	0.356	1.52	31.2
280	1330	0.378	1.52	35.7
240	1320	0.439	1.52	41.6
180	1410	0.624	1.65	55.6
170	1360	0.636	1.69	58.8
140	1065	0.605	1.80	71.5
100	680	0.540	1.92	100
60	370	0.489	2.00	167
50	320	0.509	2.03	200

Lambert absorption coefficients and optical constants in the infra-red.

In the present study we employ a similar wedge-cell technique to determine values of  $\alpha(\bar{\nu})$  in the far infra-red. Cells equipped with KRS-5 windows were used in the range 800 to 228  $\text{cm}^{-1}$ ; crystalline quartz windows were used in the range 170 to 50  $\text{cm}^{-1}$ . We employed a Perkin-Elmer Model 301 spectrophotograph. Since no insoluble windows of the required optical quality were available in the spectral range 228-170  $\text{cm}^{-1}$ , we used the transmittance data of Draeger

*et al.* [7] as a basis for interpolation in this range; these authors used polythene windows and made attempts to measure mean values of film thickness. We estimate that, in general, the uncertainties in the values obtained for  $\alpha(\bar{\nu})$  at the 24 discrete frequencies listed in the table were  $\pm 5$  per cent. The values of  $\alpha(\bar{\nu})$  obtained in the present study were in good agreement with our earlier values [6] in most of the spectral region common to the two investigations except in the vicinity of  $300\text{ cm}^{-1}$ , where the signals obtained with the CsBr prism spectrometer used in the earlier study were small.

### 3. ABSORPTION SPECTRUM

In figure 1 we give a plot of  $\alpha(\bar{\nu})$  as a function of  $\bar{\nu}$  in the spectral range 1200 to  $50\text{ cm}^{-1}$ . The spectrum in the far infra-red is dominated by a strong, broad absorption band for which  $\alpha(\bar{\nu})$  reaches its maximum values of  $3300/\text{cm}$  near  $680\text{ cm}^{-1}$ . Although this broad band shows no evidence of any complex structure, it is clearly asymmetrical; it rises rapidly on the high-frequency side and decreases gradually on the low-frequency side. A second weaker band appears as a shoulder in the vicinity of  $200\text{ cm}^{-1}$ . The absorption coefficient is decreasing rapidly at  $50\text{ cm}^{-1}$ .

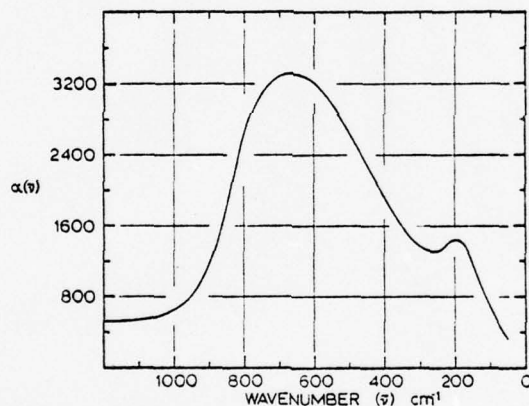


Figure 1. The Lambert absorption coefficient for water in the far infra-red;  $\alpha(\bar{\nu})$  in  $\text{cm}^{-1}$ .

The spectral transmission of a  $10\text{ }\mu\text{m}$  layer of water as computed from our measured values of  $\alpha(\bar{\nu})$  in the  $800\text{--}50\text{ cm}^{-1}$  region and our earlier [6] values of  $\alpha(\bar{\nu})$  for the  $4400\text{--}800\text{ cm}^{-1}$  region is plotted in figure 2. A layer of this thickness is essentially opaque in the  $3400\text{ cm}^{-1}$  absorption band generally attributed to monomeric fundamentals  $\nu_1$  and  $\nu_3$  and transmits less than 10 per cent at the centre of the  $1640\text{ cm}^{-1}$  band, which is attributed to monomeric fundamental  $\nu_2$ . The broad, intense band near  $680\text{ cm}^{-1}$  is usually attributed to a librational mode of oscillation  $\nu_L$  of the monomer in the field of its neighbours; the weaker band near  $200\text{ cm}^{-1}$  is similarly attributed to a hindered translational lattice mode  $\nu_T$ . The easily recognizable associational band near  $2120\text{ cm}^{-1}$  is usually interpreted as a combination of  $\nu_2$  with one or more lattice modes. The extremely weak band near  $4000\text{ cm}^{-1}$ , which appears as a depression of the transmission curve

suggested by the dashes in figure 2 was first reported by Collins [8]; the location of this band depends upon assumptions regarding the background and was listed as  $3950 \pm 30 \text{ cm}^{-1}$  by Collins.

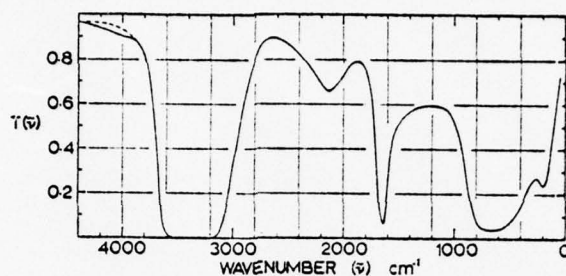


Figure 2. The spectral transmittance of a  $10 \mu\text{m}$  layer of water in the infra-red.

Water is actually highly absorbing over the entire spectral range represented in figure 2; the value of  $\alpha(\bar{\nu})$  at  $3400 \text{ cm}^{-1}$  is nearly  $10^8$  times that of water in the most transparent portion of its spectrum in the visible region. The bands shown in figure 2 are thus merely peaks superposed on a background of intense absorption. Ray [9] has recently made a survey of existing data on water absorption from the near infra-red to the millimeter and microwave region and has been able to account for the background absorption in terms of Debye dipole resonance absorption giving its maximum contribution to  $k(\bar{\nu})$  in the centimeter region.

#### 4. THE OPTICAL CONSTANTS OF WATER

The imaginary part  $k(\bar{\nu})$  of the index of refraction can be determined from the Lambert absorption coefficient  $\alpha(\bar{\nu})$  by means of the relationship

$$k(\bar{\nu}) = \alpha(\bar{\nu}) / 4\pi\bar{\nu}. \quad (4.1)$$

Using the present values of  $\alpha(\bar{\nu})$  along with those in [6], we have obtained the values of  $k(\bar{\nu})$  plotted in figure 3 and tabulated in the table for the low frequency region. For every peak for  $\alpha(\bar{\nu})$ , there is a corresponding peak for  $k(\bar{\nu})$  in

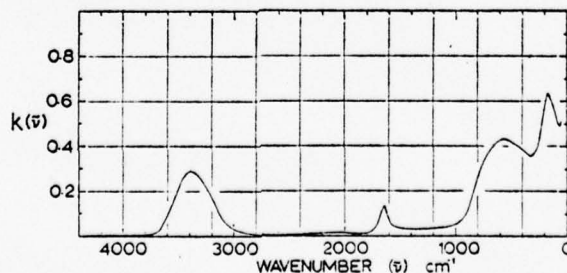


Figure 3. The imaginary part  $k(\bar{\nu})$  of the refractive index of water in the infra-red.

figure 3; however, because of the presence of  $\bar{\nu}$  in the denominator in equation (4.1), the appearance of the  $k(\bar{\nu})$  curves is quite different from that of the  $\alpha(\bar{\nu})$  curves. The maximum values of  $k(\bar{\nu})$  in the low frequency region are higher than the maximum value for the intense absorption band near  $3400\text{ cm}^{-1}$ ; the peak values of  $k(\bar{\nu})$  appear at lower frequencies than the peak values for  $\alpha(\bar{\nu})$ . The extremely broad band in the low-frequency region in figure 3 has its maximum at  $570\text{ cm}^{-1}$  and corresponds to the  $\nu_L$  band at  $680\text{ cm}^{-1}$  in figure 2; the narrower band has its maximum at  $170\text{ cm}^{-1}$  and corresponds to the  $\nu_T$  band near  $200\text{ cm}^{-1}$  in figure 2. The curve for  $k(\bar{\nu})$  in figure 3 connects smoothly at low frequencies with the  $k(\bar{\nu})$  plot given by Ray [9].

The real part  $n$  of the refractive index can be obtained from the Kramers-Kronig relation

$$n(\bar{\nu}) = 1 + (1/2\pi^2)P \int_0^{\infty} \frac{\alpha(\bar{\nu}') - \alpha(\bar{\nu})}{\bar{\nu}'^2 - \bar{\nu}^2} d\bar{\nu}' \quad (4.2)$$

provided  $\alpha(\bar{\nu})$  is known at all frequencies; since we have measured  $\alpha(\bar{\nu})$  only in the range  $4000$  to  $50\text{ cm}^{-1}$ , we cannot make direct use of equation (4.2). Fortunately, the nature of the integral in equation (4.2) is such that excellent approximate solutions can be obtained in the range  $4400\text{ cm}^{-1} > \bar{\nu} > 50\text{ cm}^{-1}$ , since there exists some knowledge of the variation of  $\alpha(\bar{\nu})$  outside this range. Bertie *et al.* [10] have shown that the values of  $n(\bar{\nu})$  for  $\bar{\nu}$  within the range of actual measurement are relatively insensitive to approximate values of  $\alpha(\bar{\nu})$  outside the range in the high-frequency region.

In making use of equation (4.2), for  $\bar{\nu} > 4400\text{ cm}^{-1}$  we used Palmer's measured values [11] of  $\alpha(\bar{\nu})$  in the range  $4400$  to  $8400\text{ cm}^{-1}$ ; we assumed that  $\alpha(\bar{\nu})$  decreases linearly with  $\bar{\nu}^{-1}$  from the measured value at  $8400\text{ cm}^{-1}$  to the value of  $1.5 \times 10^{-4}/\text{cm}$  at  $16\,960\text{ cm}^{-1}$  [12] and approaches zero at higher frequencies except for a hypothetical narrow, strong absorption band centred at  $40\,000\text{ cm}^{-1}$  introduced to take account of the effects of ultra-violet bands, which have not been measured with high precision [12]. This separate treatment of the ultra-violet bands can be justified by considering the contribution  $\Delta_{UV}n(\bar{\nu})$  of to  $n(\bar{\nu})$  at some frequency of interest in the infra-red; this can be expressed as

$$\Delta_{UV}n(\bar{\nu}) = \frac{1}{2\pi^2} P \int_0^{\infty} \frac{\alpha_{UV}(\bar{\nu}') d\bar{\nu}'}{(\bar{\nu}'^2 - \bar{\nu}^2)}. \quad (4.3)$$

For an ultra-violet absorption band centred at some high frequency  $\bar{\nu}_H$  and limited to a range  $\bar{\nu}_a$  to  $\bar{\nu}_b$ , the limits of the integral in (4.3) can be changed to  $\bar{\nu}_a$  and  $\bar{\nu}_b$ . For  $\bar{\nu} \ll \bar{\nu}_H$  and  $(\bar{\nu}_b - \bar{\nu}_a) \ll \bar{\nu}_H$ , we can, in second order approximation, write

$$\begin{aligned} \Delta_{UV}n(\bar{\nu}) &= \frac{1}{2\pi^2} \int_{\bar{\nu}_a}^{\bar{\nu}_b} \frac{\alpha_{UV}(\bar{\nu}') d\bar{\nu}'}{\bar{\nu}'^2} \left[ 1 - (\bar{\nu}/\bar{\nu}_H)^2 \right] \\ &= \text{constant} / [1 - (\bar{\nu}/\bar{\nu}_H)^2]. \end{aligned} \quad (4.4)$$

The constant in (4.4) was chosen to give  $n = 1.300$  at  $\bar{\nu} = 5000\text{ cm}^{-1}$ ; this value is based on direct reflection measurements [2, 5].

In using equation (4.2) we used  $\alpha(\bar{\nu})$  values given by Ray [9] for the region  $\bar{\nu} < 50\text{ cm}^{-1}$ ; Ray's values in this region are based largely on the work of Chamberlain *et al.* [13] together with microwave measurements.

On the basis of these values of  $\alpha(\bar{\nu})$  below and above the range of our measurements together with our measured values of  $\alpha(\bar{\nu})$ , we used a computer programme for the evaluation of  $n(\bar{\nu})$  from equation (4.2) for the region 4400 to 50  $\text{cm}^{-1}$ . The resulting values of  $n(\bar{\nu})$  are plotted in figure 4 and tabulated in the table for the low frequency region. On the basis of considerations similar to those given

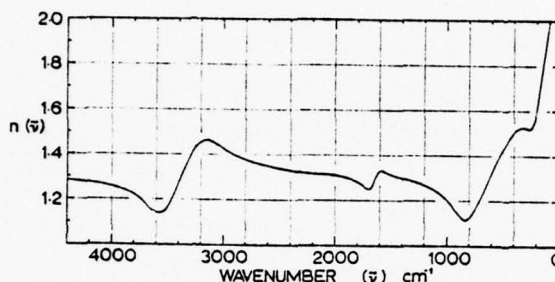


Figure 4. The real part  $n(\bar{\nu})$  of the refractive index of water in the infra-red.

by Bertie and Whalley [10] and those involved in Ahrenkiel's treatment [14] of subtractive Kramers-Kronig integrals, we believe that the errors in  $n(\bar{\nu})$  introduced by our methods of evaluating the integral in (4.2) amount to less than  $\pm 1$  per cent in the range 4400–200  $\text{cm}^{-1}$ ; in the range 200–50  $\text{cm}^{-1}$ , our values of  $n(\bar{\nu})$  are significantly influenced by the values of  $\alpha(\bar{\nu})$  in the range  $\bar{\nu} < 50 \text{ cm}^{-1}$  and by the grid size used in the computer programme employed for the numerical integration in equation (4.2); these may introduce an uncertainty of  $\pm 10$  per cent in  $n(\bar{\nu})$  at 50  $\text{cm}^{-1}$ . We estimate that uncertainties in our measured values of  $\alpha(\bar{\nu})$  lead to uncertainties of less than  $\pm 3$  per cent in values of  $n(\bar{\nu})$  listed in the table.

Since the values of  $k(\bar{\nu})$  have been previously tabulated [6] for  $\bar{\nu} > 800 \text{ cm}^{-1}$  and since our present values of  $n(\bar{\nu})$  for  $\bar{\nu} > 800 \text{ cm}^{-1}$  agree to within  $\pm 1$  per cent with previously tabulated values based on reflection measurements at two angles of incidence [5], we give values for  $k(\bar{\nu})$  and  $n(\bar{\nu})$  only in the region 800 to 50  $\text{cm}^{-1}$  in the table.

## 5. REFLECTION SPECTRUM

The optical constants  $n$  and  $k$  can be used in the Fresnel equations to compute the spectral reflectance  $R(\bar{\nu})$  of water for any angle of incidence. In the case of normal incidence, the expression for reflectance assumes the simple form

$$R = [(n-1)^2 + k^2] / [(n+1)^2 + k^2]. \quad (5.1)$$

A plot of normal-incidence spectral reflectance at a free water surface based on the values of the optical constants obtained in the present study is shown in figure 5. In the range 4400 to 400  $\text{cm}^{-1}$  the values of spectral reflectance shown in the figure are in close agreement with earlier [5] directly measured values; the computed values shown in the figure may be somewhat more

reliable than directly measured values in the vicinity of the  $R(\bar{\nu})$  minima at  $3640\text{ cm}^{-1}$  and  $910\text{ cm}^{-1}$  and in the vicinity of the  $\nu_2$  band of atmospheric water vapour near  $1626\text{ cm}^{-1}$ .

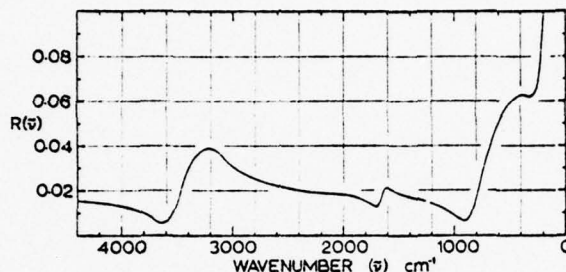


Figure 5. The normal-incidence reflectance spectrum of water in the infra-red.

The spectral reflectance curve shown in figure 5 is of considerable meteorological significance. As indicated in figure 2, any infra-red radiant flux penetrating a water surface is absorbed in the surface layers. As indicated in figure 5 nearly all normally incident flux penetrates the surface at  $3640$  and  $910\text{ cm}^{-1}$ ; thus at these frequencies and at normal incidence a water surface closely approximates that of a black body. For radiant flux emitted vertically upward, the spectral emissivity at  $910\text{ cm}^{-1}$  of a quiescent water surface is  $0.993$ ; measurement of upward-directed flux can thus be used to measure surface temperature. Since there is an 'atmospheric window' in the vicinity of  $910\text{ cm}^{-1}$ , satellite monitoring of sea temperatures is possible. Because reflectance increases with increasing angle of incidence to unity at  $90^\circ$ , the black-body approximation becomes poorer for a turbulent water surface.

## 6. DISCUSSION OF RESULTS

A comparison of the present results in the far infra-red with those obtained in earlier studies is given graphically in the expanded plots shown in figure 6, in which our present results are given by the continuous curves and the accompanying uncertainty bars.

The curves in Panel A are based directly on our transmission measurements. In the range  $800\text{--}300\text{ cm}^{-1}$  our values of  $k(\bar{\nu})$  agree within the indicated limits of uncertainty with the values of Pontier and Dechambenoy [2], which are based on measurements of absorption and of reflection at two angles of incidence, and with those of Rusk *et al.* [5], which are based on reflectance at two angles of incidence. Robertson's earlier values [6] based on absorption measurements agree with the present results over the range  $800\text{--}600\text{ cm}^{-1}$  but are lower than the present values for  $\bar{\nu} < 600\text{ cm}^{-1}$ ; the stated uncertainties in Robertson's results overlap those involved in the present study. The  $k(\bar{\nu})$  values given by Zolotarev *et al.* [3] represent results based on transmission, reflection, ATR



measurements, and, for the region  $\bar{\nu} < 400 \text{ cm}^{-1}$ , the results obtained by others [7, 13]; their values are outside our limits of uncertainty in certain spectral regions.

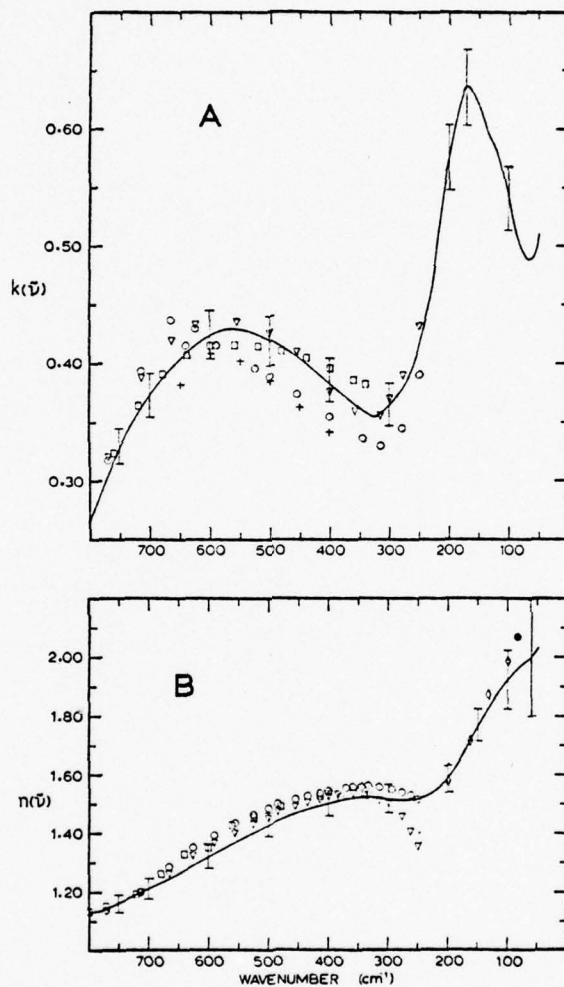


Figure 6. Optical constants of water in the far infra-red. Present results are given by the continuous curves; uncertainties in present results are indicated by error bars. Previous values as presented in the references are as follows: [2] by triangles, [3] by open circles and diamonds, [6] by '+'s, [5] by squares, and [13] by filled circles.

Our values of  $n(\bar{\nu})$  based on Kramers-Kronig analysis shown in Panel B of figure 6. The uncertainties in the range 800–200  $\text{cm}^{-1}$  are based chiefly on considerations of the uncertainties of  $\alpha(\bar{\nu})$  measurements; our computer programme for the numerical evaluation of  $n(\bar{\nu})$  in equation (3.2) employed a 10  $\text{cm}^{-1}$  grid and contributed to the progressively larger uncertainties in the region 200–50  $\text{cm}^{-1}$ , where  $\bar{\nu}$  becomes comparable with the programme grid. Present values of  $n(\bar{\nu})$  in the region 800–300  $\text{cm}^{-1}$  are somewhat lower than those based

on direct transmission and reflection measurements [2,5] and those reported by Zolotarev *et al.* [3]; the estimated uncertainties of various investigators overlap through this region. For  $\bar{\nu} < 300 \text{ cm}^{-1}$ , the values given in [2] fall below those obtained in the present study; there is general agreement in the 300–50  $\text{cm}^{-1}$  region between our results and earlier Kramers–Kronig values [3]. The value of  $n(\bar{\nu})$  given by Chamberlain *et al.* [13] for 85  $\text{cm}^{-1}$  is 5 per cent larger than our Kramers–Kronig value and thus is within our large limits of uncertainty, which are  $\pm 10$  per cent at this frequency.

The results summarized in figure 6 emphasize the desirability of further experimental work in the region  $\bar{\nu} < 300 \text{ cm}^{-1}$ . Although further quantitative studies of absorption would be desirable and would provide data for Kramers–Kronig computations employing a smaller computation grid, the major need is for quantitative measurements of reflection. We join Irvine and Pollack [1] in encouraging future investigators to give their results in tabular form, since the usual graphical representations alone do not provide values sufficiently accurate for use in calculations of optical constants. Although a thorough knowledge of  $k(\bar{\nu})$  and  $n(\bar{\nu})$  for  $\bar{\nu} < 200 \text{ cm}^{-1}$  is not of major importance to meteorology, it is of considerable importance to our understanding of the molecular properties of water.

The authors wish to express their thanks to Mr. Thomas Duell for assistance with the computer programme used in the Kramers–Kronig analysis.

## REFERENCES

- [1] IRVINE, W. H., and POLLACK, J. B., 1968, *Icarus*, **8**, 324.
- [2] PONTIER, L., and DECHAMBENOY, C., 1965, *Ann. Geophys.*, **21**, 462; 1966, *Ann. Geophys.*, **22**, 633.
- [3] ZOLATAREV, V. M., MIKHAILOV, B. A., APEROVICH, L. I., and POPOV, S. I., 1969, *Optika Spectrosk.*, **27**, 790. [Translation: *Optics Spectrosc.*, **27**, 430.]
- [4] QUERRY, M. R., CURNUTTE, B., and WILLIAMS, D., 1969, *J. opt. Soc. Am.*, **59**, 1299.
- [5] RUSK, A. N., WILLIAMS, D., and QUERRY, M. R., 1971, *J. opt. Soc. Am.*, **61**, 895.
- [6] ROBERTSON, C. W., and WILLIAMS, D., 1971, *J. opt. Soc. Am.*, **61**, 1316.
- [7] DRAECERT, D. A., STONE, N. W. B., CURNUTTE, B., and WILLIAMS, D., 1966, *J. opt. Soc. Am.*, **56**, 64.
- [8] COLLINS, J. R., 1937, *Phys. Rev.*, **52**, 88.
- [9] RAY, PETER, 1972, *Appl. Opt.*, **11**, 18.
- [10] BERTIE, J. E., LABBÉ, H. J., and WHALLEY, E., 1969, *J. chem. Phys.*, **50**, 4501.
- [11] PALMER, K. (private communication).
- [12] GOODY, R. M., 1964, *Atmospheric Radiation* (Clarendon Press), p. 415.
- [13] CHAMBERLAIN, J. E., CHANTRY, G. W., GEBBIE, H. A., STONE, N. W. B., TAYLOR, T. B., and WYLLIE, G., 1966, *Nature, Lond.*, **210**, 790.
- [14] AHRENKIEL, R. K., 1971, *J. opt. Soc. Am.*, **61**, 1651.

## Optical properties of water in the near infrared\*

Kent F. Palmer and Dudley Williams

Department of Physics, Kansas State University, Manhattan, Kansas 66506

(Received 20 March 1974)

The real  $n(\nu)$  and imaginary  $k(\nu)$  parts of the complex refractive index  $\tilde{N} = n + ik$  of water at 27°C have been determined from measurements of spectral reflectance at near-normal incidence and from measurements of the transmittance of water in carefully constructed absorption cells. Values of  $n(\nu)$  are reported in graphical and tabular form for the spectral region 3800–27 800  $\text{cm}^{-1}$ ; values of the Lambert absorption coefficient  $\alpha(\nu)$  are presented graphically and in tabular form, along with  $k(\nu)$  for the region 3800–14 500  $\text{cm}^{-1}$ . Upper limits of  $k(\nu)$  are established for the region 14 500–27 800  $\text{cm}^{-1}$ . The results are compared with earlier studies.

**Index Headings:** Refractive index; Absorption; Water; Reflectance; Infrared; Spectra.

Since the time of the Irvine–Pollack survey,<sup>1</sup> which emphasized the dearth of reliable values of the optical constants  $\tilde{N}(\nu) = n(\nu) + ik(\nu)$  for water, there have been numerous studies<sup>2–3</sup> of the spectrum of water in the frequency range below 4000  $\text{cm}^{-1}$ . In the present paper, we report new results for  $n(\nu)$  in the range 3800–27 800  $\text{cm}^{-1}$ ; these are based primarily on reflectance measurements. We also give values for the Lambert absorption coefficient  $\alpha(\nu)$  based on transmittance measurements and list the corresponding values of  $k(\nu) = \lambda\alpha(\nu)/4\pi$ .

In the course of our work, we employed a double-pass prism monochromator equipped with a type DF-2 glass prism calibrated in terms of atomic emission lines in the visible region and water-vapor bands in the near infrared. A Reeder thermocouple was employed as a detector. We used a carefully monitored tungsten iodide lamp as a source.

### REFLECTANCE MEASUREMENTS

The general procedures that we employed for the near-normal reflectance measurements were similar to those described in earlier reports<sup>5,6</sup>; we measured the ratio of the reflectance of water at 27°C to that of a reference mirror, the absolute reflectance of which was determined in an auxiliary experiment by use of a Strong reflectometer. Because water is relatively transparent in the visible and near infrared, we used water samples contained in a glass optical horn, the exterior of which was painted dull black in order to minimize spurious reflections from the walls of the container; the curved horn was constructed of 6-cm-o.d. Pyrex, had a tapered length of 16 cm, and ended in a point. We were unable to detect radiant flux reflected from the interior of the horn. As in the earlier work, we used a rapidly rotating sector disk when measuring radiant flux from the reference mirror; use of such a calibrated optical attenuator eliminates the necessity of undesirable changes of amplifier gain-control adjustments.

A plot of measured fractional spectral reflectance  $R(\nu)$  as a function of wave number is given in the curve

labeled  $R$  in Fig. 1; the curve has a slope that is small and nearly constant over most of the indicated spectral range. However, the spectral reflectance decreases rapidly in the region of 4000  $\text{cm}^{-1}$ , owing to the proximity of the strong fundamental water bands near 3400  $\text{cm}^{-1}$ . The reflectance curve shown in the figure is the smooth curve drawn through points representing many individual determinations; we believe that the fractional uncertainty  $\delta R/R$  is 0.02 over most of the range, where  $\delta R$  includes the standard deviation of the measurements of samples and reference mirror and the restrictions imposed by the calibration of the sector wheels.

### TRANSMITTANCE MEASUREMENTS

In order to obtain accurate values of the Lambert absorption coefficient  $\alpha(\nu)$ , it is necessary to have accurately measured values of the thickness  $x$  of the absorbing layers of water and to eliminate the effects of reflection and absorption by the windows of the absorption cell.<sup>7</sup> In the present study, in the 5500–14 500  $\text{cm}^{-1}$  region, we employed a set of precision absorption cells

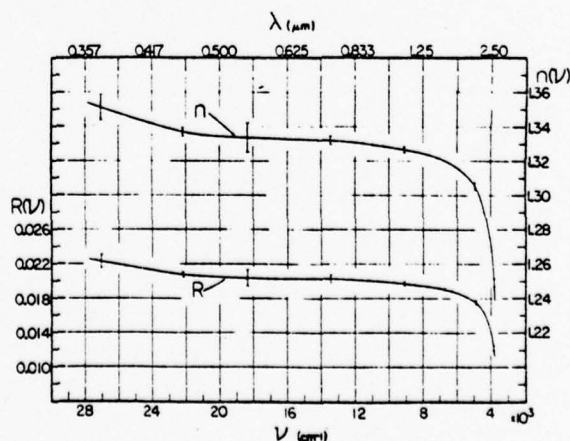


FIG. 1. Curve  $R$  gives fractional reflectance at near-normal incidence as a function of frequency in  $\text{cm}^{-1}$ . Curve  $n$  gives a plot of refractive index  $n(\nu)$  as a function of frequency.

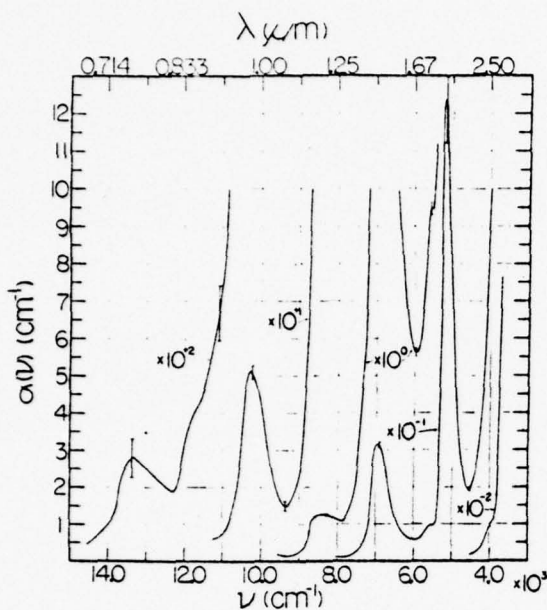


FIG. 2. Lambert absorption coefficient  $\alpha(\nu)$  as a function of frequency expressed in  $\text{cm}^{-1}$ .

of Infrasil quartz that provided path lengths of 1, 2, 5, 10, 20, 30, 40, and 50 mm; these cells, which were supplied by Markson Science, Inc., were fabricated from a single batch of fused silica in order to avoid differences of optical properties of the cell windows. In measuring the transmittance of water samples in these cells, we used a collimated beam of radiant flux.

The measured spectral transmittance  $T(\nu)$  of water in an absorption cell of length  $x$  is given by the expression

$$T(\nu) = [1 - R'(\nu)][1 - A'(\nu)]\exp[-\alpha(\nu)x], \quad (1)$$

where  $R'(\nu)$  is fraction of the incident radiant flux reflected from the inner and outer window surfaces of the filled cells and  $A'(\nu)$  is the fraction of the flux absorbed by the windows. By taking the ratios of the spectral transmittances of water-filled cells of different lengths, we eliminated the influence of  $R'(\nu)$  and  $A'(\nu)$  and obtained accurate values of the Lambert coefficient  $\alpha(\nu)$ .

In the range  $3800\text{--}5500\text{ cm}^{-1}$ , we used a Beckmann variable-path-length cell with fused-silica windows; the path length can be accurately and continuously adjusted in the range  $6\text{ mm}$  to  $30\text{ }\mu\text{m}$ .

The values of the Lambert absorption coefficient that we derived from our measurements are shown in Fig. 2. As indicated in the figure, the values of  $\alpha(\nu)$  at  $14000$  and  $4000\text{ cm}^{-1}$  differ by a factor of  $10^4$ ; uncertainty bars for various spectral regions are indicated in the figure. Values of  $\alpha(\nu)$  are listed in Table I. In arriving at each value of  $\alpha(\nu)$  given in the table we measured the transmittance of 6 to 12 absorbing layers

that had different thicknesses  $x$ . The fractional uncertainty  $\delta\alpha(\nu)/\alpha(\nu)$ , based on the standard deviation  $\delta A(\nu)$ , is fairly small in the range  $1000\text{--}5500\text{ cm}^{-1}$ ; at higher frequencies  $\alpha(\nu)$  becomes smaller and the measured absorbance  $A(\nu) = 1 - T(\nu)$  of the water for the absorption cells employed becomes too small to provide accurate values of  $\alpha(\nu)$ ; thus, the fractional uncertainty increases. At frequencies less than  $4000\text{ cm}^{-1}$ , the values of  $\alpha(\nu)$  are so great that even with the thinnest cell employed  $A(\nu)$  becomes too great for accurate determination of  $\alpha(\nu)$ ; for these low frequencies, the wedge-cell techniques described by Robertson<sup>7</sup> are to be preferred.

### OPTICAL CONSTANTS

Values of the imaginary part  $k(\nu)$  of the complex refractive index based on measured values of  $\alpha(\nu)$  are listed in Table I. A plot of  $k(\nu)$  vs  $\nu$  for the region covered in the present study joins smoothly with the curve based on Robertson's results<sup>7</sup> for lower frequency ranges.

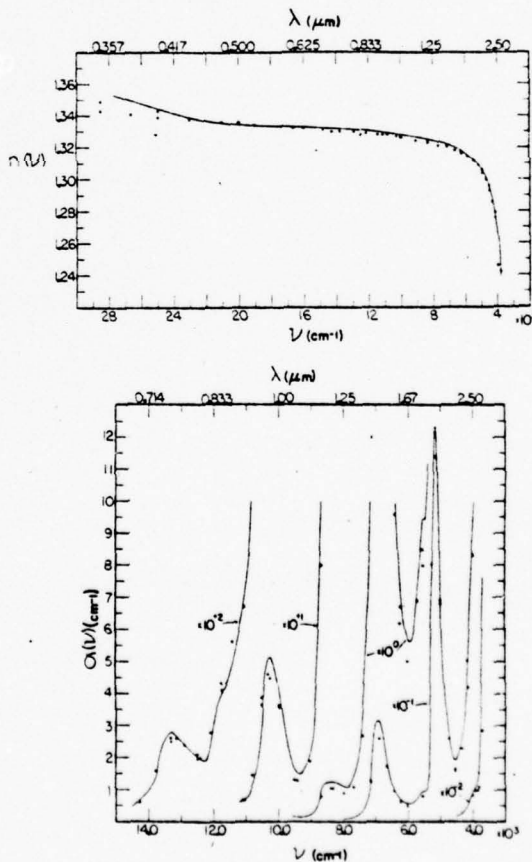


FIG. 3. The continuous curve in the upper panel gives values of  $n(\nu)$  obtained in the present study; the continuous curve in the lower panel gives values of  $\alpha(\nu)$  obtained in the present study. The crosses indicate values tabulated by Irvine and Pollack; the circles indicate values tabulated by Hale and Querry.

TABLE I. Optical constants of liquid water from the near infrared to the ultraviolet.

$\nu$ in $\text{cm}^{-1}$	$\alpha(\nu)$ in $\text{cm}^{-1}$	$k(\nu)$	$n(\nu)$	$\lambda$ in $\mu\text{m}$	$\nu$ in $\text{cm}^{-1}$	$\alpha(\nu)$ in $\text{cm}^{-1}$	$k(\nu)$	$n(\nu)$	$\lambda$ in $\mu\text{m}$
3 800	$1.93 \times 10^2$	$4.04 \times 10^{-3}$	1.239	2.632	8 600	1.18	1.09	1.326	1.163
3 900	1.11	2.26	1.257	2.564	8 700	$9.70 \times 10^{-1}$	$8.87 \times 10^{-4}$	1.326	1.149
4 000	$9.57 \times 10^1$	1.90	1.268	2.500	8 800	5.48	4.96	1.326	1.136
4 100	6.35	1.23	1.276	2.439	8 900	3.23	2.89	1.327	1.124
4 200	4.18	$7.92 \times 10^{-4}$	1.281	2.381	9 000	2.32	2.05	1.327	1.111
4 300	2.93	5.42	1.285	2.326	9 100	1.92	1.68	1.327	1.099
4 400	2.30	4.16	1.291	2.273	9 200	1.66	1.44	1.327	1.087
4 550	1.93	3.38	1.296	2.198	9 350	1.48	1.26	1.328	1.070
4 700	2.36	4.00	1.301	2.128	9 500	1.64	1.37	1.328	1.053
4 800	3.10	5.14	1.303	2.083	9 600	1.90	1.57	1.328	1.042
4 900	4.50	7.31	1.305	2.041	9 700	2.31	1.90	1.328	1.031
5 000	6.92	$1.10 \times 10^{-3}$	1.306	2.000	9 800	2.85	2.31	1.328	1.020
5 100	$1.09 \times 10^2$	1.70	1.307	1.961	9 900	3.51	2.82	1.328	1.010
5 190	1.24	1.90	1.309	1.927	10 000	4.16	3.31	1.328	1.000
5 300	$5.75 \times 10^1$	$8.63 \times 10^{-4}$	1.310	1.887	10 100	4.69	3.70	1.328	0.990
5 400	1.08	1.59	1.311	1.852	10 200	5.02	3.92	1.328	0.980
5 500	$9.44 \times 10^0$	1.37	1.312	1.818	10 280	5.14	3.98	1.328	0.973
5 550	9.48	1.36	1.312	1.802	10 400	4.71	3.60	1.328	0.962
5 600	9.18	1.30	1.313	1.786	10 500	3.22	2.44	1.328	0.952
5 700	7.60	1.06	1.314	1.754	10 600	2.14	1.61	1.329	0.943
5 800	6.23	$8.55 \times 10^{-5}$	1.314	1.724	10 700	1.58	1.18	1.329	0.935
5 900	5.65	7.62	1.315	1.695	10 800	1.19	$8.77 \times 10^{-7}$	1.329	0.926
6 000	5.65	7.49	1.316	1.667	11 000	$7.50 \times 10^{-2}$	5.43	1.329	0.909
6 100	6.07	7.92	1.317	1.639	11 200	6.09	4.33	1.329	0.893
6 200	6.80	8.73	1.318	1.613	11 400	5.06	3.53	1.330	0.877
6 300	8.07	$1.02 \times 10^{-4}$	1.318	1.587	11 600	4.28	2.94	1.330	0.862
6 400	9.68	1.20	1.319	1.563	11 800	3.87	2.61	1.330	0.847
6 500	$1.21 \times 10^1$	1.48	1.319	1.538	12 000	3.08	2.04	1.330	0.833
6 600	1.56	1.88	1.320	1.515	12 200	1.99	1.30	1.330	0.820
6 700	2.17	2.58	1.320	1.493	12 300	1.91	1.24	1.331	0.813
6 800	2.85	3.34	1.321	1.471	12 400	1.95	1.25	1.331	0.806
6 930	3.17	3.64	1.321	1.443	12 600	2.10	1.33	1.331	0.794
7 000	3.10	3.52	1.321	1.429	12 800	2.30	1.43	1.331	0.781
7 100	2.15	2.41	1.322	1.408	13 000	2.51	1.54	1.331	0.769
7 200	$9.13 \times 10^0$	1.01	1.322	1.389	13 200	2.72	1.64	1.332	0.758
7 300	5.45	$5.94 \times 10^{-5}$	1.323	1.370	13 300	2.81	1.68	1.332	0.752
7 400	3.87	4.16	1.323	1.351	13 400	2.75	1.63	1.332	0.746
7 500	2.25	2.39	1.323	1.333	13 600	2.38	1.39	1.332	0.735
7 600	1.67	1.75	1.324	1.316	13 800	1.34	$7.73 \times 10^{-5}$	1.332	0.725
7 700	1.34	1.38	1.324	1.299	14 000	$9.8 \times 10^{-3}$	5.6	1.332	0.714
7 800	1.13	1.15	1.324	1.282	14 250	6.9	3.8	1.332	0.702
7 900	1.07	1.08	1.324	1.266	14 500	4.9	2.7	1.332	0.690
8 000	1.11	1.10	1.325	1.250	18 000			1.333	0.556
8 100	1.17	1.15	1.325	1.235	22 250			1.337	0.449
8 200	1.22	1.18	1.325	1.220	24 500			1.344	0.408
8 300	1.25	1.20	1.325	1.205	27 800			1.353	0.360
8 400	1.25	1.18	1.325	1.190					
8 500	1.23	1.15	1.326	1.176					

Values of the real part  $n(\nu)$  of the complex refractive index can be obtained by use of the Fresnel expression for normal-incidence spectral reflectance

$$R = [(n-1)^2 + k^2] / [(n+1)^2 + k^2]. \quad (2)$$

Over much of the spectral region covered in the present work,  $k(\nu)$  is so small that it can be neglected; in this case,  $n(\nu)$  can be obtained in excellent approximation from

$$n = (1+R)/(1-R). \quad (3)$$

We plot  $n(\nu)$  vs  $\nu$  in curve  $n$  in Fig. 1 and list values of  $n(\nu)$  in Table I. The fractional uncertainty  $\delta n(\nu)/n(\nu)$  is approximately  $\pm 0.01$  over most of the spectral region covered.

## DISCUSSION OF RESULTS

The present study covers a region intermediate between the region of extremely high absorption in the infrared and the region of great transparency in the visible and near ultraviolet. A portion of this region was covered in the Irvine-Pollack survey<sup>1</sup>; our results are in much closer agreement with the Irvine-Pollack values in this region than were our earlier results in the intermediate and far-infrared regions.<sup>4-5</sup>

Recently Hale and Querry<sup>9</sup> have made a critical survey of the existing literature dealing with the optical properties of water and have attempted to select a set of best values. In the region of present interest, these authors base their values on the work of

Kondratyev,<sup>10</sup> Curcio and Petty,<sup>11</sup> and Zolotarev *et al.*<sup>7</sup> In Fig. 3, we compare our values of  $n$  and  $\alpha$ , as given by the continuous curves, with the results of the Irvine-Pollack survey given by crosses and the Hale-Querry survey given by circles. In general, there is fair agreement; some of the disagreements can possibly be attributed to slight differences of frequency calibration of the dispersing instruments, rather than to real differences of  $n$  and  $k$  values.

Although the values of the optical constants that we list in Table I are sufficiently accurate for use in Mie-theory calculations of scattering, more-precise values of  $n(\nu)$  in much of the range covered can be obtained from measurements of the angular deviation of beams passing through a hollow prism filled with water. The values of  $k(\nu)$  progressively decrease with increasing frequency in the visible region and attain a value of approximately  $10^{-9}$  in the 20 000–22 000  $\text{cm}^{-1}$  range. Extremely long absorption path lengths must be employed, and extreme care must be taken to avoid spurious effects associated

with scattering, if improved values of  $k(\nu)$  are to be obtained in the frequency range above 15 000  $\text{cm}^{-1}$ .

#### REFERENCES

- \* Supported in part by the Office of Naval Research.
- <sup>1</sup>W. M. Irvine and J. B. Pollack, *Icarus* **8**, 324 (1968).
- <sup>2</sup>L. Pontier and C. Dechambenois, *Ann. Geophys.* **21**, 462 (1965); *Ann. Geophys.* **22**, 633 (1966).
- <sup>3</sup>V. M. Zolotarev, B. A. Mikhailov, L. I. Aporovich, and S. I. Popov, *Opt. Spectrosk.* **27**, 790 (1969) [*Opt. Spectrosc.* **27**, 430 (1969)].
- <sup>4</sup>M. R. Querry, B. Curnutte, and D. Williams, *J. Opt. Soc. Am.* **59**, 1299 (1969).
- <sup>5</sup>A. N. Rusk, D. Williams, and M. R. Querry, *J. Opt. Soc. Am.* **61**, 895 (1971).
- <sup>6</sup>G. M. Hale, M. R. Querry, A. N. Rusk, and D. Williams, *J. Opt. Soc. Am.* **62**, 1103 (1972).
- <sup>7</sup>C. W. Robertson and D. Williams, *J. Opt. Soc. Am.* **61**, 1316 (1971).
- <sup>8</sup>C. W. Robertson, B. Curnutte, and D. Williams, *Mol. Phys.* **26**, 183 (1973).
- <sup>9</sup>G. M. Hale and M. R. Querry, *Appl. Opt.* **12**, 555 (1973).
- <sup>10</sup>K. Kondratyev, *Radiation in the Atmosphere* (Academic, New York, 1969), pp. 107–123.
- <sup>11</sup>J. A. Curcio and C. C. Petty, *J. Opt. Soc. Am.* **41**, 302 (1951).

After the experimental work done by Rusk, by Robertson, and by Palmer reported in the preceding papers, we had a wealth of quantitative knowledge of the reflection spectrum in the range  $15,000\text{ cm}^{-1}$  to  $300\text{ cm}^{-1}$  and the absorption spectrum of water from the visible region to a frequency of  $50\text{ cm}^{-1}$  in the far infrared. Over most of this range the optical constants  $n(\nu)$  and  $k(\nu)$  could be determined directly from experimental measurements. Throughout this region values of  $n(\nu)$  could also be determined by Kramers-Kronig analysis of absorption measurements; both  $n(\nu)$  and  $k(\nu)$  could be determined by Kramers-Kronig phase-shift analysis of reflection measurements. Dr. Harry D. Downing made a critical survey of the amassed data and the consistency of  $n(\nu)$  and  $k(\nu)$  as determined by various methods. The results of this survey are included in the following paper by Downing and Williams, which constitutes our definitive work on the spectrum of water at  $27^\circ\text{C}$ .

Note: Some of the data in the paper for frequencies below  $100\text{ cm}^{-1}$  are based on British work at the National Physical Laboratory in Teddington. Newer data from that source are somewhat different; thus, the tabulated values of  $n(\nu)$  and  $k(\nu)$  for very low frequencies are somewhat in question.

# Optical Constants of Water in the Infrared

HARRY D. DOWNING AND DUDLEY WILLIAMS

*Department of Physics, Kansas State University, Manhattan, Kansas 66506*

The results of our earlier studies of reflection and absorption in various spectral regions are reviewed and then used to provide values of the complex index of refraction  $\tilde{N} = n + ik$  of water at 27°C in the spectral range 5000–10 cm<sup>-1</sup>, corresponding to wavelengths in the range 2 μm to 1 mm. Values of  $n$ ,  $k$ , and the Lambert absorption coefficient  $\alpha$ , which are presented graphically and in tabular form, should prove useful in studies of the scattering of infrared radiation by water droplets in the atmosphere and in studies of radiative heat balance at water surfaces.

Although the infrared spectrum of water had been the subject of numerous investigations, *Irvine and Pollack* [1968] made a critical survey of published results that revealed many inconsistencies and a general paucity of quantitative data on which to base values of the real and imaginary parts of the complex index of refraction  $\tilde{N} = n + ik$ . In view of the importance of  $n$  and  $k$  in calculations of the transmission, scattering, and absorption of electromagnetic radiation by water droplets in the earth's atmosphere, our laboratory group has devoted considerable attention to the quantitative determination of the optical properties of water in the infrared. We have based our earlier listings of the optical constants  $n$  and  $k$  on quantitative measurements of various types in various spectral regions. The purpose of the present paper is to give a critical review of our earlier studies with the purpose of providing a set of 'best values' for use in atmospheric studies.

In our initial study, covering the 5000- to 400-cm<sup>-1</sup> region, *Querry et al.* [1969] attempted to measure the reflectance of polarized radiation at two large angles of incidence and to determine  $n$  and  $k$  by solution of the generalized Fresnel equations. In the range 5000–330 cm<sup>-1</sup>, *Rusk et al.* [1971] employed reflectance measurements at near-normal incidence and at an angle of 53° near Brewster's angle. Although there was fair agreement in the values of  $n$  and  $k$  obtained in these two studies, serious uncertainties were introduced as a result of the imperfect polarizers employed at nonnormal incidence in the first study and the failure to achieve Brewster's angle in the vicinity of absorption bands in the second study.

In view of these uncertainties, *Hale et al.* [1972] applied a Kramers-Kronig (KK) phase shift analysis to obtain values of the optical constants from *Rusk's* measurements of reflectance at near-normal incidence. The values of  $n$  based on the KK analysis represented an improvement on the earlier values; the KK analysis gave good values of  $k$  in the vicinity of strong absorption maximums but was unreliable in spectral regions where  $k$  is small. In general, reflectance measurements can give reliable values for  $n$  and also for large  $k$ ; they thus complement careful absorption measurements, which can provide reliable values for small  $k$  but somewhat questionable values for large  $k$ .

Our next study by *Robertson and Williams* [1971] was the quantitative measurement of the Lambert absorption coefficient  $\alpha$  defined by  $I = I_0 \exp[-\alpha x]$ ; in this work we used a wedge-shaped absorption cell designed by *Robertson*, and we covered the spectral range 4300–300 cm<sup>-1</sup>. The values of  $k = \lambda\alpha/4\pi$  based on absorption measurements were more precise than those based on reflectance in spectral regions of

small  $k$  and agreed, within the stated limits of uncertainty, in the centers of absorption bands where  $k$  is large; in the spectral range  $\nu < 600$  cm<sup>-1</sup> the uncertainties in  $k$  became larger because of limitations imposed by the spectrometers employed. The values of  $k$  were measured in this low-frequency region by *Robertson et al.* [1973], who used a far infrared grating instrument to determine  $\alpha$  in the spectral range between 800 and 50 cm<sup>-1</sup>; these authors also obtained values of  $n$  by means of a KK analysis of measured values of  $\alpha$ .

In the spectroscopy of the remote infrared, interferometers used with Fourier transform techniques have marked advantages over conventional grating instruments. Using interferometric methods, *John Chamberlain* and his associates at the National Physical Laboratory (NPL) have obtained values of  $n$  and  $k$  in the range 100–20 cm<sup>-1</sup>; in the course of this work, *Davies et al.* [1970] employed absorption techniques, and *Zafar et al.* [1973] employed reflection techniques. Existing water data in the microwave and radiofrequency regions have been summarized by *Ray* [1972].

## PRESENT STUDY

In preparing the present summary of our work on water we have based our values of the optical constants primarily on (1) *Robertson's* absorption measurements and (2) *Rusk's* measurements of spectral reflectance at near-normal incidence. In extensions of these primary data to the near-infrared and visible we have made use of the recent work of *Palmer and Williams* [1974]; in the extreme infrared we have used the NPL results in the 100- to 20-cm<sup>-1</sup> region and results taken from *Ray's* survey in the frequency range below 20 cm<sup>-1</sup>. In spectral regions where accurate values of absorption coefficients and reflectances have been determined independently we have obtained values of  $n$  and  $k$  from Fresnel's equation; in other regions we have employed KK methods.

The refractive index  $n$  can be determined from the KK relation

$$n(\nu) = 1 + (1/2\pi^2)P \int_0^\infty \frac{\alpha(\nu') - \alpha(\nu)}{\nu'^2 - \nu^2} d\nu' \quad (1)$$

where  $\alpha$  represents the Lambert absorption coefficient, for which we have values in the range between the radiofrequency region and 14,500 cm<sup>-1</sup> in the visible. In order to obtain values of  $n$  in the infrared from (1) it is sufficient to take account of ultraviolet contributions by assuming a single far ultraviolet band which will give the proper value of  $n$  at some frequency for which it is accurately known from independent measurements; we chose characteristics for the hypothetical ultraviolet band that would yield a value  $n = 1.306$  at 5000 cm<sup>-1</sup> in agreement with all our own earlier measurements.



On the basis of  $n$  evaluated from (1) and of direct experimental values of  $k = \lambda\alpha/4\pi$  we calculated the values of the normal incidence reflectance  $R$  in the range 800–120  $\text{cm}^{-1}$ ; these calculated values of  $R$  served to check Rusk's values in the 800- to 350- $\text{cm}^{-1}$  range and to provide values of  $R$  in the 350- to 120- $\text{cm}^{-1}$  range, where no reflectance measurements have been made. In the 120- to 90- $\text{cm}^{-1}$  range we joined our calculated values to a reflectance curve for the 90- to 10- $\text{cm}^{-1}$  range calculated from the NPL optical constants and those listed by Ray. On the basis of measured and calculated values of reflectance over the whole range from the near ultraviolet to the radiofrequency range, we then employed the KK phase shift theorem

$$\phi(\nu) = (2\nu/\pi)P \int_0^{\infty} \frac{\ln [R(\nu')]^{1/2}}{\nu^2 - \nu'^2} d\nu' \quad (2)$$

where  $[R(\nu)]^{1/2}$  is the modulus of the complex reflectivity  $\hat{R} = [R(\nu)]^{1/2} \exp[i\phi(\nu)]$ . In terms of  $\phi$  and  $R$  the values of  $n$  and  $k$  at any frequency are given by the relations

$$n = (1 - R)/(1 + R - 2R^{1/2} \cos \phi) \quad (3)$$

$$k = (-2R^{1/2} \sin \phi)/(1 + R - 2R^{1/2} \cos \phi) \quad (4)$$

We have used (2) along with (3) and (4) to provide  $n$  and  $k$  over the entire frequency range of present interest.

In the computer programs used for the solution of (1) and (2) we have employed methods based on Simpson's rule with a basic increment of 10  $\text{cm}^{-1}$  except in the vicinity of the singularity at  $\nu$ , where analytic solutions involving quadratic approximations of  $\alpha(\nu)$  and  $\ln [R(\nu)]^{1/2}$  were used. The 10- $\text{cm}^{-1}$  mesh is satisfactory over most of the range of present interest but becomes coarse at the lowest frequencies.

#### OPTICAL CONSTANTS

In Figure 1 we give our final values of the absorption index  $k$  as a function of frequency in waves per centimeter and wavelength in micrometers. The values represent the weighted average of  $k$  based on direct measurements of  $\alpha$  and on KK analyses; greater weight is given to the values based on direct measurement. The error bars shown in the figure represent the maximum differences between measured values and values based on (1), (2), and (4); the error bars thus give a measure of the in-

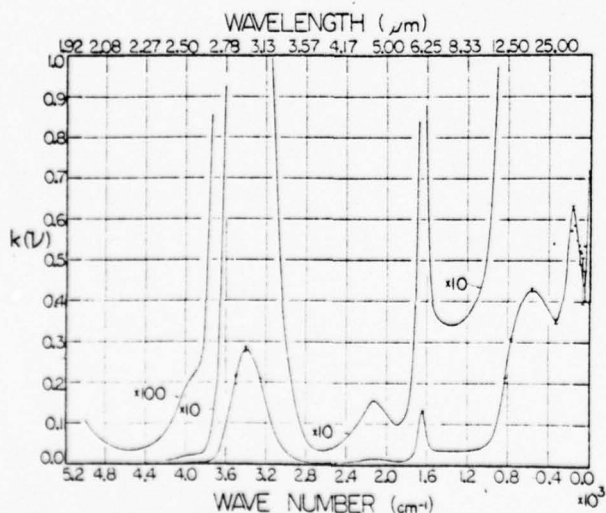


Fig. 1. Absorption index  $k$  as a function of wave number and wavelength.

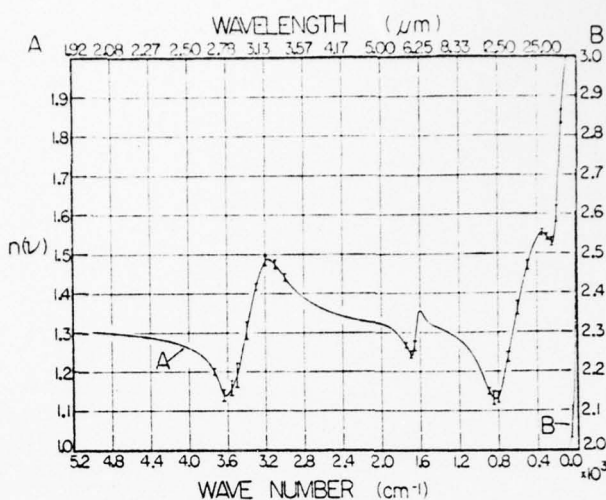


Fig. 2. Refractive index  $n$  as a function of wave number and wavelength.

ternal consistency of our work. In general, the actual uncertainties, which have been estimated in our earlier papers, are comparable with those given by the error bars except in the vicinity of the strong absorption band near 3400  $\text{cm}^{-1}$ , for which *Robertson and Williams* [1971] list an uncertainty of  $\pm 4\%$  in  $k$ ; thus since transmission measurements tend to give an underestimate of  $k$  at the centers of strong absorption bands, our results indicate that  $k$  may be as large as 0.294 at 3390  $\text{cm}^{-1}$ .

Our final values of the refractive index  $n$  are plotted as a function of wave number and wavelength in Figure 2. The curve shown represents a weighted average of direct determinations in regions where  $\alpha$  and  $R$  have been determined directly by experiment, of KK determinations from (1), and of KK determinations from (2) and (3); greater weight has been accorded to direct determinations. It should be noted that our values of  $n$  in the range 350–120  $\text{cm}^{-1}$  are based entirely on

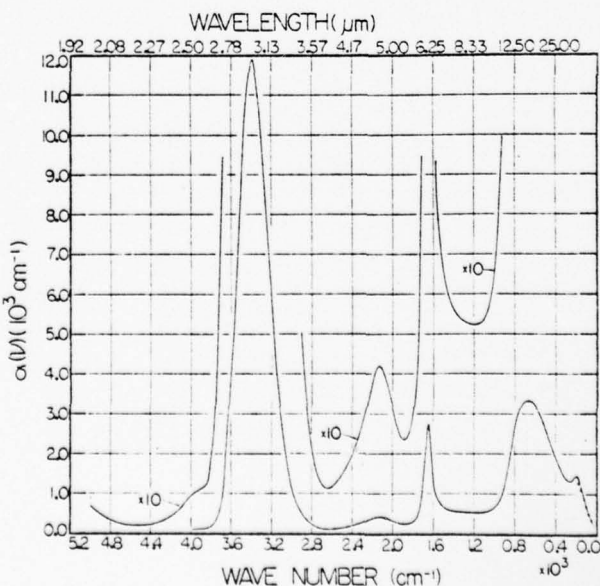


Fig. 3. Lambert absorption coefficient  $\alpha$  as a function of wave number and wavelength. Values shown are based on direct measurement of absorption.

KK analyses, since we have made no reflection measurements in this range. The error bars on the curve in the figure are a measure of the self-consistency of our work and at a given frequency represent the maximum differences between  $n$  as determined by various techniques; the large uncertainties in spectral regions where  $n$  is changing rapidly are probably due in part to spectrometer calibration problems and in part to the size of the increments employed in the KK analysis.

TABLE 1. Optical Constants of Water in the Infrared

$\nu$	$n(\nu)$	$k(\nu)$	$\alpha(\nu)$	$\lambda$
5000	1.303	0.00110	69.2	2.000
4950	1.301	0.000900	56.0	2.020
4900	1.301	0.000731	45.0	2.041
4850	1.300	0.000617	37.6	2.062
4800	1.298	0.000514	31.0	2.083
4750	1.298	0.000452	27.0	2.105
4700	1.296	0.000400	23.6	2.128
4650	1.295	0.000359	21.0	2.151
4600	1.294	0.000341	19.7	2.174
4550	1.293	0.000338	19.3	2.198
4500	1.291	0.000345	19.5	2.222
4450	1.289	0.000376	21.0	2.247
4400	1.287	0.000416	23.0	2.273
4350	1.285	0.000465	25.4	2.299
4300	1.282	0.000542	29.3	2.326
4250	1.280	0.000652	34.8	2.353
4200	1.277	0.000792	41.8	2.381
4150	1.274	0.000968	50.5	2.410
4100	1.270	0.00123	63.5	2.439
4050	1.265	0.00156	79.5	2.469
4000	1.261	0.00190	95.7	2.500
3990	1.260	0.00195	97.5	2.506
3980	1.259	0.00200	100.0	2.513
3970	1.257	0.00205	102.0	2.519
3960	1.256	0.00207	103.0	2.525
3950	1.255	0.00210	104.0	2.532
3940	1.254	0.00212	105.0	2.538
3930	1.252	0.00215	106.0	2.545
3920	1.250	0.00219	108.0	2.551
3910	1.249	0.00224	110.0	2.558
3900	1.247	0.00227	111.0	2.564
3890	1.246	0.00231	113.0	2.571
3880	1.243	0.00234	114.0	2.577
3870	1.241	0.00239	116.0	2.584
3860	1.240	0.00243	118.0	2.591
3850	1.238	0.00248	120.0	2.597
3840	1.235	0.00257	124.0	2.604
3830	1.232	0.00270	130.0	2.611
3820	1.230	0.00298	143.0	2.618
3810	1.227	0.00330	158.0	2.625
3800	1.224	0.00402	192.0	2.632
3790	1.221	0.00437	208.0	2.639
3780	1.218	0.00482	229.0	2.646
3770	1.214	0.00536	254.0	2.653
3760	1.210	0.00627	296.0	2.660
3750	1.205	0.00732	345.0	2.667
3740	1.200	0.00855	402.0	2.674
3730	1.195	0.0105	490.0	2.681
3720	1.191	0.0127	593.0	2.688
3710	1.185	0.0145	677.0	2.695
3700	1.179	0.0164	762.0	2.703
3690	1.172	0.0186	862.0	2.710
3680	1.166	0.0205	946.0	2.717
3670	1.157	0.0282	1300.0	2.725
3660	1.149	0.0380	1930.0	2.732
3650	1.144	0.0462	2270.0	2.740
3640	1.139	0.0548	2600.0	2.747
3630	1.138	0.0649	2970.0	2.755
3620	1.138	0.0744	3340.0	2.762
3610	1.139	0.0836	3720.0	2.770

TABLE 1. (continued)

$\nu$	$n(\nu)$	$k(\nu)$	$\alpha(\nu)$	$\lambda$
3600	1.141	0.0927	4070.0	2.778
3590	1.144	0.102	4420.0	2.786
3580	1.149	0.112	4750.0	2.793
3570	1.154	0.121	5110.0	2.801
3560	1.158	0.131	5530.0	2.809
3550	1.161	0.142	6020.0	2.817
3540	1.165	0.154	6510.0	2.825
3530	1.171	0.167	7070.0	2.833
3520	1.177	0.180	7670.0	2.841
3510	1.183	0.194	8230.0	2.849
3500	1.191	0.206	8750.0	2.857
3490	1.199	0.218	9270.0	2.865
3480	1.212	0.229	9660.0	2.874
3470	1.220	0.239	10120.0	2.882
3460	1.233	0.249	10500.0	2.890
3450	1.246	0.258	10850.0	2.899
3440	1.258	0.265	11150.0	2.907
3430	1.271	0.271	11370.0	2.915
3420	1.282	0.276	11600.0	2.924
3410	1.293	0.280	11780.0	2.933
3400	1.305	0.281	11850.0	2.941
3390	1.317	0.282	11900.0	2.950
3380	1.329	0.282	11870.0	2.959
3370	1.342	0.279	11720.0	2.967
3360	1.353	0.276	11600.0	2.976
3350	1.364	0.272	11400.0	2.985
3340	1.376	0.267	11150.0	2.994
3330	1.386	0.262	10920.0	3.003
3320	1.398	0.255	10570.0	3.012
3310	1.407	0.250	10300.0	3.021
3300	1.417	0.243	10000.0	3.030
3290	1.426	0.236	9670.0	3.040
3280	1.434	0.228	9300.0	3.049
3270	1.442	0.220	8950.0	3.058
3260	1.450	0.212	8570.0	3.067
3250	1.457	0.204	8270.0	3.077
3240	1.465	0.195	7820.0	3.086
3230	1.471	0.183	7320.0	3.096
3220	1.476	0.173	6830.0	3.106
3210	1.480	0.163	6400.0	3.115
3200	1.483	0.153	6010.0	3.125
3190	1.486	0.144	5610.0	3.135
3180	1.487	0.134	5210.0	3.145
3170	1.487	0.125	4840.0	3.155
3160	1.487	0.117	4550.0	3.165
3150	1.486	0.110	4320.0	3.175
3140	1.485	0.0994	3890.0	3.185
3130	1.482	0.0920	3620.0	3.195
3120	1.479	0.0855	3390.0	3.205
3110	1.477	0.0785	3120.0	3.215
3100	1.474	0.0716	2840.0	3.226
3090	1.472	0.0653	2590.0	3.236
3080	1.467	0.0600	2390.0	3.247
3070	1.464	0.0550	2190.0	3.257
3060	1.461	0.0504	2010.0	3.268
3050	1.457	0.0462	1840.0	3.279
3040	1.454	0.0422	1680.0	3.289
3030	1.451	0.0385	1530.0	3.300
3020	1.448	0.0348	1390.0	3.311
3010	1.444	0.0315	1260.0	3.322
3000	1.441	0.0297	1120.0	3.333
2990	1.437	0.0279	1050.0	3.344
2980	1.434	0.0262	980.0	3.356
2970	1.431	0.0250	933.0	3.367
2960	1.427	0.0229	850.0	3.378
2950	1.425	0.0210	780.0	3.390
2940	1.421	0.0193	713.0	3.401
2930	1.418	0.0177	650.0	3.413
2920	1.415	0.0163	599.0	3.425
2910	1.413	0.0151	551.0	3.436
2900	1.410	0.0138	503.0	3.448
2890	1.407	0.0128	466.0	3.460

TABLE 1. (continued)

$\nu$	$n(\nu)$	$k(\nu)$	$\alpha(\nu)$	$\lambda$
2880	1.405	0.0118	428.0	3.472
2870	1.403	0.0110	398.0	3.484
2860	1.400	0.0101	363.0	3.497
2850	1.398	0.00941	337.0	3.509
2840	1.396	0.00866	309.0	3.521
2830	1.394	0.00807	287.0	3.534
2820	1.392	0.00737	261.0	3.546
2810	1.390	0.00683	241.0	3.559
2800	1.388	0.00625	220.0	3.571
2790	1.387	0.00579	203.0	3.584
2780	1.385	0.00538	188.0	3.597
2770	1.383	0.00506	176.0	3.610
2760	1.382	0.00473	164.0	3.623
2750	1.379	0.00449	155.0	3.636
2740	1.378	0.00424	146.0	3.650
2730	1.377	0.00405	139.0	3.663
2720	1.375	0.00389	133.0	3.676
2710	1.374	0.00376	128.0	3.690
2700	1.372	0.00365	123.0	3.704
2690	1.371	0.00355	120.0	3.717
2680	1.370	0.00347	117.0	3.731
2670	1.369	0.00340	114.0	3.745
2660	1.367	0.00335	112.0	3.759
2650	1.366	0.00336	112.0	3.774
2640	1.365	0.00335	111.0	3.788
2630	1.363	0.00339	112.0	3.802
2620	1.361	0.00340	112.0	3.817
2610	1.361	0.00348	114.0	3.831
2600	1.360	0.00352	115.0	3.846
2590	1.358	0.00365	118.0	3.861
2580	1.358	0.00370	120.0	3.876
2570	1.357	0.00378	122.0	3.891
2560	1.355	0.00389	125.0	3.906
2550	1.354	0.00399	128.0	3.922
2540	1.353	0.00410	131.0	3.937
2530	1.352	0.00422	134.0	3.953
2520	1.351	0.00433	137.0	3.968
2510	1.350	0.00450	142.0	3.984
2500	1.349	0.00465	146.0	4.000
2490	1.348	0.00479	150.0	4.016
2480	1.348	0.00494	154.0	4.032
2470	1.347	0.00512	159.0	4.049
2460	1.346	0.00531	164.0	4.065
2450	1.345	0.00549	169.0	4.082
2440	1.344	0.00568	174.0	4.098
2430	1.344	0.00586	179.0	4.115
2420	1.343	0.00608	185.0	4.132
2410	1.342	0.00631	191.0	4.149
2400	1.341	0.00653	197.0	4.167
2390	1.340	0.00673	202.0	4.184
2380	1.340	0.00696	208.0	4.202
2370	1.338	0.00722	215.0	4.219
2360	1.337	0.00749	222.0	4.237
2350	1.337	0.00779	230.0	4.255
2340	1.335	0.00806	237.0	4.274
2330	1.334	0.00833	244.0	4.292
2320	1.334	0.00864	252.0	4.310
2310	1.333	0.00896	260.0	4.329
2300	1.332	0.00927	268.0	4.348
2290	1.332	0.00966	278.0	4.367
2280	1.331	0.0100	287.0	4.386
2270	1.330	0.0104	297.0	4.405
2260	1.330	0.0108	308.0	4.425
2250	1.330	0.0112	318.0	4.444
2240	1.329	0.0117	330.0	4.464
2230	1.329	0.0122	342.0	4.484
2220	1.329	0.0126	352.0	4.505
2210	1.328	0.0131	364.0	4.525
2200	1.328	0.0136	376.0	4.545
2190	1.327	0.0140	386.0	4.566

TABLE 1. (continued)

$\nu$	$n(\nu)$	$k(\nu)$	$\alpha(\nu)$	$\lambda$
2180	1.327	0.0145	396.0	4.587
2170	1.327	0.0149	406.0	4.608
2160	1.327	0.0152	412.0	4.630
2150	1.327	0.0154	417.0	4.651
2140	1.326	0.0156	419.0	4.673
2130	1.326	0.0157	419.0	4.695
2120	1.326	0.0157	418.0	4.717
2110	1.325	0.0157	416.0	4.739
2100	1.325	0.0155	410.0	4.762
2090	1.325	0.0153	402.0	4.785
2080	1.325	0.0151	394.0	4.808
2070	1.325	0.0148	386.0	4.831
2060	1.325	0.0146	377.0	4.854
2050	1.324	0.0143	368.0	4.878
2040	1.324	0.0140	359.0	4.902
2030	1.323	0.0137	349.0	4.926
2020	1.322	0.0133	338.0	4.950
2010	1.322	0.0129	327.0	4.975
2000	1.321	0.0126	317.0	5.000
1990	1.320	0.0122	306.0	5.025
1980	1.319	0.0118	294.0	5.051
1970	1.318	0.0115	284.0	5.076
1960	1.318	0.0110	272.0	5.102
1950	1.317	0.0108	264.0	5.128
1940	1.316	0.0105	255.0	5.155
1930	1.314	0.0103	249.0	5.181
1920	1.313	0.0101	244.0	5.208
1910	1.311	0.0100	240.0	5.236
1900	1.310	0.00993	237.0	5.263
1890	1.308	0.00990	235.0	5.291
1880	1.306	0.00995	235.0	5.319
1870	1.304	0.0100	236.0	5.348
1860	1.302	0.0102	238.0	5.376
1850	1.299	0.0104	242.0	5.405
1840	1.297	0.0107	247.0	5.435
1830	1.294	0.0110	253.0	5.464
1820	1.291	0.0115	262.0	5.495
1810	1.288	0.0120	274.0	5.525
1800	1.285	0.0128	289.0	5.556
1790	1.282	0.0138	311.0	5.587
1780	1.278	0.0150	336.0	5.618
1770	1.275	0.0166	370.0	5.650
1760	1.271	0.0185	409.0	5.682
1750	1.267	0.0205	451.0	5.714
1740	1.262	0.0242	529.0	5.747
1730	1.256	0.0293	637.0	5.780
1720	1.251	0.0332	734.0	5.814
1710	1.247	0.0429	947.0	5.848
1700	1.242	0.0544	1200.0	5.882
1690	1.241	0.0688	1515.0	5.917
1680	1.241	0.0840	1840.0	5.952
1670	1.247	0.1021	2175.0	5.988
1660	1.265	0.117	2430.0	6.024
1650	1.289	0.130	2670.0	6.061
1640	1.311	0.132	2738.0	6.098
1630	1.332	0.124	2566.0	6.135
1620	1.349	0.106	2139.0	6.173
1610	1.354	0.0880	1760.0	6.211
1600	1.356	0.0740	1465.0	6.250
1590	1.354	0.0618	1200.0	6.289
1580	1.350	0.0535	1025.0	6.329
1570	1.345	0.0484	934.0	6.369
1560	1.341	0.0447	863.0	6.410
1550	1.337	0.0420	806.0	6.452
1540	1.333	0.0398	758.0	6.494
1530	1.330	0.0383	726.0	6.536
1520	1.326	0.0373	703.0	6.579
1510	1.324	0.0370	683.0	6.623
1500	1.322	0.0366	666.0	6.667

TABLE 1. (continued)

$\nu$	$n(\nu)$	$k(\nu)$	$a(\nu)$	$\lambda$
1490	1.320	0.0363	652.0	6.711
1480	1.319	0.0360	638.0	6.757
1470	1.318	0.0357	624.0	6.803
1460	1.317	0.0355	612.0	6.849
1450	1.316	0.0352	602.0	6.897
1440	1.315	0.0350	593.0	6.944
1430	1.314	0.0347	582.0	6.993
1420	1.313	0.0346	575.0	7.042
1410	1.311	0.0343	564.0	7.092
1400	1.310	0.0342	558.0	7.143
1390	1.309	0.0342	554.0	7.194
1380	1.308	0.0342	550.0	7.246
1370	1.307	0.0343	547.0	7.299
1360	1.306	0.0342	543.0	7.353
1350	1.305	0.0342	540.0	7.407
1340	1.303	0.0342	537.0	7.463
1330	1.302	0.0342	535.0	7.519
1320	1.301	0.0342	532.0	7.576
1310	1.300	0.0344	530.0	7.634
1300	1.298	0.0345	530.0	7.692
1290	1.296	0.0346	529.0	7.752
1280	1.295	0.0349	528.0	7.813
1270	1.294	0.0351	527.0	7.874
1260	1.293	0.0351	526.0	7.937
1250	1.291	0.0351	525.0	8.000
1240	1.288	0.0352	524.0	8.065
1230	1.286	0.0356	524.0	8.130
1220	1.285	0.0359	523.0	8.197
1210	1.283	0.0361	523.0	8.264
1200	1.281	0.0362	522.0	8.333
1190	1.279	0.0366	522.0	8.403
1180	1.276	0.0370	523.0	8.475
1170	1.274	0.0374	523.0	8.547
1160	1.271	0.0378	523.0	8.621
1150	1.269	0.0383	524.0	8.696
1140	1.267	0.0387	525.0	8.772
1130	1.264	0.0392	527.0	8.850
1120	1.261	0.0398	529.0	8.929
1110	1.259	0.0405	532.0	9.009
1100	1.256	0.0411	536.0	9.091
1090	1.253	0.0417	540.0	9.174
1080	1.249	0.0424	546.0	9.259
1070	1.246	0.0434	553.0	9.346
1060	1.242	0.0443	561.0	9.434
1050	1.238	0.0453	571.0	9.524
1040	1.234	0.0467	583.0	9.615
1030	1.230	0.0481	596.0	9.709
1020	1.224	0.0497	613.0	9.804
1010	1.220	0.515	631.0	9.901
1000	1.214	0.0534	651.0	10.000
990	1.208	0.0557	673.0	10.101
980	1.202	0.0589	702.0	10.204
970	1.194	0.0622	733.0	10.309
960	1.189	0.0661	770.0	10.417
950	1.181	0.0707	817.0	10.526
940	1.174	0.0764	866.0	10.638
930	1.168	0.0823	927.0	10.753
920	1.162	0.0898	993.0	10.870
910	1.156	0.0973	1064.0	10.989
900	1.149	0.107	1165.0	11.111
890	1.143	0.118	1270.0	11.236
880	1.139	0.130	1396.0	11.364
870	1.135	0.144	1533.0	11.494
860	1.132	0.159	1682.0	11.628
850	1.132	0.176	1833.0	11.765
840	1.131	0.192	1987.0	11.905
830	1.132	0.208	2143.0	12.048
820	1.130	0.226	2309.0	12.195
810	1.130	0.243	2467.0	12.346
800	1.134	0.260	2618.0	12.500
790	1.138	0.277	2760.0	12.658

TABLE 1. (continued)

$\nu$	$n(\nu)$	$k(\nu)$	$a(\nu)$	$\lambda$
780	1.142	0.292	2883.0	12.821
770	1.157	0.305	2969.0	12.987
760	1.171	0.317	3040.0	13.158
750	1.182	0.328	3100.0	13.333
740	1.189	0.338	3150.0	13.514
730	1.201	0.347	3192.0	13.699
720	1.213	0.356	3231.0	13.889
710	1.223	0.365	3263.0	14.085
700	1.236	0.373	3287.0	14.286
690	1.249	0.379	3298.0	14.493
680	1.264	0.386	3307.0	14.706
670	1.277	0.392	3308.0	14.925
660	1.289	0.397	3307.0	15.152
650	1.303	0.403	3301.0	15.385
640	1.313	0.408	3291.0	15.625
630	1.324	0.412	3276.0	15.873
620	1.335	0.417	3259.0	16.129
610	1.348	0.420	3234.0	16.393
600	1.361	0.423	3203.0	16.667
590	1.372	0.425	3167.0	16.949
580	1.385	0.427	3126.0	17.241
570	1.396	0.428	3077.0	17.544
560	1.407	0.427	3022.0	17.857
550	1.419	0.427	2964.0	18.182
540	1.431	0.426	2903.0	18.519
530	1.441	0.425	2842.0	18.868
520	1.451	0.423	2779.0	19.231
510	1.462	0.421	2709.0	19.608
500	1.470	0.418	2638.0	20.000
490	1.480	0.415	2565.0	20.408
480	1.488	0.411	2494.0	20.833
470	1.496	0.408	2423.0	21.277
460	1.504	0.404	2347.0	21.739
450	1.510	0.401	2280.0	22.222
440	1.515	0.397	2210.0	22.727
430	1.521	0.394	2143.0	23.256
420	1.527	0.390	2072.0	23.810
410	1.532	0.386	2004.0	24.390
400	1.537	0.382	1933.0	25.000
390	1.541	0.377	1862.0	25.641
380	1.545	0.372	1793.0	26.316
370	1.549	0.368	1724.0	27.027
360	1.552	0.363	1658.0	27.778
350	1.552	0.359	1593.0	28.571
340	1.552	0.356	1532.0	29.412
330	1.550	0.352	1472.0	30.303
320	1.546	0.353	1412.0	31.250
310	1.543	0.357	1401.0	32.258
300	1.541	0.361	1374.0	33.333
290	1.539	0.368	1351.0	34.483
280	1.537	0.375	1331.0	35.714
270	1.534	0.385	1317.0	37.037
260	1.532	0.398	1311.0	38.462
250	1.529	0.414	1310.0	40.000
240	1.525	0.436	1323.0	41.667
230	1.528	0.469	1364.0	43.478
220	1.542	0.505	1407.0	45.455
210	1.567	0.539	1434.0	47.619
200	1.600	0.571	1445.0	50.000
190	1.640	0.597	1437.0	52.652
180	1.689	0.618	1412.0	55.556
170	1.746	0.629	1358.0	58.824
160	1.801	0.622	1266.0	62.500
150	1.848	0.608	1165.0	66.667
140	1.890	0.593	1065.0	71.429
130	1.929	0.577	967.0	76.923
120	1.960	0.557	872.0	83.333
110	1.982	0.532	773.0	90.909
100	1.997	0.507	678.0	100.000
90	2.000	0.487	594.0	111.111
80	2.010	0.466	509.0	125.000

TABLE 1. (continued)

$\nu$	$n(\nu)$	$k(\nu)$	$\alpha(\nu)$	$\lambda$
70	2.020	0.450	429.0	142.857
60	2.040	0.444	360.0	166.667
50	2.070	0.438	290.0	200.000
40	2.110	0.460	240.0	250.000
30	2.150	0.527	210.0	333.333
20	2.225	0.718	192.0	500.000
10	2.600	1.0902	137.0	1000.000

Frequencies  $\nu$  are expressed in waves per centimeter ( $\text{cm}^{-1}$ ),  $n(\nu)$  and imaginary  $k(\nu)$  parts of the dielectric constant  $\epsilon = n + ik$  are dimensionless, the Lambert absorption coefficient  $\alpha(\nu)$  defined by the relation  $I = I_0 \exp[-\alpha x]$  is expressed in waves per centimeter ( $\text{cm}^{-1}$ ), and wavelengths  $\lambda$  are given in micrometers ( $\mu\text{m}$ ). The values of  $n(\nu)$ ,  $k(\nu)$ , and  $\alpha(\nu)$  are given for water at 27°C.

Although the values of  $n$  and  $k$  provide all the information actually required for a quantitative description of the optical properties of water, a set of values of the Lambert coefficient  $\alpha$  is of direct use in providing information of importance to studies of radiative heat balance at horizontal water surfaces. We have therefore included a plot of  $\alpha$  versus  $\nu$  in Figure 3; values of  $\alpha$  given in the plot are based entirely on direct measurements and thus differ slightly from  $\alpha$  values calculated from our averaged values of  $k$ . The values of  $\alpha$  given in Figure 3 would apply in good approximation to clear freshwater lakes and can provide rough approximations of the properties of clear seawater, as suggested by *Hobson and Williams* [1971].

Irvine and Pollack have emphasized the importance of presenting optical constants in tabular as well as graphical form. In Table 1 we list our best values of  $k$ ,  $n$ , and  $\alpha$  at frequency intervals of  $10 \text{ cm}^{-1}$  over most of the range between 5000 and  $10 \text{ cm}^{-1}$ ; the values in the table correspond to those plotted in Figures 1-3 and involve the same uncertainties. These values apply to water at a laboratory temperature of approximately 27°C; values at other temperatures can be estimated from the plots given by *Hale et al.* [1972]. A molecular interpretation of the water spectrum was given by *Robertson et al.* [1973].

#### COMPARISON WITH OTHER STUDIES

Our values for the optical constants can be compared with those obtained in earlier studies by *Pontier and Dechambeno* [1965, 1966] in France and by *Zolotarev et al.* [1969] in Russia. The present results for  $k$  are in excellent agreement with both of these studies in the range 5000-4000  $\text{cm}^{-1}$  but are in somewhat serious disagreement in the vicinity of the strong absorption band near 3400  $\text{cm}^{-1}$ , where plots of the earlier studies differ by several percent from those in Figure 1. The peak values of  $k$  in the two studies are 0.305, a value somewhat higher than our present highest estimate and 8% higher than the value given in our plot; the absorption band obtained by the French workers is centered at a slightly lower frequency than the frequency given in the other studies.

In the frequency range 2800-800  $\text{cm}^{-1}$  there is truly excellent agreement between the present  $k$  values and those reported by the Russian group; throughout most of this region the French values of  $k$  are significantly higher than our values. At frequencies lower than 800  $\text{cm}^{-1}$  the French values are generally

greater than ours, and the Russian values generally lower; through the entire region below 800  $\text{cm}^{-1}$  the  $k$  values reported by the other groups fall within  $\pm 10\%$  of the values we give in Figure 1.

In comparing our present values for  $n$  with the earlier studies we find that in the 5000- to 3600- $\text{cm}^{-1}$  region our values are in good agreement with the values obtained in the French study; throughout this region the Russian values are considerably lower than ours and are in serious disagreement in the 3800- to 3600- $\text{cm}^{-1}$  range, where the Russian values are much lower than ours. In the range 3200-400  $\text{cm}^{-1}$  the  $n$  values obtained in the earlier studies generally fall within  $\pm 1\%$  of our values as plotted in Figure 2; however, at the minimum near 840  $\text{cm}^{-1}$  the earlier results are lower than ours by 1.5%. At frequencies below 400  $\text{cm}^{-1}$  we have continued satisfactory agreement with the Russians, who based their values in this region on published results of others including *Draeger et al.* [1966] which are shown by the points in Figures 1 and 3 for  $\nu < 200 \text{ cm}^{-1}$ . In the region  $\nu < 400 \text{ cm}^{-1}$  the French results fall below our values and are apparently in serious error; they are based on prism spectrograph results, which we find are subject to stray radiation problems in the low-frequency region.

*Acknowledgments.* We wish to acknowledge our debt to all the participants in our laboratory studies and to generous support by the Office of Naval Research. We should also like to express our appreciation to the late John Chamberlain and his associates at the NPL and to Peter Ray for their generous cooperation.

#### REFERENCES

- Davies, M., G. W. Pardoe, J. Chamberlain, and H. A. Gebbie, Submillimetre- and millimetre-wave absorption of some polar and non-polar liquids, *Trans. Faraday Soc.*, 66, 273, 1970.
- Draeger, D. A., N. W. B. Stone, B. Curnutte, and D. Williams, Far-infrared spectrum of liquid water, *J. Opt. Soc. Amer.*, 56, 64, 1966.
- Hale, G. M., M. R. Querry, A. N. Rusk, and D. Williams, Influence of temperature on the spectrum of water, *J. Opt. Soc. Amer.*, 62, 1103, 1972.
- Hobson, D. E., and D. Williams, Infrared spectral reflectance of sea water, *Appl. Opt.*, 10, 2372, 1971.
- Irvine, W. M., and J. B. Pollack, Infrared optical properties of water and ice spheres, *Icarus*, 8, 324, 1968.
- Palmer, K. F., and D. Williams, Optical properties of water in the near infrared, *J. Opt. Soc. Amer.*, 64, 1107, 1974.
- Pontier, L., and C. Dechambeno, Mesure du pouvoir reflecteur de l'eau, *Ann. Geophys.*, 21, 462, 1965.
- Pontier, L., and C. Dechambeno, Détermination des constantes optiques de l'eau, *Ann. Geophys.*, 22, 633, 1966.
- Querry, M. R., B. Curnutte, and D. Williams, Refractive index of water in the infrared, *J. Opt. Soc. Amer.*, 59, 1299, 1969.
- Ray, P. S., Broadband complex refractive indices of ice and water, *Appl. Opt.*, 11, 1836, 1972.
- Robertson, C. W., and D. Williams, Lambert absorption coefficients of water in the infrared, *J. Opt. Soc. Amer.*, 61, 1316, 1971.
- Robertson, C. W., B. Curnutte, and D. Williams, The infra-red spectrum of water, *Mol. Phys.*, 26, 183, 1973.
- Rusk, A. N., D. Williams, and M. R. Querry, Optical constants of water in the infrared, *J. Opt. Soc. Amer.*, 61, 895, 1971.
- Zafar, M. S., J. B. Hasted, and J. Chamberlain, Submillimetre-wave dielectric dispersion in water, *Nature London Phys. Sci.*, 243, 106, 1973.
- Zolotarev, V. M., B. A. Mikhailov, L. I. Aperovich, and S. I. Popov, Dispersion and absorption of water in the infrared, *Opt. Spectrosc.*, 27, 790, 1969. (*Opt. Spectrosc.*, Engl. Transl., 27, 430, 1969.)

(Received September 11, 1974;  
accepted November 25, 1974.)

The next subject to be investigated involved a study of the influence of temperature on the optical constants of water by Dr. L. W. Pinkley and Dr. P. P. Sethna. The results of that study are given in graphical and tabular form in the following paper by Pinkley, Sethna, and Williams.

# Optical constants of water in the infrared: Influence of temperature\*

Lary W. Pinkley, P. P. Sethna, and Dudley Williams

Department of Physics, Kansas State University, Manhattan, Kansas 66506

(Received 16 September 1976)

We have compared the near-normal-incidence spectral reflectance of water at 1, 16, 39, and 50°C with the corresponding spectral reflectance of water at 27°C, at which temperature the optical constants  $n(\nu)$  and  $k(\nu)$  have been previously determined. By applying Kramers-Kronig analyses to the resulting values of spectral reflectance we have obtained the optical constants of water at each of the above temperatures. We present the results in graphical form for the spectral region 400–5000  $\text{cm}^{-1}$  and in tabular form in the vicinity of major absorption and dispersion features. The bearing of our results on the intermolecular structure of water is discussed.

In an earlier investigation<sup>1</sup> we measured the near-normal-incidence spectral reflectance  $R(\nu)$  of water in the infrared by comparing the reflectance of a water surface with that of a calibrated reference mirror; we employed water samples at 5, 27, and 70 °C. By the use of conventional Kramers-Kronig phase-shift analysis of the spectral reflectance, we obtained values of the real  $n(\nu)$  and imaginary  $k(\nu)$  parts of the complex index of refraction  $\hat{N}(\nu) = n(\nu) + ik(\nu)$  in the infrared.

Since the time of the earlier study we have made more detailed studies of the optical properties of water at 27 °C by additional measurements of reflection and by quantitative measurements of the Lambert absorption coefficient  $\alpha(\nu) = 4\pi k(\nu)/\lambda$  in the spectral region between the near ultraviolet and the remote infrared. The subsequent studies have been discussed along with related results in the submillimeter and microwave regions in a critical survey by Downing and Williams,<sup>2</sup> who presented an extensive table of the values of  $n(\nu)$  and  $k(\nu)$  in the infrared. On the basis of these tabulated values, the near-normal-incidence spectral reflectance of water at 27 °C can be computed from the Fresnel relation

$$R(\nu) = \frac{[n(\nu) - 1]^2 + [k(\nu)]^2}{[n(\nu) + 1]^2 + [k(\nu)]^2}. \quad (1)$$

By the use of the resulting computed values of  $R(\nu)_S$  for water at 27 °C as a standard we can now determine  $R(\nu)_T$  for water at other temperatures by direct comparison. This technique has the advantages of avoiding possible errors in the positioning of a reference mirror in the reflectometer and in the measurement of the absolute spectral reflectance of the reference mirror itself. Because the spectral reflectances of water at other temperatures are comparable in magnitude with the spectral reflectance of water at 27 °C, comparisons can be made without the use of optical attenuators or of changes in amplifier gain settings that are required when a metallic reference mirror is employed.

In view of these advantages, we have undertaken a re-examination of the influence of temperature on the optical constants of water by making direct comparisons of near-normal-incidence reflection of water at various temperatures with that of water at 27 °C. In the present study we have employed water samples at 1, 16, 39, and 50 °C.

The measured ratios of the spectral reflectance of water at other temperatures to the reflectance of water at 27 °C are shown in Fig. 1. The measured ratios

shown in the figure are reproducible to within  $\pm 1\%$  of the plotted values over most of the infrared and can thus be of future value when values of the optical constants of water at 27 °C more exact than those tabulated by Downing and Williams<sup>2</sup> become available. On the basis of the values of the ratios plotted in Fig. 1 and our standard values of  $R(\nu)$  for water at 27 °C as computed from Eq. (1), we obtain the values of spectral reflectance shown in Fig. 2. The most obvious change in  $R(\nu)$  with temperature occurs in the vicinity of 3200  $\text{cm}^{-1}$ ; as indicated in Fig. 2,  $R(\nu)$  in this region decreases monotonically with increasing temperature. Even larger changes in spectral reflectance with temperature occur in the vicinity of 600  $\text{cm}^{-1}$ , where increasing temperature is also accompanied by decreasing spectral reflectance; changes near 600  $\text{cm}^{-1}$  are associated with a shift of the librational band to lower frequencies with increasing temperature.<sup>3</sup> Changes in temperature produce smaller changes in  $R(\nu)$  in other spectral regions.

In arriving at values of the optical constants of water at various temperatures we have made use of the fact that  $n(\nu)$  and  $k(\nu)$  are well known<sup>2</sup> for water at 27 °C and that spectral reflectances  $R(\nu)_T$  of water at other temperatures were determined in terms of the spectral reflectance of water at 27 °C. We treat the spectral re-

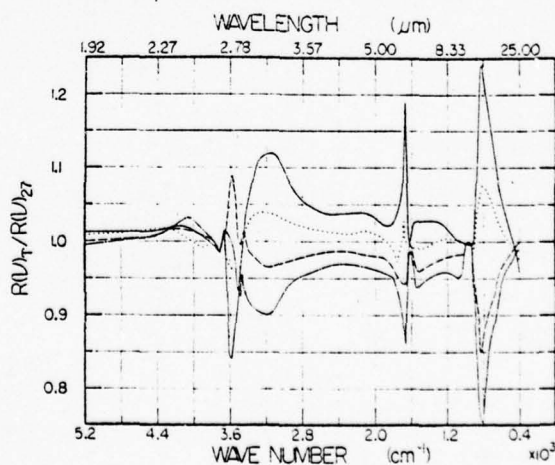


FIG. 1. Ratio of the near-normal-incidence spectral reflectance of water at various temperatures  $R(\nu)_T$  to the spectral reflectance  $R(\nu)_{27}$  of water at 27 °C. The ratios are given by the light continuous curve, 1 °C; dotted curve, 16 °C; dashed curve, 39 °C; and dash-dot-dash curve, 50 °C.

flectance at 27 °C as computed from Eq. (1) as a standard  $R(\nu)_S$ . Because we know the values of  $R(\nu)_S$  for frequency ranges<sup>4</sup> well outside the present measurement range, 350–5200  $\text{cm}^{-1}$ , we can arrive at a value of the phase shift for water at 27 °C from the Kramers-Kronig relation

$$\phi(\nu)_{SK} = \frac{2\nu}{\pi} P \int_0^{\infty} \frac{\ln[R(\nu')_S]^{1/2}}{\nu'^2 - \nu^2} d\nu', \quad (2)$$

where  $[R(\nu)]^{1/2}$  is the modulus of the complex reflectivity  $R(\nu) = [R(\nu)]^{1/2} \exp[i\phi(\nu)]$ ; the resulting values of  $\phi(\nu)_{SK}$  are extremely close approximations of  $\phi(\nu)_S$  as computed directly from tabulated values<sup>2</sup> of  $n(\nu)$  and  $k(\nu)$ . The values of  $\phi(\nu)_{SK}$  obtained from Eq. (2) can be considered as the sum of three parts

$$\phi(\nu)_{SK} = \phi(\nu)_{SK\text{-HFE}} + \phi(\nu)_{SK\text{-M}} + \phi(\nu)_{SK\text{-LFE}} \quad (3)$$

where the subscript M indicates the contributions to  $\phi(\nu)_{SK}$  associated with values of  $R(\nu)$  in the present range of *measurement* and the subscripts HFE and LFE indicate contributions associated with *high-frequency extrapolation* and *low-frequency extrapolation*, respectively.

From our present values of  $R(\nu)_T$  for water at other temperatures  $T$ , we can obtain corresponding values of  $\phi(\nu)_{TK}$  based on Eq. (2) and write

$$\phi(\nu)_{TK} = \phi(\nu)_{TK\text{-HFE}} + \phi(\nu)_{TK\text{-M}} + \phi(\nu)_{TK\text{-LFE}}. \quad (4)$$

By using  $R(\nu)_T = R(\nu)_S$  in the HFE and LFE ranges for all temperatures, we obtain values of the differences  $\Delta(\nu)_T$  between  $\phi(\nu)_{TK}$  and  $\phi(\nu)_{SK}$  that are based only on actual measurements:  $\Delta(\nu)_T = \phi(\nu)_{TK\text{-M}} - \phi(\nu)_{SK\text{-M}}$ . Thus, we can write  $\phi(\nu)_{TK} = \phi(\nu)_{SK} + \Delta(\nu)_T$ . In order to obtain a still more precise value for  $\phi(\nu)_T$  we may write

$$\phi(\nu)_T = \phi(\nu)_S + \Delta(\nu)_T, \quad (5)$$

where  $\phi(\nu)_S$  is the value of the phase shift for water at 27 °C as computed directly from tabulated values<sup>2</sup> of  $n(\nu)$  and  $k(\nu)$  supported by measurements of absorption as well as reflection. On the basis of the phase shifts given by Eq. (5) along with the experimental values of  $R(\nu)$ , we proceed to obtain values of  $n(\nu)$  and  $k(\nu)$  by well known relationships.

The values of the refractive index  $n(\nu)$  are plotted as a function of  $\nu$  in Fig. 3. The dispersion features exhibited by the curves in Fig. 3 are, in general, similar to the corresponding features in the plots of spectral reflectance given in Fig. 2. The influences of temperature changes on  $n(\nu)$  are greatest near 3200 and 600  $\text{cm}^{-1}$ .

The values of the absorption index  $k(\nu)$  as a function of frequency  $\nu$  are shown by the curves in Fig. 4. The strong absorption band near 3400  $\text{cm}^{-1}$  is associated with the  $\nu_1$  and  $\nu_2$  fundamentals of the water molecule with some contribution from  $2\nu_2$ . The peak values of  $k(\nu)$  as well as the band strength  $S = \int k(\nu) d\nu$  for this band decrease monotonically with increasing temperature, while the frequency at which  $k(\nu)$  is a maximum increases in similar fashion with increasing temperature. The sharp absorption band near 1640  $\text{cm}^{-1}$  is associated with the  $\nu_2$  fundamental of the water molecule

and is virtually unaffected by temperature over the range covered in the present study. The strong absorption band in the vicinity of 600  $\text{cm}^{-1}$ , which is associated with the librational motion of the water molecule in the field of its neighbors, shifts to lower frequencies with increasing temperature without appreciable change in the maximum value of  $k(\nu)$ . The band strength  $S = \int k(\nu) d\nu$  computed on the assumption that the band is symmetrical about its peak is nearly constant. The weak associational band near 2200  $\text{cm}^{-1}$  shifts toward lower frequencies with increasing temperature and shows an apparent decrease in strength  $S = \int k(\nu) d\nu$  at the higher temperatures; because of the low values of  $k(\nu)$  involved, this associational band can best be studied by absorption methods.<sup>3</sup> The absorption in the spectral region between the  $\nu_2$  fundamental and the librational band shows little change with temperature.

## DISCUSSION OF RESULTS

The results of the present study are those typical of *intensity spectroscopy* as contrasted with conventional *frequency spectroscopy*. We have obtained quantitative values of the optical constants of water at the expense of some loss in information regarding precise band positions and band contours, which can be obtained more reliably from absorption studies provided corrections are made for reflections at absorption cell windows and for interference phenomena in the thin absorbing layers that are required. The present work gives more precise information regarding the intensities of strong absorption bands; more reliable information regarding weak bands can be obtained by absorption studies provided the thickness of absorbing layers are carefully measured and provided proper corrections for reflections at cell windows are made.

The present study provides quantitative values of the refractive index  $n(\nu)$  that are not directly available from absorption studies. In many spectral regions values of  $n(\nu)$  for water at other temperatures can be obtained from the values tabulated<sup>2</sup> for water at 27 °C. The Lorentz-Lorenz relation between  $n(\nu)$  and density  $\rho$  can be conveniently expressed in the form

$$\frac{(n(\nu)^2 - 1)}{(n(\nu)^2 + 2)} \cdot \frac{1}{\rho} = \text{const.} \quad (6)$$

On the basis of the tabulated values for water at 27 °C, we find that the Lorentz-Lorenz relation provides values of  $n(\nu)$  that agree to within  $\pm 0.005$  with our experimental values in the spectral range 5200–3650  $\text{cm}^{-1}$  for all temperatures covered in the present study. Agreement to within  $\pm 0.01$  is provided in the spectral ranges 2650–1700  $\text{cm}^{-1}$  and 1600–820  $\text{cm}^{-1}$ . The Lorentz-Lorenz relation can probably be used in these regions for temperatures considerably above 50 °C.

The values of  $n(\nu)$  in the vicinity of the major dispersion features in Fig. 3 are presented in Table I along with the corresponding values of  $k(\nu)$ . Values of the optical constants of water at other temperatures in the range 1–50 °C can be obtained by interpolation from the values tabulated for the temperatures covered in the present study; some extrapolation to higher temperatures is possible.



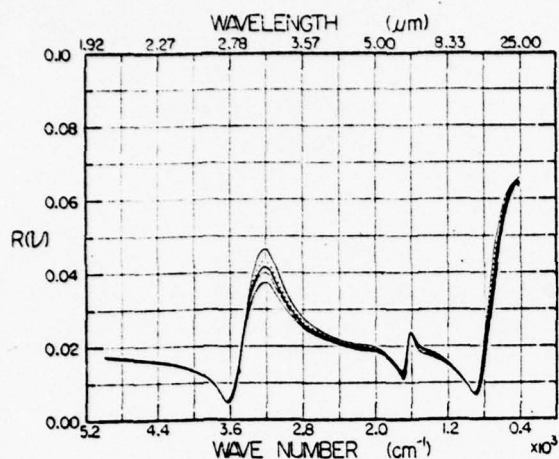


FIG. 2. Near-normal-incidence spectral reflectance  $R(\nu)$  for water at various temperatures: light continuous curve, 1°C; dotted curve, 16°C; heavy continuous curve, 27°C; dashed curve, 39°C; and dash-dot-dash curve, 50°C.

In Table II we present a summary of our results for each of the major absorption bands of water. The table gives a listing of the frequency  $\nu_{max}$  at which the absorption index attains its maximum value  $k_{max}$ , which is also indicated in Table II. The band strength or integrated absorption  $S = \int k(\nu) d\nu$  is listed for each band along with an estimation of the corresponding bandwidth parameter  $\Gamma$ , which gives the full width of the band between the frequencies at which the absorption index is  $\frac{1}{2}k_{max}$ . We note that the values of  $S$  and  $\Gamma$  listed for the librational band  $\nu_L$  are based on the assumption that the band is symmetrical about  $\nu_{max}$ ; other studies indicate that this assumption is valid except for a sharp band due to hindered translation  $\nu_T$  that appears as a shoulder on the low-frequency wing of the librational band.<sup>2</sup>

Also listed in Table II are values of integrated absorption  $\int k(\nu) d\nu$  for the spectral region between  $\nu_{1,3}$  and

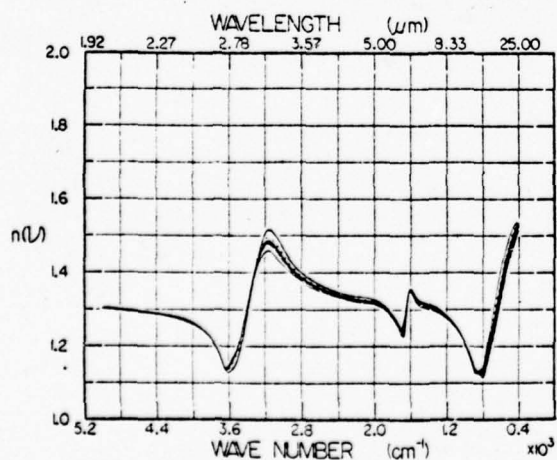


FIG. 3. Refractive index  $n(\nu)$  for water at various temperatures: light continuous curve, 1°C; dotted curve, 16°C; heavy continuous curve, 27°C; dashed curve, 39°C; and dash-dot-dash curve, 50°C.

$\nu_2$ , in which the weak associational band occurs, and for the spectral interval between  $\nu_2$  and  $\nu_L$ . Although  $k(\nu)$  never attains large values in these interband regions, the integrated absorption in the two regions is not negligible and is indeed comparable with the value of  $S$  for the  $\nu_2$  band.

#### RELATION TO THE INTERMOLECULAR STRUCTURE OF WATER

Although no entirely satisfactory theoretical description of the intermolecular structure of liquid water has yet been developed, the local-lattice model of Bryan and Curnutte<sup>5</sup> has many features that provide an insight into an interpretation of our present results. These authors interpret the far-infrared spectrum in terms of the hindered motions of a water molecule connected tetrahedrally by hydrogen bonds to a rigid cage of neighboring molecules. When a single molecule is enclosed in a rigid cage of four neighboring molecules, there are three modes of librational motion in the range 450–720  $\text{cm}^{-1}$  and three modes of hindered translational motion in the vicinity of 165  $\text{cm}^{-1}$ ; the computed frequencies for a molecule in an incomplete cage are generally lower. Extending this model to the case of a nonrigid central unit of five water molecules inside a larger rigid cage of surrounding molecules, Bandekar and Curnutte<sup>7</sup> find a larger number of librational modes in the range 450–720  $\text{cm}^{-1}$  and a large number of hindered-translational modes in the range 160–220  $\text{cm}^{-1}$  along with three new modes in the vicinity of 75  $\text{cm}^{-1}$ ; in the actual water structure there are presumably motions occurring at still lower frequencies.

Although earlier studies<sup>3,8,9</sup> have failed to reveal any well-defined infrared absorption bands in the spectral range below 100  $\text{cm}^{-1}$ , clear evidence of a hindered translation band has been obtained; at 27°C this band is associated with a maximum<sup>2,8</sup> in  $k(\nu)$  at 170  $\text{cm}^{-1}$  and shifts toward lower frequencies with increasing temperature.<sup>3</sup> The hindered translational absorption band appears as a weak shoulder on the much stronger libra-

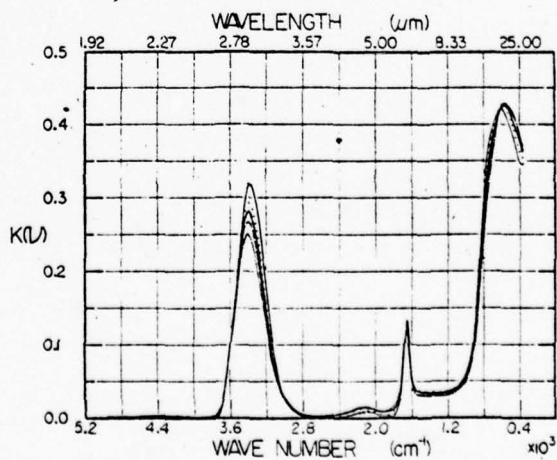


FIG. 4. Absorption index  $k(\nu)$  for water at various temperatures: light continuous curve, for 1°C; dotted curve, 16°C; heavy continuous curve, 27°C; dashed curve, for 39°C; and dash-dot-dash curve, 50°C.



TABLE II. Absorption regions in the water spectrum.

Temp. (°C)	Band	$\nu_{\max}$ (cm <sup>-1</sup> )	$k_{\max}$	$S = \int k(\nu) d\nu$ (cm <sup>-1</sup> )	$\Gamma$ (cm <sup>-1</sup> )
1	$\nu_{1,3}$	3380	0.32	124	358
16		3390	0.29	114	360
27		3390	0.28	112	365
39		3400	0.27	103	367
50		3400	0.25	97	378
1		~ 2100		8	
16		~ 2100		6	
27		~ 2100		8	
39		~ 2100		4	
50		~ 2100		4	
1	$\nu_2$	1640	0.12	17	118
16		1640	0.13	16	100
27		1640	0.13	17	100
39		1640	0.13	15	90
50		1640	0.14	15	86
1				16	
16				17	
27				14	
39				15	
50				14	
1	$\nu_L$	590	0.42	222	514
16		590	0.43	222	485
27		570	0.43	224	520
39		555	0.43	228	524
50		560	0.43	218	500

tional band in a plot of the Lambert absorption coefficient  $\alpha(\nu) = 4\pi k(\nu)/\lambda = 4\pi\nu k(\nu)$  as a function of wave number  $\nu$ ; in a plot of  $k(\nu)$  vs  $\nu$ , the translational band is narrow and well defined with a value of  $k(\nu)_{\max}$  that is 50% larger than that of the librational band. Further studies of the translational band by reflection or ATR (attenuated-total-reflection) techniques at various temperatures are highly desirable.

The shift of the observed librational band toward lower frequencies with increasing temperature has been noted in our earlier study of absorption<sup>3</sup> and is probably associated with a weakening of the hydrogen bonded local lattice. It is interesting that  $k(\nu)_{\max}$  at the band center and the band strength  $\int k(\nu) d\nu$  remain nearly unchanged over the entire temperature range covered in the present study. The strength of the interaction between the hindered rotational motion of the water molecule and the electromagnetic field associated with the radiation thus seems to be largely independent of the molecule's immediate environment.

The sharp  $\nu_2$  fundamental absorption band near 1640 cm<sup>-1</sup>, which is associated with the bending motion of the water molecule, remains nearly unchanged in frequency  $\nu_{\max}$  and its strength  $\int k(\nu) d\nu$  decreases by only 11% as does its corresponding value of  $k(\nu)_{\max}$  as the water temperature is changed from 1 to 50 °C. The  $\nu_2$  band strength at 1 °C is nearly the same as that of the corresponding band<sup>10</sup> in ice at -7 °C.

The influence of temperature on the overlapping  $\nu_{1,3}$  bands of water near 3400 cm<sup>-1</sup> is considerably different from its influence on the other characteristic bands. With increasing temperature the observed maximum

shifts to higher frequencies, away from the lower frequencies of the corresponding bands in ice and toward the higher frequencies of the corresponding bands in water vapor. More impressive is the 22% decrease in  $k(\nu)_{\max}$  and in  $\int k(\nu) d\nu$  as the water temperature increases from 1 to 50 °C. As both the  $\nu_1$  and  $\nu_3$  fundamentals of the water molecule are "valence vibrations" involving changes in the distances between the hydrogen atoms and the oxygen atom in the water molecule, the changes in intensity can be interpreted on a semiclassical basis in terms of a greater amplitude of the motion of the proton in the modified potentials involved in the hydrogen bonding between adjacent water molecules. Alternatively, the observed changes in band strength might be interpreted in terms of larger numbers of incompletely hydrogen bonded molecules in water at the higher temperatures; there may be difficulties in reconciling this latter view with the observed behavior of the librational band.

The absorption in the interband region 1100-1600 cm<sup>-1</sup> is interesting in that  $\int k(\nu) d\nu$  for the region is nearly independent of temperature. Since there is no absorption maximum in the region, it is impossible to attribute the absorption to a single mechanism. The general absorption in this region is probably due to many overlapping bands representing harmonics and combinations of various librational modes. It is possible that some of the absorption may be due to hot bands representing transitions from molecules in the low-lying librational and translational states to the first excited level of the  $\nu_2$  bending vibration of the water molecule.

Absorption in the second interband region between 1800 and 2800 cm<sup>-1</sup> decreases with increasing temperature and is characterized by a maximum near 2100 cm<sup>-1</sup>. This so-called associational band, which has no counterpart in the spectrum of water vapor, is usually attributed to a combination of  $\nu_2$  with a librational mode of vibration. At 27 °C the observed band maximum occurs at 2120 cm<sup>-1</sup>; if we employ the frequency of the peak of the observed librational band as the required frequency for the combination with  $\nu_2$ , we obtain  $\nu_A = \nu_2 + \nu_L = (1640 + 570 \text{ cm}^{-1}) = 2210 \text{ cm}^{-1}$  as the frequency of the combination band. The frequency of the associational band decreases with increasing temperature<sup>3</sup>; in view of the observed decrease in the frequency of the librational band, this behavior is to be expected if the associational band is actually a combination band. However, since the band strengths of  $\nu_2$  and  $\nu_L$  remain nearly independent of temperature, the decrease in the strength of the associational band presents problems. It is possible that the coupling between the bending motions of the water molecule and its librational motion decreases with increasing temperature as a result of the decrease in anharmonicity of the proton potential with increasing oxygen-oxygen separation in the hydrogen bonded liquid structure.

Absorption studies have revealed the presence of two more weak associational bands in the spectrum of liquid water. One of these  $\nu_B$  appears<sup>11</sup> near 3950 cm<sup>-1</sup> and the other  $\nu_C$  appears<sup>12</sup> near 5600 cm<sup>-1</sup>. These can be accounted for in terms of the combinations:  $\nu_B = \nu_3 + \nu_L$

$= 3950 \text{ cm}^{-1}$  and  $\nu_C = \nu_2 + \nu_3 + \nu_L = 5590 \text{ cm}^{-1}$ . It should be noted that in selecting values for  $\nu_L$  we have chosen the frequency at which  $k(\nu)$  is a maximum and not the frequency at which  $\alpha(\nu) = 4\pi\nu k(\nu)$  is a maximum; the difference between these frequencies becomes large for broad bands at low frequencies.<sup>2</sup> We note that earlier interpretations of  $\nu_A$ ,  $\nu_B$ , and  $\nu_C$  in terms of  $\alpha(\nu)$  maxima have been unsuccessful unless combinations involving hindered translation frequencies as well as librational frequencies are involved.<sup>13</sup>

Other investigators<sup>14,15</sup> have reported phenomena that suggest sudden changes in the structure of water occurring at  $35^\circ\text{C}$ . The greatest and most reliably measured effect of temperature on the infrared spectrum of water obtained in the present study is the change in the strength  $S = \int k(\nu) d\nu$  of the  $\nu_{1,3}$  band. In the range  $1-50^\circ\text{C}$  the strength of this band decreases monotonically with increasing temperature with no indications of sudden change in the vicinity of  $35^\circ\text{C}$ . In order to check the reported effect further we have made isochromatic spectral reflectance measurements near 600 and  $3200 \text{ cm}^{-1}$  over the temperature range  $1-70^\circ\text{C}$  without detecting any discontinuities in the  $R(\nu)$ -vs- $T$  curves. Although studies of the infrared spectrum of water as a function of temperature provide significant information regarding the water structure, we have not been able to observe any *sudden* spectral changes at  $35^\circ\text{C}$  or at any other temperatures in the range covered in the present work.

We should like to thank Professor Basil Curnutte for his helpful advice and criticism of the present work.

\*Supported in part by the Office of Naval Research.

<sup>1</sup>G. M. Hale, M. R. Querry, A. N. Rusk, and D. Williams,

"Influence of Temperature on the Spectrum of Water," *J. Opt. Soc. Am.* **62**, 1103-1108 (1972).

<sup>2</sup>H. D. Downing and D. Williams, "Optical Constants of Water in the Infrared," *J. Geophys. Res.* **80**, 1656-1661 (1975).

<sup>3</sup>D. A. Draeger, N. W. B. Stone, B. Curnutte, and D. Williams, "Far-Infrared Spectrum of Water," *J. Opt. Soc. Am.* **56**, 64-69 (1966).

<sup>4</sup>K. F. Palmer and D. Williams, "Optical Properties of Water in the Near Infrared," *J. Opt. Soc. Am.* **64**, 1107-1110 (1974).

<sup>5</sup>L. W. Pinkley and D. Williams, "Optical constants of sea water in the infrared," *J. Opt. Soc. Am.* **66**, 554-558 (1976).

<sup>6</sup>J. B. Bryan and B. Curnutte, "A Normal Coordinate Analysis Based on the Local Structure of Liquid Water," *J. Mol. Spectrosc.* **41**, 512-533 (1972).

<sup>7</sup>J. Bandekar and B. Curnutte, "The Intramolecular Vibrations of the Water Molecular in the Liquid State," *J. Mol. Spectrosc.* **41**, 500-511, (1972); "A Local-Structure Model for Calculations of Lattice Vibrations in Liquid Water," *ibid.* **58**, 169-177 (1975).

<sup>8</sup>C. W. Robertson, B. Curnutte, and D. Williams, "The Infrared Spectrum of Water," *Mol. Phys.* **26**, 183-191 (1973).

<sup>9</sup>M. S. Zafar, J. B. Hasted, and J. Chamberlain, "Submillimetre-Wave Dielectric Dispersion in Water," *Nature London Phys. Soc.* **243**, 106-111 (1973).

<sup>10</sup>J. W. Schaaf and D. Williams, "Optical Constants of Ice in the Infrared," *J. Opt. Soc. Am.* **63**, 726-732 (1973).

<sup>11</sup>J. R. Collins, "A New Infrared Absorption Band of Liquid Water at  $2.52 \mu\text{m}$ ," *Phys. Rev.* **55**, 470-472 (1939).

<sup>12</sup>D. Williams and W. M. Millett, "Effects of Various Ions on the Infrared Absorption of Water," *Phys. Rev.* **63**, 6-8 (1944).

<sup>13</sup>D. Williams, "Frequency Assignments in the Infrared Spectrum of Water," *Nature* **210**, 194-195 (1966).

<sup>14</sup>H. M. Dobbins and E. R. Peck, "Change of Refractive Index of Water as a Function of Temperature," *J. Opt. Soc. Am.* **63**, 318-320 (1973).

<sup>15</sup>J. B. Hawkes and R. W. Astheimer, "Optical Properties of Water in the Neighborhood of  $35^\circ\text{C}$ ," *J. Opt. Soc. Am.* **64**, 105-106 (1974).

The results given in the immediately preceding papers can be used in the Mie theory of scattering to predict the transmission through aerosols consisting of water droplets. The results thus have an important bearing on problems involving infrared signal transmission as well as on meteorological problems. However, because ice particles are sometimes present as aerosols, it is desirable to have a knowledge of the optical constants of ice at a temperature of meteorological importance. A study of the reflection spectrum of ice was carried out by Dr. Joel W. Schaaf in connection with his doctoral dissertation. The results of his study are summarized in the following paper by Schaaf and Williams.

## Optical constants of ice in the infrared\*

Joel W. Schaaf and Dudley Williams

Department of Physics, Kansas State University, Manhattan, Kansas 66506

(Received 5 February 1973)

The normal-incidence spectral reflectance of ice at  $-7^{\circ}\text{C}$  has been measured in the range  $300\text{--}5000\text{ cm}^{-1}$ . A Kramers-Kronig phase-shift analysis of the measured spectral reflectance has been employed to provide values of the real and imaginary parts of the refractive index. The resulting values of these optical constants are suitable for use in Mie-theory computations of scattering by ice particles in planetary atmospheres. The optical constants of ice at  $-7^{\circ}\text{C}$  are compared in detail with those of liquid water at several temperatures and with those recently determined for ice at  $-170^{\circ}\text{C}$ .

Index Headings: Refractive index; Ice; Infrared; Reflectance.

Irvine and Pollack<sup>1</sup> have made a critical survey of the existing literature<sup>2-13</sup> dealing with the optical properties of ice in the infrared and have attempted to establish values of the real  $n_r$  and imaginary  $n_i$  parts of the refractive index for use in the Mie-theory calculations of the scattering of infrared radiation by ice particles in the earth's atmosphere. In view of the difficulties involved in matching results obtained by different investigators working under widely different conditions and in different spectral regions, Irvine and Pollack emphasized the importance of further quantitative studies of ice in the infrared. The present work was undertaken with a view to obtaining pertinent values of the optical constants in the near and intermediate

infrared for ice at a temperature of meteorological importance.

Since the time of the Irvine-Pollack survey, Bertie, Labbé, and Whalley<sup>14</sup> have determined values of  $n_r$  in the spectral range  $4000\text{--}30\text{ cm}^{-1}$  for ice at  $-170^{\circ}\text{C}$  from measurements of the transmittance of thin layers of ice formed by the condensation of water vapor on a cold transparent substrate. These authors then used Kramers-Kronig techniques for the determination of corresponding values of  $n_r$ . Although they apply to ice at a temperature considerably lower than those commonly encountered in the earth's atmosphere, the results obtained by Bertie *et al.* represent the most complete single study of the properties of ice in the infrared.

The purpose of the present study was to measure the near-normal-incidence reflectance of ice at  $-7^{\circ}\text{C}$  in the range  $5000\text{--}300\text{ cm}^{-1}$  and to use a Kramers-Kronig phase-shift dispersion analysis of measured spectral reflectance to obtain values of  $n_r$  and  $n_i$ . It was hoped that the results, in combination with the low-temperature results of Bertie *et al.*,<sup>14</sup> would provide satisfactory values of optical constants for use in Mie-theory calculations.

## EXPERIMENTAL WORK

The reflectometer and spectrometer used in the present study are those used in our earlier studies of the near-normal-incidence reflectance of water.<sup>15</sup> The experimental methods employed were essentially similar to those employed in the earlier work. The first step was the measurement of the nominal spectral reflectance  $R_n$  of ice relative to a reference mirror. After the absolute spectral reflectance  $\mu$  of the reference mirror had been determined by means of a Strong reflectometer,<sup>16</sup> the spectral reflectance  $R$  of ice was obtained from the relation  $R = \mu R_n$ .

In the course of the reflectance measurements, the ice sample under study was positioned in the reflectometer by means of the device shown schematically in Fig. 1. The ice sample  $S$  was mounted in an aluminum receptacle  $R$ , which was surrounded by an ice-salt

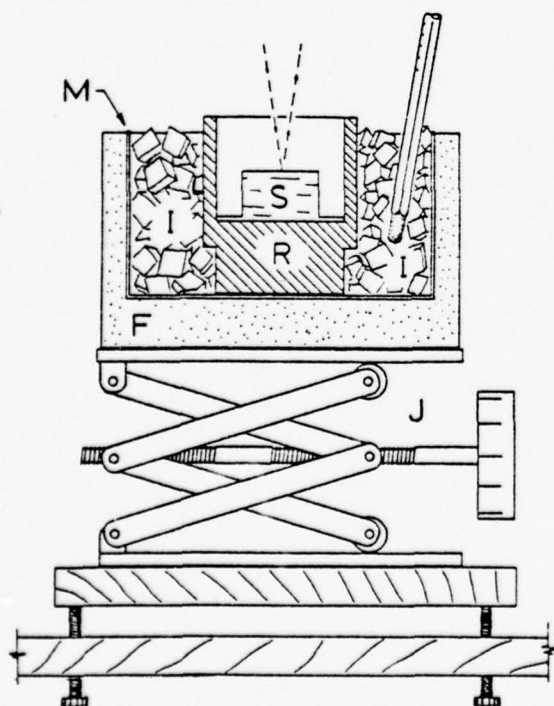


Fig. 1. Schematic diagram of sample holder.

mixture I in a metal container, which was encased in a polystyrene-foam sheath F. The plane reflecting surface of the ice sample could be positioned vertically by means of a laboratory jack J and could be made horizontal by means of the leveling screws shown in the figure. An auxiliary He-Ne laser beam was employed to advantage in the process of positioning the ice sample and the reference mirror. The temperature of the ice-salt mixture was continuously monitored by means of an ordinary thermometer and was maintained in the range  $-11 \pm 4$  °C; the corresponding temperature of the ice sample, which was monitored by means of an embedded thermocouple, was in the range  $-7 \pm 4$  °C. All reflectance measurements were made during winter months when the humidity of the surrounding air was low; during summer, formation of frost on the sample surface made reflectance measurements impossible.

The polycrystalline ice samples were prepared from freshly boiled distilled de-ionized water samples, which were frozen against flat Plexiglass plates in the ice tray of a commercial refrigerator. In a laboratory cold room at 5 °C, we removed an ice sample from the tray, snapped off the Plexiglass, and cemented the sample to the bottom of the pre-cooled sample receptacle R with a layer of water. In comparing the reflectance of ice with that of the reference mirror, it is necessary to use a plane ice surface of good optical quality. After a sample had been cemented to the cold receptacle, the entire receptacle-bath assembly was tilted to approximately 40° with the horizontal; with the sample in this position, we pressed the surface of a highly polished aluminum block at approximately 5 °C gently against the sample surface so as to melt the surface layer, after which a thin layer of liquid water was observed to flow along the surface. After several applications of the polished aluminum block, we were able to produce a crack-free surface capable of producing undistorted images by reflection at large angles of incidence. The close agreement between the values of nominal reflectance  $R_n$  subsequently obtained with different ice samples indicates that our procedures resulted in satisfactory sample surfaces.

### REFLECTION SPECTRUM

The spectral reflectance of ice at near-normal incidence is shown in Fig. 2. The reflectance curve shown in the figure is based on eight completely independent sets of reflectance measurements; the error bars shown in the figure are based upon the standard deviations involved in the determination of nominal reflectance  $R_n$  and in the determination of reference-mirror reflectance  $\mu$ . The uncertainties represented by the error bars are largest in spectral regions where the spectral-reflectance curve has a large slope; the increase of uncertainty in these regions is associated with the spectrometer's failure to reproduce prism settings. The spectral slit widths used in different parts of the

spectrum are indicated by vertical bars in the figure and were, in general, small compared with the dispersive features shown in the reflectance curve.

A major dispersive feature in the spectral-reflectance curve is centered at 3385  $\text{cm}^{-1}$ ; the reflectance has a minimum value of 0.0011 at 3530  $\text{cm}^{-1}$  and a maximum of 0.0866 at 3240  $\text{cm}^{-1}$ . A barely identifiable inflection occurs at 3415  $\text{cm}^{-1}$ , and a clearly visible shoulder appears at 3180  $\text{cm}^{-1}$ . A less-prominent dispersive feature centered at 2225  $\text{cm}^{-1}$  has a minimum reflectance of 0.0208 at 2285  $\text{cm}^{-1}$  and a reflectance maximum of 0.0220 at 2165  $\text{cm}^{-1}$ . A comparable feature centered near 1648  $\text{cm}^{-1}$  has a reflectance minimum of 0.0157 at 1725  $\text{cm}^{-1}$  and a reflectance maximum of 0.0198 at 1570  $\text{cm}^{-1}$ . A second major dispersive feature centered near 848  $\text{cm}^{-1}$  exhibits a reflectance minimum of 0.0055 at 950  $\text{cm}^{-1}$  and a reflectance maximum of 0.0608 at 745  $\text{cm}^{-1}$ . There are some indications of shoulders at 600 and 510  $\text{cm}^{-1}$ . Values of spectral reflectance for selected frequencies are listed in Table I; Fig. 2 provides a basis for interpolation between the tabulated values.<sup>17</sup>

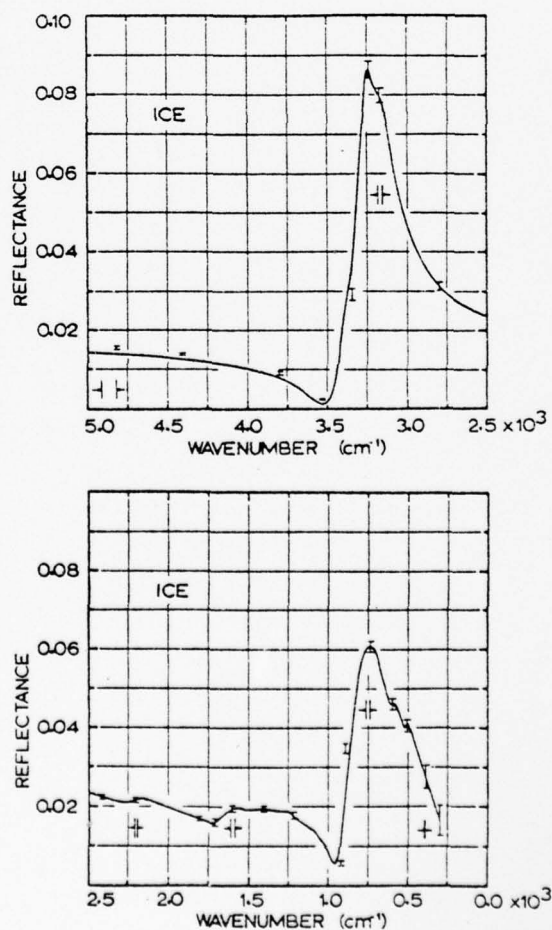


Fig. 2. Normal-incidence spectral reflectance of ice at  $-7$  °C.

TABLE I. Reflectivity and optical constants of ice at  $-7^{\circ}\text{C}$ .

$\nu$ ( $\text{cm}^{-1}$ )	$R$	$n_r$	$n_i$	$\lambda$ ( $\mu\text{m}$ )	$\nu$ ( $\text{cm}^{-1}$ )	$R$	$n_r$	$n_i$	$\lambda$ ( $\mu\text{m}$ )
5000	0.0143	1.272	0.000	2.000	1750	0.0159	1.287	0.035	5.714
4800	0.0138	1.267	0.000	2.083	1740	0.0158	1.285	0.038	5.747
4600	0.0133	1.260	0.001	2.174	1730	0.0158	1.284	0.042	5.780
4400	0.0125	1.252	0.001	2.273	1720	0.0158	1.283	0.046	5.814
4200	0.0115	1.241	0.003	2.381	1710	0.0158	1.283	0.052	5.848
4000	0.0102	1.225	0.004	2.500	1700	0.0161	1.285	0.057	5.882
3900	0.0092	1.212	0.004	2.564	1650	0.0180	1.301	0.069	6.061
3800	0.0077	1.192	0.005	2.632	1630	0.0188	1.309	0.070	6.135
3700	0.0056	1.162	0.008	2.703	1600	0.0195	1.316	0.067	6.250
3600	0.0027	1.108	0.020	2.778	1590	0.0197	1.318	0.065	6.289
3550	0.0013	1.065	0.038	2.817	1580	0.0197	1.320	0.064	6.329
3540	0.0012	1.056	0.044	2.825	1570	0.0198	1.321	0.062	6.369
3530	0.0011	1.046	0.052	2.833	1560	0.0198	1.321	0.059	6.410
3520	0.0012	1.037	0.060	2.841	1550	0.0198	1.321	0.057	6.452
3510	0.0013	1.027	0.068	2.849	1540	0.0196	1.320	0.056	6.494
3500	0.0016	1.016	0.079	2.857	1520	0.0193	1.317	0.055	6.579
3480	0.0031	0.995	0.110	2.874	1500	0.0191	1.315	0.057	6.667
3460	0.0055	0.979	0.146	2.890	1480	0.0193	1.317	0.058	6.757
3440	0.0100	0.960	0.193	2.907	1450	0.0194	1.318	0.057	6.897
3420	0.0171	0.967	0.257	2.924	1420	0.0194	1.318	0.055	7.042
3410	0.0192	0.978	0.276	2.933	1400	0.0194	1.318	0.055	7.143
3400	0.0217	0.987	0.295	2.941	1380	0.0193	1.318	0.054	7.246
3380	0.0266	1.004	0.331	2.959	1360	0.0192	1.317	0.052	7.353
3360	0.0321	1.021	0.367	2.976	1340	0.0190	1.315	0.052	7.463
3340	0.0395	1.035	0.411	2.994	1320	0.0189	1.314	0.052	7.576
3320	0.0494	1.064	0.466	3.012	1300	0.0189	1.314	0.052	7.692
3300	0.0603	1.104	0.522	3.030	1280	0.0189	1.314	0.050	7.812
3280	0.0732	1.170	0.584	3.049	1260	0.0187	1.313	0.047	7.937
3270	0.0797	1.217	0.612	3.058	1240	0.0185	1.311	0.043	8.065
3260	0.0841	1.273	0.627	3.067	1220	0.0179	1.306	0.039	8.197
3250	0.0858	1.330	0.625	3.077	1200	0.0170	1.297	0.037	8.333
3240	0.0866	1.384	0.614	3.086	1180	0.0165	1.292	0.039	8.475
3230	0.0858	1.432	0.593	3.096	1150	0.0156	1.282	0.040	8.696
3220	0.0839	1.469	0.564	3.106	1120	0.0147	1.272	0.042	8.929
3210	0.0826	1.499	0.539	3.115	1100	0.0141	1.265	0.044	9.091
3200	0.0816	1.527	0.515	3.125	1080	0.0135	1.258	0.045	9.259
3190	0.0809	1.553	0.491	3.135	1050	0.0122	1.244	0.046	9.524
3180	0.0803	1.578	0.465	3.145	1020	0.0102	1.219	0.047	9.804
3170	0.0797	1.603	0.438	3.155	1000	0.0085	1.197	0.051	10.0
3160	0.0786	1.623	0.406	3.165	980	0.0068	1.167	0.065	10.2
3150	0.0771	1.640	0.372	3.175	970	0.0061	1.150	0.075	10.3
3140	0.0750	1.650	0.336	3.185	960	0.0055	1.132	0.088	10.4
3120	0.0700	1.653	0.267	3.205	950	0.0055	1.113	0.108	10.5
3100	0.0648	1.641	0.210	3.226	940	0.0062	1.097	0.134	10.6
3050	0.0544	1.593	0.121	3.279	930	0.0082	1.088	0.168	10.8
3000	0.0467	1.545	0.074	3.333	920	0.0111	1.085	0.204	10.9
2950	0.0416	1.511	0.041	3.390	900	0.0197	1.101	0.280	11.1
2900	0.0370	1.476	0.024	3.448	880	0.0292	1.150	0.341	11.4
2850	0.0337	1.449	0.015	3.509	860	0.0370	1.202	0.379	11.6
2800	0.0311	1.428	0.009	3.571	840	0.0445	1.259	0.409	11.9
2750	0.0290	1.410	0.008	3.636	820	0.0504	1.320	0.422	12.2
2700	0.0275	1.398	0.007	3.704	800	0.0558	1.387	0.422	12.5
2600	0.0250	1.376	0.007	3.846	780	0.0587	1.445	0.403	12.8
2500	0.0234	1.361	0.010	4.000	770	0.0598	1.472	0.389	13.0
2400	0.0219	1.348	0.012	4.167	760	0.0606	1.496	0.374	13.2
2350	0.0214	1.343	0.015	4.255	750	0.0608	1.517	0.354	13.3
2300	0.0209	1.337	0.020	4.348	740	0.0608	1.534	0.335	13.5
2280	0.0209	1.337	0.023	4.386	730	0.0607	1.549	0.315	13.7
2250	0.0210	1.338	0.026	4.444	720	0.0607	1.563	0.294	13.9
2220	0.0213	1.340	0.029	4.505	710	0.0603	1.575	0.271	14.1
2200	0.0217	1.344	0.030	4.545	700	0.0592	1.581	0.246	14.3
2170	0.0220	1.347	0.025	4.608	680	0.0564	1.583	0.198	14.7
2150	0.0219	1.347	0.021	4.651	660	0.0524	1.565	0.164	15.2
2100	0.0213	1.341	0.015	4.762	650	0.0509	1.558	0.152	15.4
2000	0.0198	1.327	0.012	5.000	640	0.0497	1.552	0.142	15.6
1900	0.0182	1.312	0.014	5.263	620	0.0471	1.536	0.128	16.1
1800	0.0167	1.296	0.024	5.556	610	0.0463	1.531	0.125	16.4



TABLE I. (continued)

$\nu$ ( $\text{cm}^{-1}$ )	$R$	$n_r$	$n_i$	$\lambda$ ( $\mu\text{m}$ )	$\nu$ ( $\text{cm}^{-1}$ )	$R$	$n_r$	$n_i$	$\lambda$ ( $\mu\text{m}$ )
600	0.0464	1.532	0.123	16.7	500	0.0412	1.504	0.067	20.0
590	0.0464	1.534	0.116	16.9	490	0.0404	1.500	0.055	20.4
580	0.0461	1.534	0.107	17.2	480	0.0393	1.492	0.045	20.8
550	0.0433	1.519	0.079	18.2	450	0.0352	1.461	0.029	22.2
530	0.0406	1.498	0.072	18.9	400	0.0289	1.408	0.030	25.0
520	0.0402	1.495	0.076	19.2	350	0.0227	1.350	0.053	28.6
510	0.0408	1.500	0.075	19.6	300	0.0167	1.274	0.106	33.3

## KRAMERS-KRONIG ANALYSIS

The real and imaginary parts of the refractive index of a material are given by the expressions

$$n_r = [1 - R] / [1 + R - 2\sqrt{R} \cos\phi], \quad (1)$$

$$n_i = [-2\sqrt{R} \sin\phi] / [1 + R - 2\sqrt{R} \cos\phi], \quad (2)$$

where  $R$  is the normal-incidence reflectance and  $\phi$  is the phase angle used in expressing the complex reflectivity  $\hat{r}$  in polar form:  $\hat{r} = \sqrt{R}e^{i\phi}$ . The phase angle  $\phi(\nu_0)$  at frequency  $\nu_0$  to be used in Eqs. (1) and (2) can be calculated rigorously from the Kramers-Kronig integral

$$\phi(\nu_0) = (2\nu_0/\pi)P \int_0^\infty \frac{\ln\sqrt{R(\nu)}d\nu}{\nu_0^2 - \nu^2}, \quad (3)$$

where  $P$  denotes the Cauchy principal value, provided that the reflectance  $R(\nu)$  is known for all frequencies. If values of  $R(\nu)$  have been accurately measured for a finite frequency interval, Eq. (3) can be used to provide values of phase angles  $\phi$  within this interval, provided

TABLE II. Band characteristics at various temperatures.

Band Characteristics	Water <sup>a</sup>			Ice		
	70 °C	27 °C	5 °C	-7 °C <sup>b</sup>	-170 °C <sup>c</sup>	
$\nu_{1,3}$	$n_r$ min	1.126	1.119	1.104	0.958	1.015
	$\nu_r$ min ( $\text{cm}^{-1}$ )	3620	3590	3560	3430	3430
	$n_r$ max	1.440	1.484	1.501	1.653	1.861
	$\nu_r$ max ( $\text{cm}^{-1}$ )	3150	3150	3155	3125	3120
	$n_i$ max	0.236	0.297	0.316	0.627	0.815
	$\nu_i$ max ( $\text{cm}^{-1}$ )	3450	3395	3380	3260	3230
$\Gamma$ ( $\text{cm}^{-1}$ )	380	390	370	260	180	
$\nu_2$	$n_r$ min	1.218	1.232	1.246	1.283	1.310
	$\nu_r$ min ( $\text{cm}^{-1}$ )	1680	1680	1680	1715	1715
	$n_r$ max	1.338	1.349	1.338	1.321	1.337
	$\nu_r$ max ( $\text{cm}^{-1}$ )	1590	1600	1585	1565	1445
	$n_i$ max	0.107	0.137	0.109	0.070	0.060
	$\nu_i$ max ( $\text{cm}^{-1}$ )	1640	1650	1640	1640	1600
$\Gamma$ ( $\text{cm}^{-1}$ )	80	110	120	220	330	
$\nu_L$	$n_r$ min	1.113	1.116	1.086	1.085	1.105
	$\nu_r$ min ( $\text{cm}^{-1}$ )	840	840	845	920	950
	$n_r$ max	...	1.553 <sup>d</sup>	1.544 <sup>d</sup>	1.584	1.565
	$\nu_r$ max ( $\text{cm}^{-1}$ )	...	330 <sup>d</sup>	330 <sup>d</sup>	690	760
	$n_i$ max	0.430	0.443	0.438	0.462	0.395
	$\nu_i$ max ( $\text{cm}^{-1}$ )	510	580	590	810	830
$\Gamma$	540 <sup>d</sup>	500 <sup>d</sup>	500 <sup>d</sup>	230	195	

<sup>a</sup> Reference 18.

<sup>b</sup> Present study.

<sup>c</sup> Reference 14.

<sup>d</sup> Estimated value.

that approximate values of  $R(\nu)$  can be established outside the frequency interval.

Because our measurements were confined to the frequency range 300–5000  $\text{cm}^{-1}$ , it was necessary to use estimated values of  $R(\nu)$  outside this range. For the far-infrared region  $10 \leq \nu < 300 \text{ cm}^{-1}$ , we assumed values of  $R(\nu)$  based primarily on the low-temperature data of Bertie *et al.*<sup>14</sup>; their values were scaled to  $-7^\circ\text{C}$  on the basis of considerations given by Irvine and Pollack<sup>1</sup> together with the earlier far-infrared data of Bertie and Whalley.<sup>9</sup> Our initial estimates of  $R(\nu)$  were adjusted to match the absorption feature at 215  $\text{cm}^{-1}$  reported by Zimmerman and Pimentel<sup>6</sup> for ice at  $-7^\circ\text{C}$  and were also adjusted for a smooth match at 300  $\text{cm}^{-1}$  with our spectral-reflectance curve. For the low-frequency region  $0 \leq \nu \leq 10 \text{ cm}^{-1}$ , we assumed that the value of  $R(\nu)$  was constant and equal to its value at 10  $\text{cm}^{-1}$ .

In selecting values of  $R(\nu)$  for use in Eq. (3) in the range  $\nu > 5000 \text{ cm}^{-1}$ , we extended our reflectance measurements to 7800  $\text{cm}^{-1}$ . The resulting values were then matched to values of  $R(\nu)$  based on the Irvine-Pollack survey in the range 8000–10 000  $\text{cm}^{-1}$ . At frequencies higher than 10 000  $\text{cm}^{-1}$ ,  $R(\nu)$  was assigned a constant value equal to its value at 10 000  $\text{cm}^{-1}$ .

Values of  $\phi(\nu)$  were obtained from Eq. (3) by means of a computer program written by Hale and Query and used in our earlier study of water<sup>18</sup>; the resulting values were tabulated at 10- $\text{cm}^{-1}$  intervals throughout the range 300–5000  $\text{cm}^{-1}$ . Since the value of  $\phi(\nu_0)$  at frequency  $\nu_0$  depends on values of  $R(\nu)$  at all frequencies covered by the integral in (3), evaluation of the uncertainties in  $\phi(\nu_0)$  presents difficulties; however, for the range of uncertainties in measured reflectance indicated in Fig. 2, computer results indicate an average uncertainty  $\delta\phi(\nu_0) = \pm 0.003 \text{ rad}$  for most of the frequency range covered in our experimental work. Values of  $\phi(\nu_0)$  for most of the range for which we have measured  $R(\nu)$  are relatively insensitive to detailed assumptions regarding values of  $R(\nu)$  outside the range provided that the assumed spectral-reflectance curves are matched smoothly to the measured curve.

## OPTICAL CONSTANTS

Values of the optical constants  $n_r$  and  $n_i$  were obtained from Eqs. (1) and (2) by use of measured values

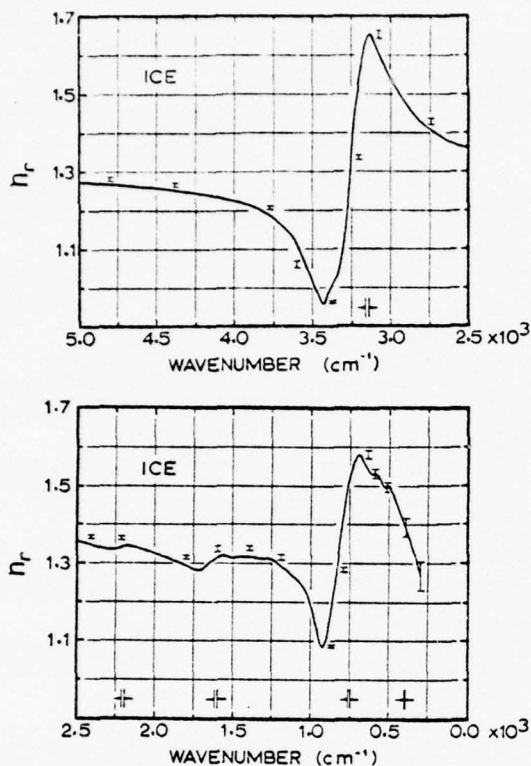


FIG. 3. Real part  $n_r$  of the refractive index of ice as a function of frequency, in wave numbers.

of reflectance  $R$  and values of  $\phi$  given by the Kramers-Kronig integral in Eq. (3). Values of optical constants are listed for selected frequencies in Table I and are presented graphically as a function of wave number in Figs. 3 and 4; the curves in the figures provide a basis of interpolation between values of  $n_r$  and  $n_i$  listed in the table.

The plot of  $n_r$  in Fig. 3 shows a major dispersive feature centered at 3278  $\text{cm}^{-1}$  with  $n_{r \text{ min}} = 0.958$  at 3430  $\text{cm}^{-1}$  and  $n_{r \text{ max}} = 1.653$  at 3125  $\text{cm}^{-1}$ . The minor dispersive feature centered at 2223  $\text{cm}^{-1}$  is characterized by  $n_{r \text{ min}} = 1.337$  at 2285  $\text{cm}^{-1}$  and  $n_{r \text{ max}} = 1.348$  at 2160  $\text{cm}^{-1}$ ; the minor feature centered at 1640  $\text{cm}^{-1}$  is characterized by  $n_{r \text{ min}} = 1.283$  at 1715  $\text{cm}^{-1}$  and  $n_{r \text{ max}} = 1.321$  at 1565  $\text{cm}^{-1}$ . A second major dispersive feature centered at 805  $\text{cm}^{-1}$  is characterized by  $n_{r \text{ min}} = 1.085$  at 920  $\text{cm}^{-1}$  and  $n_{r \text{ max}} = 1.584$  at 690  $\text{cm}^{-1}$ ; two small shoulders appear near 593 and 510  $\text{cm}^{-1}$ . Estimated uncertainties in  $n_r$  are indicated by the error bars in Fig. 3.

In Fig. 4, our values of  $n_i$  are plotted as a function of wave number; over the range 5000–4000  $\text{cm}^{-1}$ , values of  $n_i$  based on our reflection measurements are not significantly different from zero. The  $n_i$  plot in the upper panel is dominated by the strong absorption band with  $n_{i \text{ max}} = 0.627$  at 3260  $\text{cm}^{-1}$ ; the bandwidth parameter  $\Gamma$  giving full width at half-maximum is

260  $\text{cm}^{-1}$  for this band. The much-weaker band at 2210  $\text{cm}^{-1}$  has peak value  $n_{i \text{ max}} = 0.030$  and bandwidth parameter  $\Gamma = 260 \text{ cm}^{-1}$ ; a second weak band at 1640  $\text{cm}^{-1}$  has  $n_{i \text{ max}} = 0.070$  and  $\Gamma = 290 \text{ cm}^{-1}$ . A second major absorption band centered at 810  $\text{cm}^{-1}$  has  $n_{i \text{ max}} = 0.425$  and  $\Gamma = 225 \text{ cm}^{-1}$ ; two small shoulders can be distinguished at 590 and 520  $\text{cm}^{-1}$ . Uncertainties in  $n_i$  are indicated at various points along the curve.

## DISCUSSION OF RESULTS

The results of the present study are compared in Figs. 5 and 6 with the values of  $n_r$  and  $n_i$  listed by Irvine and Pollack<sup>1</sup> on the basis of their survey of earlier work; the continuous curves in these figures give the present results and the points represent values obtained in the earlier survey. The most-serious disagreements between the present results and those of Irvine and Pollack occur in the vicinity of the strong absorption bands near 3260 and 810  $\text{cm}^{-1}$ ; these are the regions in which reflectance data are most useful, because it is extremely difficult to prepare the thin films of uniform thickness required for quantitative measurements of transmittance. Comparison of the results for  $n_r$ , shown in Fig. 5 indicates best agreement in the region between 5000 and 3750  $\text{cm}^{-1}$  and rather poor agreement in other spectral regions; in Fig. 6 our values for  $n_i$  are much larger at the centers of the strong absorption bands but

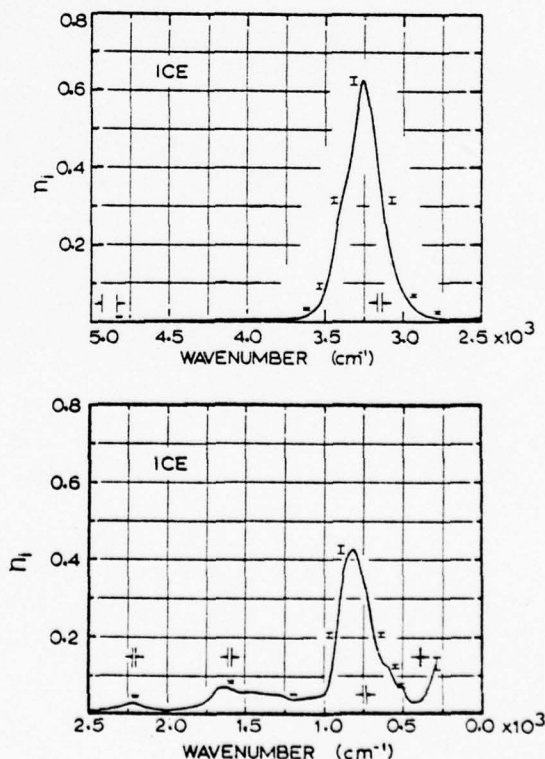


FIG. 4. Imaginary part  $n_i$  of the refractive index of ice as a function of frequency, in wave numbers.

are in fair agreement with the Irvine-Pollack values in the region between 3000 and 1000  $\text{cm}^{-1}$ . In view of the fair agreement between our values of  $n_r$  and those based on the survey in the region between 5000 and 3750  $\text{cm}^{-1}$ , it is probable that the Irvine-Pollack values of  $n_i$  in this region, which are based largely on transmittance measurements, are satisfactory for atmospheric calculations; our reflectance measurements gave no valid values of  $n_i$  in this region of weak absorption.

The strong absorption band centered near 3260  $\text{cm}^{-1}$  in Fig. 6 occurs in the region where OH groups have characteristic vibration bands and is usually attributed chiefly to the  $\nu_1$  and  $\nu_3$  fundamentals of  $\text{H}_2\text{O}$  monomers in the lattice. The weaker band centered at 1640  $\text{cm}^{-1}$  is similarly attributed to the bending  $\nu_2$  fundamental of the  $\text{H}_2\text{O}$  monomer. The strong absorption band with maximum at 810  $\text{cm}^{-1}$  is attributed to a hindered-rotational or librational mode  $\nu_L$  of the  $\text{H}_2\text{O}$  monomer in the field of its neighbors. The weak band with maximum near 2210  $\text{cm}^{-1}$  is usually referred to as an associational band and attributed to a combination of  $\nu_2$  with a librational mode. It is of interest to consider the variation of these bands with temperature changes in water and in ice.

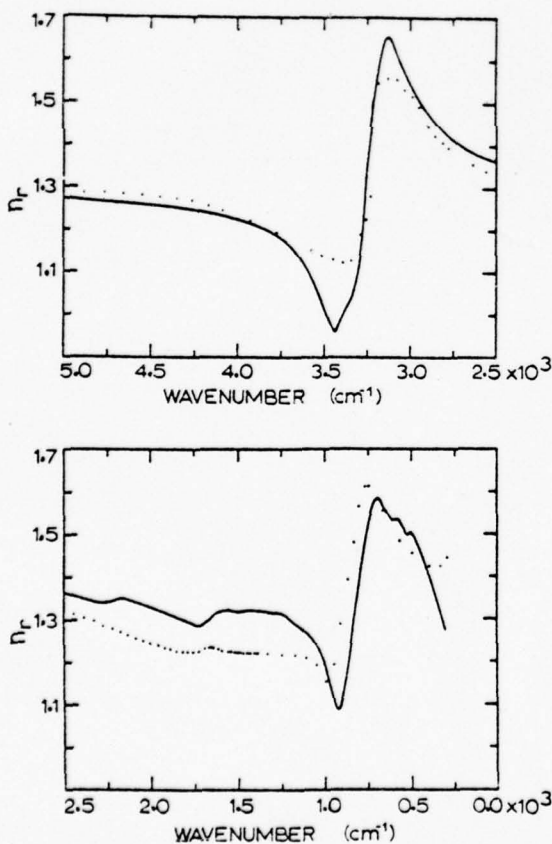


FIG. 5. Comparison of present results for  $n_r$ , given by the continuous curve, with values of  $n_r$  listed in the Irvine-Pollack survey given by points.

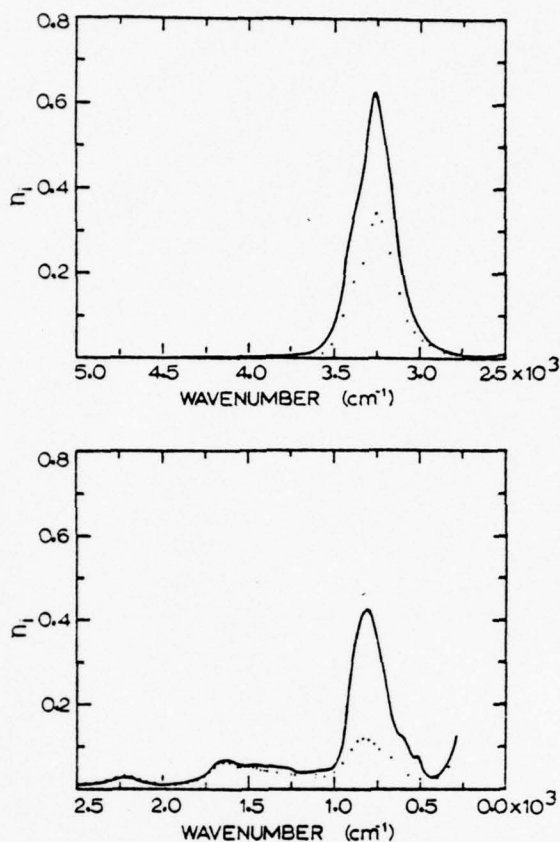


FIG. 6. Comparison of present results for  $n_i$ , given by the continuous curve, with values of  $n_i$  listed in the Irvine-Pollack survey given by points.

Table II gives a summary of major-band characteristics as a function of temperature in water and ice. The absorption band, which is designated as  $\nu_{1,3}$  since it is primarily due to the monomer fundamentals  $\nu_1$  and  $\nu_3$ , shifts to lower frequencies and becomes narrower as the temperature is decreased; the value of  $n_{i, \max}$  and the difference  $n_{r, \max} - n_{r, \min}$  increase monotonically with decrease of temperature. The  $\nu_2$  band in liquid water remains virtually unchanged in position and in peak values of absorption  $n_{i, \max}$  with change of temperature; in ice, the frequency and the value of  $n_{i, \max}$  decrease as the temperature decreases. In both water and ice, the bandwidth parameter  $\Gamma$  increases as the temperature is reduced. The frequency of the librational band  $\nu_L$  increases monotonically with decreasing temperature; the phase change from liquid to solid is accompanied by a sudden increase of the frequency of  $\nu_L$ . The peak value of  $n_i$  for the  $\nu_L$  band is nearly independent of temperature in both water and ice; however, a marked narrowing of the band accompanies freezing.

The data for the associational band centered at 2210  $\text{cm}^{-1}$  in Fig. 6 are not included in Table II; the

frequency of this band increases to  $2240\text{ cm}^{-1}$  and the bandwidth nearly doubles in ice as the temperature is reduced to  $-170\text{ }^{\circ}\text{C}$ .

The values of  $n_r$  and  $n_i$  given in Table I should be of use in calculations of the scattering of infrared radiation by ice particles in the lower telluric atmosphere. For ice in planetary atmospheres at lower temperatures, it is possible that interpolation between the optical constants at  $-7$  and  $-170\text{ }^{\circ}\text{C}$  may provide useful values of  $n_r$  and  $n_i$ . Some of the features of Table II should be useful in making the interpolation.

It is highly desirable that quantitative reflectance measurements be made in the vicinity of the hindered-translational band near  $215\text{ cm}^{-1}$  to serve as a supplement to earlier transmission studies of this band.

#### ACKNOWLEDGMENTS

We wish to thank Professor Basil Curnutte and Professor Marvin Querry for numerous helpful discussions.

#### REFERENCES

\*Supported in part by the Office of Naval Research. Paper presented at 1973 Spring Meeting [J. Opt. Soc. Am. 63, 493A (1973)].

- <sup>1</sup>W. M. Irvine and J. B. Pollack, *Icarus* 8, 324 (1968).
- <sup>2</sup>W. Luck, *Ber. Bunsenges. Phys. Chem.* 67, 186 (1963).
- <sup>3</sup>N. Ockmann, *Adv. Phys.* 7, 199 (1958); Doctoral dissertation, University of Michigan (1957).
- <sup>4</sup>F. P. Reding, Thesis, Brown University (1951).
- <sup>5</sup>J. J. Fox and A. E. Martin, *Proc. R. Soc. A* 174, 234 (1940).
- <sup>6</sup>R. Zimmerman and G. C. Pimentel, *Proc. Intern. Meeting Mol. Spectry, Bologna* 2, 726 (1962).
- <sup>7</sup>C. H. Cartwright and J. Errera, *Proc. R. Soc. A* 154, 138 (1936).
- <sup>8</sup>J. E. Bertie and E. Whalley, *J. Chem. Phys.* 40, 1637 (1964).
- <sup>9</sup>J. E. Bertie and E. Whalley, *J. Chem. Phys.* 46, 1271 (1967).
- <sup>10</sup>M. Weingeroff, *Z. Phys.* 70, 104 (1931).
- <sup>11</sup>G. Bode, *Ann. Phys. (Leipz.)* 30, 326 (1909).
- <sup>12</sup>L. D. Kislovski, *Opt. Spektrosk.* 7, 201 (1959) [*Opt. Spectrosc.* 7, 311 (1959)].
- <sup>13</sup>A. J. Alkezweeny and P. V. Hobbs, *J. Geophys. Res.* 71, 1083 (1966).
- <sup>14</sup>J. E. Bertie, H. J. Labbé, and E. Whalley, *J. Chem. Phys.* 50, 4501 (1969).
- <sup>15</sup>A. N. Rusk, D. Williams, and M. R. Querry, *J. Opt. Soc. Am.* 61, 895 (1971).
- <sup>16</sup>J. Strong, *Procedures in Experimental Physics* (Prentice-Hall, New York, 1938), p. 376.
- <sup>17</sup>More-detailed tabulation of results along with a more detailed analysis of uncertainties are presented in the doctoral dissertation of J. W. Schaaf, Kansas State University (1973).
- <sup>18</sup>G. M. Hale, M. R. Querry, A. N. Rusk, and D. Williams, *J. Opt. Soc. Am.* 62, 1103 (1972).

Of special importance to meteorological studies of the earth's heat balance is a knowledge of the optical constants of sea water. Sea water is also an important component of marine aerosols at altitudes near the surface of the sea. A knowledge of the optical constants of sea water is of obvious importance in many naval problems. Therefore, we made an investigation of this subject, which is summarized in the following article by Pinkley and Williams.

## Optical properties of sea water in the infrared\*

Lary W. Pinkley and Dudley Williams  
Kansas State University, Manhattan, Kansas 66506  
(Received 11 December 1975)

We have made quantitative measurements of the ratio of the infrared spectral reflectance of standard sea water at near-normal incidence to the corresponding spectral reflectance of pure water at 27°C. The infrared spectral reflectance of standard sea water was determined from the measured ratio and the known optical constants for pure water. The real  $n(\nu)$  and the imaginary  $k(\nu)$  parts of the complex index of refraction of standard sea water were then determined by Kramer-Kronig methods. The results obtained for the standard sea water are compared with previous results obtained for pure water and with previous studies of sea water.

In view of the fact that three-quarters of the earth's surface is covered by sea water, the optical properties of sea water have an important bearing on the earth's radiative heat balance; because the emission spectrum of the earth is largely in the intermediate infrared, a knowledge of the optical constants of sea water in this spectral region is of special importance. Detailed knowledge of these constants is also of importance to remote sensing of the earth's atmospheric and surface features from satellites and to infrared signal transmission through the atmosphere near the surface of the sea, where droplets of sea water are an important aerosol component of the atmosphere.

The present infrared study of sea water is a part of a research program dealing with the infrared properties of water, in which we have used quantitative measurements of absorption<sup>1</sup> and reflection<sup>2</sup> to determine the real  $n$  and imaginary  $k$  parts of the complex index of refraction  $\tilde{N} = n + ik$ . In a critical summary<sup>3</sup> of earlier work, we compare the  $n$  and  $k$  values obtained by Kramers-Kronig (KK) analyses of separate reflection and absorption measurements with the values of these constants based on a combination of absorption and reflec-

tion measurements. In general, KK analysis of reflection measurements provided excellent values of  $n$  and yielded good values of  $k$  in spectral regions of strong absorption. In the present study we have determined the reflectance  $R$  at near-normal incidence and have employed KK analysis to obtain  $n$  and  $k$  for sea water in the infrared.

In earlier studies we have investigated the influence of temperature<sup>4</sup> and various inorganic solutes<sup>5</sup> on the infrared reflectance of water; the results have a bearing on the spectrum of sea water, which, apart from its particulate and biologic components, is merely a dilute solution of certain salts. Hobson and Williams<sup>5</sup> have compared the spectral reflectance of sea water from various geographical locations with the reflection of pure water and with the reflection of the solutions of salts known to be present in sea water; the presence of the  $\text{SO}_4^{2-}$  ion produces readily observable effects in sea water. Querry and his associates<sup>7</sup> have also studied the reflection spectra of sea water from various sources and have made a detailed investigation of the influence of NaCl on the spectrum of water.

Because the concentration of the solutes in ocean

water varies with geographic location, various varieties of *standard sea water* (SSW) have been devised and used in laboratory studies. In the present investigation we have employed SSW prepared from the complete prescription of Lyman and Fleming,<sup>8</sup> which provides an extremely close approximation to clean ocean water. Friedman<sup>9</sup> has made a detailed study of SSW in which he measured spectral reflectance at large angles of incidence and, in certain spectral regions, made comparisons of the spectral transmittance of SSW and pure water. The SSW employed by Friedman included only  $\text{MgCl}_2 \cdot 6\text{H}_2\text{O}$ ,  $\text{NaCl}$ ,  $\text{MgSO}_4 \cdot 7\text{H}_2\text{O}$ , and  $\text{CaCl}_2$ , which are the major components of the Lyman-Fleming prescription; the concentration of minor components is so small that their contributions to the observable spectrum of sea water is probably completely negligible. In the course of his work, Friedman also employed solutions having 0.5 the normal solute concentration (SSW-0.5), along with multiples 1.5 (SSW-1.5) and 2 (SSW-2) of the normal concentration; the use of these solutions facilitated estimates of the effects of salinity on the spectral properties of sea water.

In the present study we made a careful comparison of the spectral reflectances of SSW and SSW-2 with that of pure water at near-normal incidence in the spectral range 350–6700  $\text{cm}^{-1}$ . The results are shown in Fig. 1 in which we plot the measured ratios  $R(\nu)_{\text{SSW}}/R(\nu)_w$  and  $R(\nu)_{\text{SSW-2}}/R(\nu)_w$  as a function of wave number in the range 400–5200  $\text{cm}^{-1}$ . The length of the uncertainty bars shown at selected wave numbers on the SSW curve also apply to the SSW-2 curve. In most spectral regions the uncertainty in the ratio plotted in Fig. 1 amounts to approximately  $\pm 0.01$  but becomes larger in regions of low spectral reflectance near 3700 and 900  $\text{cm}^{-1}$  and in regions where spectral reflectance changes rapidly with frequency. The results shown in Fig. 1 indicate that the spectral reflectance of sea water is greater than that of pure water in most of the infrared region but is significantly lower in the vicinity of 800  $\text{cm}^{-1}$ .

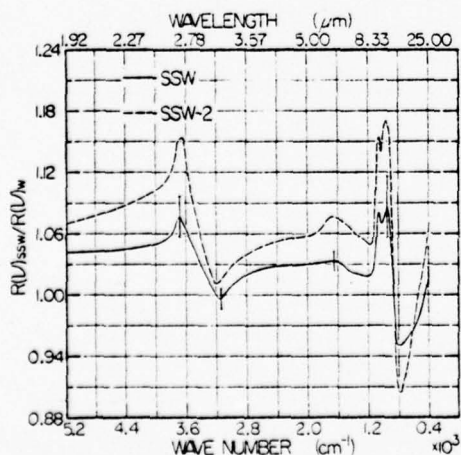


FIG. 1. Ratio of the near-normal-incidence spectral reflectances of SSW and SSW-2 to that of water. Samples were at 27°C.

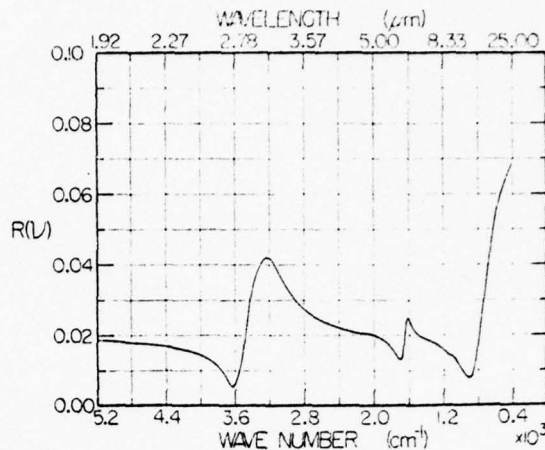


FIG. 2. Near-normal-incidence spectral reflectance  $R(\nu)$  of standard sea water at 27°C.

The spectral reflectances  $R(\nu)$  for SSW and SSW-2 were obtained by using the measured ratios of their reflectance to water reflectance. In arriving at values for the spectral reflectance  $R(\nu)_w$  of water we used values of reflectance computed from tabulated values<sup>3</sup> of  $n(\nu)$  and  $k(\nu)$ , which in turn are based on numerous quantitative measurements of reflection and absorption covering the spectral range 28 000 to 1  $\text{cm}^{-1}$ . The resulting values of  $R(\nu)$  for SSW are shown in Fig. 2. The low values of  $R(\nu)$  near 3600 and 900  $\text{cm}^{-1}$  were verified by direct measurements involving a calibrated reference mirror. Except for small shifts in frequency, the major features of  $R(\nu)$  for SSW bear a close resemblance to the reflectance spectrum of pure water. However, a clearly visible small feature near 1100  $\text{cm}^{-1}$  has no counterpart in the spectrum of pure water. We also obtained the spectral reflectance spectrum of SSW-2, which as expected from Fig. 1 is also roughly comparable with the reflectance spectrum of pure water.

The values of  $R(\nu)$  shown in Fig. 2 were used in KK analysis to calculate values of the optical constants  $n(\nu)$  and  $k(\nu)$  for SSW. In arriving at these values we employed the KK phase-shift theorem

$$\phi(\nu) = \frac{2\nu}{\pi} P \int_0^{\infty} \frac{\ln[R(\nu')]^{1/2}}{\nu'^2 - \nu^2} d\nu', \quad (1)$$

where  $[R(\nu)]^{1/2}$  is the modulus of the complex reflectivity  $\hat{R} = [R(\nu)]^{1/2} \exp[i\phi(\nu)]$ . In terms of  $\phi$  and  $R$ , calculated values of  $n$  and  $k$  at any frequency are given by the relations

$$n = (1 - R)/(1 + R - 2R^{1/2} \cos\phi), \quad (2)$$

$$k = (-2R^{1/2} \sin\phi)/(1 + R - 2R^{1/2} \cos\phi). \quad (3)$$

We have used Eqs. (1)–(3) to obtain values for  $n(\nu)$  and  $k(\nu)$  for SSW and SSW-2 in the range 400–5200  $\text{cm}^{-1}$ . We have used a computer program based on Simpson's rule except in the vicinity of  $\nu$  where quadratic approximations of  $[R(\nu)]^{1/2}$  based on measured values of  $R(\nu)$  in the vicinity were used. Beyond the spectral range of actual measurement, 6700  $\text{cm}^{-1}$  to  $\infty$  and 0 to 350  $\text{cm}^{-1}$ , we employed extrapolations based on  $R(\nu)$  for pure

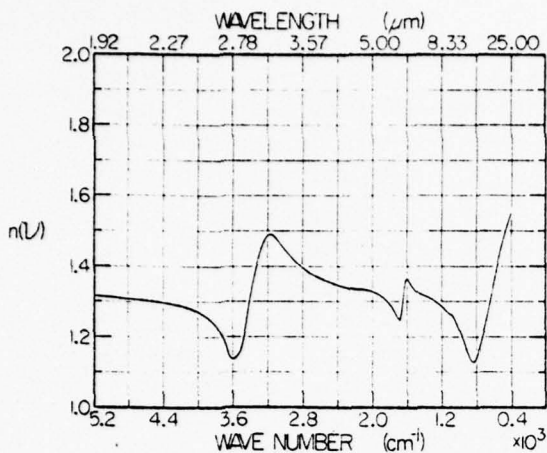


FIG. 3. Refractive index  $n(\nu)$  of standard sea water at 27 °C.

water,<sup>3,10</sup> which is known in the range 1 to 28 000  $\text{cm}^{-1}$ .

The values of  $n(\nu)$  for SSW are plotted as a function of wave number in Fig. 3. As in the case of  $R(\nu)$ , the general features of the  $n(\nu)$  curve strongly resemble those of the corresponding curve for pure water. In most spectral regions  $n(\nu)$  for SSW is slightly larger than the corresponding value for water. There are slight shifts in the major dispersion features near 3400 and 600  $\text{cm}^{-1}$  with respect to the corresponding features for pure water. The small inflection near 1100  $\text{cm}^{-1}$  is easily noted in Fig. 3. In general, the uncertainties in the values of  $n(\nu)$  amount to approximately  $\pm 0.005$ .

The values of the absorption index  $k(\nu)$  for SSW are plotted as a function of wave number in Fig. 4. The major absorption band near 3400  $\text{cm}^{-1}$  is attributed to the  $\nu_3$  and  $\nu_1$  fundamentals of the water molecule along with some contribution from the overtone  $2\nu_2$ ; the position and shape of this major band are strongly influenced by temperature changes<sup>4</sup> and by the nature and concentration of solutes<sup>5</sup> that modify the molecular surroundings of the water molecule. In SSW the band is shifted to slightly higher frequencies from its position in pure water. The sharp absorption band near 1650  $\text{cm}^{-1}$  is due to the  $\nu_2$  fundamental of the water molecule; although slightly altered in shape, its frequency in SSW is the same as in pure water. The major absorption band near 600  $\text{cm}^{-1}$  is associated with the librational or hindered rotational motion of the water molecule in the field of its neighbors; as in the case of the 3400  $\text{cm}^{-1}$  band, the position of the librational band  $\nu_L$  is dependent on water temperature<sup>4</sup> and on the nature and concentration of solutes.<sup>5</sup> In SSW it is shifted from its position in pure water to slightly lower frequencies.

The readily observable small absorption band near 1100  $\text{cm}^{-1}$  can be attributed to the  $\nu_3$  fundamental of the  $\text{SO}_4^{2-}$  ion.<sup>11</sup> Comparison of the spectrum of SSW-2 with SSW reveals that absorption near 1100  $\text{cm}^{-1}$  increases with increasing salt concentration. There are several small variations in  $k(\nu)$  in the 1200–1500  $\text{cm}^{-1}$  region but are not measurably different in the spectra of SSW-2.

In view of the direct dependence of the value of  $k(\nu)$  on  $\sin\phi(\nu)$  in (3), the absolute values of  $k(\nu)$  in regions of low absorption are strongly influenced by uncertainties in  $\phi(\nu)$  as determined by KK phase shift analysis (1). We have found that  $k(\nu)$  values based on KK analysis are highly unreliable for  $k(\nu) \leq 0.03$  but become increasingly reliable with increasing values of  $k(\nu)$ . The  $k(\nu)$  values in Fig. 4 are virtually meaningless in the spectral ranges 3700–5200  $\text{cm}^{-1}$  and 2900–1700  $\text{cm}^{-1}$ ; in these regions absorption measurements are needed.

Because the spectrum of SSW so closely resembles the spectrum of pure water, Friedman has proposed that its optical properties can best be provided by the use of small corrections to the values of  $n(\nu)$  and  $k(\nu)$  that have been established for pure water. In view of the fact that we have measured the ratio of the reflectance of SSW and SSW-2 to pure water, we have adopted this procedure since the small corrections will remain applicable in good approximation when more exact values of the optical constants of water become available. In arriving at values of the small corrections we have compared our own values of the optical constants<sup>3</sup> of pure water with those obtained for SSW and SSW-2 in the present study.

The curve shown in Fig. 5 gives the difference between  $n(\nu)$  for SSW and  $n(\nu)$  for pure water. In most spectral regions  $n(\nu)$  for SSW is greater than that of water. The two major exceptions to this statement are associated with the minima near 3550 and 650  $\text{cm}^{-1}$ , which are associated with changes in the frequency and contours of the major band near 3400  $\text{cm}^{-1}$  and the librational band near 600  $\text{cm}^{-1}$ , respectively. The corresponding curve for SSW-2 is shown in Fig. 6; the general features are similar to those for SSW except for larger differences between SSW-2 and water over much of the spectral range. Since the values of  $n(\nu)$  for the solutions are based on the properties of water, the length of the uncertainty bars are closely related to those shown in Fig. 1. The influence of the  $\text{SO}_4^{2-}$  absorption band near 1100  $\text{cm}^{-1}$  is clearly discernable in Figs. 5 and 6.

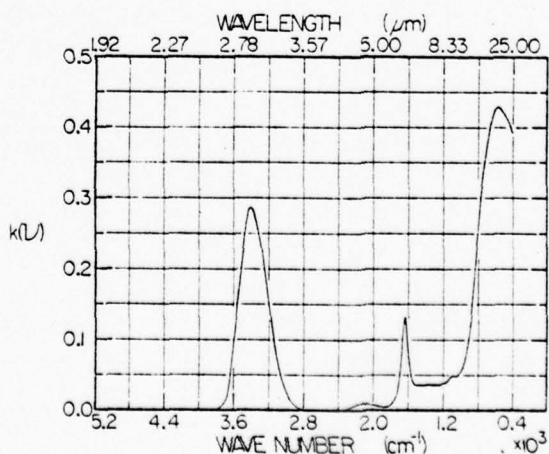


FIG. 4. Absorption index  $k(\nu)$  of standard sea water at 27 °C.



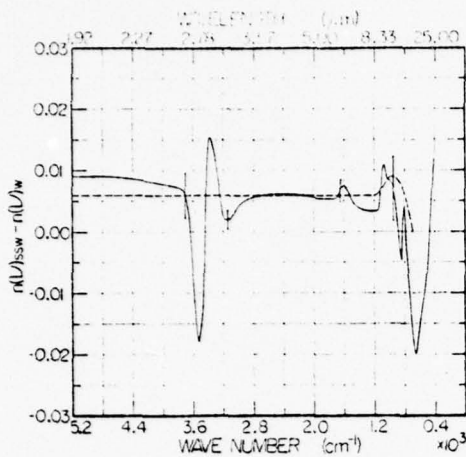


FIG. 5. Difference between the refractive index  $n(\nu)$  for SSW and that of pure water.

The dashed curves shown in Figs. 5 and 6 represent Friedman's proposed corrections to the  $n(\nu)$  for water that would give values of  $n(\nu)$  for SSW and SSW-2. The present results are in close agreement with those of Friedman between 3000 and 1500  $\text{cm}^{-1}$ ; our slightly larger values in the 5000–3800  $\text{cm}^{-1}$  region may be due to the fact that Friedman's values are based on the  $n(\nu)$  values of Pontier and Dechambenois<sup>12</sup> that differ from our values in this region. Friedman's corrections do not include those associated with changes in the 3400  $\text{cm}^{-1}$  water band produced by the solutes.

In view of our criticism of the absolute values of  $k(\nu)$  based on KK analysis (1) and (3) in regions where  $k(\nu)$  is small, it would appear that the present study would provide little basis for establishing corrections of  $k(\nu)$  for water to give corresponding values of  $k(\nu)$  for SSW. Closer examination of the actual computation of  $\phi(\nu)$  from (1) indicates that it is possible to provide significant corrections. In arriving at  $\phi(\nu)$  from (1), we ob-

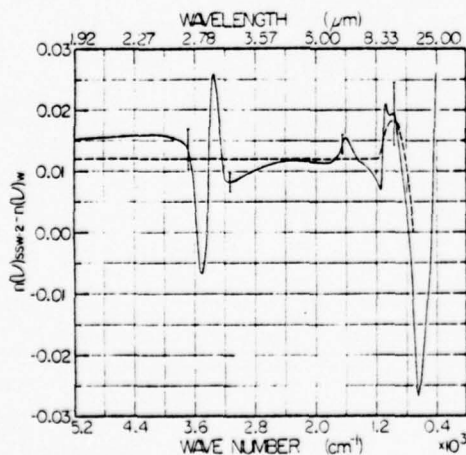


FIG. 6. Difference between the refractive index  $n(\nu)$  for double-concentration standard sea water (SSW-2) and that of pure water.

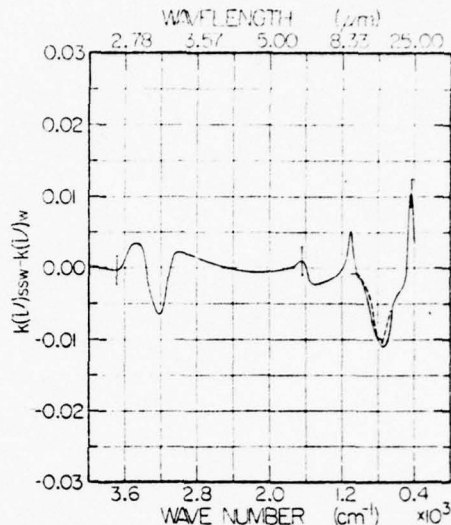


FIG. 7. Difference between the absorption index  $k(\nu)$  of SSW and that of pure water.

tain a value of  $\phi(\nu)$  that is the sum of  $\phi(\nu)_{\text{HFE}}$  based on high-frequency extrapolation,  $\phi(\nu)_M$  based on measured values of  $R(\nu)$ , and  $\phi(\nu)_{\text{LFE}}$  based on low-frequency extrapolation. In spectral regions where  $\phi(\nu)$  is small, its value given by (1) is strongly influenced by the extrapolations; this fact accounts for the large uncertainties in the absolute values of  $k(\nu)$  in regions of low absorption. In spectral regions where  $\phi$  is large, the magnitudes of  $\phi(\nu)_{\text{HFE}}$  and  $\phi(\nu)_{\text{LFE}}$  are small as compared with that of  $\phi(\nu)_M$ .

However, if we employ identical extrapolations for water and for SSW, we can obtain significant differences  $k(\nu)_{\text{SSW}} - k(\nu)_W$  even though the calculated values of these separate absorption indices may be unreliable. In establishing these corrections, we note that  $\phi(\nu)_{\text{SSW}} - \phi(\nu)_W = [\phi(\nu)_{\text{HFE}} + \phi(\nu)_M + \phi(\nu)_{\text{LFE}}]_{\text{SSW}} - [\phi(\nu)_{\text{HFE}} + \phi(\nu)_M + \phi(\nu)_{\text{LFE}}]_W = \phi(\nu)_{M-\text{SSW}} - \phi(\nu)_{M-W}$  provided identical high-frequency and low-frequency extrapolations are employed.

In Figs. 7 and 8 we show the results of values of  $k(\nu)_{\text{SSW}} - k(\nu)_W$  and  $k(\nu)_{\text{SSW-2}} - k(\nu)_W$ , respectively. In arriving at the values shown in these figures we used extrapolations based on  $R(\nu)_{\text{SSW}} = R(\nu)_W$  for  $\nu > 8000 \text{ cm}^{-1}$  and  $\nu < 350 \text{ cm}^{-1}$ . On the basis of uncertainties  $\pm 0.01$   $R(\nu)$  in measured values of the spectral reflectance of SSW, we estimate that the uncertainties in the differences in absorption indices plotted in Figs. 7 and 8 amount to less than  $\pm 0.002$  over most of the spectral range between 4000 and 400  $\text{cm}^{-1}$ . For  $\nu > 4000 \text{ cm}^{-1}$ , the calculated differences in absorption indices are influenced by the way in which the measured reflectance curves for sea water are merged with the values of  $R(\nu)_W$  used in the high-frequency extrapolation.

Over most of the spectral region 4000–400  $\text{cm}^{-1}$  the differences between  $k(\nu)$  values for SSW-1 and SSW-2 and the values of  $k(\nu)$  for water are small and the difference amounts to less than  $\pm 0.002$ . Differences larger than this occur in the 3400  $\text{cm}^{-1}$  region and in-

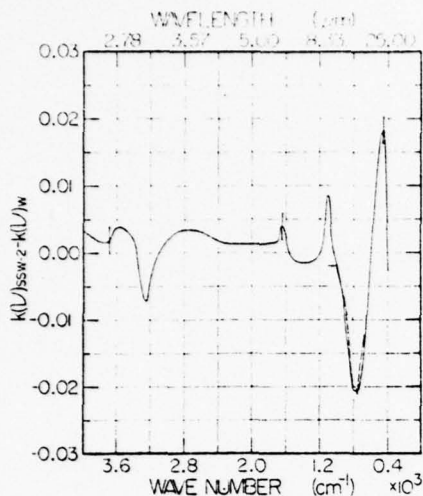


FIG. 8. Difference between the absorption index  $k(\nu)$  of double-concentration standard sea water (SSW-2) and that of pure water.

dicating a slight shift to higher frequency and possible changes in the contours of the water band caused by the influence of the solutes. Similar but larger differences are noted in the  $600\text{ cm}^{-1}$  region and are associated with a shift of the librational band to lower frequencies; the dashed curve in this region represents the differences in absorption index reported by Friedman on the basis of absorption measurements. The sharp peak near  $1100\text{ cm}^{-1}$  is associated with the  $\text{SO}_4^{2-}$  absorption band mentioned earlier; the total absorption  $\int k(\nu) d\nu$  associated with this band is roughly proportional to concentration.

It is gratifying to note the general agreement between the present results based on reflection measurements at near-normal incidence and the earlier results of Friedman,<sup>9</sup> who measured reflectance at large angles of incidence along with transmission measurements in certain restricted spectral ranges. In the present

study we have extended quantitative measurements to lower frequencies and have detected shifts in the  $3400\text{ cm}^{-1}$  water band not reported in Friedman's study.

On the basis of the refractive-index differences plotted in Fig. 5 and the absorption-index differences plotted in Fig. 7 one may obtain values of  $n(\nu)$  and  $k(\nu)$  for standard sea water by adding these differences to the values of these quantities tabulated by Downing and Williams.<sup>3</sup> Comparisons of Figs. 5 and 7 with Figs. 6 and 8 provide a measure of the variations in  $n(\nu)$  and  $k(\nu)$  with salinity. We emphasize that comparisons of the reflection and emission of real sea water may be somewhat different from those computed on the basis of the present values of the optical constants for standard sea water, which contains no particulate or biologic constituents.

We should like to express our appreciation to Professor Basil Curnutte and to Dr. Harry Downing for helpful suggestions and to Keith Consani who prepared our standard sea water samples under the supervision of Professor William G. Fateley.

\*Supported in part by the Office of Naval Research.

<sup>1</sup>C. W. Robertson and D. Williams, *J. Opt. Soc. Am.* **61**, 1316 (1971).

<sup>2</sup>A. N. Rusk, D. Williams, and M. R. Querry, *J. Opt. Soc. Am.* **61**, 895 (1971).

<sup>3</sup>H. D. Downing and D. Williams, *J. Geophys. Res.* **80**, 1656 (1975).

<sup>4</sup>G. M. Hale, M. R. Querry, A. N. Rusk, and D. Williams, *J. Opt. Soc. Am.* **62**, 1103 (1972).

<sup>5</sup>P. Rhine, D. Williams, G. M. Hale, and M. R. Querry, *J. Phys. Chem.* **78**, 238 (1974); **78**, 1405 (1974).

<sup>6</sup>D. E. Hobson and D. Williams, *Appl. Opt.* **10**, 2372 (1971).

<sup>7</sup>M. R. Querry (private communication).

<sup>8</sup>J. Lyman and R. H. Fleming, *J. Marine Res.* **3**, 134 (1940).

<sup>9</sup>D. Friedman, *Appl. Opt.* **8**, 2073 (1969).

<sup>10</sup>K. F. Palmer and D. Williams, *J. Opt. Soc. Am.* **64**, 1107 (1974).

<sup>11</sup>G. Herzberg, *Infrared and Raman Spectra* (Van Nostrand-Reinhold, New York, 1945), p. 167.

<sup>12</sup>L. Pontier and C. Dechambenoy, *Ann. Geophys.* **22**, 633 (1966).

## II. Summary of Work on Inorganic Hydrated Materials

Most of our work on hydrated materials has involved studies of the optical properties of aqueous solutions. The first such study was carried out by Dr. David A. Draeger in work involved with his doctoral dissertation. Draeger's study involved the study of the absorption spectra aqueous solutions of strong electrolytes in the far-infrared regions of the spectrum. This investigation, which was carried out by means of the conventional techniques of infrared spectroscopy, is summarized in the following paper by Draeger and Williams.

## Far-Infrared Absorption Spectra of Aqueous Solutions of Strong Electrolytes\*

DAVID A. DRAEGERT AND DUDLEY WILLIAMS

Kansas State University, Manhattan, Kansas

(Received 12 July 1967)

The infrared absorption of solutions of LiCl, KF, KCl, KBr, KI, NaCl, NaBr, NaI, NaNO<sub>3</sub>, NaClO<sub>3</sub>, NaClO<sub>4</sub>, DCl, and NaOD in D<sub>2</sub>O has been studied in the spectral region 75 to 650 cm<sup>-1</sup>; the absorption of HCl and NaOH solutions in H<sub>2</sub>O in the region 75 to 1000 cm<sup>-1</sup> has also been investigated. Even for the highest concentrations, the solution spectra have a striking resemblance to the spectrum of the solvent. A broad, intense band attributable to the hindered rotation of water molecules and a much less intense band attributable to the hindered translation of water molecules appear in the spectrum of each solution. The frequencies, widths, and shapes of these bands are compared in some detail with the corresponding bands in the spectrum of pure water. Small but significant differences between the spectra of the solutions and the spectrum of water are noted.

Because of their importance and their interesting physical properties, aqueous solutions have been studied by many experimental techniques, including infrared<sup>1</sup> and Raman spectroscopy.<sup>2-5</sup> Most of the earlier infrared investigations covered frequencies higher than 1000 cm<sup>-1</sup>, and the observed absorption bands involved transitions between *intramolecular* vibrational states. Information regarding the *intermolecular* structure of the liquids was obtained only because the intermolecular forces have some influence on the frequencies and intensities of intramolecular bands. Direct transitions between states involving motions of entire water molecules restrained by relatively weak intermolecular forces produce absorption at frequencies lower than 1000 cm<sup>-1</sup>. Hence, studies of the far-infrared absorption spectra of solutions can, in principle, provide additional information concerning the intermolecular forces and the effects of solutes on the structure of water.

The present study of aqueous solutions is a continuation of our earlier work on the far-infrared spectrum of liquid water,<sup>6</sup> which revealed general absorption<sup>7</sup> throughout the region with at least two well-defined absorption bands. One is a broad, intense band with an absorption maximum near 680 cm<sup>-1</sup> in H<sub>2</sub>O and near 500 cm<sup>-1</sup> in D<sub>2</sub>O; the contour of this major band is smooth but decidedly asymmetric. A much weaker band

produces a shoulder on the low-frequency wing of the major band. After allowance is made for the contour of the major band, it appears that the shoulder band is centered near 170 cm<sup>-1</sup> in H<sub>2</sub>O and near 165 cm<sup>-1</sup> in D<sub>2</sub>O. Bands in these regions have been observed in Raman<sup>3</sup> and in inelastic neutron-scattering studies.<sup>8</sup> Because of their isotopic shifts, the major and shoulder bands have been attributed, respectively, to hindered rotations or "librations" and to hindered translations of water molecules. For both H<sub>2</sub>O and D<sub>2</sub>O it was found that the frequency of the absorption maximum of the major band decreases with increasing temperature. The major band also broadens, and the maximum absorption coefficient appears to decrease with increasing temperature. The central frequency and the maximum absorption coefficient of the shoulder band apparently decrease with increasing temperature. The spectra of the electrolytic solutions observed in the present study will be compared with the spectrum of water.

The solutes selected for study included eight alkali halides, three sodium salts with more complex anions, hydrochloric acid, and sodium hydroxide. To permit comparison of the effects of the different solutes, most of the solutions were studied at a common concentration; since the observed spectral effects generally increase with concentration, the highest common concentration attainable (4*M*) was used. Concentration effects were studied in detail in certain selected solutions.

### EXPERIMENTAL METHODS

The far-infrared spectra were obtained with a Perkin-Elmer Model 301 double-beam spectrophotometer. The spectral slitwidth rarely exceeded 4 cm<sup>-1</sup> and was usually considerably less. The ambient temperature of the sample compartment was approximately 28°C.

The samples consisted of thin layers of liquid between polyethylene windows spaced a few microns apart.

\* Work supported in part by the U.S. Air Force Cambridge Research Laboratories and in part by the U.S. Office of Naval Research.

<sup>1</sup> E. Ganz, *Ann. Physik* **28**, 445 (1937); D. Williams and W. Millet, *Phys. Rev.* **66**, 6 (1944); G. R. Choppin and K. Buijs, *J. Chem. Phys.* **39**, 2042 (1963); H. Yamatera, B. Fitzpatrick, and G. Gordon, *J. Mol. Spectry.* **14**, 268 (1964).

<sup>2</sup> W. R. Busing and D. F. Hornig, *J. Chem. Phys.* **65**, 284 (1961); J. W. Schultz and D. F. Hornig, *ibid.* **65**, 2131 (1961).

<sup>3</sup> G. E. Wairafén, *J. Chem. Phys.* **36**, 1035 (1962); **40**, 3249 (1964).

<sup>4</sup> G. E. Wairafén, *J. Chem. Phys.* **44**, 1546 (1966).

<sup>5</sup> D. E. Irish and G. E. Wairafén, *J. Chem. Phys.* **46**, 378 (1967); G. E. Wairafén, *ibid.* **46**, 1870 (1967).

<sup>6</sup> D. A. Draegert, N. W. B. Stone, B. Curnutte, and D. Williams, *J. Opt. Soc. Am.* **56**, 64 (1966).

<sup>7</sup> R. M. Goody, *Atmospheric Radiation* (Oxford University Press, New York, 1964), App. 13. The ratio of the absorption coefficients in the intermediate infrared to those in the visible is approximately 10<sup>8</sup>.

<sup>8</sup> K. E. Larsson and V. Dahlborg, *React. Sci. Tech. (J. Nucl. Eng.)* **16**, 81 (1962).

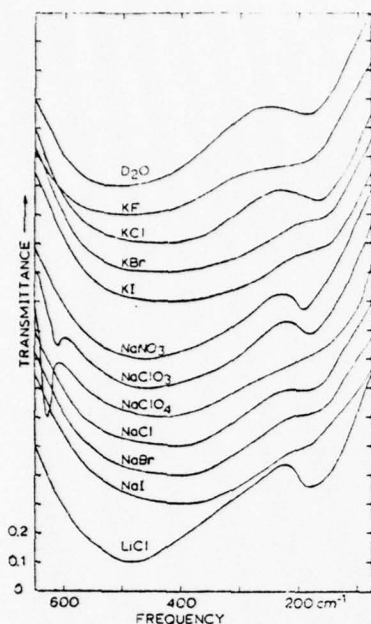


Fig. 1. Normalized spectral transmittance curves for  $D_2O$  and  $4M$  solutions of strong electrolytes. The interval between marks on the transmittance axis in this and subsequent figures is 0.1; the upper curves have been displaced by multiples of this interval. In general, spectral transmittance values based on independent measurements differ from those given in the curves by at most  $\pm 0.03$ .

Liquid  $D_2O$  was used as a solvent, because its interesting spectral features occur in the frequency region below  $650\text{ cm}^{-1}$ , where polyethylene is transparent; most other window materials dissolve or react with the solutions. Reagent-grade salts were dissolved in 99.5%  $D_2O$  obtained from Coleman, Matheson, and Bell, Inc. Solutions of 25%  $NaOD$  and 20%  $DCl$  in  $D_2O$  were supplied by Calbiochem, Inc.

Because of the experimental difficulties encountered in our earlier quantitative study of the water spectrum,<sup>6</sup> no precise measurements of sample thickness were undertaken in the present work. Thus, absorption coefficients were not determined. Each of the transmittance curves shown in the figures is a composite, based on four or more spectra of the same solution. Several spectra for each solution were averaged after they had been "normalized" by Lambert's law to give a minimum transmittance of 0.10; the minimum transmittances actually measured were between 0.06 and 0.22. The normalization procedure facilitates comparison of frequency shifts and band shapes. However, it should be noted that no comparison of the relative absorption coefficients of *different* solutions is possible.

#### EXPERIMENTAL RESULTS

Normalized transmittance curves for  $D_2O$  and for  $4M$  solutions of 11 different solutes are shown in Fig. 1.

The spectra of all solutions show a marked resemblance to the spectrum of  $D_2O$ . The major band in the potassium and sodium halide solutions shifts to lower frequencies as the halide ions increase in size. The shoulder band is barely discernible in the bromide and iodide solutions. In the lithium chloride solution, the major band is narrow and well separated from the shoulder band. Careful examination reveals differences in the shape of the major band for lithium, sodium, and potassium salts in solutions having a common halide ion. The shapes of the transmittance curves for sodium nitrate and sodium chlorate solutions are similar; replacement of nitrate ions by chlorate ions shifts the entire curve to lower frequencies. The sharp bands near  $610\text{ cm}^{-1}$  in the sodium chlorate solution and near  $628\text{ cm}^{-1}$  in the sodium perchlorate solution are due to normal vibrations of the anion groups.

Normalized transmittance curves for  $D_2O$  and for different concentrations of potassium fluoride, potassium iodide, and sodium perchlorate are shown in Fig. 2. The principal effect of concentration increase in the potassium fluoride solution is a broadening of the major band; the shoulder band is extremely broad in the  $12M$  solution. In the potassium iodide solutions the major band shifts to lower frequencies with increasing concentration. Similar shifts are observed for the sodium perchlorate solutions; the curve for the  $8M$  solution has an "angular contour," with definite changes in the slope near  $520$  and  $370\text{ cm}^{-1}$ .

Normalized transmittance curves for  $D_2O$  and for two different concentrations of deuterated sodium hydrox-

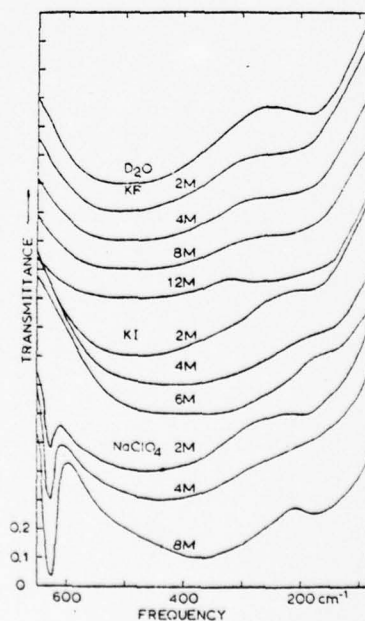


Fig. 2. Normalized spectral transmittance curves for  $D_2O$  and  $KF$ ,  $KI$ , and  $NaClO_4$  solutions with the indicated concentrations.

ide and hydrochloric acid are shown in Fig. 3. In the hydroxide solution, increase in concentration broadens the major band. In the acid solution, increase in concentration shifts the major band to lower frequencies.

Because the major band is extremely broad, it is difficult to determine the frequency of maximum absorbance by casual inspection of the normalized transmittance curves. This frequency, denoted by  $\nu_L$ , was determined by the procedure suggested on the  $D_2O$  curve in Fig. 3. For this curve,  $\nu_1$  and  $\nu_2$  are the frequencies at which the normalized transmittance is 0.2; the mean of  $\nu_1$  and  $\nu_2$  is denoted by  $\bar{\nu}(0.2)$ . The corresponding mean frequencies for smaller values of transmittance, along with estimated uncertainties, are also shown in Fig. 3. The frequency  $\nu_L$  is given by the limit of these mean frequencies as the normalized transmittance approaches 0.1. The values of  $\nu_L$  for

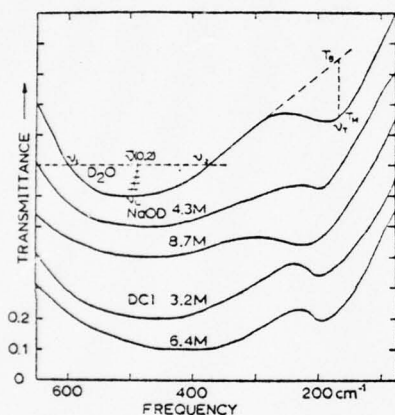


Fig. 3. Normalized spectral transmittance curves for  $D_2O$  and  $NaOD$  and  $DCl$  solutions with the indicated concentrations.

deuterated solutions are listed in Table I; the indicated uncertainties are based on consideration of band shape and scatter in the original data points. The values of  $\nu_L$  for several solutions are plotted in the left panel of Fig. 4 as a function of concentration. The right panel of Fig. 4 gives the values of  $\nu_L$  for 4M solutions of the indicated compounds of lithium, sodium, and potassium.

It can be seen from Fig. 4 that the frequencies  $\nu_L$  for all solutions are generally less than  $\nu_L$  for pure  $D_2O$ . For 4M solutions of potassium salts, the frequency  $\nu_L$  decreases in the order:  $KF$ ,  $KCl$ ,  $KBr$ , and  $KI$ ; for 4M solutions of sodium compounds, the corresponding order of decrease is:  $NaOD$ ,  $NaNO_3$ ,  $NaClO_3$ ,  $NaClO_4$ ,  $NaCl$ ,  $NaBr$ , and  $NaI$ . For the 4M solutions of chlorides, bromides, and iodides, the frequency  $\nu_L$  is less for sodium salts than for potassium salts; however, it should be noted from Fig. 1 that the shapes of the major bands in sodium and potassium salts are quite different. In the 4M chloride solutions,  $\nu_L$  decreases in the order  $LiCl$ ,  $DCl$ ,  $KCl$ , and  $NaCl$ . For the solutions studied at various concentrations,  $\nu_L$  decreases rapidly

TABLE I. The frequencies  $\nu_L$  of the "major band" and  $\nu_T$  of the "shoulder band" for  $D_2O$  solutions.

Solution	Concentration (M)	$\nu_L$ ( $cm^{-1}$ )	$\nu_T$ ( $cm^{-1}$ )
$D_2O$		$500 \pm 10$	$165 \pm 10$
KF	2	$500 \pm 10$	$186 \pm 12$
	4	$491 \pm 12$	$169 \pm 12$
	8	$484 \pm 10$	$182 \pm 12$
	12	$482 \pm 12$	230-140*
KCl	4	$441 \pm 12$	$153 \pm 12$
KBr	4	$440 \pm 10$	$149 \pm 14$
KI	2	$479 \pm 10$	$166 \pm 12$
	4	$423 \pm 10$	$140 \pm 14$
	6	$401 \pm 12$	$140 \pm 14$
$NaNO_3$	4	$459 \pm 10$	$185 \pm 12$
$NaClO_3$	4	$452 \pm 12$	$164 \pm 12$
$NaClO_4$	2	$464 \pm 12$	$176 \pm 12$
	4	$433 \pm 12$	$177 \pm 15$
	8	$371 \pm 12$	$140 \pm 12$
NaCl	4	$412 \pm 12$	$166 \pm 12$
NaBr	4	$408 \pm 12$	$162 \pm 14$
NaI	4	$398 \pm 12$	$183 \pm 14$
LiCl	4	$486 \pm 10$	$163 \pm 12$
NaOD	4.3	$470 \pm 12$	$186 \pm 12$
	8.7	$476 \pm 12$	$202 \pm 12$
DCl	3.2	$454 \pm 12$	$176 \pm 12$
	6.4	$412 \pm 12$	$177 \pm 12$

\* A broad band with abrupt changes in slope near the indicated frequencies.

with increasing concentration except for  $KF$  and  $NaOD$  solutions. The lowest frequency  $\nu_L$  observed was for the 8M solution of  $NaClO_4$ ; this frequency is 26% less than the frequency of  $\nu_L$  in pure  $D_2O$ .

As indicated in the normalized transmittance curves in Figs. 1-3, there is considerable variation in the width of the major band in the spectra of various solutions. In view of the general far-infrared absorption mentioned earlier, any definition of the bandwidth of the major band is perhaps arbitrary. The frequency difference  $\nu_1 - \nu_2$  between the frequencies at which the normalized transmittance is 0.2 was selected as a measure of bandwidth; at this value of normalized transmittance, the "width index"  $\nu_1 - \nu_2$  is large com-

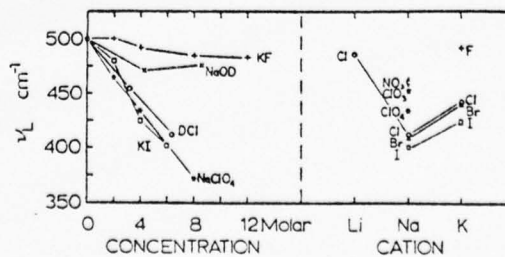


Fig. 4. The frequency  $\nu_L$  of maximum spectral absorbance. The left panel gives  $\nu_L$  for several solutions as a function of concentration. The right panel gives  $\nu_L$  for 4M solutions of compounds of lithium, sodium, and potassium; the anion is listed for each point.

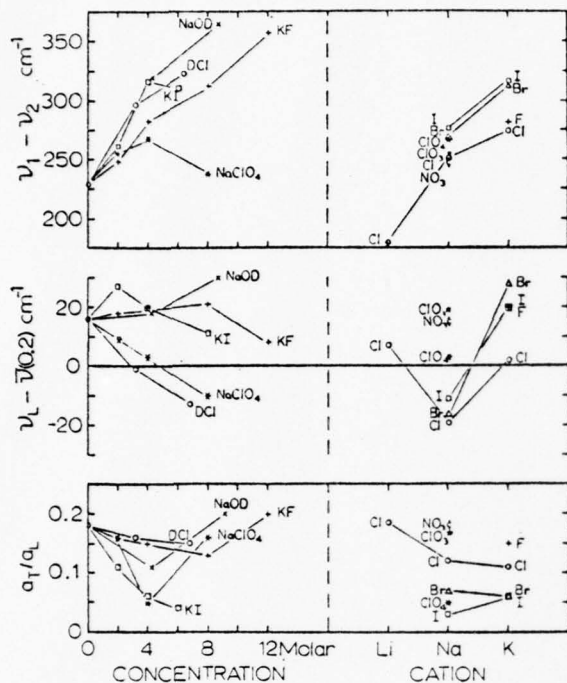


Fig. 5. The width index  $\nu_1 - \nu_2$  of the major band, the asymmetry index  $\nu_L - \bar{\nu}(0.2)$  of the major band, and the ratio  $a_T/a_L$  of the absorption coefficients of the shoulder and major band are shown as a function of concentration in the left panels. These parameters, which are defined in the text, are shown in the right panels for 4M solutions of the indicated salts.

pared with uncertainties in  $\nu_1$  and  $\nu_2$ . Absorbance by the shoulder band is usually negligible in the spectral region between  $\nu_1$  and  $\nu_2$ , but was taken into account in some cases before  $\nu_2$  was determined.

In the upper part of Fig. 5, the width index  $\nu_1 - \nu_2$  is plotted as a function of concentration in the left panel and is shown for 4M solutions of various compounds of lithium, sodium, and potassium in the right panel. The figure indicates that, with the exception of LiCl, the width index for the major band is larger for all solutions than for D<sub>2</sub>O. The width generally increases with concentration, but for KI and NaClO<sub>4</sub> the band appears to narrow as the concentration increases beyond 4M. For 4M solutions of potassium halides, the width index increases in the order: KCl, KF, KBr, and KI; for 4M solutions of sodium compounds, the order of increase is: NaNO<sub>3</sub>, NaCl, NaClO<sub>3</sub>, NaClO<sub>4</sub>, NaBr, NaI, and NaOD. Except for the positions of NaCl and NaOD, these orders are identical with those for decreasing  $\nu_L$ . For chloride solutions, the width index increases in the order: LiCl, NaCl, KCl, and DCl. For bromide and iodide solutions, the width index is larger for the potassium than for the sodium salts.

In discussing the effects of various solutes on the shape of the central portion of the major band in the spectral region, where the normalized transmittance is less than 0.2, it is helpful to introduce an "asymmetry

index"  $\nu_L - \bar{\nu}(0.2)$ . For a symmetrical band, this index is zero. If the asymmetry index is positive, as in the case of the D<sub>2</sub>O curve in Fig. 3, the integral of the spectral absorbance from  $\nu_1$  to  $\bar{\nu}(0.2)$  is greater than this integral from  $\bar{\nu}(0.2)$  to  $\nu_2$ . Values of the asymmetry index, which is seldom zero, are plotted in the central portion of Fig. 5. As indicated in the left panel, with increasing concentration the asymmetry index increases for NaOD and decreases steadily for DCl and NaClO solutions. The plot in the right panel gives the asymmetry parameters for various 4M solutions. For the sodium halides, the asymmetry index has large negative values; for the potassium halides, the index is positive and has large values for the fluoride, bromide, and iodide. These differences in the asymmetry indices for the sodium and potassium halides thus reflect the marked differences in band contours noted in Fig. 1; a decrease in the asymmetry index implies a relative increase in spectral absorbance in the lower-frequency portion of the band.

In assigning a central frequency  $\nu_T$  to the shoulder band, it is necessary to make some assumption regarding the portion of the measured spectral absorbance that should be attributed to this band. The values of  $\nu_T$  listed in Table I were obtained by drawing a straight line  $T_B$  tangent to the normalized measured transmittance curve  $T_M$  at the point of inflection between the major and shoulder bands, as indicated in Fig. 3. The frequency  $\nu_T$  is the frequency for which the difference  $T_B - T_M$  is greatest; the use of an analogous technique involving logarithmic plots of transmittance gave only slightly different values for  $\nu_T$ . The estimated uncertainties in  $\nu_T$  listed in Table I take into consideration the arbitrary manner in which the "boundary lines"  $T_B$  were constructed on linear or logarithmic plots of normalized transmittance.

Some of the values of  $\nu_T$  for the solutions listed in Table I are lower than  $\nu_T$  for D<sub>2</sub>O; others are higher. For the 4M solutions of potassium halides,  $\nu_T$  clearly decreases in the "usual order": KF, (D<sub>2</sub>O), KCl, KBr, and KI. Differences in the values of  $\nu_T$  for the 4M solutions of sodium compounds are smaller and in some cases not significant; the observed order of decrease is: NaNO<sub>3</sub>, NaOD, NaI, NaClO<sub>4</sub>, NaCl, (D<sub>2</sub>O), NaClO<sub>3</sub>, NaBr. For the 4M bromide and iodide solutions,  $\nu_T$  is less for potassium salts than for sodium salts; for the chloride solutions,  $\nu_T$  decreases in the order DCl, NaCl, (D<sub>2</sub>O), LiCl, and KCl.

Although no determinations of absorption coefficients  $a(\nu)$  were made, it is possible to determine from the normalized transmittance curves the relative values of  $a(\nu)$  for various frequencies in the spectrum of a given solution. The ratio of the part  $a_T$  of the absorption coefficient at  $\nu_T$  attributable to the shoulder band to the total absorption coefficient  $a_L$  at  $\nu_L$  was obtained. For a sample thickness  $l$ , Lambert's law gives

$$a_T l = -\ln(T_M/T_B) \quad \text{and} \quad a_L l = -\ln(T_L), \quad (1)$$

where  $T_L$  has the value 0.1 in the normalized transmittance curves. The ratio  $a_T/a_L$  is then given by the expression

$$a_T/a_L = \ln(T_M/T_B) / \ln(T_L). \quad (2)$$

The ratios  $a_T/a_L$  for various solutions are shown in the lower portion of Fig. 5. Because of the arbitrary method of selecting  $T_B$ , the uncertainties in the ratio  $a_T/a_L$  may be as great as  $\pm 40\%$ .

For the 4M solutions of potassium salts, the ratio  $a_T/a_L$  decreases in the order: KF, KCl, KBr, and KI; for the sodium compounds,  $a_T/a_L$  decreases in the order: NaNO<sub>3</sub>, NaClO<sub>3</sub>, NaCl, NaOD, NaBr, NaClO<sub>4</sub>, and NaI. For the chloride solutions, the ratio decreases in the order: LiCl, DCl, NaCl, and KCl;  $a_T/a_L$  is very small for the iodide and bromide solutions of sodium and potassium. The ratio  $a_T/a_L$  generally decreases with increasing concentration to about 6M and then increases for the more concentrated solutions of NaOD and KF.

For purposes of comparison with the deuterated solutions, normalized transmittance curves for H<sub>2</sub>O and solutions of NaOH and HCl are shown in Fig. 6. The portions of the curves between 1000 and 550 cm<sup>-1</sup> are based on data obtained with a Perkin-Elmer Model 421 spectrometer. For H<sub>2</sub>O and the less concentrated HCl solutions, silver chloride cell windows were used for frequencies as low as 400 cm<sup>-1</sup>; the other solutions reacted with silver chloride. Spectral data for frequencies below 650 cm<sup>-1</sup> were obtained by the techniques described earlier. Values of  $\nu_L$ ,  $\nu_T$ , and  $a_T/a_L$  are listed in Table II.

A comparison of the spectra of the acid and base solutions shown in Figs. 3 and 6 is rather interesting. The major bandwidth is large for both classes of solutions and increases rapidly with increasing concentration. The frequency  $\nu_L$  decreases with increasing

TABLE II. The frequency  $\nu_L$  of the "major band," the frequency  $\nu_T$  of the "shoulder band," and the ratio  $a_T/a_L$  of absorption coefficients for H<sub>2</sub>O solutions.

Solution	Concentration (M)	$\nu_L$ (cm <sup>-1</sup> )	$\nu_T$ (cm <sup>-1</sup> )	$a_T/a_L$
H <sub>2</sub> O	...	680±10	170±12	0.22±40%
NaOH	2	...	176	0.21
	4	...	191	0.24
	8	...	194	0.32
HCl	2	620±12	166	0.22
	4	624	173	0.24
	8	...	167	0.26
	12	...	171	0.31

concentration—rapidly in the acid, slowly in the base. With increasing concentration, the asymmetry index rapidly decreases for the acid and slowly increases for the base. The frequency  $\nu_T$  is nearly constant in acid solutions, but increases with concentration in the base. In both acid and base, the ratio of absorption coefficients  $a_T/a_L$  is not significantly different from that of water, except at the highest concentrations.

## DISCUSSION OF RESULTS

The far-infrared absorption of pure water is presumably produced by rotational and translational motions of molecules restrained by intermolecular forces exerted by neighboring water molecules. X-ray studies of water<sup>9</sup> have shown that, on a short time scale, a given water molecule is likely to have four nearest neighbors located at the corners of a tetrahedron. Motions of a given molecule are restricted chiefly by hydrogen bonds linking it to its nearest neighbors; displacement of a molecule from its equilibrium orientation and position gives rise to restoring forces.

Under these circumstances, it is to be expected that a given molecule will have three modes of hindered rotation about the principal axes of the molecule. Two of these modes would be strongly infrared active, since they involve changes in the direction of the molecular dipole moment; rotation about the symmetry axis would possibly produce absorption by an indirect process involving changes in molecular polarizations. Because the water structure does not have the regularity of a true crystal and is subject to change in times at least comparable with and probably shorter than the dielectric relaxation time  $\sim 10^{-11}$  sec, broad absorption bands due to hindered rotation are to be expected.

Although the observed water band attributed to

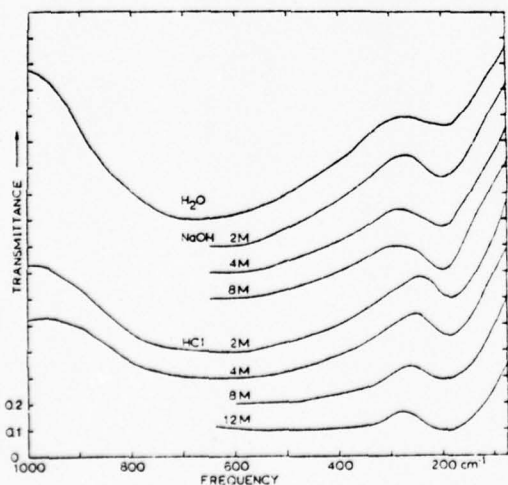


Fig. 6. Normalized spectral transmittance curves for H<sub>2</sub>O and for solutions of NaOH and HCl.

<sup>9</sup> J. Morgan and B. Warren, *J. Chem. Phys.* 6, 666 (1938); G. Brady and W. Romanow, *ibid.* 32, 306 (1960); M. D. Danford and H. A. Levy, *J. Am. Chem. Soc.* 84, 3965 (1962).



hindered rotation is asymmetric, we have not obtained any direct evidence that this band consists of unresolved components. The clearest evidence for the existence of more than one component has been obtained by Terhune, Maker, and Savage<sup>10</sup> in their studies of inelastic harmonic light scattering; Savage reports H<sub>2</sub>O bands near 485 and 760 cm<sup>-1</sup>, which can be distinguished by polarization measurements. The observed Raman band has been analytically decomposed into two or three components by Walrafen.<sup>11</sup> Thus, it is probable that the major far-infrared band of water consists of two or more unresolved components.

Although there are three degrees of freedom for hindered translation, no evidence of a multi-component structure has been reported for the observed water band attributed to motion of this type.

In view of current interpretations of the far-infrared spectrum of water, the striking resemblance of the observed spectra of solutions to the spectrum of pure water is possibly surprising. In the most concentrated solutions, in which there is one solute ion pair for every four molecules, the restraining forces acting on a given water molecule would be expected to be quite different from the restraining forces acting on a molecule in pure water. Because major bands and shoulder bands grossly similar to those in water are discernible in all solution spectra, it appears reasonable to attribute these bands, respectively, to hindered rotation and hindered translation of water molecules in the solutions.

In some superficial respects, changes in temperature and the addition of solutes to water cause similar spectral effects; both result in changes of  $\nu_L$  and changes in the width index of the major band. As indicated earlier in our description of experimental results, solutes with equal concentrations can be listed in a definite order of increasing effectiveness in producing spectral changes. Similar orders have been noted in studies of other physical quantities,<sup>12</sup> including the frequencies of near-infrared absorption bands,<sup>1</sup> the frequencies and intensities of Raman bands,<sup>2-4</sup> and the shifts of NMR peaks.<sup>13</sup> By comparing the effects of various solutes with the effects produced by temperature change, earlier workers have classified various ions as "structure makers" and "structure breakers." From this point of view, the results of the present far-infrared study of salt solutions indicate that Na<sup>+</sup> and K<sup>+</sup> should be regarded as structure breakers and Li<sup>+</sup> and F<sup>-</sup> should be regarded as structure makers; in the order of increasing effectiveness as structure breakers, the other negative ions should be listed as follows: NO<sub>3</sub><sup>-</sup>, ClO<sub>3</sub><sup>-</sup>, ClO<sub>4</sub><sup>-</sup>, Cl<sup>-</sup>, Br<sup>-</sup>, and I<sup>-</sup>. This classification of various ions is in essential agreement with those based on studies of other physical properties.

<sup>10</sup> R. W. Terhune, P. D. Maker, and C. M. Savage, Phys. Rev. Letters 14, 681 (1965); and private communication.

<sup>11</sup> G. E. Walrafen, J. Chem. Phys. (to be published).

<sup>12</sup> F. S. Feates and D. J. G. Ives, J. Chem. Soc. 1956, 2798.

<sup>13</sup> J. C. Hindman, J. Chem. Phys. 36, 1000 (1962).

Another scheme for comparing the effects of various solutes with the effects of temperature change involves the concept of a "structure temperature," which is defined as the temperature at which pure water would have the same properties as those of a given solution. In the temperature range between 5° and 75°C, the frequency  $\nu_L$  in pure D<sub>2</sub>O shifts at the rate of approximately -0.8 cm<sup>-1</sup>/C deg. Use of this rate of change leads to structure temperatures of about 105°C for 4M solutions of NaClO<sub>4</sub> and NaI and 180°C for an 8M solution of NaClO<sub>4</sub>. As these temperatures are above the normal boiling point of water, it appears that the concept of structure temperature is of questionable value when applied to concentrated solutions of electrolytes.

The present study provides evidence that the spectra of solutions have certain features which *cannot* be duplicated by changing the temperature of pure water. Even casual observation of the normalized transmittance curves in Figs. 1-3 reveals that the *shapes* of the hindered rotational bands for some solutions are different from the hindered rotational band in pure D<sub>2</sub>O. The sudden changes in the slope of the curve for the 8M solution of NaClO<sub>4</sub> suggest the existence of unresolved components in the hindered rotational band in this solution. The large negative values of the asymmetry index for the sodium halide solutions indicate that the low-frequency absorptance of the bands in these solutions is relatively more intense than for the corresponding band in D<sub>2</sub>O. With increasing concentration of NaClO<sub>4</sub>, the asymmetry index decreases rapidly, but the width index first increases and then decreases; this behavior would be expected if one or more unresolved low-frequency components gradually increased in intensity until they dominated the spectrum, with accompanying decrease in the intensity of high-frequency components associated with the undisturbed water structure. A somewhat similar variation of the asymmetry and width indices is noted for the potassium iodide solution. The observed major bands in the spectra of solutions can thus be considered as having unresolved components involving hindered rotations of water molecules, some of which are closely associated with solute ions. Walrafen has drawn similar conclusions from his studies of the Raman spectra of solutions.<sup>4</sup>

Other evidence for hindered rotation of water molecules associated with ions has been obtained by Van der Elsken and Robinson<sup>14</sup> in their far-infrared studies of crystal hydrates. For water molecules in the halogen environment X···H-O-H···X, the rotational frequencies progressively decrease in the order X = Cl, Br, I; for water molecules in the environment X···H-O-H···O, the rotational frequencies are higher than for water molecules in the corresponding X···H-O-H···X environment. These observations offer some support for

<sup>14</sup> J. van der Elsken and D. E. Robinson, Spectrochim. Acta 17, 1249 (1961).

the interpretation of the present results in terms of unresolved components involving water molecules associated with solute ions.

Whereas increase in temperature decreases the frequency of hindered translation in pure water, some solutes containing ions usually regarded as structure breakers cause an increase in the observed frequency  $\nu_T$ . The observed shifts in  $\nu_T$  can be interpreted in terms of new unresolved components involving water molecules associated with various ions. The sudden changes in the slope of the very broad hindered translational band for the 12M solution of KF are further evidence for the existence of unresolved components.

In summary, the results of the present study show that, even for the most concentrated solutions, the

observed spectra have a striking resemblance to the spectrum of pure water. Although the observed differences may be attributed in part to a disturbance of the general intermolecular structure of water by the ions similar to those produced by temperature changes, they also involve direct interaction of ions with the water molecules responsible for the observed absorption; such direct interactions become increasingly important as concentration increases.

#### ACKNOWLEDGMENTS

We wish to express our appreciation to Dr. George Walrafen, Professor Basil Curnutte, and Mr. Jon Bryan for helpful discussions.

The initial work on the far infrared spectra, which must be considered semi-quantitative so far as band intensities are concerned, was followed by studies of the near-normal-incidence reflection of solutions of strong electrolytes. The reflection spectra of these solutions and the optical constants obtained by Kramers-Kronig phase-shift analysis are presented in the following articles by Rhine, Williams, Hale, and Querry. These articles are based on the doctoral dissertation of Dr. Paul Rhine; the Kramers-Kronig analysis was carried out at the University of Missouri at Kansas City at a time when the necessary computing facilities were not available to us here. Our thanks go to Dr. Marvin Querry for the design of the original computer programs, which were later refined here in the course of our subsequent studies.

## Infrared Optical Constants of Aqueous Solutions of Electrolytes. The Alkali Halides

Paul Rhine, Dudley Williams,\*

Department of Physics, Kansas State University, Manhattan, Kansas 66506

G. Michael Hale, and Marvin R. Querry

Department of Physics, University of Missouri, Kansas City, Missouri 64110 (Received July 5, 1973)

The normal-incidence spectral reflectance of aqueous solutions of alkali halides has been measured in the spectral range 350–5000  $\text{cm}^{-1}$ . From the measured values of reflectance we have used Kramers-Kronig phase-shift analysis to provide values of the real and imaginary parts of the complex refractive indices  $\tilde{N} = n + ik$  of the solutions. The plots of  $k(\nu)$  vs.  $\nu$  give quantitative measures of absorption band intensities as well as positions; we find that the negative ions produce greater changes in the absorption spectrum of the solvent than do the positive ions. Similarly, we find that the negative ions have greater influence on  $n(\nu)$  in the near infrared; all the halide ions increase  $n(\nu)$  to values above that of water but, at a common concentration, the iodide ion has the greatest effect. The primary influence of the ions on  $n(\nu)$  in the near infrared can be attributed to electronic bands in the ultraviolet. The influence of the ions on the characteristic water bands is related to the influence of the ions on the intermolecular structure of water.

### Introduction

Although the infrared spectrum of water has been the subject of numerous investigations dating from the early days of infrared spectroscopy, a critical survey by Irvine and Pollack<sup>1</sup> revealed many inconsistencies in published results and emphasized the importance of further quantitative studies of transmission and reflection for the purpose of obtaining more precise values of the real and imaginary parts of the refractive index  $\tilde{N} = n + ik$  in the infrared. Several such quantitative studies of water have recently been reported.<sup>2-8</sup> These studies have revealed that the values of the optical constants  $n$  and  $k$  obtained

in much of the infrared by Kramers-Kronig (KK) analysis<sup>6</sup> of near-normal-incidence-reflectance measurements were in much of the infrared in essential agreement with values based on reflectance measurements at two angles of incidence and with values based on a combination of reflection and absorption measurements.<sup>5</sup> The KK analysis of reflectance measurements provides reliable values of  $n$  in most of the range covered by the reflectance measurements and good values of  $k$  in the vicinity of strong bands; the fractional uncertainties in  $k$  increase as  $k$  decreases.

The KK theorem for phase-shift analysis of reflectance  $R(\nu)$  data asserts that if the modulus  $\rho(\nu) = [R(\nu)]^{1/2}$  of

the complex reflectivity  $\rho(\nu)e^{i\phi(\nu)}$  is known for all frequencies  $\nu$ , then the phase  $\phi(\nu_0)$  at any frequency  $\nu_0$  is given by

$$\phi(\nu_0) = \frac{2\nu_0}{\pi} P \int_0^\infty \frac{\ln \rho(\nu)}{\nu_0^2 - \nu^2} d\nu \quad (1)$$

where  $\rho(\nu)$  and  $\phi(\nu)$  must satisfy conditions that allow contour integration in the complex plane. Although the value of  $\phi(\nu_0)$  in eq 1 is most strongly influenced by values of  $\rho(\nu)$  in the vicinity of  $\nu_0$ , values of  $\rho(\nu)$  for all frequencies must be known if the KK theorem is to apply with rigor. Our earlier experience with water<sup>6</sup> has shown that  $\phi(\nu_0)$  in the range 300–5000  $\text{cm}^{-1}$ , in which we had actually measured  $R(\nu)$  is relatively insensitive to the type of extrapolation of  $R(\nu)$  to higher frequencies provided the extrapolation joins smoothly to the measured reflectance curve; values based on extrapolation to lower frequencies have increasingly greater uncertainties as  $\nu_0$  in eq 1 approaches the lower limit covered by experiment. In making the extrapolation of  $R(\nu)$  to low frequencies, we found it desirable to make use of approximate values based on the experimental work of others.<sup>4,9</sup>

In the present study, we report the results of measurements of the near-normal incidence spectral reflectance  $R(\nu)$  of aqueous solutions of alkali halides in the range 350–5000  $\text{cm}^{-1}$  and present the values of  $n$  and  $k$  provided by KK phase-shift analysis of the measured values of  $R$ . In addition to providing some insight into the influence of dissolved monatomic ions on the intermolecular lattice structure of liquid water, the study provides results that are of practical importance to meteorological studies of the transmission of infrared radiation through aerosols encountered in fog and cloud formation near the surface of the sea.

### Experimental Section

The general experimental techniques have been described in detail in earlier papers. We determined the spectral reflectance of a sample by comparing the radiant flux reflected from the free liquid surface with the flux reflected by a reference mirror, the absolute reflectivity of which was determined in an auxiliary experiment. In the comparison of the sample with the reference mirror we used a calibrated optical attenuator consisting of a rapidly rotating sector wheel, which was placed in front of the spectrometer slit when flux from the mirror was being measured; by use of the attenuator we avoided the necessity of changing amplifier gain settings. In spectral regions where the spectral reflectance of water had been well established, we made direct comparison of sample reflectance with the reflectance of water.

At least four independent measurements of reflectance were made for each solution studied. We believe that the averaged values of  $R$  presented in the figures have an experimental uncertainty of  $\pm 1\%$  of the plotted values; the uncertainties may have been slightly larger in spectral regions where  $R$  is changing rapidly with frequency and also at the lowest frequency range covered 450–350  $\text{cm}^{-1}$ .

The computer program used to determine  $\phi(\nu_0)$  from eq 1 employed a basic wave number interval of 10  $\text{cm}^{-1}$  for numerical integration except in the vicinity of the singularity at  $\nu = \nu_0$ , where the wave number interval was reduced to approximately 1  $\text{cm}^{-1}$ . In providing values of  $R$  for use in eq 1 outside the 350–5000- $\text{cm}^{-1}$  range covered by actual measurement, we made use of the values of the optical constants of water tabulated by Zolotarev, *et al.*;<sup>4</sup>

the computed values of water reflectance were raised to match and join smoothly with our  $R$  curves at 5000 and at 350  $\text{cm}^{-1}$ . Since the gross features of the reflectance curves for the solutions are similar to those for water, the adjustment of the Zolotarev data probably gives a satisfactory approximation of solution reflectance outside our range of measurement. We further assumed that the reflectance of a solution was constant for  $\nu > 10,000 \text{ cm}^{-1}$  and equal to the reflectance at 10,000  $\text{cm}^{-1}$ ; this eliminated remote ultraviolet reflection bands from the integral. Similarly, we assumed that solution reflectance at extremely low frequencies was constant and equal to its reflectance at 0.37  $\text{cm}^{-1}$ , thereby eliminating the effects of bands at lower radio frequencies.

On the basis of our earlier work on water together with considerations of uncertainties in our present work, we estimate that the uncertainty in  $\phi(\nu_0)$  in eq 1 is  $\pm 0.003$  rad. This indicates that uncertainties in  $n$  amount to  $\pm 1\%$  of the values shown in our graphs over most of the frequency range indicated but may increase to  $\pm 2\%$  at the lowest frequencies. The numerical uncertainty  $\delta k$  amounts to approximately  $\pm 0.03$  over most of the range; thus, our uncertainties amount to  $\pm 10\%$  at the maximum of the strong band near 3400  $\text{cm}^{-1}$ ,  $\pm 25\%$  at the maximum of the weaker band near 1640  $\text{cm}^{-1}$ , and  $\pm 7.5\%$  at the maximum of the strong band near 500  $\text{cm}^{-1}$ . These uncertainties are large but are smaller than those involved in values based on transmission measurements unless extreme care is taken in the preparation of the absorption cell.<sup>7</sup> For values of  $k < 0.10$ , values of  $k$  based on transmission measurements are usually to be preferred provided suitable cell windows of high optical quality are available.

Reagent grade materials were employed. Reflectance was measured for solutions at ambient laboratory temperature, which was approximately 27°.

### Results

The results of our study are summarized in the figures. The top panel in each figure gives measured reflectance  $R$  as a function of frequency. The center panel of each figure gives a corresponding plot of  $n$ , and the bottom panel gives  $k$  as a function of frequency. In each panel a light continuous curve gives the corresponding parameter for pure water at 27° for purposes of comparison.

A. *The 5000–2500- $\text{cm}^{-1}$  Region.* Figures 1–4 gives plots for the spectral region 5000–2500  $\text{cm}^{-1}$ , which is dominated by the intense absorption band near 3400  $\text{cm}^{-1}$  in water; this band, which occurs in a region where molecules containing OH groups have characteristic absorption, is usually attributed primarily to the  $\nu_1$  and  $\nu_3$  fundamentals of the  $\text{H}_2\text{O}$  molecule but includes some contribution from  $2\nu_2$  of the molecule.

Figure 1 gives the results obtained with 4 *M* solutions of three alkali bromides in the 5000–2500- $\text{cm}^{-1}$  region. The general contours of the reflectance feature are changed somewhat and the reflectances of the solutions are generally higher than those of water. The values of  $n$  for the solutions in the 5000–4000- $\text{cm}^{-1}$  region are practically indistinguishable from one another; this indicates that the difference between  $n$  of the solutions from that of water in this region is due primarily to the common halide ion  $\text{Br}^-$  and the alkali ions have relatively little effect on  $n$ . Similar results were obtained in studies of  $\text{Li}^+$ ,  $\text{Na}^+$ , and  $\text{K}^+$  in the presence of the halide ions  $\text{Cl}^-$  and  $\text{I}^-$ ; related but less clear-cut results were obtained with alkali fluorides.

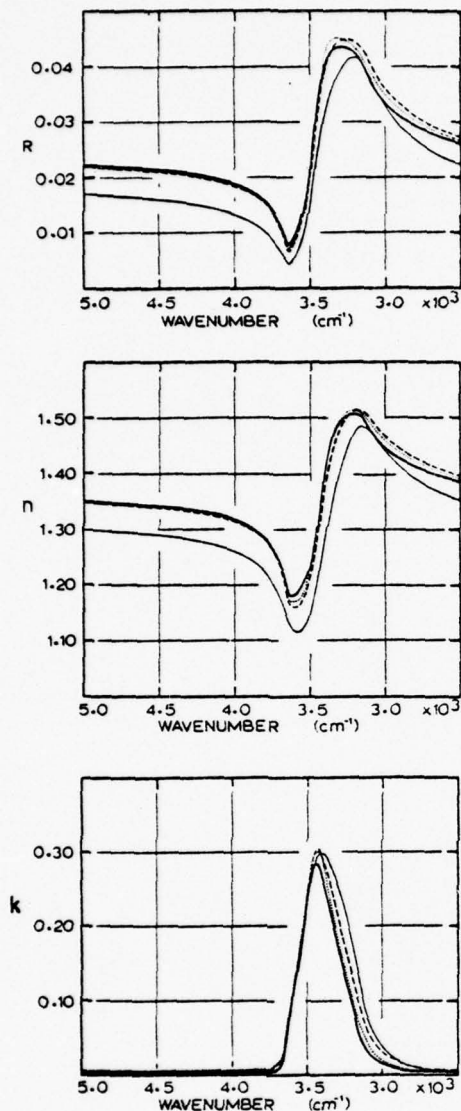


Figure 1. Normal-incidence reflectance and optical-constant curves for 4 *M* solutions of LiBr (dashed), NaBr (dotted), and KBr (heavy continuous). The light continuous curves give corresponding plots for water.

In view of our uncertainty  $\Delta k = \pm 0.03$ ,  $k$  is not significantly different from zero in the 5000–3800- $\text{cm}^{-1}$  range; in the vicinity of the 3400- $\text{cm}^{-1}$  absorption band of pure water, the  $k$  bands for the solutions are shifted to higher frequencies and are narrower than the water band; the slight shift of the peaks and the slight decrease in the half-width are progressively greater in the order  $\text{Li}^+$ ,  $\text{Na}^+$ , and  $\text{K}^+$ . The  $k$  peak heights are essentially the same within the limits of uncertainty, but the KBr peak is slightly lower than the other peaks shown in the figure; the maximum value of  $k$  for the solutions is very nearly equal to the  $k = 0.30$  maximum for water.

Figure 2 gives plots of  $R$ ,  $n$ , and  $k$  in the 5000–2500- $\text{cm}^{-1}$  region for 4 *M* solutions of potassium halides. The values of  $R$  and  $n$  for the solutions differ markedly from the corresponding values for water in the 5000–4000- $\text{cm}^{-1}$  range; the values of  $R$  and  $n$  increase in the order  $\text{F}^-$ ,  $\text{Cl}^-$ ,  $\text{Br}^-$ , and  $\text{I}^-$ . The peak values of  $k$  for the bands in

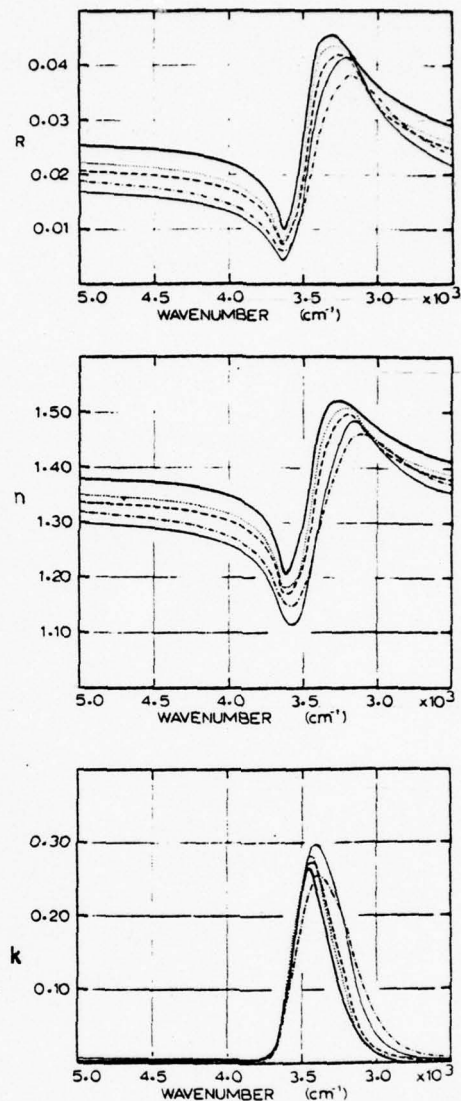


Figure 2. Normal-incidence reflectance and optical-constant curves for 4 *M* solutions of KF (dash-dot-dash), KCl (dashed), KBr (dotted), and KI (heavy continuous). The light continuous curves give corresponding plots for water.

the solutions are lower than that of the 3400- $\text{cm}^{-1}$  water band and decrease in the order  $\text{Cl}^-$ ,  $\text{Br}^-$ , and  $\text{I}^-$  for the heavier halides; the half-widths of the band are less than that of the water band and show a corresponding decrease with increasing ion size; however, the frequency at which maximum  $k$  occurs is greater than that of the water maximum and increases in the order  $\text{Cl}^-$ ,  $\text{Br}^-$ , and  $\text{I}^-$ . The appearance of the  $k$  band in the KF solution is different from its appearance in the other halide solutions; its peak value is considerably lower than those in the other halide solutions; its half-width is greater than that of the corresponding band in pure water; the  $k$  peak is shifted to a lower frequency than that of the water band.

On the basis of the plots in Figures 1 and 2 we conclude that the influence of negative ions on the 3400- $\text{cm}^{-1}$  water band is greater than the influence of positive ions. The influences of the  $\text{I}^-$  and  $\text{F}^-$  ions are greatly different; the smaller effects of  $\text{Cl}^-$  and  $\text{Br}^-$  are more nearly like those

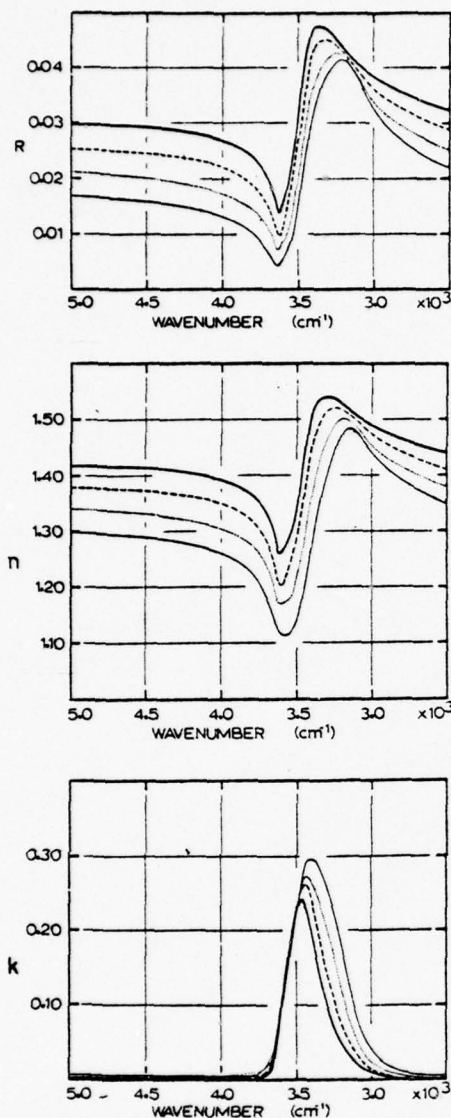


Figure 3. Normal-incidence reflectance and optical-constant curves for KI solutions: 2 (dotted), 4 (dashed), and 6 M (heavy continuous). The light continuous curves give corresponding plots for water.

of  $I^-$  than like those of  $F^-$ . These conclusions have been borne out in studies of alkali halide solutions other than those shown in the figures.

In order to ascertain the influences of concentration on the infrared spectra, we studied KI and KF solutions at several concentrations. Figure 3 gives the results obtained for KI. The difference between  $n$  for the solutions and  $n$  for water in the 5000-4000- $\text{cm}^{-1}$  region is roughly proportional to concentration. With increasing concentration: (1) the frequency at which the  $k$  peak occurs shifts progressively to higher frequencies, (2) the maximum value of  $k$  progressively decreases, and (3) the half-width of the absorption band progressively decreases. The corresponding results for KF solutions are shown in Figure 4. The value of  $n$  in the 5000-4000- $\text{cm}^{-1}$  region shows a small monotonic increase with increasing concentration. The peak value of  $k$  and the frequency at which the peak occurs become progressively lower with increasing concentration of KF;

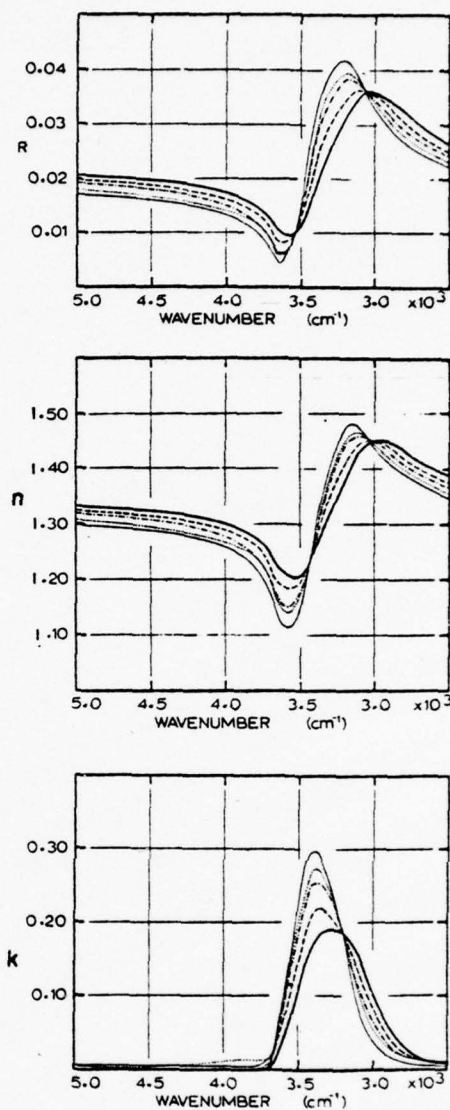


Figure 4. Normal-incidence reflectance and optical-constant curves for KF solutions: 2 (dotted), 4 (dot-dash-dot), 8 (dashed), and 12 M (heavy continuous). The light continuous curves give corresponding plots for water.

the half-width of the band becomes increasingly greater. For the 12 M solution the shape of the band bears little resemblance to that of the water band.

Consideration of Figures 3 and 4 reveals no anomalies with increasing concentration. All effects noted in Figures 1 and 2 appear to increase monotonically, although not necessarily linearly, with increasing concentration. Similar results have been obtained in concentration studies of other alkali halide solutions not shown in the figures.

*B. The 2500-350- $\text{cm}^{-1}$  Region.* In the 2500-350- $\text{cm}^{-1}$  region in the spectrum of water occur the weak associational band  $\nu_A$  near 2120  $\text{cm}^{-1}$ , the  $\nu_2$  fundamental of the  $\text{H}_2\text{O}$  molecule near 1640  $\text{cm}^{-1}$  and the strong, broad band  $\nu_L$  attributed to the librational or hindered rotational motion of  $\text{H}_2\text{O}$  molecules in the fields of their neighbors. The librational band in water at 27° is characterized by a maximum in  $k$  at 580  $\text{cm}^{-1}$ ; the peak position of the  $\nu_L$  band is strongly influenced by temperature. Our present

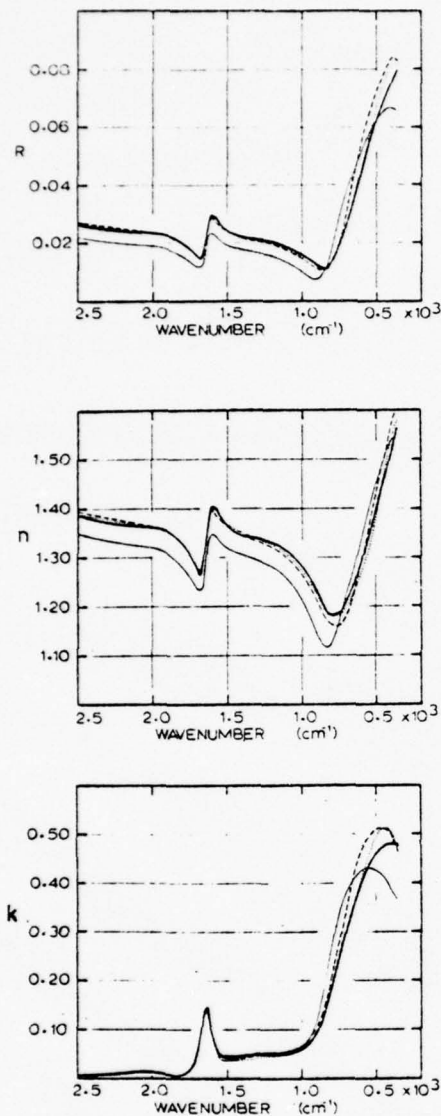


Figure 5. Normal-incidence reflectance and optical-constant curves for 4 *M* solutions of LiBr (dashed), NaBr (dotted), and KBr (heavy continuous). The light continuous curves give corresponding plots for water.

results in the 2500–350-cm<sup>-1</sup> region are summarized in Figures 5–8.

Figure 5 gives the results obtained with alkali bromide solutions. The spectral reflectance *R* is nearly the same for all the bromides and is greater for all solutions than for water except in the 800–350-cm<sup>-1</sup> region, where the reflectance curves of the solutions cross that of water; similar behavior is exhibited by the *n* curves, in which the minimum corresponding to the water minimum at 840 cm<sup>-1</sup> is shifted to lower frequencies. In the plot of *k* the small maximum associated with the associational band  $\nu_A$  is clearly visible near 2120 cm<sup>-1</sup>; however, in the view of experimental uncertainties in *k*, we can, on the basis of the present work, draw no conclusions regarding the influence of solutes on the associational band, which can be more readily studied by measurements of transmission.<sup>7</sup> The position and shape of the  $\nu_2$  fundamental are not measurably influenced by the presence of the solutes. The *k* peak position for the librational band in the alkali bro-

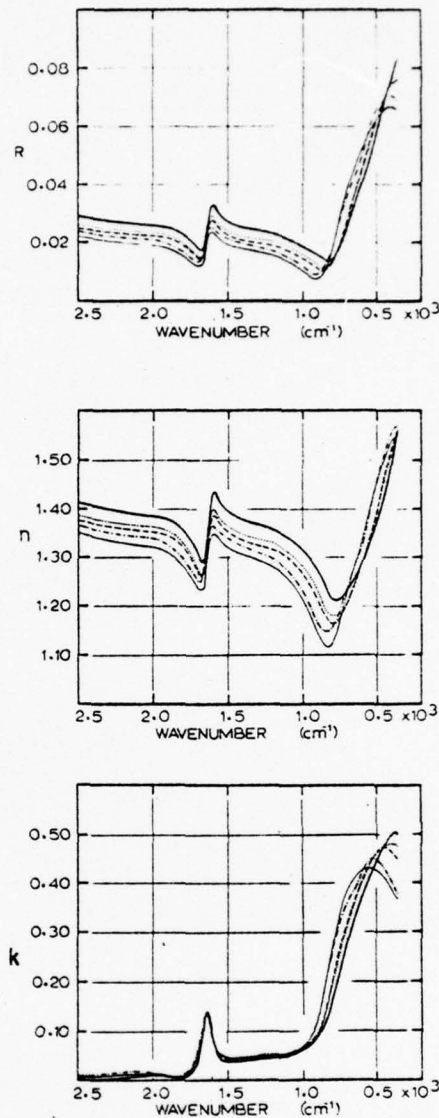


Figure 6. Normal-incidence reflectance and optical-constant curves for 4 *M* solutions of KF (dash-dot-dash), KCl (dashed), KBr (dotted), and KI (solid continuous). The light continuous curves give corresponding plots for water.

mid solutions is shifted to lower frequencies, relative to its position in the spectrum of water; the shift is large for all the bromides but increases slightly in the order Li<sup>+</sup>, Na<sup>+</sup>, K<sup>+</sup>.

Figure 6 summarizes our results for alkali halide solutions. In the 2500–800-cm<sup>-1</sup> range the *R* and *n* curves for the solutions are higher than the corresponding curves for water; the difference between *n* for the solutions and *n* for water in this region increases in the order F<sup>-</sup>, Cl<sup>-</sup>, Br<sup>-</sup>, I<sup>-</sup>. In the 2500–800-cm<sup>-1</sup> region, the *k* curves for the solutions coincide within the limits of uncertainty with the *k* curve for water; we can conclude that the solutes have little influence on  $\nu_2$ . In the 800–350-cm<sup>-1</sup> regions, the *R* and *n* curves cross; the minimum in *n* occurs at a slightly higher frequency for KF and at increasingly lower frequencies for the other potassium halides in the order Cl<sup>-</sup>, Br<sup>-</sup>, I<sup>-</sup>. The position of the *k* peak for  $\nu_L$  is strongly influenced by the solute and is shifted to lower frequencies in the order F<sup>-</sup>, Cl<sup>-</sup>, Br<sup>-</sup>, I<sup>-</sup>; there is a slight indica-



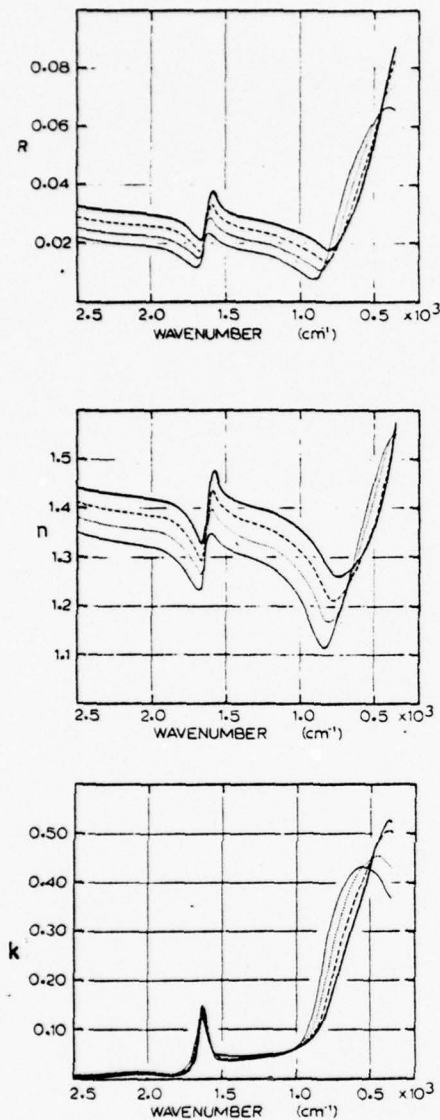


Figure 7. Normal-incidence reflectance and optical-constant curves for KI solutions: 2 (dotted), 4 (dashed), and 6 *M* (heavy continuous). The light continuous curves give corresponding plots for water.

tion of a high-frequency shoulder on the KF curve. The magnitude of  $k$  at the peak is greater than that for water; peak values of  $k$  increase in the order  $F^-$ ,  $Cl^-$ ,  $Br^-$ ,  $I^-$ .

Figure 7 gives the results of our study KI solutions as a function of concentration. In the 2500–800- $cm^{-1}$  region, the  $R$  and  $n$  curves become increasingly higher than the water curves as the KI concentration increases; the  $k$  curves for KI nearly coincide with the water curve at all concentrations. In the frequency range below 800  $cm^{-1}$  the  $R$  and  $n$  curves cross; the minima in the  $n$  curves for the KI solutions occur at progressively lower frequencies as the concentration increases. The  $k$  maxima of the  $\nu_L$  band in the solution spectra shift to progressively lower frequencies as the concentration of KI increases; for the 6 *M* solution the  $k$  maximum may actually occur at a frequency below our limit of measurements at 350  $cm^{-1}$ .

Figure 8 gives the results of our study of KF as a function of concentration. In the 2500–800- $cm^{-1}$  region the  $R$  and  $n$  curves are higher than the corresponding water

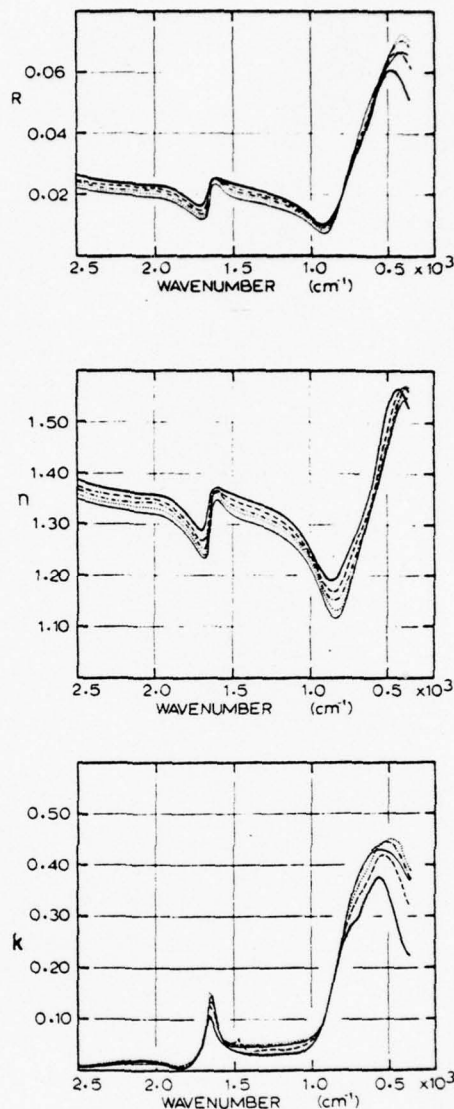


Figure 8. Normal-incidence reflectance and optical-constant curves for KF solutions: 2 (dotted), 4 (dot-dash-dot), 8 (dashed), and 12 *M* (heavy continuous). The light continuous curves show corresponding plots for water.

curves by a relatively small amount that increases with increasing concentration of KF. The  $\nu_2$  peak in the  $k$  curve remains at the same frequency in the solutions, but the peak value of  $k$  appears to decrease with increasing concentration. Differences in the levels of the  $k$  curves for the KF solutions can be noted in the relatively flat parts of the curves between 1500 and 1000  $cm^{-1}$ . In the spectral range below 1000  $cm^{-1}$ , the  $R$  curves nearly coincide until the  $R$  maximum is reached; the reflectance maximum is attained at a higher frequency for the 12 *M* solution than for water or the less concentrated solutions. The minimum in the  $n$  curves occurs at a progressively higher frequency relative to the minimum in the water curve as the KF concentration increases. The  $k$  peak position for the  $\nu_L$  band in the 2, 4, and 8 *M* solutions appears at slightly lower frequencies than for water and at a slightly higher frequency for the 12 *M* solution than for water. The height of the  $\nu_L$  peak in the  $k$  curves decreases with increasing concentration; evidence for the existence of a high-fre-

quency shoulder appears in the spectra of the more concentrated solutions.

### Discussion

The results obtained for values of  $n$  in the infrared indicate that this parameter is influenced more by negative ions than by positive ions. Its value in the visible and infrared is determined primarily by the intensities and positions of electronic bands in the ultraviolet; at a given frequency in the infrared, the increase of  $n$  for the solutions over  $n$  for water is directly proportional to the intensities of the ultraviolet bands of the solutions and is greater for electronic bands in the near ultraviolet than in the far ultraviolet. Since our values of  $n$  in the near infrared show little dependence on the positive ions (Figure 1), we can conclude that the ultraviolet bands of the tightly bound electronic structures of the positive ions  $\text{Li}^+$ ,  $\text{Na}^+$ , and  $\text{K}^+$  are either weak or located in the remote ultraviolet or both; conversely, since our values of  $n$  are strongly dependent on the negative ions (Figure 2), we can conclude that the ultraviolet bands of the loosely bound electronic structures of the negative ions  $\text{F}^-$ ,  $\text{Cl}^-$ ,  $\text{Br}^-$ , and  $\text{I}^-$  are either strong or located in the near ultraviolet or both.

Our determinations of  $k$  have given good values of this quantity at the centers of strong bands where values of  $k = \lambda\alpha/4\pi$  cannot be determined with high precision by transmission techniques because of large uncertainties in the Lambert coefficient  $\alpha$  resulting from difficulties in the preparation of extremely thin absorbing layers of uniform and precisely measured thickness and because of the presence of small amounts of stray radiation in nearly all spectrometers.<sup>7</sup> Because of our limiting uncertainty  $\delta k \cong 0.03$ , the fractional uncertainty  $\delta k/k$  increases in the wings of absorption bands and in other spectral regions where  $k$  is small. Thus, we have not made any important contributions to existing knowledge of band contours; for example, the  $3400\text{-cm}^{-1}$  band of liquid water, which is actually a complex region of absorption consisting of several overlapping unresolved components, we have treated in our discussion of Figures 1-4 as a single band with characteristic frequency, peak height, and half-width.

Earlier studies<sup>10-12</sup> of the infrared absorption of solutions of alkali halides have revealed certain superficial similarities between the effects of dissolved ions and the effects of temperature on the positions of the absorption bands of water. The comparison between these types of effects was prompted by the early theoretical work of Bernal and Fowler,<sup>13</sup> who attempted to explain various phenomena on the basis of disruptive effects of ions on the tetrahedrally bonded intermolecular lattice of water; according to this theory the disruptive effects were related to the ratio of the magnitude of the ionic charge to ionic radius; large ions such as  $\text{I}^-$  were supposed to have a greater disruptive effect than small ions such as  $\text{Li}^+$ . Bernal and Fowler also introduced the concept of the *equivalent structural temperature* of a solution; this equivalent temperature of a solution is the temperature of a pure water sample that would exhibit the same properties as those of the solution. On the basis of these theoretical considerations as modified by subsequent refinements and extensions, some investigators have attempted to classify various ions as "structure makers," which actually contribute to the regularity of the water structure of the type produced by decreasing the temperature of pure water, and as "structure breakers," which have the reverse effect.

Our recent study of the optical constants of water at different temperatures<sup>8</sup> and studies of ice<sup>14</sup> make it possible to compare parameters other than band position in solution with water at various temperatures. For the  $3400\text{-cm}^{-1}$  water band a summary of our results given in Table II of ref 14 indicates that (1) the peak value of  $k$  decreases, (2) the frequency of the  $k$  peak increases, and (3) the width of the band between points of half-maximum  $k$  increases with increasing temperature. Our present results for alkali bromides (Figure 1) show little significant change in the  $k$  peak height, a small shift of the band maximum to higher frequencies with barely significant differences produced by  $\text{Li}^+$ ,  $\text{Na}^+$ , and  $\text{K}^+$ , and a narrowing of the absorption band with the width of the peak in  $\text{LiBr}$  somewhat larger than for the other two solutions. Thus, (1) the nearly constant peak value of  $k$  would indicate a nearly unchanged equivalent temperature; (2) the shift of the peak to higher frequencies would indicate an increase in equivalent temperature; (3) the narrowing of the absorption peak would indicate a decrease in equivalent temperature. In the case of the potassium halide solutions (1) the decrease in  $k$  peak height is characteristic of a temperature increase in the expected order for the large ions  $\text{Cl}^-$ ,  $\text{Br}^-$ , and  $\text{I}^-$  but is even greater for the smaller  $\text{F}^-$  ion; (2) the shift of the peak to increasingly higher frequencies for the  $\text{Cl}^-$ ,  $\text{Br}^-$ , and  $\text{I}^-$  would indicate an increasing structural temperature, while the shift of the band to lower frequencies in  $\text{KF}$  is characteristic of a decrease in structural temperature; (3) the progressive narrowing of the band for  $\text{Cl}^-$ ,  $\text{Br}^-$ , and  $\text{I}^-$  would indicate a progressive decrease in structural temperature, but the greatly broadened peak for  $\text{F}^-$  would indicate an increase in structural temperature. These ambiguous interpretations are further emphasized in the analysis of Figures 4 and 5, which show the influence of concentration of  $\text{KI}$  and  $\text{KF}$ , respectively.

Thus, it would appear that any interpretation of our results for the  $3400\text{-cm}^{-1}$  band in terms of an equivalent structural temperature or in terms of various ions as structure makers or breakers leads to such serious ambiguities that it is of questionable value. It is, of course, possible that future studies in which the individual components of the  $3400\text{-cm}^{-1}$  band are resolved can alter our present conclusion on this subject.

In the case of the  $\nu_2$  band near  $1640\text{ cm}^{-1}$  our studies of liquid water and ice show that (1) the peak value of  $k$  shows no significant change in temperature for liquid water but is considerably smaller for ice; (2) the peak frequency of  $1640\text{ cm}^{-1}$  is not significantly altered with temperature change in water or in ice near the melting point but shifts to  $1600\text{ cm}^{-1}$  in ice at  $-170^\circ$ ; and (3) that the width of the band decreases monotonically with increasing temperature. Comparison of the results for the  $\nu_2$  band in Figures 5-7 indicate that solutes also have little influence on the  $\nu_2$  band characteristics; the results shown in Figure 8 indicate some possible influences of  $\text{KF}$  on the  $\nu_2$  band, but these marginally significant changes cannot be interpreted with clarity in terms of changes in structural temperature.

In the case of the librational band  $\nu_L$ , our earlier studies of water and ice have shown that (1) the peak value of  $k$  does not change significantly with temperature; (2) the peak shifts to lower frequency with increasing temperature; and (3) that the band width increases with increasing temperature. For the alkali bromides (Figure 5), (1) the peak values of  $k$  are all significantly larger than the  $k$

maximum for water; (2) the frequency of the band maximum is shifted to lower frequencies in the order  $\text{Li}^+$ ,  $\text{Na}^+$ ,  $\text{K}^+$ ; (3) no valid conclusions can be drawn with regard to band width. For the potassium halides (Figure 6), (1) peak values of  $k$  are all greater than for water; (2) the position of the peak is shifted to lower frequencies in the increasing order  $\text{F}^-$ ,  $\text{Cl}^-$ ,  $\text{Br}^-$ , and  $\text{I}^-$ ; (3) no conclusions can be drawn with regard to band width. With increasing concentration of KI (Figure 7), (1) peak height increases monotonically; (2) the peak position shifts to lower frequencies; (3) there is some evidence of progressive narrowing of the band. With increasing concentration of KF (Figure 8), (1) the peak value of  $k$  decreases monotonically; (2) the position of the peak shifts monotonically to higher frequencies; (3) there is some indication of band narrowing and there is increasing evidence of a high-frequency shoulder. For the  $\nu_L$  band, (1) there is thus no temperature analog of the observed change in peak values of  $k$ ; (2) at a common 4 M concentration, the shift of the band peak to lower frequencies would indicate an increased structural temperature; with increasing concentration of KI the progressive shift of the peak to lower frequencies would indicate an increased structural temperature; with increasing concentration of KF, we might conclude that the equivalent structural temperature of the solution is initially greater than 27° but decreases to much lower values at the highest concentrations; (3) the progressive narrowing of the librational band can be interpreted as progressive reduction of the structural temperature for increasing concentration of KF; no valid conclusions can be drawn for the other solutions.

Thus, for the  $\nu_L$  band there seems to be no unique way to interpret the observed solution spectra in terms of an equivalent structural temperature. The situation for the  $\nu_L$  band is worse than in the case of the 3400  $\text{cm}^{-1}$  in view of the fact that the large observed changes in the maximum value of  $k$  for the  $\nu_L$  band cannot be produced by either increase or decrease in the temperature of pure water.

In the Bernal-Fowler theory the concept of structural temperature was introduced to account for perturbation of the water lattice by ions; the concept should thus be applied only to dilute solutions in which the number density of ions is small as compared with the number density of water molecules constituting the lattice. In the more concentrated solutions used in the present study of reflection and in earlier studies of absorption, this concentration limitation has not been fulfilled; thus, it is not surprising that the concept of structural temperature involving the classification of various ions as structure makers and structure breakers should fail. In the most concentrated solutions used in the present study nearly every  $\text{H}_2\text{O}$  molecule interacts directly or indirectly with one or more ions; Draeger and Williams<sup>16</sup> have pointed out that it is remarkable that the spectra of such concentrated solutions bear any resemblance to the spectrum of water, particularly in the far infrared.

The present study has been concerned with the quantitative measurements of the spectral reflectance and with the determination of absolute values of refractive indices  $n$  and absorption indices  $k$  from measured values of reflectance. Our results for the absorption indices  $k$  are closely related to the results of numerous earlier studies of infrared absorption spectra, which have recently been discussed in considerable detail by Verrill.<sup>17</sup> Many of the results obtained in the present study have also been ob-

tained in studies of absorption. However, unless extreme care is taken in absorption measurements,<sup>7,8</sup> it is difficult to obtain accurate values of the Lambert absorption coefficients  $\alpha$  or the associated absorption indices  $k$  in the vicinity of strong absorption bands. In the vicinity of the strong absorption band with maximum at 3400  $\text{cm}^{-1}$  in the spectrum of water, the difficulties are particularly great; under conditions of low resolution the observed band center as given in a plot of spectral transmittance can actually shift with cell thickness.<sup>18</sup> Inadequate control of absorption cell thickness in the early study of aqueous solutions by Millet and Williams<sup>19</sup> apparently led to spurious results for the 3400- $\text{cm}^{-1}$  band but caused no difficulties in other spectral regions.<sup>17</sup>

Recent absorption studies have given valuable information<sup>17</sup> concerning the influence of solutes on the  $\nu_1$  and  $\nu_2$  bands by making effective use of isotopic shifts. In HDO the  $\nu_1$  and  $\nu_3$  are widely separated in frequency; by absorption studies of HDO as an impurity in liquid  $\text{H}_2\text{O}$  and in liquid  $\text{D}_2\text{O}$ , the  $\nu_1$  and  $\nu_3$  bands of HDO can be studied separately under conditions where neither is overlapped by the overtone band  $2\nu_2$ . Although the results of these absorption studies have given valuable information concerning interactions between ions and HDO molecules, it is possibly doubtful whether the HDO results can be applied directly to quantitative studies of the optical properties of liquid  $\text{H}_2\text{O}$  or of ordinary aqueous solutions. In liquid  $\text{H}_2\text{O}$  the frequencies of the molecular vibrations  $\nu_1$ ,  $\nu_3$ , and  $2\nu_2$  are so nearly the same that resonance effects producing band splittings and intensity anomalies may occur.

However, it would possibly seem desirable to consider various models for the association of monatomic ions with individual water molecules. In the Bernal-Fowler theory, the effects produced by ions depend on ionic charge and ionic radius and not on the sign of the charge; although this theory and subsequent refinements of it account satisfactorily for many observed effects, it has failed in explaining the effects observed in the present study and in studies of infrared absorption, which reveal that negative ions have more influence than do positive ions; for example, the influence of the  $\text{F}^-$  ion is much greater than the effects produced by the  $\text{K}^+$  ion even though the two ions have nearly the same radius.

In the  $\nu_1$ ,  $\nu_2$ ,  $\nu_3$ , and  $\nu_L$  modes of water, most of the actual motion is associated with H atoms rather than with the more massive O atoms. In the association of a water molecule with a negative monatomic ion, the effect of the energetically favored close proximity of the negative ion to the H atoms of the polar water molecule would be expected to be greater than the effect of a positive ion of the same size, for which the energetically favored position would be near the O atom of the polar water molecule. Elaboration of a simple model of this type to include possible ion clustering might lead to an interpretation of some of the observed effects of ions on the water spectrum.

We might close by pointing out that carefully executed ATR measurements are capable of providing greater precision<sup>20</sup> in the determination of  $n$  and  $k$  from directly measured quantities without the necessity of employing KK analysis. ATR techniques should provide further information regarding band contours. We hope that our present results can soon be checked by ATR techniques. It would also be desirable to extend the measurements to frequencies lower than our present limit of 350  $\text{cm}^{-1}$  to include the hindered-translation band<sup>8</sup> near 180  $\text{cm}^{-1}$ .

*Acknowledgments.* We wish to express our appreciation to the Office of Naval Research for support of the work at Kansas State University and to the National Science Foundation for support at the University of Missouri—Kansas City.

#### References and Notes

- (1) W. M. Irvine and J. B. Pollack, *Icarus*, **8**, 324 (1968).
- (2) L. Pontier and C. Dechambenoy, *Ann. Geophys.*, **21**, 462 (1965); **22**, 633 (1966).
- (3) M. R. Querry, B. Curnutte, and D. Williams, *J. Opt. Soc. Amer.*, **59**, 1299 (1969).
- (4) V. M. Zolotarev, B. A. Mikhailov, L. I. Aperovich, and S. I. Popov, *Opt. Spectrosc.*, **27**, 790 (1969). [Translation, *Opt. Spectrosc.*, **27**, 430 (1969)].
- (5) A. N. Rusk, D. Williams, and M. R. Querry, *J. Opt. Soc. Amer.*, **61**, 895 (1971).
- (6) G. M. Hale, M. R. Querry, A. N. Rusk, and D. Williams, *J. Opt. Soc. Amer.*, **62**, 1103 (1972).
- (7) C. W. Robertson and D. Williams, *J. Opt. Soc. Amer.*, **61**, 1316 (1971).
- (8) C. W. Robertson, B. Curnutte, and D. Williams, *Mol. Phys.*, **26**, 183 (1973).
- (9) P. S. Ray, *Appl. Opt.*, **11**, 1836 (1972).
- (10) D. Williams and W. Millett, *Phys. Rev.*, **66**, 6 (1944).
- (11) G. R. Choppin and K. Buijs, *J. Chem. Phys.*, **39**, 2042 (1963).
- (12) H. Yamatera, B. Fitzpatrick, and G. Gordon, *J. Mol. Spectrosc.*, **4**, 268 (1964).
- (13) J. D. Bernal and R. H. Fowler, *J. Chem. Phys.*, **1**, 515 (1933).
- (14) J. W. Schaaf and D. Williams, *J. Opt. Soc. Amer.*, **63**, 726 (1973).
- (15) J. E. Bertie, J. J. Labbe, and E. Whalley, *J. Chem. Phys.*, **50**, 4501 (1969).
- (16) D. A. Draeger and D. Williams, *J. Chem. Phys.*, **48**, 401 (1968).
- (17) R. E. Verrall, "Water: A Comprehensive Treatise," Vol. 3, F. Franks, Ed., Plenum Press, New York, N. Y., 1973, Chapter 5, pp 211-264.
- (18) E. K. Plyler and C. J. Craven, *J. Chem. Phys.*, **2**, 303 (1934).
- (19) D. Williams and W. Millett, *Phys. Rev.*, **66**, 6 (1944).
- (20) B. L. Crawford, private communication.

## Infrared Optical Constants of Aqueous Solutions of Electrolytes, Acids and Bases<sup>1</sup>

Paul Rhine, Dudley Williams,\*

Department of Physics, Kansas State University, Manhattan, Kansas 66506

G. Michael Hale, and Marvin R. Querry

Department of Physics, University of Missouri, Kansas City, Missouri 64110 (Received January 7, 1974)

Publication costs assisted by Kansas State University and the University of Missouri—KC

The normal-incidence spectral reflectances of aqueous solutions of HCl, NaOH, and KOH have been measured in the spectral range 350–5000  $\text{cm}^{-1}$ . From the measured values of reflectance we have used a Kramers–Kronig phase-shift analysis to obtain values of the real  $n$  and imaginary  $k$  parts of the refractive indices of the solutions. The spectral reflectance and the refractive index  $n$  of the solutions in the 5000–4000- $\text{cm}^{-1}$  region and in other spectral regions that are remote from characteristic water bands increase monotonically with concentration. Plots of absorption index  $k$  for HCl as a function of concentration indicate (1) a gradual decrease in the peak height and frequency of the 3400- $\text{cm}^{-1}$  water band, (2) strong general absorption in the 3200–2000- $\text{cm}^{-1}$  region, (3) an apparent shift of the  $\nu_2$  water band toward high frequencies, (4) the appearance of a new band near 1100  $\text{cm}^{-1}$ , and (5) shifts of the librational water band to lower frequencies. Plots of  $k$  for NaOH as a function of concentration reveal (1) a reduction of the  $k$  peak for water near 3400  $\text{cm}^{-1}$ , (2) the appearance of strong additional absorption near 2800  $\text{cm}^{-1}$  along with strong general absorption in the 3000–1700- $\text{cm}^{-1}$  region, and (3) shifts in the position of the librational water band. The observed effects are discussed qualitatively.

### Introduction

In an earlier paper<sup>2</sup> we have given the results of a study of near-normal-incidence spectral reflectance of aqueous solutions of alkali halides in the 350–5000- $\text{cm}^{-1}$  region of the infrared. By applying the Kramers–Kronig (KK) theorem for phase-shift analysis, we obtained values of the real  $n$  and imaginary  $k$  parts of the complex refractive index  $\tilde{N} = n + ik$  for the spectral region covered in our measurements of reflectance.

In the present paper we report a similar study of solutions of the strong acid HCl and two strong bases, NaOH and KOH. None of the alkali or halide ions involved in our earlier studies had characteristic bands in the infrared. In the present study, the  $\text{OH}^-$  ion was expected to exhibit a characteristic vibrational band; the hydrogen ions are presumably strongly attached to one or more water molecules in such a way that new characteristic bands could result.

### Experimental Section

The experimental arrangements employed in the reflectance measurements were similar in all details to those described in our previous paper; similar methods of carry-

ing out the KK analysis were also employed. The uncertainties  $\delta n$  in  $n$  amount to  $\pm 1\%$  of the plotted values over most of the range but increase to as much as  $\pm 3\%$  in the 500–350- $\text{cm}^{-1}$  region. The uncertainty  $\delta k$  is approximately  $\pm 0.03$  over most of the range but may increase to  $\pm 0.05$  at 350  $\text{cm}^{-1}$ .

### Results

Our results are presented graphically in Figures 1–6. The upper panel in each figure gives measured spectral reflectance  $R$  at near-normal incidence; the center panel gives the values of the refractive index  $n$  as given by the KK analysis; the bottom panel gives the values of the absorption index  $k$ . In each panel, for purposes of comparison, we indicate the corresponding values for water by a light continuous curve.

*A. Hydrochloric Acid.* The spectrum in the 5000–2500- $\text{cm}^{-1}$  region is dominated by a strong absorption band, which appears in the vicinity of 3400  $\text{cm}^{-1}$  in the spectrum of water at 27°. Figure 1 gives our results for HCl at the concentrations indicated in the legend. The values of  $R$  and  $n$  for the solutions in the 5000–3800- $\text{cm}^{-1}$  range are greater than the values of water; the difference between

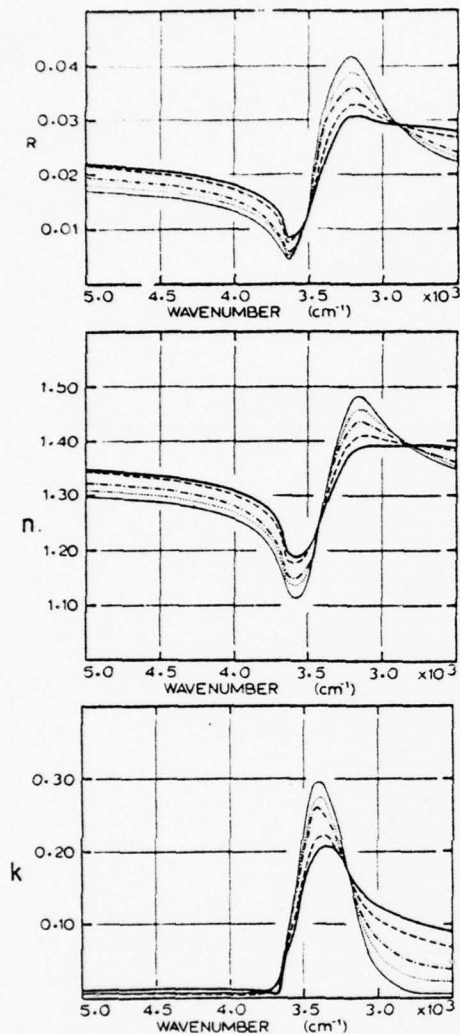


Figure 1. Reflectivity, refractive index, and absorption index curves for HCl solutions: 12 M, heavy continuous; 8 M, dashed; 4 M, dash-dot-dash; 2 M, dotted; water, light continuous.

the curves for the solutions and the curve for water increases monotonically with increasing concentration. In the vicinity of the resonance feature near  $3400\text{ cm}^{-1}$  the  $R$  and  $n$  curves cross and the resonance feature becomes less sharp with increasing concentration. In view of our uncertainty  $\delta k = 0.03$ , the values of the absorption index are not measurably different from zero in the  $5000\text{--}3800\text{ cm}^{-1}$  range. The absorption peak at  $3400\text{ cm}^{-1}$  in pure water shifts to noticeably lower frequencies with increasing concentration of HCl; the peak value of  $k$  becomes progressively lower with increasing concentration. Although the  $k$  peak appears to increase in width at half-height, this effect may be due to the greatly increased absorption in the low-frequency wing of the band. General absorption occurs in the region between  $3200$  and  $2500\text{ cm}^{-1}$  and increases with increasing concentration; there is no evidence of a separate peak in  $k$  associated with the general absorption.

The spectra of HCl solutions in the  $2500\text{--}350\text{ cm}^{-1}$  region are shown in Figure 2. The spectral reflectance of all solutions is higher than that of water for all regions except

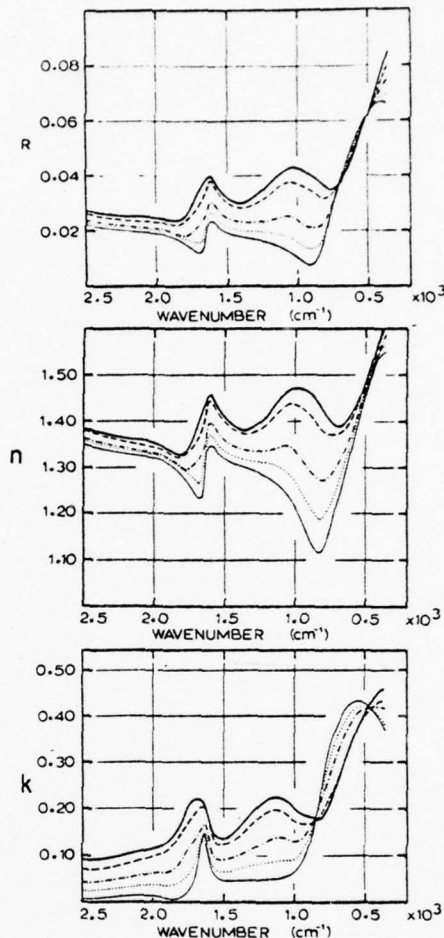


Figure 2. Reflectivity, refractive index, and absorption index curves for HCl solutions: 12 M, heavy continuous; 8 M, dashed; 4 M, dash-dot; 2 M, dotted; water, light continuous.

the  $700\text{--}500\text{ cm}^{-1}$  range, where all the measured reflectance curves nearly coincide; the same is true for the  $n$  curves. In both  $R$  and  $n$  curves, the resonance features in the vicinity of the  $1640\text{ cm}^{-1}$  water band apparently become broader and shift to higher frequency. An additional resonance feature not present in the spectrum of pure water produces a broad  $n$  maximum near  $1000\text{ cm}^{-1}$  in the 8 and 12 M solutions.

The absorption characteristics of the solutions are shown by the plots of  $k$  in the bottom panel. All solutions exhibit stronger absorption than water in the  $2500\text{--}1800\text{ cm}^{-1}$  region; the absorption in this region is general and is not characterized by clearly discernible peaks. The  $k$  peak appearing at  $1640\text{ cm}^{-1}$  in the spectrum of pure water appears to increase in height, to broaden, and to shift to higher frequencies with increasing concentration. At the highest HCl concentrations a new broad band having no counterpart in the water spectrum appears in the vicinity of  $1100\text{ cm}^{-1}$ . The librational band with maximum  $k$  near  $600\text{ cm}^{-1}$  in the water spectrum shifts to progressively lower frequencies with increasing HCl concentration.

*B. Sodium and Potassium Hydroxide.* The results obtained for NaOH and KOH in the  $5000\text{--}2500\text{ cm}^{-1}$  region

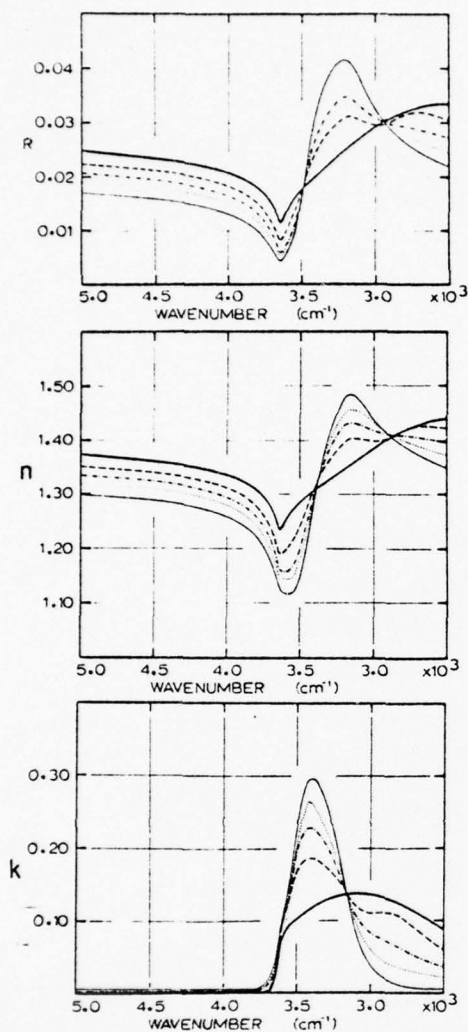


Figure 3. Reflectivity, refractive index, and absorption index curves for NaOH solutions: 16 *M*, heavy continuous; 8 *M*, dashed; 4 *M*, dash-dot-dash; 2 *M*, dotted; water, light continuous.

are shown in Figures 3 and 4, respectively. In spectral regions remote from absorption bands, the values of  $R$  and  $n$  are slightly larger for KOH than for NaOH; in other respects the contours of the  $R$  and  $n$  curves for the solutions are similar for corresponding concentrations. In the vicinity of the  $3400\text{-cm}^{-1}$  water band, the dispersion features in the  $R$  and  $n$  curves for the 2 and 4 *M* solutions become progressively less pronounced with increasing concentration. The curves for the 8 *M* solutions for both hydroxides show clearly an additional small dispersion feature near  $3000\text{ cm}^{-1}$ ; further evidence of this feature appears in the  $n$  and  $R$  curves for the 16 *M* solution of KOH but is less apparent in the corresponding curves for NaOH.

The plots of the absorption index  $k$  in the bottom panels of Figures 3 and 4 indicate a progressive reduction of peak height of the  $3400\text{-cm}^{-1}$  water band along with a progressive broadening of the band toward lower frequencies with increasing concentration. For the 8 *M* solutions, there is some evidence of a second incompletely resolved band near  $2800\text{ cm}^{-1}$ . In the 16 *M* solution of KOH, there is clear evidence of a peak near  $2800\text{ cm}^{-1}$ , where the value of  $k$  is greater than that of  $k$  at  $3400\text{ cm}^{-1}$ . In the  $k$

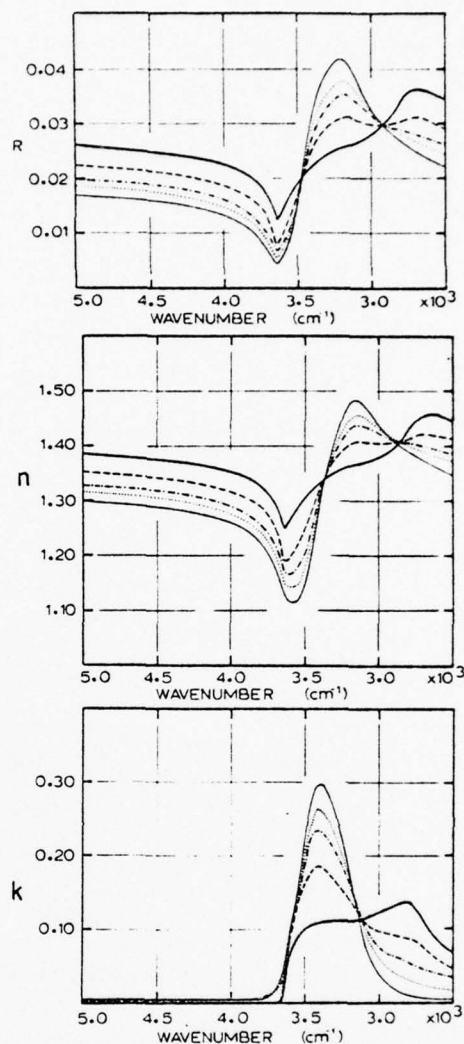


Figure 4. Reflectivity, refractive index, and absorption index curves for KOH solutions: 16 *M*, heavy continuous; 8 *M*, dashed; 4 *M*, dash-dot-dash; 2 *M*, dotted; water, light continuous.

curve for 16 *M* NaOH, a single broad region of absorption replaces the two peaks appearing at  $3400$  and  $2800\text{ cm}^{-1}$  in the spectrum of the 8 *M* solution.

The results obtained in the  $2500\text{-}350\text{-cm}^{-1}$  region for NaOH and KOH are shown in Figures 5 and 6, respectively. In most of this spectral region, values of  $R$  and  $n$  become progressively greater with increasing concentration; however, in the  $600\text{-}400\text{-cm}^{-1}$  region, the  $R$  and  $n$  curves for the 16 *M* solutions cross the corresponding curves for lower concentrations and attain lower values at  $400\text{ cm}^{-1}$ . In the vicinity of the  $1640\text{-cm}^{-1}$  water band all  $R$  and  $n$  curves for the hydroxide solutions exhibit dispersion features. However, for the 8 and 16 *M* solutions there is some evidence of a narrower additional dispersion feature near  $1500\text{ cm}^{-1}$ ; this narrow feature is clearly separated from the  $1640\text{-cm}^{-1}$  water band in the NaOH solutions but is barely resolved in the KOH solutions. Except for the 16 *M* solutions, the major dispersion feature near  $600\text{ cm}^{-1}$  shifts to progressively lower frequencies with increasing concentration; for the 16 *M* solution the maxima in  $R$  and  $n$  appear at considerably higher frequencies than for the less concentrated solutions.

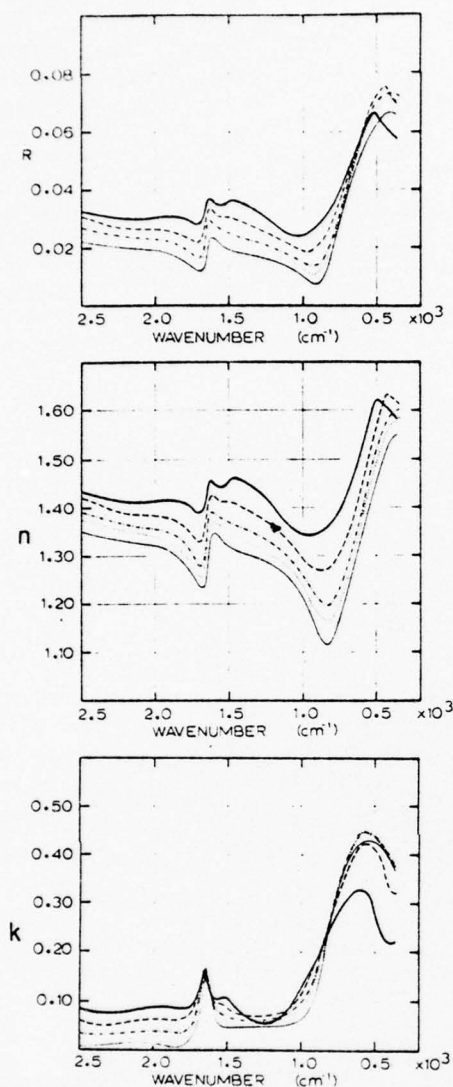


Figure 5. Reflectivity, refractive index, and absorption index curves for NaOH: 16 M, heavy continuous; 8 M, dashed; 4 M, dash-dot-dash; 2 M, dotted; water, light continuous.

The absorption indices  $k$  for the hydroxides are plotted in the bottom panels of Figures 5 and 6. In the entire spectral region between 3400 and 1640  $\text{cm}^{-1}$  the values of  $k$  for all solutions are much greater than the corresponding  $k$  values for water; for the more concentrated hydroxide solutions the absorption indices  $k$  at all frequencies in the interband region maintain values that are nearly half the value of  $k$  at the center of the 1640- $\text{cm}^{-1}$  band in pure water. The value of  $k$  at 1640  $\text{cm}^{-1}$  remains constant in all solutions within our limits of uncertainty  $\delta k = 0.03$ ; there is some evidence of a splitting of the band at higher concentrations. The values of  $k$  for the 2 and 4 M solutions in the vicinity of the 600- $\text{cm}^{-1}$  water band are also within the limits of uncertainty equal to the  $k$  value for pure water. There is a small progressive shift of the 600- $\text{cm}^{-1}$  band to lower frequencies in the 2, 4, and 8 M KOH solutions but little change in band position for the corresponding NaOH solutions; this band becomes narrower, has a smaller maximum value of  $k$ , and shifts noticeably to higher frequencies in the 16 M solutions.

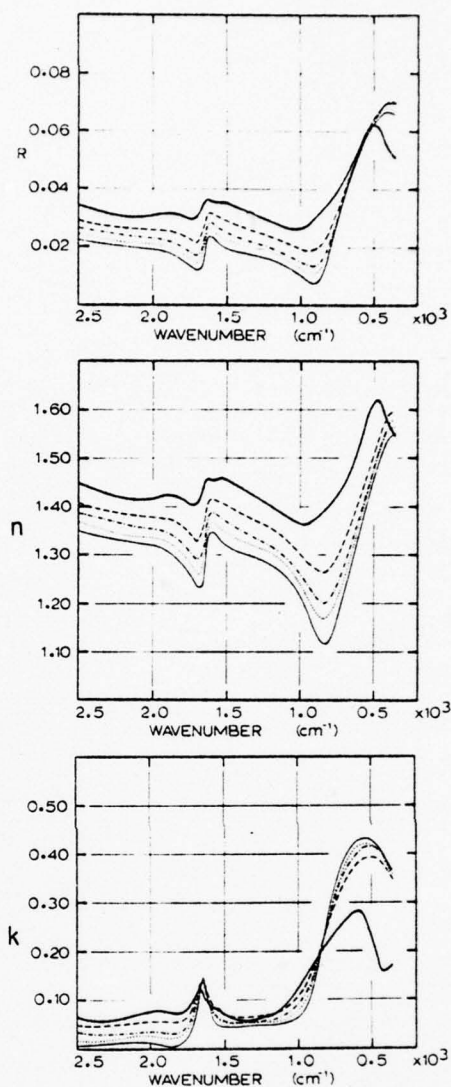


Figure 6. Reflectivity, refractive index, and absorption index curves for KOH: 16 M, heavy continuous; 8 M, dashed; 4 M, dash-dot-dash; 2 M, dotted; water, light continuous.

#### Discussion of Results

The major portion of the new information regarding solutions obtainable from the present reflectance studies is connected with the quantitative measurements of the refractive indices  $n$  and the absorption indices  $k$ . Many earlier measurements of transmission spectra of acids and bases have provided only qualitative values of Lambert absorption coefficients  $\alpha(\nu)$ , since the published curves were labeled "absorption" or "transmission" with no numbers on the ordinate scales; in view of the difficulties<sup>3</sup> involved in preparing uniform absorption layers of well-measured thickness, these earlier transmission studies could not have been expected to yield quantitative results. However, many of the features shown in the  $k(\nu)$  vs.  $\nu$  plots of Figures 1-6 have been noted in earlier studies. No earlier studies have provided values of the refractive index  $n(\nu)$  for comparison with the present work.

A. *Hydrochloric Acid*. In a beautiful piece of work Falk and Giguere<sup>4</sup> have investigated the transmission spectra of aqueous solutions of five mineral acids with the purpose



of identifying spectral features characteristic of the  $\text{H}_3\text{O}^+$  ion; these authors also reviewed earlier work on the subject. Falk and Giguere observed increased absorption associated with broad bands with maxima at 1205, 1750, and 2900  $\text{cm}^{-1}$ , which they attributed to the  $\text{H}_3\text{O}^+$  ion, and report that the lifetime of this ion in aqueous solution is longer than  $10^{-13}$  sec. These band positions are in close agreement with the positions of  $\text{H}_3\text{O}^+$  bands reported in earlier infrared studies of crystalline hydrates of strong acids<sup>5-7</sup> and in related Raman studies.<sup>8,9</sup>

In view of these results and other structural information, the observed spectrum has been interpreted<sup>7</sup> in terms of a pyramidal form of  $\text{H}_3\text{O}^+$ , which is isoelectronic with  $\text{NH}_3$ ; the incompletely resolved  $\nu_1$  and  $\nu_3$  fundamentals are associated with the broad band near 2900  $\text{cm}^{-1}$ , the  $\nu_4$  fundamental with the band near 1205  $\text{cm}^{-1}$ , and the  $\nu_2$  fundamental with the band near 1750  $\text{cm}^{-1}$ . However, Pavia and Giguere<sup>10</sup> have shown that the spectrum of perchloric acid dihydrate gives evidence of the ion  $\text{H}_5\text{O}_2^+$ . Gilbert and Sheppard<sup>11</sup> have recently obtained infrared spectra of crystalline mono- and higher hydrates of HCl and HBr; the higher hydrates exhibit features not clearly attributable to  $\text{H}_3\text{O}^+$ ; in particular, in the di- and trihydrates there is evidence for the  $\text{H}_5\text{O}_2^+$  ion. In the spectrum of the  $\text{H}_5\text{O}_2^+$  ion, the existence of which is supported by X-ray diffraction measurements,<sup>12,13</sup> bands corresponding to  $\nu_2$  and  $\nu_4$  in  $\text{H}_3\text{O}^+$  in the monohydrate spectrum are split into sharp components in the dihydrate and broaden in the trihydrate; the  $\nu_1$  and  $\nu_3$  bands in  $\text{H}_3\text{O}^+$  coalesce into a single somewhat narrower band in the di- and trihydrate spectra.

The broad regions of absorption shown in our plots of  $k$  for HCl shown in Figures 1 and 2 doubtless include contributions from both  $\text{H}_3\text{O}^+$  and  $\text{H}_5\text{O}_2^+$  ions. However, attempts to divide the integrals  $\int k(\nu) d\nu$  or  $\int \alpha(\nu) d\nu$  between the two forms of hydrated  $\text{H}^+$  ions would at present represent mere speculation; however, evaluation of these integrals in restricted spectral intervals for various HCl concentrations might be used in testing various possible future theories.

We have also compared the reflection spectra of HCl with HBr. Although HBr solutions have higher reflectivity as a result of stronger  $\text{Br}^-$  bands in the ultraviolet,<sup>2</sup> the general shape of the two reflectance curves exhibit marked similarity. Similarities in the spectra of HCl and HBr crystal hydrates were also noted by Gilbert and Sheppard.<sup>11</sup>

The observed shift of the libration band of the solutions in the 600- $\text{cm}^{-1}$  region to lower frequencies with increasing HCl concentration confirms the results obtained in the earlier transmission study of Draeger and Williams.<sup>14</sup>

*B. Sodium and Potassium Hydroxide.* Although there has been little discussion of the nature of the hydration of the  $\text{OH}^-$  ion, the general absorption of the hydroxides in the region between the 3400- and 1640- $\text{cm}^{-1}$  water bands is nearly as intense as the corresponding HCl absorption, which we have attributed to the  $\text{H}_3\text{O}^+$  and  $\text{H}_5\text{O}_2^+$  ions. The absorption spectrum of crystalline NaOH is characterized by a sharp band at 3637  $\text{cm}^{-1}$  attributed to the  $\text{OH}^-$  ion;<sup>15</sup> a similar band at 3600  $\text{cm}^{-1}$  occurs in the spectrum of KOH.<sup>16-18</sup> Jones<sup>19</sup> has reported an extremely sharp  $\text{OH}^-$  band at 3678  $\text{cm}^{-1}$  in crystalline LiOH; in the hydrated crystal LiOH· $\text{H}_2\text{O}$  Jones found a somewhat broadened  $\text{OH}^-$  band at 3574  $\text{cm}^{-1}$  and an extremely broad, intense band with a maximum at 2850  $\text{cm}^{-1}$ , which he attributed to the overlapping  $\nu_1$  and  $\nu_3$  bands of

the strongly hydrogen-bonded water molecule of crystallization. The frequency of the band due to the water of crystallization is even lower than that of the  $\text{H}_2\text{O}$  molecule in ice. In a Raman study of KOH solutions Busing and Hornig<sup>20</sup> report a band with a sharp peak near 3600  $\text{cm}^{-1}$  with an accompanying broad band extending to frequencies as low as 2200  $\text{cm}^{-1}$ ; these authors attribute the sharp peak to  $\text{OH}^-$  and the broad band to three overlapping unresolved bands associated with molecules of the solvent.

Although there is no evidence of a resolved sharp  $\text{OH}^-$  band in the bottom panels of Figures 3 and 4, the absorption index curves rise abruptly near 3700  $\text{cm}^{-1}$ ; this abrupt rise may correspond to the sharp band noted by Busing and Hornig in their Raman study. However, if a sharp  $\text{OH}^-$  band is present in the infrared, its intensity is small as compared with the broader bands at lower frequencies. It would appear from Figures 3 and 4 that there are two such bands with frequencies in the vicinity of 3400 and 2800  $\text{cm}^{-1}$ , respectively; it is tempting to attribute the former to the normally hydrogen-bonded molecules of liquid water and the latter to water molecules strongly hydrogen-bonded to  $\text{OH}^-$  ions. If this interpretation involving two types of differently hydrogen-bonded molecules is correct, it might also account for the apparent splitting of the band at 1640  $\text{cm}^{-1}$  associated with the  $\nu_2$  bending fundamental of the  $\text{H}_2\text{O}$  molecule in liquid water; this splitting is particularly pronounced in the 16  $M$  solution curves in Figures 5 and 6.

We note that in the  $k(\nu)$  vs.  $\nu$  curves for the 16  $M$  hydroxide solutions there is an apparent shift of the librational maximum to higher frequencies and a marked narrowing of the band. The curves for the other less concentrated solutions are in general agreement with the earlier work of Draeger and Williams,<sup>14</sup> whose study was limited to hydroxide solutions with concentrations of 12  $M$  and less and was hampered by the lack of suitable absorption cell windows.

We note that the influence of  $\text{Na}^+$  and  $\text{K}^+$  ions on the water structure is nearly negligible as compared with the influence of the  $\text{OH}^-$  ions, which are capable of forming hydrogen bonds with water molecules. In the case of acids, the influence of  $\text{Cl}^-$  and  $\text{Br}^-$  ions on the water structure is similarly small as compared with the hydroxide ions that are responsible for the hydrates  $\text{H}_3\text{O}^+$  and  $\text{H}_5\text{O}_2^+$ , or possibly even higher hydrates.

The structure of the crystal monohydrate LiOH· $\text{H}_2\text{O}$  has been determined by Pepinsky<sup>21</sup> on the basis of X-ray diffraction measurements; his results indicate that the distance between the oxygen of the  $\text{H}_2\text{O}$  unit and the oxygen of the nearest  $\text{OH}^-$  unit is 2.68 Å as compared with the 2.76 Å O-O distance in ice. This short distance implies strong hydrogen bonds  $\text{H}_2\text{O} \cdots \text{OH}^-$ ; thus, it seems probable that the broad band with maximum near 2850  $\text{cm}^{-1}$  in the spectrum of the monohydrate crystal is indeed due to strongly hydrogen-bonded  $\text{H}_2\text{O}$  molecules. The increasingly strong absorption noted in this region in the present study would seem to indicate increasingly great numbers of strong  $\text{H}_2\text{O} \cdots \text{OH}^-$  hydrogen bonds as the concentration increases. In the case of the 16  $M$  concentration, there are no longer sufficient numbers of water molecules to approximate a normal water structure; this paucity of solvent molecules results in the marked decrease in  $k(\nu)$  in the 3400- $\text{cm}^{-1}$  region and also near 600  $\text{cm}^{-1}$ , where stronger bonds to  $\text{OH}^-$  units could also account for the apparent increase in the frequency of the li-

bration band of water. If this interpretation is correct, the lack of significant decrease of  $k(\nu)$  near  $1640\text{ cm}^{-1}$  together with the apparent splitting of the  $\nu_2$  peak would indicate greater transition probabilities for the more strongly bonded  $\text{H}_2\text{O}$  units than for the  $\text{H}_2\text{O}$  units in liquid water; this would be in contrast to the situation in ice, for which peak  $k(\nu)$  values in this region are somewhat smaller<sup>22</sup> than for liquid water.

As for the mean lifetimes of the local environment of hydrogen-bonded  $\text{H}_2\text{O} \cdots \text{OH}^-$  units, the reasonably well-defined bands observed in the present study and in earlier Raman studies indicate that local lattice structures exist for times long compared with  $10^{-13}$  sec. However, the fact that single proton resonances<sup>23</sup> are observed in nmr studies of concentrated solutions of strong bases indicates that the mean lifetimes of local lattice structures are short compared with  $10^{-7}$  sec.

In closing, we note that many of our interpretations of the observed spectra in the  $2500\text{--}300\text{-cm}^{-1}$  region can be tested by extending studies of crystalline  $\text{LiOH}\cdot\text{H}_2\text{O}$  into the far infrared and that more detailed information regarding band shapes can probably be obtained by ATR studies of solutions.

We also note that Zundel and his associates<sup>24,25</sup> have recently discussed the properties of  $\text{H}_3\text{O}_2^+$  ions. Their theoretical work dealing with the hydrogen bonds involved may provide an interpretation of some of the continuous general absorption that we have observed in the spectra of acids and bases in the present study.

*Acknowledgment.* It is a pleasure to acknowledge help-

ful discussions with Professors C. H. Moser, R. M. Hamaker, K. F. Purcell, and B. Curnutte.

#### References and Notes

- (1) Supported in part at Kansas State University by the Office of Naval Research and at the University of Missouri, Kansas City, by the National Science Foundation.
- (2) P. Rhine, D. Williams, G. M. Hale, and M. R. Querry, *J. Phys. Chem.*, **78**, 238 (1974).
- (3) (a) A. N. Rusk, M. R. Querry, and D. Williams, *J. Opt. Soc. Amer.*, **61**, 895 (1971); (b) C. W. Robertson and D. Williams, *ibid.*, **61**, 1316 (1971).
- (4) M. Falk and P. A. Giguere, *Can. J. Chem.*, **35**, 1195 (1957).
- (5) D. E. Bethell and N. J. Sheppard, *J. Chim. Phys.*, **50**, C72 (1953).
- (6) C. C. Ferriso and D. F. Hornig, *J. Amer. Chem. Soc.*, **75**, 4113 (1953).
- (7) C. C. Ferriso and D. F. Hornig, *J. Chem. Phys.*, **23**, 1464 (1959).
- (8) J. T. Mulhaupt and D. F. Hornig, *J. Chem. Phys.*, **24**, 169 (1956).
- (9) R. C. Taylor and G. L. Vidale, *J. Amer. Chem. Soc.*, **78**, 5999 (1956).
- (10) A. C. Pavia and P. A. Giguere, *J. Chem. Phys.*, **52**, 3551 (1970).
- (11) A. S. Gilbert and N. Sheppard, *Chem. Commun.*, 337 (1971).
- (12) J. O. Lundgren and I. Olovsson, *Acta Crystallogr.*, **23**, 966 (1967).
- (13) J. O. Lundgren and I. Olovsson, *Acta Crystallogr.*, **23**, 971 (1967).
- (14) D. A. Draegert and D. Williams, *J. Opt. Soc. Amer.*, **48**, 401 (1968).
- (15) W. R. Busing, *J. Chem. Phys.*, **23**, 933 (1955).
- (16) J. A. Ibers, J. Kumamoto, and R. G. Snyder, *J. Chem. Phys.*, **33**, 1164 (1960).
- (17) R. G. Snyder, J. Kumamoto, and J. A. Ibers, *J. Chem. Phys.*, **33**, 1171 (1960).
- (18) R. A. Buchanan, *J. Chem. Phys.*, **31**, 870 (1959).
- (19) L. H. Jones, *J. Chem. Phys.*, **22**, 217 (1954).
- (20) W. R. Busing and D. F. Hornig, *J. Phys. Chem.*, **65**, 284 (1961).
- (21) R. Pepinsky, *Z. Kristallogr., Abt. A*, **102**, 119 (1940).
- (22) J. Schaaf and D. Williams, *J. Opt. Soc. Amer.*, **63**, 726 (1973).
- (23) H. S. Gutowsky and A. Saika, *J. Chem. Phys.*, **21**, 1688 (1953).
- (24) R. Lindemann and G. Zundel, *J. Chem. Soc., Faraday Trans. 2*, **68**, 979 (1972).
- (25) R. Janoschek, E. G. Wiedemann, and G. Zundel, *J. Chem. Soc., Faraday Trans. 2*, **69**, 505 (1973).

The initial work on solutions of strong electrolytes, which involved solutions of alkali halides and strong acids and bases, was extended to include other salts by Dr. Harry D. Downing. The results of his studies are summarized in the following publication by Downing and Williams, which covers work on solutions of alkaline-earth halides and certain other salts.

**Infrared Optical Constants of Aqueous Solutions of Electrolytes. Further Studies of Salts**

Publication costs assisted by the Office of Naval Research

Sir: In earlier studies of reflection spectra we have used Kramers-Kronig methods to obtain values of the real  $n(\nu)$  and imaginary  $k(\nu)$  parts of the complex index of refraction for aqueous solutions of the alkali halides<sup>1</sup> and of strong acids and bases.<sup>2,3</sup> Because our chief interest has been on the influence of these solutes on the infrared spectrum and on the structure of water itself, we have limited our studies to simple salts which do not have characteristic absorption bands of their own in the infrared. There are certain extremely intense bands in the water spectrum that cannot be studied by absorption methods without resorting to rather elaborate techniques;<sup>4,5</sup> for this reason we have employed reflection methods.

This note summarizes the results we have obtained with solutions not previously studied by reflection methods. These include solutions of several alkaline-earth halides, of cupric chloride, and of sodium cyanide. Although the  $\text{CN}^-$  ion of sodium cyanide has a single characteristic vibration band in the infrared, the band is weak as compared with the major water bands and occurs in a spectral region remote from the major water bands.

Our methods of investigation were the same as those employed in earlier studies and involved measurements of spectral reflectance at near-normal incidence in the range 5500–350  $\text{cm}^{-1}$ . Kramers-Kronig analysis provided reliable values of  $n(\nu)$  and  $k(\nu)$  in the range 5000–400  $\text{cm}^{-1}$  within the

TABLE I: Valence Band<sup>a</sup>

Material	Concn, M	$\nu_0$ , $\text{cm}^{-1}$	$k(\nu_0)$	$\Gamma$ , $\text{cm}^{-1}$	$\int k(\nu) d\nu$ , $\text{cm}^{-1}$
Water		3385	0.28	370	112
MgCl <sub>2</sub>	1.9	3400	0.31	380	122
	3.8	3390	0.33	370	121
CaCl <sub>2</sub>	2.2	3420	0.29	380	108
	4.4	3420	0.30	320	100
CaBr <sub>2</sub>	2.0	3420	0.29	360	106
	4.0	3460	0.31	280	98
CuCl <sub>2</sub>	2.15	3390	0.27	410	122
	4.30	3370	0.22	500	114
NaCN	4.0	3440	0.22	420	85
	8.0	3440	0.18	400	76

<sup>a</sup> Values of  $\nu_0$  and  $\Gamma$  are stated to the nearest 10  $\text{cm}^{-1}$ ; values of  $k(\nu_0)$  and  $\int k(\nu) d\nu$  are accurate to  $\pm 10\%$ .

TABLE II: Librational Band<sup>a</sup>

Material	Concn, M	$\nu_0$ , $\text{cm}^{-1}$	$k(\nu_0)$	$\nu'$ , $\text{cm}^{-1}$
Water		570	0.43	830
MgCl <sub>2</sub>	1.9	560	0.43	820
	3.8	540	0.45	800
CaCl <sub>2</sub>	2.2	540	0.48	760
	4.4	530	0.46	760
CaBr <sub>2</sub>	2.0	540	0.46	760
	4.0	540	0.48	720
CuCl <sub>2</sub>	2.15	520	0.42	820
	4.30	440 <sup>b</sup>	0.40	800
NaCN	4.0	500	0.46	790
	8.0	450 <sup>b</sup>	0.49	760

<sup>a</sup> Values of  $\nu_0$  and  $\nu'$  are stated to the nearest 10  $\text{cm}^{-1}$ . The value of  $k(\nu_0)$  are accurate to  $\pm 10\%$ . <sup>b</sup> Indication of splitting.

ranges of uncertainty specified in reports of our earlier studies.

The two major features of the water spectrum are a very strong absorption band occurring near 3400  $\text{cm}^{-1}$  and a second band near 570  $\text{cm}^{-1}$  in water at ambient temperatures. Although the band near 3400  $\text{cm}^{-1}$  involves the  $\nu_3$ ,  $\nu_1$ , and  $2\nu_2$  bands of water molecules, we shall for reasons of brevity refer to it as the *valence band*. The band near 570  $\text{cm}^{-1}$  is the so-called *librational band* and is associated with the hindered rotational motion of the  $\text{H}_2\text{O}$  molecule in the field of its neighbors. The results of the present study are summarized in Tables I and II, which apply to the valence band and the librational band, respectively.

In Table I we list the frequency  $\nu_0$  at which the maximum value of  $k(\nu)$  occurs, the value of the absorption index  $k(\nu_0)$  for this frequency, the full width  $\Gamma$  of the band at half maximum, and the integrated absorption  $\int k(\nu) d\nu$  for the valence band in each of the solutions studied; the concentrations of the solutes are listed. The band maximum shifts to higher frequencies relative to  $\nu_0$  for water in all the solutions except for the 4.3 M solution of  $\text{CuCl}_2$ , in which it is shifted to slightly lower frequencies. The value of  $k(\nu_0)$  for all the alkaline-earth halides is slightly higher than  $k(\nu_0)$  for water; in  $\text{CuCl}_2$  and  $\text{NaCN}$  solutions the value  $k(\nu_0)$  is significantly lower than  $k(\nu_0)$  for water. As compared with water, the band-width parameter  $\Gamma$  shows little change for  $\text{MgCl}_2$ ,  $\text{CaCl}_2$ , and 2 M  $\text{CaBr}_2$  but is significantly smaller for 4 M  $\text{CaBr}_2$ ; for the  $\text{CuCl}_2$  and  $\text{NaCN}$  solutions  $\Gamma$  is significantly larger than for water. Except for  $\text{NaCN}$ , the value of the integrated absorption  $\int k(\nu)$

$d\nu$  for the valence band in solution is within  $\pm 12\%$  of the value for water; in the spectra of the NaCN solutions the value of  $\int k(\nu) d\nu$  is strikingly smaller.

In Table II we list the frequency  $\nu_0$  at which the maximum value of  $k(\nu)$  occurs for the librational band and the value  $k(\nu_0)$  noted for this frequency; also listed is the value  $\nu'$  at which  $k(\nu)$  attains half its maximum value in the high-frequency wing of the band. The librational band for all solutions is shifted to lower frequencies relative to its position in the water spectrum as indicated by the listed values for both  $\nu_0$  and  $\nu'$ . The values of  $k(\nu_0)$  for the solutions are, in general, equal to or greater than  $k(\nu_0)$ ; the only exceptions to this are the  $\text{CuCl}_2$  solutions, for which  $k(\nu_0)$  is slightly smaller than that for water.

In our earlier study of alkali-halide solutions we noted some qualitative agreement with predictions based on the Bernal-Fowler<sup>6</sup> theory, but detailed analysis of the results led to certain discrepancies between observations and predictions. Bernal and Fowler introduced the concept of a *structural temperature* involving an intermolecular, hydrogen-bonded structure that is extensive and tightly bound at low temperatures and becomes less extensive and less tightly bound at higher temperatures. According to their theory ions in aqueous solution affect the structural temperature in a manner that depends on the ratio of ionic charge to ionic radius; large singly charged ions are supposed to produce a greatly increased structural temperature, while smaller ions are supposed to be less effective in breaking up the normal water structure and thus to have less effect on the structural temperature. In our studies of the alkali halide spectra we found that negative ions had greater effects on the water spectrum than did positive ions.

In the case of the valence band, our earlier studies of water have shown that (1)  $k(\nu_0)$  decreases, (2)  $\nu_0$  increases, and (3)  $\Gamma$  increases with increasing temperature. The values of these quantities listed in Table I are accurate to approximately  $\pm 10\text{ cm}^{-1}$  for  $\nu_0$  and  $\Gamma$  and to  $\pm 10\%$  for  $k(\nu_0)$  and  $\int k(\nu) d\nu$ . For the alkaline-earth halides listed Table I, we would conclude that the combined effects of anions and cations (1) have little influence on the structural temperature as measured by  $k(\nu_0)$ , (2) increase the structural temperature as measured by  $\nu_0$ , and (3) decrease the structural temperature as measured by  $\Gamma$ . No startlingly large effects can be attributed to multiply charged cations of the alkaline earths as compared with the singly charged cations of the alkalis studied earlier. With the regard to the valence band, both  $\text{CuCl}_2$  and NaCN greatly increase the structural temperatures as measured by  $k(\nu_0)$  and as measured by  $\Gamma$ ;  $\text{CuCl}_2$  greatly decreases and NaCN greatly increases the structural temperature as measured by  $\nu_0$ .

In the case of the *librational band*, our earlier studies of water have shown that (1)  $k(\nu_0)$  does not change significantly with temperature, (2)  $\nu_0$  decreases with increasing temperature, and (3) the band width increases with increasing temperature. Except for  $\text{CuCl}_2$ , all solutes listed in Table II have values of  $k(\nu_0)$  that are somewhat but not significantly higher than  $k(\nu_0)$  for water. All solutes increase the structural temperature as measured by  $\nu_0$ . All alkaline-earth halides listed in Table II decrease the band width as estimated from  $\nu' - \nu_0$  and thus decrease the structural temperature as measured by this parameter;  $\text{CuCl}_2$  and NaCN increase the structural temperature as measured by the band width parameter.

In view of various discrepancies between structural temperatures of solutions as measured by various spectroscopic parameters we can only conclude that the Bernal-Fowler theory does not provide a satisfactory basis for interpreting the spectra of solutions. Various effects are observed in the

solution spectra that cannot be duplicated by merely changing the temperature of water itself.

Recent progress has been made in quantum-mechanical calculations of the energies of interaction between small ions and water molecules and has recently been summarized by Schuster et al.<sup>7</sup> These calculations also provide information regarding the intermolecular configuration and electron densities involved in the solvation complexes. They indicate that specific properties of the ions other than the Bernal-Fowler parameters of charge and ionic radius must be considered. In the hope that the newer calculations will eventually be extended to the *spectral changes* produced by various ions, plots of the reflection spectra  $R(\nu)$  vs.  $\nu$ , the values of  $n(\nu)$  vs.  $\nu$ , and the values of  $k(\nu)$  vs.  $\nu$  are available as supplementary material (see paragraph at end of text regarding supplementary material); the plots should be of use in testing new theoretical predictions.

In comparing the plots of  $k(\nu)$  vs.  $\nu$  with earlier plots of absorption spectra, it should be noted that absorption spectra are usually presented as curves purporting to give fractional transmittance  $T(\nu)$  vs.  $\nu$  or as plots of the Lambert absorption coefficient  $\alpha(\nu)$  vs.  $\nu$ , where  $\alpha(\nu)$  is defined by the relation  $T(\nu) = \exp(-\alpha(\nu)x)$ , in which  $x$  is the thickness of the absorbing layer. The absorption index  $k(\nu)$  is a dimensionless optical constant related to  $\alpha(\nu)$  by the expression  $k(\nu) = \alpha(\nu)/4\pi\nu$  with  $\alpha(\nu)$  and  $\nu$  expressed in  $\text{cm}^{-1}$ . The separation of the  $k(\nu)$  and  $\alpha(\nu)$  peaks becomes important only when  $\Gamma/\nu_0$  is large; for example, the librational band of water occurs at  $570\text{ cm}^{-1}$  in a  $k(\nu)$  vs.  $\nu$  plot and at  $680\text{ cm}^{-1}$  in a plot of  $\alpha(\nu)$  vs.  $\nu$ .

We note that  $k(\nu)$  is a maximum for the frequency  $\nu_{nm}$  at which the matrix element  $|R^{nm}|^2$  is a maximum. The spectral absorbance is a maximum at the frequency for which  $\nu_{nm}|R^{nm}|^2$  is a maximum, and spectral emission is a maximum at the frequency for which  $\nu_{nm}^4|R^{nm}|^2$  is a maximum. Thus, the peak in  $k(\nu)$  appears at the frequency most directly associated with the matrix elements involved in the transition probability.<sup>8</sup>

*Acknowledgments.* We wish to acknowledge the support of the Office of Naval Research for this work.

*Supplementary Material Available:* Plots of  $R(\nu)$  vs.  $\nu$ , the values of  $n(\nu)$  vs.  $\nu$ , and the values of  $k(\nu)$  vs.  $\nu$  for the materials shown in Tables I and II (40 pages). Ordering information is available on any current masthead page.

## References and Notes

- P. Rhine, D. Williams, G. M. Hale, and M. R. Querry, *J. Phys. Chem.*, **78**, 238 (1974).
- P. Rhine, D. Williams, G. M. Hale, and M. R. Querry, *J. Phys. Chem.*, **78**, 1405 (1974).
- H. D. Downing and D. Williams, *J. Phys. Chem.*, in press.
- C. W. Robertson and D. Williams, *J. Opt. Soc. Am.*, **61**, 1316 (1971).
- J. P. Hawranek and R. N. Jones, *Spectrochim. Acta, Part A*, **32**, 99 (1976).
- J. D. Bernal and R. H. Fowler, *J. Chem. Phys.*, **1**, 515 (1933).
- P. Schuster, W. Jakubetz, and W. Marius, *Top. Current Chem.*, **60**, 1 (1975).
- G. Herzberg, "Spectra of Diatomic Molecules", Van Nostrand, Princeton, N.J., 1950, p 20.

Department of Physics  
Kansas State University  
Manhattan, Kansas 66506

Harry D. Downing  
Dudley Williams\*

Received April 19, 1976

A further elaboration on our work on strong acids and bases is summarized in the following publication by Downing and Williams, who point out certain features of the solutions of HCl and HBr that can be attributed to the  $\text{H}_3\text{O}^+$  ion. Marked differences between the spectra of acids and bases are emphasized.

## Infrared Spectra of Strong Acids and Bases<sup>1</sup>

Publication costs assisted by the Office of Naval Research

Sir: In an earlier paper on this subject<sup>2</sup> we reported the results of a study of the reflectance spectra of aqueous solutions of strong acids and bases; from measured values of spectral reflectance  $R(\nu)$  we used a Kramers-Kronig analysis to obtain the real  $n(\nu)$  and imaginary  $k(\nu)$  parts of the complex index of refraction  $\tilde{N} = n(\nu) + ik(\nu)$  in the spectral region 400–5000  $\text{cm}^{-1}$ . With regard to major absorption bands, our results were in general agreement with those obtained in the earlier absorption study of Falk and Giguere,<sup>3</sup> and we adopted their assignment of certain bands in the spectrum of HCl solutions to the ion  $\text{H}_3\text{O}^+$ .

It has been brought to our attention that our results and this assignment are in disagreement with those obtained by Ackermann,<sup>4</sup> who has made a quantitative study of the transmission spectra of strong acids and bases in the range 1100–4000  $\text{cm}^{-1}$ . Ackermann reported that the absorption spectra of acids and bases are essentially similar and can be interpreted as mere radical modifications of the spectrum of water. In particular, he raised questions as to the assignment of bands to the  $\text{H}_3\text{O}^+$  ion.

In order to check our earlier results we have remeasured the reflection spectrum of HBr at two concentrations and are including our results for spectral reflectance  $R(\nu)$ ,  $n(\nu)$ , and  $k(\nu)$  in Figures 1'–7' (supplementary material; see paragraph at end of text regarding supplementary material). In order to determine the differences between the solution spectra and the spectrum of water, we have also prepared curves showing the differences between the absorption indices  $k(\text{solution})$  and  $k(\text{water})$  as a function of wave number; the curve for a 48% solution of HBr is shown in Figure 1. In spectral regions where  $k(\text{solution}) - k(\text{water})$  is negative, the solution is more transparent than water; one such region occurs near 3400  $\text{cm}^{-1}$  and is probably associated with a shift of the strong valence-vibration band of water; a second such region occurs near 700  $\text{cm}^{-1}$  and is probably associated with a shift in the librational band of water.<sup>5</sup>

Three strong maxima occur near 2800, 1750, and 1100  $\text{cm}^{-1}$  in the curve shown in Figure 1. Each of these maxima is in close proximity to a band reported for the  $\text{H}_3\text{O}^+$  ion in crystal hydrates.<sup>6–8</sup> This agreement between the frequencies of bands observed in solution and in hydrated crystals is our major reason for attributing the solution bands to the  $\text{H}_3\text{O}^+$  ion. Since the  $\text{H}_3\text{O}^+$  ion is isoelectronic with  $\text{NH}_3$  and is probably pyramidal, the observed bands appear in the anticipated spectral regions.<sup>2</sup>

The value  $k(\text{solution}) - k(\text{water})$  in Figure 1 is positive throughout the entire spectral region between 3200 and 900  $\text{cm}^{-1}$ ; this indicates that the HBr solution is more strongly absorbing than water. Similar strong general absorption was noted for solutions of HCl, NaOH, and KOH in our

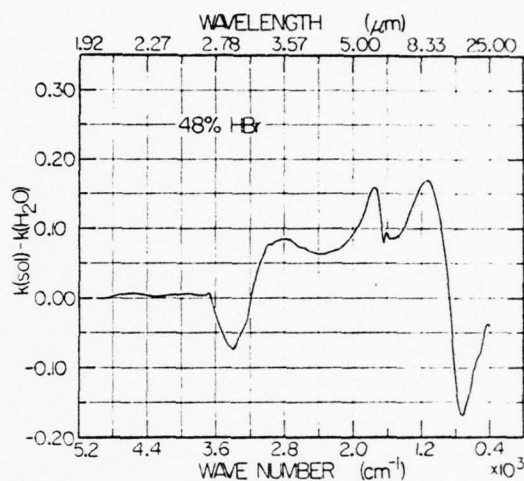


Figure 1. Difference between the spectral absorption index of a 48% aqueous solution of HBr and the corresponding index of water ( $T = 25^\circ\text{C}$ ).

earlier study.<sup>2</sup> With respect to this generally increased absorption for both acids and bases as compared with water, our results agree with those of Ackermann. However, the shapes of the absorption curves for acids and bases are quite different. No strong absorption maxima near 1750 and 1100  $\text{cm}^{-1}$  appear in the hydroxide spectra. Although a region of strong absorption occurs near 2800  $\text{cm}^{-1}$  in the hydroxide spectra, the shape of the hydroxide absorption curve in this region is quite different from the shape of the acid absorption curve.

We conclude by noting that our results agree with the experimental results of Ackermann with regard to generally increased absorption of acid and hydroxide solutions throughout most of the near infrared but disagree with his results with regard to the shapes of the absorption curves. Our interpretation of the peaks shown in Figure 1 in terms of the  $\text{H}_3\text{O}^+$  ion is in sharp disagreement with Ackermann's conclusions.

*Supplementary Material Available:* Spectral reflectance at near-normal incidence, refractive index, and absorption index for 24 and 48% HBr solutions (Figures 1'–7', 7 pages). Ordering information is available on any current masthead page.

## References and Notes

- (1) Supported in part by the Office of Naval Research.
- (2) P. Rhine, D. Williams, G. M. Hale, and M. R. Query, *J. Phys. Chem.*, **78**, 1405 (1974).
- (3) M. Falk and P. A. Giguere, *Can. J. Chem.*, **35**, 1195 (1957).
- (4) T. Ackermann, *Z. Phys. Chem. (Frankfurt am Main)*, **27**, 253 (1961).
- (5) D. A. Draeger and D. Williams, *J. Chem. Phys.*, **48**, 401 (1968).
- (6) D. E. Bethell and N. J. Sheppard, *J. Chim. Phys.*, **50**, C72 (1953).
- (7) C. C. Ferriso and D. F. Hornig, *J. Am. Chem. Soc.*, **75**, 4113 (1953).
- (8) C. C. Ferriso and D. F. Hornig, *J. Chem. Phys.*, **23**, 1464 (1959).

Editor's note: Professor Ackermann<sup>4</sup> has communicated to us his agreement with the assignment of the solution bands to  $\text{H}_3\text{O}^+$ , based on these new data obtained with an improved experimental technique. He further indicates his conclusion that "there are two different types of characteristic changes in the infrared spectra of strong acids:

- (i) The appearance of characteristic absorption bands, which can be attributed to the  $\text{H}_3\text{O}^+$  ion;
- (ii) A generally increased absorption, which can be observed in the infrared spectra of bases as well as acids."

Department of Physics  
Kansas State University  
Manhattan, Kansas 66506

Harry D. Downing  
Dudley Williams\*

Received February 13, 1976



In the work covered thus far in this report, the bands attributed to the  $\text{H}_3\text{O}^+$  ion in acid solutions together with the marked changes of the shapes of the water bands in fluoride solutions represent the only cases in which we have obtained evidence for stable or quasi-stable groups involving association of solutes and water molecules. However, we have recently obtained evidence for quasi-stable groups involving association between the cupric ion  $\text{Cu}^{++}$  and water molecules. The first evidence for this type of association was reported in the following article by Sethna, Pinkley, and Williams and was based on work done under other sponsorship.

AD-A052 267

KANSAS STATE UNIV MANHATTAN DEPT OF PHYSICS  
INFRARED STUDIES OF WATER AND HYDRATED MATERIALS. (U)  
MAR 78 D WILLIAMS

F/G 7/2

N00014-67-A-0403-0001

UNCLASSIFIED

NL

2 OF 2  
AD  
A052 267



END  
DATE  
FILMED  
5 - 78  
DDC

## Optical constants of cupric sulfate in the infrared\*

P. P. Sethna, Lary W. Pinkley, and Dudley Williams

*Department of Physics, Kansas State University, Manhattan, Kansas 66506*

(Received 8 November 1976)

We have measured the spectral reflectance of a cupric sulfate single crystal for unpolarized radiation at near-normal incidence. Values of the refractive index  $n(\nu)$  and the absorption index  $k(\nu)$  have been obtained by subtractive Kramers-Kronig phase-shift analysis. The values of  $\int k(\nu) d\nu$  for the characteristic  $\text{SO}_4^{--}$  bands in the spectrum of the crystal are compared with values of  $\int k(\nu) d\nu$  for these bands obtained by extrapolation of values of  $k(\nu)$  determined for cupric sulfate solutions.

Elsewhere<sup>1</sup> we have reported a moderately successful attempt to obtain a synthetic spectrum of crystalline ammonium sulfate by extrapolating the values of  $k(\nu)$  characteristic of the  $\text{NH}_4^+$  and  $\text{SO}_4^{--}$  ions in aqueous solution to the number densities of these ions in the crystal. The method offers some promise of providing approximate values of the optical constants  $n(\nu)$  and  $k(\nu)$  in the infrared for soluble materials that cannot be easily obtained as single crystals sufficiently large for use in absorption and reflection measurements.

One of the basic assumptions involved in the method

is that the value of  $\int k(\nu) d\nu$  for an absorption band characteristic of a well-defined atomic group such as the  $\text{SO}_4^{--}$  ion depends only on the number density of the group and is independent of the electric and magnetic fields produced by neighboring atomic groups in a crystal or in solution. In order to test this assumption further we have attempted to make a quantitative comparison of  $\int k(\nu) d\nu$  for the  $\text{SO}_4^{--}$  ion in a single crystal of the hydrated salt  $\text{CuSO}_4 \cdot 5\text{H}_2\text{O}$  with extrapolated values of  $\int k(\nu) d\nu$  for the  $\text{SO}_4^{--}$  bands in aqueous solution; absorption due to water of crystallization in the crystal introduces some complications not encountered in the earlier

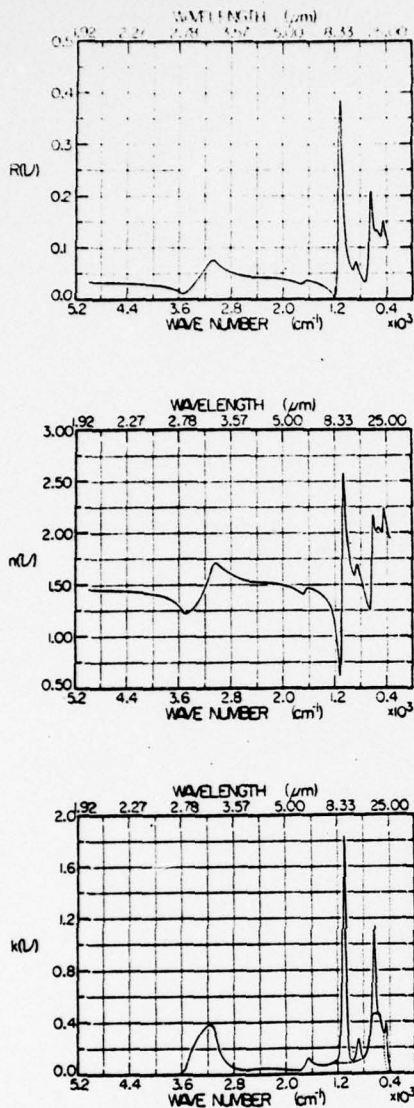


FIG. 1. Top panel: Spectral reflectivity  $R(\nu)$  of a single cupric sulfate crystal for unpolarized radiation at near-normal incidence. Center panel: Refractive index  $n(\nu)$  of the crystal. Bottom panel: Absorption index  $k(\nu)$  of the crystal.

study. In making the comparison we have based our values of  $k(\nu)$  on a subtractive Kramers-Kronig (K-K) phase-shift analysis of the measured spectral reflectance  $R(\nu)$  for unpolarized radiation at near-normal incidence. In the case of the single crystal this technique eliminates birefringence complications that are not pertinent to the problem at hand.

We employed an initially unpolarized beam but recognize that the radiation reaching the detector becomes partially polarized during passage through the spectrograph. Therefore, in order to eliminate the effects of birefringence in the crystal, we mapped the reflection spectrum for several different orientations of the crystal in the reflectometer. The composite of the results is shown in the upper panel of Fig. 1, which gives a plot of  $R(\nu)$  vs  $\nu$  for the crystal. The dispersion features near 3200

and 1670  $\text{cm}^{-1}$  as well as the general rise in  $k(\nu)$  in the low-frequency region can be attributed to the water of crystallization. The sharper features in the 1200 to 400  $\text{cm}^{-1}$  region are associated with the  $\text{SO}_4^{2-}$  ion.

By subtractive K-K phase-shift analysis of the reflectance spectrum of the crystal, we obtained the values of the optical constants  $n(\nu)$  and  $k(\nu)$  shown in the lower panels of Fig. 1. The plot of  $n(\nu)$  vs  $\nu$  shown in the middle panel has features similar to the  $R(\nu)$  vs  $\nu$  plot in the top panel. The plot of the absorption index  $k(\nu)$  vs  $\nu$  in the bottom panel shows certain peaks that can be readily identified. The broad absorption band near 3160  $\text{cm}^{-1}$  is attributed to the  $\nu_1$ ,  $\nu_3$ , and  $2\nu_2$  bands of  $\text{H}_2\text{O}$  in the water of crystallization; the weaker band near 1650  $\text{cm}^{-1}$  is the corresponding  $\nu_2$  band of  $\text{H}_2\text{O}$ . The sharp bands in the range below 1200  $\text{cm}^{-1}$  are associated with fundamentals<sup>2</sup> of the  $\text{SO}_4^{2-}$  bands:  $\nu_3$  at 1090  $\text{cm}^{-1}$ ,  $\nu_1$  at 870  $\text{cm}^{-1}$ ,  $\nu_4$  at 630  $\text{cm}^{-1}$ , and  $\nu_2$  near 450  $\text{cm}^{-1}$ . Because of uncertainties in our K-K analyses our estimates of the shape and magnitude of the  $\nu_2$  band may be seriously in error even though this band produces readily observable features in the experimentally observed reflectance spectrum. The sharp  $\text{SO}_4^{2-}$  bands are superposed on a broad feature associated with the librational motion of  $\text{H}_2\text{O}$  molecules in the crystal lattice. The dotted curve in the figure gives a qualitative estimate of the contributions of the water of crystallization in this region based on earlier studies of water, ice, and water of crystallization in other crystals.<sup>3</sup>

For comparison with our results for the single crystal of  $\text{CuSO}_4 \cdot 5\text{H}_2\text{O}$  we have studied the reflection spectra of 0.75M and 1.25M solutions of cupric sulfate in water and have subjected the results to K-K analysis in the manner described in our earlier study.<sup>1</sup> The curves shown in Fig. 2 give a plot of the difference between the absorption indices for the 0.75M and 1.25M solutions and the absorption index for water with [ $k(\text{solution}) - k(\text{water})$ ] extrapolated to the number densities of the

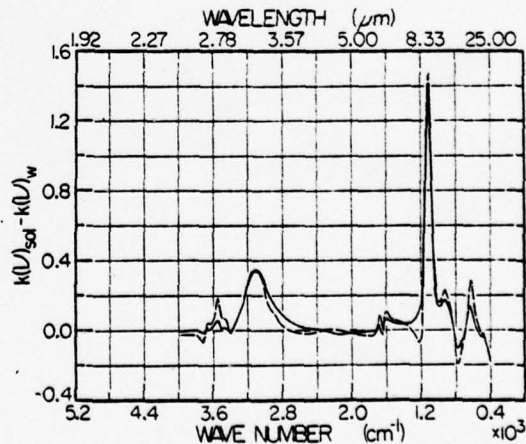


FIG. 2. Difference of absorption indices [ $k(\text{solution}) - k(\text{water})$ ] for a 0.75M and a 1.25M cupric sulfate solution as a function of frequency in the infrared as extrapolated to the number density of  $\text{CuSO}_4 \cdot 5\text{H}_2\text{O}$  units in crystalline cupric sulfate. The solid curve refers to the 1.25M solution; dashed curve to the 0.75M solution.

TABLE I. Comparison of  $\text{SO}_4^{2-}$  band strengths in the  $\text{CuSO}_4 \cdot 5\text{H}_2\text{O}$  crystal spectrum and in the spectrum extrapolated from solution.

Band	$\int k(\nu) d\nu$	
	Crystal	Extrapolation
$\nu_3$	$128 \pm 9 \text{ cm}^{-1}$ ( $114 \pm 9$ )	$132 \pm 10 \text{ cm}^{-1}$
$\nu_1$	$28 \pm 14$ ( $10 \pm 8$ )	$24 \pm 5$
$\nu_4$	$69 \pm 15$ ( $30 \pm 10$ )	$47 \pm 12$
$\nu_2$	$22 \pm 8$ ( $13 \pm 8$ )	$14 \pm 5$

$\text{CuSO}_4 \cdot 5\text{H}_2\text{O}$  units in the crystal; there are marked similarities between the plots in Fig. 2, which are a measure of the absorption of the solute, and the plot given in the bottom panel of Fig. 1.

The positive peaks near 3550, 3090, 1680, and 1600  $\text{cm}^{-1}$  differ from corresponding spectra obtained in our earlier studies of alkali-halide solutions<sup>4</sup>; these peaks may be due to  $\text{H}_2\text{O}$  molecules in quasistable association with  $\text{Cu}^{2+}$  ions in the solutions.<sup>5,6</sup> We are making a further study of this possibility in other solutions containing cupric ions. The  $\nu_3$ ,  $\nu_1$ , and  $\nu_4$  bands of the  $\text{SO}_4^{2-}$  ion appear as sharp peaks superposed on a generally decreasing background, which is associated with a shift of the librational water band to lower frequency in the solution.<sup>4</sup> The  $\nu_2$  band of  $\text{SO}_4^{2-}$  is incompletely resolved. The gradual decrease of  $[k(\text{solution}) - k(\text{water})]$  for low frequencies is even greater in the plot for the 1.25M solution than for the 0.75M solution.

On the basis of plots similar to the one in Fig. 2 we have obtained estimates of  $\int k(\nu) d\nu$  for the  $\text{SO}_4^{2-}$  bands and list the results in Table I, in which they are compared with  $\int k(\nu) d\nu$  for the corresponding bands of the  $\text{CuSO}_4 \cdot 5\text{H}_2\text{O}$  single crystal. For each band in the crystal we list two values; the larger of these attributes all of the observed absorption to the  $\text{SO}_4^{2-}$  ion, while the smaller value given in parenthesis attempts to eliminate absorption due to the water of crystallization as given by the dotted curve in the bottom panel of Fig. 1. The actual value of  $\int k(\nu) d\nu$  for each band probably falls between the estimated limits. The uncertainties in the

values of  $\int k(\nu) d\nu$  for absorption bands in solution are attributable in large part to difficulties in estimating the effects of the shift of the librational band of  $\text{H}_2\text{O}$  molecules in the solvent with respect to the corresponding band in pure water; the uncertainties in  $\int k(\nu) d\nu$  for the bands in the crystal are associated in part with uncertainties in the K-K analysis as well as uncertainties involving absorption by the water of crystallization.

Despite the indicated large uncertainties involving corrections due to absorption by the water of crystallization, we regard the rough agreement between the values of  $\int k(\nu) d\nu$  for bands in the crystal and the corresponding values of  $\int k(\nu) d\nu$  extrapolated from the solutions as sufficiently good to prompt further work on the general subject. We believe that the use of more dilute solutions along with the special K-K techniques that we employed in our study of sea water<sup>7</sup> should reduce the uncertainties in the band intensities based on solution results. The use of crystals not containing water of crystallization should eliminate some of the uncertainties in the estimation of band intensities.

We should like to thank Professor Dana Johnson for the crystal employed in the study and to express our appreciation to Professor H. C. Moser and Professor J. D. Petersen for helpful discussion of hydrates of the cupric ion.

\*Supported in part by the National Aeronautics and Space Administration.

<sup>1</sup>H. D. Downing, L. W. Pinkley, P. P. Sethna, and D. Williams, "Optical constants of ammonium sulfate in the infrared," *J. Opt. Soc. Am.* 67, 186-190 (1977).

<sup>2</sup>G. Herzberg, *Infrared and Raman Spectra* (Van Nostrand, New York, 1945), p. 167.

<sup>3</sup>V. Seidl, O. Knop, and M. Falk, "Infrared Studies of Water in Crystalline Hydrates: Gypsum,  $\text{CaSO}_4 \cdot 2\text{H}_2\text{O}$ ," *Can. J. Chem.* 47, 1361-1368 (1969).

<sup>4</sup>P. Rhine, D. Williams, G. M. Hale, and M. R. Querry, "Infrared Optical Constants of Aqueous Solutions of Electrolytes: The Alkali Halides," *J. Phys. Chem.* 75, 238-246 (1974).

<sup>5</sup>L. E. Orgel, *Transition-Metal Chemistry: Ligand-Field Theory* (Methuen and Company, London, 1960), Chap. 4.

<sup>6</sup>T. J. Swift and R. E. Connick, "NMR Relaxation of  $\text{O}^{17}$ ," *J. Chem. Phys.* 37, 307-320 (1962).

<sup>7</sup>L. W. Pinkley and D. Williams, "Optical properties of sea water in the infrared," *J. Opt. Soc. Am.* 66, 554-558 (1976).

We were rather surprised that the absorption bands associated with water of crystallization in crystalline  $\text{CuSO}_4 \cdot 5\text{H}_2\text{O}$  remained clearly visible in the spectra of solutions of this salt. Subsequent studies of the spectra of solutions of  $\text{CuCl}_2$  and  $\text{CuBr}_2$  showed that similar bands appear. We have attributed these bands to quasi-stable groups in the solution that involve the attachment of water molecules to  $\text{Cu}^{++}$  ions by ligands of the type involved in the crystal. The groups can be represented formally by the ions  $(\text{Cu} \cdot 4\text{H}_2\text{O})^{++}$  or  $(\text{Cu} \cdot 6\text{H}_2\text{O})^{++}$ . An article on the subject is currently in press in the Journal of Physical Chemistry. Similar association by ligands are possibly to be expected in solutions of salts of the other transition elements.

### III. Other Publications

Although the major results of our project are given in the articles included in the present report, we are including the following complete list of our publications. Reprints of most of the publications listed are still available on request.

### List of Publications

1. "Far-Infrared Absorption Spectra of Aqueous Solutions of Strong Electrolytes: (Draegert and Williams), J. Chem. Phys. 48, 401 (1968).
2. "Explicit Solution of Generalized Fresnel Reflection Equations" (Marvin Querry), J. Opt. Soc. Amer. 58, 1560 (1968). P\*.
3. "The Infrared Reflectance of Water" (Williams, Querry, and Curnutte), J. Opt. Soc. Amer. 58, 1560 (1968). P.
4. "Direct Solution of the Generalized Fresnel Equations" (Querry) J. Opt. Soc. Amer. 59, 876 (1969).
5. "Infrared Spectral Absorption Coefficients of Water" (Querry and Williams), Bull. Am. Phys. Soc. II 14, 621 (1969). P.
6. "Infrared Reflectance of Water at Normal Incidence" (Rusk and Williams) J. Opt. Soc. Amer. 59, 500 (1969). P.
7. "Refractive Index of Water in the Infrared", Rusk, Curnutte, and Williams, J. Opt. Soc. Amer. 59, 1299 (1969).
8. "Infrared Reflection Spectrum of Water", Rusk, Querry, and Williams, Proc. of Symposium on Structures of Water and Aqueous Solutions, University of Chicago, June 1969. P.
9. "Infrared Spectral Absorption Coefficients of Water", Querry and Williams, Bull. Am. Phys. Soc. II 14, 621 (1969). P.
10. "Optical Constants of Water in the Infrared", Rusk and Williams, J. Opt. Soc. Amer. 60, 1569 (1970) P.
11. "Infrared Spectral Reflectance of Sea Water", Hobson and Williams, Bull. Am. Phys. Soc. II 15, 1312 (1970). P.

---

\*P denotes a paper presented at a scientific meeting and published as an abstract.



12. "Optical Constants of Water in the Infrared", Rusk, Williams, and Querry. J. Opt. Soc. Amer. 61, 895 (1971).
13. "Lambert Absorption Coefficient of Water in the Infrared", Robertson and Williams, J. Opt. Soc. Amer. (Spring Meeting 1971, p.32). P.
14. "Lambert Absorption Coefficient of Water in the Infrared," Robertson and Williams, J. Opt. Soc. Amer. 61, 1316 (1971).
15. "Optical Properties of Water in the Infrared", Williams, Rusk, and Querry, Bull. Am. Phys. Soc. II. 16, 501 (1971). P.
16. "Infrared Spectral Reflectance of Sea Water", Hobson and Williams, Appl. Opt. 10, 2372 (1971).
17. "Reflection Spectra of Alkali Halide Solutions", Rhine and Williams, Bull. Am. Phys. Soc. II 17, 575 (1972). P.
18. "Optical Constants of Water", Williams, Proceedings Twenty-Seventh Symposium on Molecular Spectra and Structure, Ohio State University 1972, p.109. P.
19. "Influence of Temperature on the Spectrum of Water", Hale, Querry, Rusk, and Williams, J. Opt. Soc. Amer. 62, 1104 (1972).
20. "The Optical Constants of Water in the Far Infrared", Robertson, Curnutte, and Williams, J. Opt. Soc. Amer. 62, 1381 (1972). P.
21. "The Infrared Spectrum of Water", Robertson, Curnutte, and Williams, Molecular Physics 26, 183 (1973).
22. "The Infrared Reflection Spectrum of Ice", Schaaf and Williams, OSA J. Opt. Soc. Am. 63, 493 (1973). P.
23. "Lambert Absorption Coefficient of Water in the Near Infrared", K. F. Palmer, J. Opt. Soc. Am. 63, 475 (1973). P.

24. "Optical Constants of Ice in the Infrared", Schaaf and Williams, J. Opt. Soc. Amer. 63, 726 (1973).
25. "The Infrared Reflectance of Aqueous Solutions of H<sub>2</sub>SO<sub>4</sub>", K. F. Palmer, Proceedings of the 28th Symposium on Molecular Spectroscopy, Ohio State University, p. 168. P.
26. "Infrared Optical Constants of Aqueous Solutions of Electrolytes: The Alkali Halides", Rhine, Williams, Hale, and Querry, J. Phys. Chem. 78, 238 (1974).
27. "Optical Properties of Particulate Constituents of Planetary Atmospheres", Williams, Proceedings of the Copernicus Symposium 1973 (In Press).
28. "The Far Infrared Spectrum of Water," Curnutte and Williams, Structure of Water, Ed. A.P. Luck (Verlag Chemie/Physik Marburg) pp. 207-219.
29. "Optical Constants of Water in the Infrared", Downing and Williams, Bull. Am. Phys. Soc. 19, 448 (1974). P.
30. "The Optical Properties of Water in the Near Infrared", Palmer and Williams, J. Opt. Soc. Amer. 64, 1107 (1974).
31. "Infrared Properties of Aqueous Solutions of Electrolytes: Acids and Bases", Rhine, Williams, Hale, and Querry., J. Chem. Phys. 78, 1405 (1974).
32. "Optical Constants of Water in the Infrared," Downing and Williams, J. Geophys. Res. 80, 1656 (1975).
33. "Infrared Spectra of Matter in Condensed States", D. Williams Proceedings of XII Congress of European Molecular Spectroscopists: "Molecular Spectroscopy of Dense Phases" (ELSEVIER, Amsterdam, 1976). p. 765.

34. "Infrared Spectra of Strong Acids and Bases," H. D. Downing and J. Phys. Chem. 80, 1640 (1976).
35. "Optical Constants of Sea Water in the Infrared," L. W. Pinkley and D. Williams, J. Opt. Soc. Amer. 66, 554 (1976).
36. "Infrared Optical Constants of Aqueous Solutions of Electrolytes: Further Studies of Salts," H. D. Downing and D. Williams, J. Phys. Chem. 80, 1950 (1976).
37. "Optical Constants of Water in the Infrared: Influence of Temperature," L. W. Pinkley, P. P. Sethna, and D. Williams, J. Opt. Soc. Amer. 67, 494 (1977).
38. "The Influence of Cupric Ions on the Infrared Spectrum of Water", P. P. Sethna, H. D. Downing, and D. Williams, J. Opt. Soc. Amer. (In Press).
39. "Optical Constants of D<sub>2</sub>O in the Infrared", P. P. Sethna and D. Williams, J. Opt. Soc. Amer. (In Press).
40. "The Influence of Fluoride Ions on the Infrared Spectrum of Water", P. P. Sethna and D. Williams (In Preparation).

#### Technical Reports

Reprints of publications 1, 4, and 7 are listed above and have been distributed as Technical Reports No. 1, No. 2, and No. 3, respectively. A reprint of publication 12 was distributed as Technical Report No. 4 and was assigned No. AD730204 by DDC; a reprint of publication 14 as Technical Report No. 5 was assigned No. AD733820 and a reprint of publication 16 as Technical Report No. 6 was assigned No. AD733821 by DDC. Reprints of publication 32 and 35 were issued as a technical report DDC No. ADA034071.

## APPENDIX

Although the major work done under the present contract was an experimental determination of the optical properties of water and of aqueous solutions of electrolytes, theoretical work under different sponsorship has been going on under the direction of Professor Basil Curnutte, who has also served as senior research associate under this contract. In the likely event that this theoretical work will prove of useful interest to readers of this report, we are adding several of Professor Curnutte's contributions as an appendix to the report.

In earlier work Professor Curnutte and one of his graduate students had made a study of the influence of hydrogen bonding on the intramolecular vibrations of  $H_2O$ . Two of the following journal articles by Bandekar and Curnutte deal with the influence of hydrogen bonding on the intermolecular or lattice vibrations of water. Also included is an article by Curnutte and Williams, who interpret the observed spectrum of water in terms of several theories of the water structure.

## A Local-Structure Model for Calculation of Lattice Vibrations in Liquid Water<sup>1</sup>

JAGDEESH BANDEKAR<sup>2</sup> AND BASIL CURNUTTE

*Department of Physics, Kansas State University, Manhattan, Kansas 66506*

The local-structure model of Bryan and Curnutte, which treated a single molecule in a rigid cage, has been extended to include a central water molecule and its four nearest neighbors surrounded by a rigid cage of next-nearest neighbors. The influence of the next-nearest neighbors is accounted for by the average forces they exert on the five-molecule local-structure group. With parameters based on water at 25°C, we give calculations of the spectra of liquid H<sub>2</sub>O and D<sub>2</sub>O at 25°C and for ice I. The results of the calculations are compared with observed spectra and with recent molecular-dynamics calculations.

### INTRODUCTION

The far-infrared spectrum of water vapor is that of an asymmetric rotator with rotational lines extending from 800 cm<sup>-1</sup> to 1 cm<sup>-1</sup> and is well understood. When water vapor is condensed, the absorption spectrum of the liquid as given by a plot of the Lambert absorption coefficient  $\alpha(\nu)$  in this same region consists of a strong broad band with little structure having an absorption maximum at 685 cm<sup>-1</sup>, a weaker band with a maximum at 193 cm<sup>-1</sup> (1), and an inflection in the  $\alpha(\nu)$ -vs- $\nu$  curves near 10 cm<sup>-1</sup> (2). From the isotopic frequency shifts observed in the spectra of D<sub>2</sub>O and H<sub>2</sub>O, the absorption of liquid water in the region near 685 cm<sup>-1</sup> has been attributed to the librational motion of individual molecules in a liquid lattice and the absorption at 193 cm<sup>-1</sup> has been attributed to hindered translational motion. The Raman spectrum of water shows a broad band in the range 300-950 cm<sup>-1</sup> which Walrafen (3, 4) has analyzed into three librational bands with maxima at 450, 550, and 722 cm<sup>-1</sup> and weaker Raman scattering in the frequency range below 300 cm<sup>-1</sup> with maxima at 166 and about 60 cm<sup>-1</sup>. The resolution of the Raman librational band into three broad, nearly Gaussian bands is supported by inelastic neutron scattering (5) and hyper-Raman (6, 7) observations.

Considering the lack of spatial ordering as evidenced in X-ray scattering measurements and the short lifetime of lattice structure in liquid water as inferred from dielectric relaxation measurements, Bryan and Curnutte (8) proposed a simple model for the calculation of the librational and hindered translational modes of the water lattice. This model consisted of a single rigid water molecule, tetrahedrally hydrogen bonded to its four nearest neighbors in their average positions. The force constants for the hydrogen bonds were taken from the Lippincott-Schroeder (9, 10) potential function,  $V_{LS}(R, r, \theta)$ , for a hydrogen bond. The Lippincott-Schroeder potential function gives

<sup>1</sup> Based on part of a dissertation submitted by J. Bandekar to the Kansas State University in partial fulfillment of the requirements of the Doctor of Philosophy degree.

<sup>2</sup> Present address: Department of Biophysics, Indian Institute of Science, Bangalore-560012, India.

the binding energy of a pair of hydrogen-bonded water molecules as a function of the oxygen-oxygen distance  $R$ , the oxygen-hydrogen distance  $r$ , bond bending angle  $\theta$ , and parameters which characterize the dispersion forces between the oxygen atoms and the covalent bonding between the oxygen and hydrogen atoms. In addition to these hydrogen bond forces it was necessary to include a term representing the forces resulting from the interaction of the dipole moment of the central molecule with the electric field due to the electric dipole moments of its neighbors. The potential was adjusted once at an O-O distance of 2.85 Å to fit the measured Raman scattering maxima of water at 25°C. The frequencies of major features in the spectrum of ice *I* were also reproduced with the same potential when the O-O distances were set equal to 2.76 Å with no other changes.

The liquid was treated by assigning the distances to the nearest neighbors at random in a Monte Carlo calculation and a frequency distribution histogram was obtained. This calculation was successful in reproducing the vibrational and hindered translational frequencies for H<sub>2</sub>O at 25°C, H<sub>2</sub>O at 75°C, and D<sub>2</sub>O at 25°C with appropriate bandwidths and temperature shifts. However, in this analysis no frequency maximum was obtained for any frequency lower than that of the hindered translational band at 166 cm<sup>-1</sup>.

Frequencies observed below 166 cm<sup>-1</sup> could be due to lattice modes involving more than just one molecule since the dielectric relaxation time would permit correlated motion of up to about ten molecules. The present calculation was undertaken to extend the local structure model to include the motion of a central molecule in a nonrigid cage of its nearest neighbors, surrounded by a rigid cage of next-nearest neighbors in order to see what additional librational and translational frequencies would be obtained for this more realistic local-structure unit.

The present calculations thus concentrate on the motion of the central molecule and its four nearest neighbors as shown in Fig. 1. The internal vibrations are assumed to take place independently of the intermolecular vibrations, so that the three internal degrees of freedom will be neglected in this calculation. The five molecules, which contribute to the kinetic energy of the local structure unit, have 30 degrees of translational and rotational freedom in all. Since this five-molecule group is embedded in the average fields of the next-nearest neighbors, all the 30 degrees of freedom contribute to nontrivial solutions of the secular equation. In Fig. 1, complete tetrahedral hydrogen bonding is shown between the molecules. We note, however, that after the O-O distance reaches a distance of 3.5 Å, the hydrogen bond may be considered to have broken. At greater distances the hydrogen-bond force becomes nearly zero. The structure shown in Fig. 1 illustrates the situation for the case in which all the hydrogen bonds are of the same length; this does not occur in the liquid and this fact was accounted for in the calculations. The molecules in Fig. 1 are shown aligned with respect to the central molecule and the dipole moments of the nearest molecules are all parallel to that of the central molecule. This type of ordering of the hydrogen atoms does not actually occur; we show later that the disorder of the dipoles has little effect on the observed spectrum.

#### COMPUTATION

A normal coordinate analysis was carried out by using a small-vibration treatment similar to that of Bryan, except that the 30 external coordinates of five molecules are

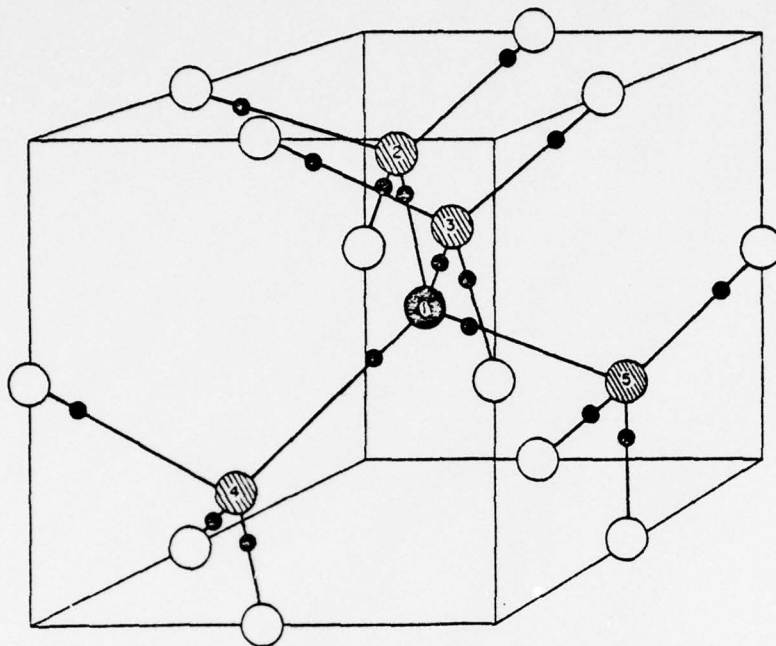


FIG. 1. Local structure unit, used to define nomenclature used in this calculation. The molecules are shown for the most symmetrical, ordered arrangement. In the calculations the sixteen O-O distances are assigned values at random. The effect of the orientational ordering is discussed in the text.

now explicitly included in the analysis. The specific expressions for  $T$  and  $V$  in the case of our local structure unit as shown by Fig. 1 were obtained. The expression for the kinetic energy of the unit is (11)

$$2T = \sum_{j=1}^5 [M_j \dot{R}^2 + I_{xz} \dot{R}_{zj}^2 + I_{yy} \dot{R}_{yj}^2 + I_{zz} \dot{R}_{zj}^2],$$

where  $R_{zj}$ ,  $R_{yj}$ , and  $R_{xj}$  denote rotational displacements from equilibrium in radians about the  $x$ ,  $y$ , and  $z$  axes, respectively, of molecule  $j$  and the quantity  $R$ , denotes a translational displacement of molecule  $j$  from its equilibrium position. The valence-bond form of the potential energy expression in the harmonic approximation is

$$2V = \sum_{\beta=1}^{16} k_{\beta} \rho_{\beta}^2 + g_{\beta} \sigma_{\beta}^2 + h_{\beta} \tau_{\beta}^2 + \sum_{\alpha=1}^5 (\rho E)_{\alpha} (R_{z\alpha}^2 + R_{y\alpha}^2),$$

where the summation on  $\beta$  is over 16 bonds and the summation on  $\alpha$  is over five molecules;  $\rho$ ,  $\sigma$ ,  $\tau$  represent the stretching, in-plane bending, and out-of-plane bending displacements of hydrogen bonds from their positions of equilibrium and  $k$ ,  $g$ , and  $h$  are the corresponding force constants. The last term is the interaction energy of the electric dipole moment of a molecule with the local electric field due to its neighbors ( $\beta$ ). The force constant  $k$  associated with the stretching of the oxygen-oxygen distance and the

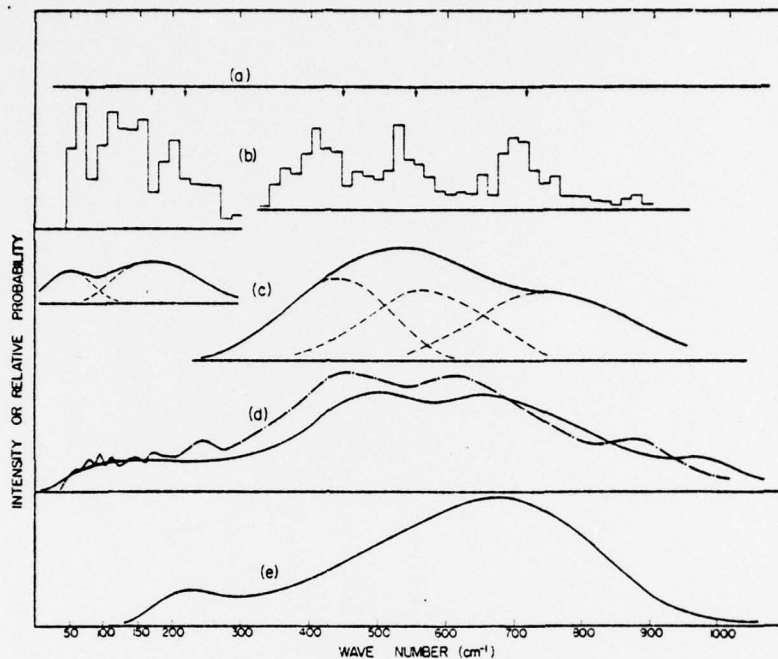


FIG. 2. Observed spectra (50–1000  $\text{cm}^{-1}$ ) and results of this calculation. (a) Frequencies calculated for the symmetrical local structure unit with all O–O distances at 2.85 Å are shown by arrows. (b) Results of a 600-configuration Monte Carlo calculation for water at 25°C. (c) Raman scattering spectrum (3, 4). (d) Neutron inelastic scattering spectrum (5). The solid curve is for scattering angle of  $\phi = 45^\circ$  at  $T = 25^\circ\text{C}$ , the dashed curve is for  $\phi = 0^\circ$  at  $T = 0^\circ\text{C}$ . (e) Far-infrared spectrum (1).

hydrogen-bond bending constants  $g$  and  $h$  were obtained from the Lippincott–Schroeder potential function (9, 10). Expressions for these quantities have been given in Ref. (8).

It was assumed that the local electric field  $\mathbf{E}$  is constant at the site of the central molecule and at the sites of each of the nearest neighbors. The product  $\mathbf{p} \cdot \mathbf{E}$ , where  $\mathbf{p}$  is the dipole moment of a water molecule in the liquid state, was assumed to depend only on the distances to the nearest neighbors and hence varied according to the average value of the reciprocal of the O–O distances cubed, where the average is taken over the four hydrogen bonds of the molecule of interest. The possible change in this contribution due to angle bending was neglected.

The potential-energy expression was transformed from valence bond coordinates  $\rho$ ,  $\sigma$ , and  $\tau$ , to cartesian displacement coordinates  $R_i$  and rotational coordinates  $R_j$  by using the geometrical relationships between these sets of coordinates. The classical Euler–Lagrange equations were then constructed for the local structure unit.

Calculations of the vibrational frequencies for the model were first made for a symmetric configuration of  $\text{H}_2\text{O}$  molecules with all O–O distances set to 2.85 Å. The values of  $k$ ,  $g$ ,  $h$ , and  $pE$  were chosen so that the frequencies obtained agreed with the Raman scattering maxima of water at 25°C given by Walrafen (3, 4) as shown in Fig. 2c. The resulting force constants for  $R_0 = 2.85 \text{ \AA}$  and  $r_0 = 0.99 \text{ \AA}$  were:  $k = 1.92 \times 10^4 \text{ dyne}$



TABLE I  
Frequencies and Symmetry Coordinates for Water in the Symmetric  
Case with  $C_{2v}$  Symmetry  
Hindered Rotations

Liquid Water $R = 2.85 \text{ \AA}$				"Ice" $R = 2.76 \text{ \AA}$
Frequency ( $\text{cm}^{-1}$ )	Symmetry	Symmetry Coordinate		Frequency ( $\text{cm}^{-1}$ )
$\text{H}_2\text{O}$	$\text{D}_2\text{O}$			
450	319	$A_2$	$0.71(R_{z4}+R_{z5})$	561
450	320	$B_1$	$0.71(R_{z4}-R_{z5})$	563
450	318	$A_2$	$R_{z1}$	561
452	320	$B_2$	$0.71(R_{z3}-R_{z2})$	563
452	319	$A_2$	$0.71(R_{z3}+R_{z2})$	561
553	397	$A_1$	$0.71(R_{x4}-R_{x5})$	651
553	399	$B_2$	$0.69(R_{x4}+R_{x5})+0.10(R_{x3}+R_{x2})$	651
554	397	$A_2$	$0.71(R_{x3}-R_{x2})$	653
554	398	$B_2$	$0.16(R_{x4}+R_{x5})+0.69(R_{x3}+R_{x2})$	651
553	397	$B_2$	$R_{x1}$	653
722	538	$B_1$	$0.69(R_{y4}+R_{y5})+0.16(R_{y3}+R_{y2})$	810
722	539	$B_1$	$R_{y1}$	811
722	538	$A_2$	$0.71(R_{y5}-R_{y4})$	810
723	539	$B_1$	$-0.16(R_{y4}+R_{y5})+0.69(R_{y3}+R_{y2})$	811
723	538	$A_1$	$0.71(R_{y2}-R_{y3})$	810

$\text{cm}^{-1}$ ,  $g/r_0R_0 = G = 2.40 \times 10^3 \text{ dyne cm}^{-1}$ ,  $h/r_0R_0 = H = 2.375 \times 10^3 \text{ dyne cm}^{-1}$ , and  $pE = 0.119 \times 10^{-11} \text{ erg}$ .

The algebraic expressions for  $k$ ,  $g$ , and  $h$  obtained from the Lippincott-Schroeder potential function ( $\delta$ ) were then scaled by a simple constant multiplication to yield these values of  $k$ ,  $g$ , and  $h$  for  $R = 2.85 \text{ \AA}$ . At all other O-O distances the force constants were obtained from the potential function without further changes. The resulting frequencies for the symmetrical configuration are given in the first columns of Tables I and II. The normal coordinates for these symmetrical modes and their symmetry classes under  $C_{2v}$  symmetry are shown in the center two columns of Tables I and II.

The resulting frequencies in  $\text{cm}^{-1}$  when the calculations were extended without change of parameters to liquid  $\text{D}_2\text{O}$  are shown in the second columns of Tables I and II and are

TABLE II  
Frequencies and Symmetry Coordinates for Water in the  
Symmetric Case with  $C_{2v}$  Symmetry  
Hindered Translations

Liquid Water R = 2.85Å				"Ice" R = 2.76Å
Frequency ( $\text{cm}^{-1}$ )	Symmetry	Symmetry Coordinate		Frequency ( $\text{cm}^{-1}$ )
H <sub>2</sub> O	D <sub>2</sub> O			
71	68	B <sub>2</sub>	$0.72y_1 - 0.41(x_4 + x_5) + 0.27(z_4 - z_5)$	96
77	74	B <sub>1</sub>	$0.72x_1 + 0.41(y_3 + y_2) + 0.27(z_3 - z_2)$	104
75	72	A <sub>1</sub>	$0.27(x_5 - x_4) + 0.27(y_3 - y_2) + 0.32(z_4 + z_5) + 0.71z_1$	101
164	157	B <sub>2</sub>	$0.71(x_2 + x_3)$	227
164	157	A <sub>2</sub>	$0.71(x_2 - x_3)$	227
160	152	A <sub>2</sub>	$0.71(y_5 - y_4)$	222
163	155	B <sub>1</sub>	$0.71(y_5 + y_4)$	225
164	157	A <sub>1</sub>	$0.59(x_5 - x_4) + 0.39(y_2 - y_3)$	227
162	154	B <sub>2</sub>	$0.39(x_4 + x_5) - 0.59(z_5 - z_4)$	224
165	157	A <sub>1</sub>	$0.5(z_2 + z_3 - z_5 - z_4)$	228
165	157	B <sub>1</sub>	$0.39(y_3 + y_2) - 0.59(z_3 - z_2)$	228
165	157	A <sub>2</sub>	$-0.20(x_5 - x_4) + 0.43(y_2 - y_3) + 0.37(z_4 + z_5 + z_3 + z_2)$	228
217	206	B <sub>2</sub>	$0.43(x_4 + x_5) + 0.69y_1 - 0.28(z_4 - z_5)$	303
219	208	B <sub>1</sub>	$0.71x_1 - 0.42(y_3 + y_2) - 0.27(z_3 + z_2)$	303
219	207	A <sub>1</sub>	$0.27(x_5 - x_4) - 0.27(y_2 - y_3) + 0.32(z_4 + z_5) - 0.71z_1$	301

in good agreement with the maxima in the observed spectra for liquid D<sub>2</sub>O. The calculations were also extended with no changes in parameters to H<sub>2</sub>O ice by calculating the frequencies for the symmetrical case corresponding to an O-O distance of 2.76 Å and using the corresponding force constants. The values obtained, as given in the last columns of Tables I and II compare very favorably with the values obtained experimentally (12) except for the lowest two observed frequencies at 45 and 63  $\text{cm}^{-1}$  for which no corresponding frequencies are obtained with this model.

The dielectric relaxation time for ice I and 0°C is about  $2 \times 10^{-6}$  sec (13), a time during which motions of a large number of neighbors might be expected to correlate with those of a given molecule; thus, correlations of order higher than the ones incorporated in our model might give rise to the bands of ice at 45 and 63  $\text{cm}^{-1}$ . The symmetrical configurations with O-O distance of 2.76 Å of our local structure unit represent the unit cells for ice as used in solid-state physics except that we have introduced

boundary conditions at the edges of the unit cells, so that the molecules there are assumed to be stationary.

An approximate distribution function for the O-O distance of the hydrogen bond in liquid water was obtained from the experimental data of Narten *et al.* (14) in the manner discussed in Ref. (8). This approximate distribution function was used as the basis for a Monte Carlo calculation. The Monte Carlo technique consisted in picking the configuration of the local structure unit at random by assigning lengths at random to the 16 hydrogen bonds in the model and calculating the corresponding frequencies. The random lengths were chosen by using random numbers generated by means of an IBM subroutine, RANDU (15). Each two-digit number represents a particular interval out of 100 equal intervals in the O-O distance distribution. The height of the distribution function at each interval represents the probability that an O-H-O bond has the corresponding O-O length at equilibrium. If we assume that the hydrogen bond lengths are all independent, the product of the 16 heights represents the probability of finding that particular configuration. From the randomly selected O-O distances, the appropriate stretching and bending constants were assigned for each bond by using the Lippincott-Schroeder potential function as originally scaled; the potential-energy matrix was then normalized with respect to the kinetic-energy matrix and was then diagonalized. For each configuration a set of 30 frequencies was obtained along with the corresponding probability of the configuration.

The histogram shown in Fig. 2b is the result of calculations of 600 randomly chosen configurations. Until calculations for about 250 configurations were obtained, the trend of the shape of the curve was uncertain. When the number of configurations was increased to 350, there was a definite trend which remained unchanged as the number of configurations in the calculations was increased to 600. The band at  $75\text{ cm}^{-1}$  is a well-defined peak as are the three librational bands. The band at  $220\text{ cm}^{-1}$  is well peaked but is broadened considerably to the high-frequency side. The  $165\text{ cm}^{-1}$  maximum is rather broad; this is so because it has the highest, ninefold, degeneracy for the symmetrical configuration.

It must be noted that the histogram gives just the probability of the occurrence of a frequency without regard to any selection rules peculiar to the technique of study. The intensity of the observed infrared or Raman band is related to the density of states modified by the absorption or scattering probability of the fundamentals and overtone and combination bands. Since the infrared absorption probability expression is proportional to  $|M_{if}|^2$  and to  $\nu$ , the observed infrared absorption is enhanced toward high frequencies. The Raman scattering intensity is proportional to  $(\partial\alpha/\partial Q)^2$  and to  $1/\nu$ , where  $\alpha$  is the polarizability tensor and  $Q$  is a normal coordinate. Thus, the Raman scattering curve is expected to be enhanced toward the low-frequency end of the spectrum. The neutron-scattering cross section depends on the momentum transfer, so that the curve does not give a pure density of states. In view of the above selection rules and limitations, only the peak positions and bandwidths should be compared with experimental data.

The calculations reported here are for only one ordered orientation of the molecular dipoles of the molecules. From a calculation of the largest and smallest values available to the  $\mathbf{p}\cdot\mathbf{E}$  term, one can estimate that inclusion of the disordering of the molecular

dipoles would only give rise to an additional breadth of the librational bands of about  $50 \text{ cm}^{-1}$ .

#### COMPARISON WITH MOLECULAR-DYNAMICS STUDIES

It is instructive to compare the results of these local structure calculations with the results of the molecular dynamics calculation of Rahman and Stillinger (16).

The potential used in the Rahman and Stillinger calculations gives equilibrium positions at tetrahedral angles and at O-O distances of  $2.76 \text{ \AA}$  and was not adjusted to fit any observed spectral data so that the comparison should be made for qualitative features and not for precise frequencies. The best comparison is between the histogram of Fig. 2b, which gives probability of occurrence of a vibrational frequency in the local structure unit, and the Fourier transforms of various autocorrelation functions of Ref. (16). The total angular momentum autocorrelation function yields a Fourier transform (16, Fig. 29) which shows three well-defined maxima at  $424$ ,  $636$ , and  $850 \text{ cm}^{-1}$  which can be compared to the three librational maxima at  $425$ ,  $525$ , and  $710 \text{ cm}^{-1}$  of Fig. 2b. It is interesting that the 217-molecule unit of the molecular-dynamics study shows only three broad maxima as do our local structure calculations.

Comparison of the Fourier transforms of the proton total velocity autocorrelation function (16, Fig. 32), which has maxima at  $53$ ,  $212$ , and  $425 \text{ cm}^{-1}$ , inflections at  $636$ ,  $850 \text{ cm}^{-1}$  and is nonzero in the range  $1000$ – $1300 \text{ cm}^{-1}$ , with Fig. 2b, which has maxima at  $70$ ,  $100$ – $170$ ,  $200$ ,  $425$ ,  $525$ , and  $710 \text{ cm}^{-1}$ , shows considerable similarity; however, the molecular-dynamics calculation shows no maxima in the  $100$ – $170 \text{ cm}^{-1}$  region and the local structure model no vibrations above  $1000 \text{ cm}^{-1}$ .

The occurrence of vibrations in the region  $1000$ – $1300 \text{ cm}^{-1}$  in the molecular-dynamics calculations and their absence in the local structure model can be due to the fact that the local-structure calculations are for fundamental modes only, while overtone and combination frequencies involving translational and librational motion should be expected in the molecular-dynamics calculation. The fundamental translational modes in the region  $100$ – $170 \text{ cm}^{-1}$  in the local-structure calculation appear to correspond to the  $212 \text{ cm}^{-1}$  peak in the molecular-dynamics calculation. The  $200 \text{ cm}^{-1}$  peak in the local-structure calculation appears to have no counterpart in the molecular dynamics unless it is masked by the librational band.

#### DISCUSSION

One of the objectives in model calculations for any physical system is to identify those features of the system which make important contributions to the observed phenomena and those features which are not essential for understanding the phenomena under consideration. From such model calculations one can discover what features of the physical system can be studied by a given technique. It is also clear that a model which contains only those details necessary to understand one kind of observation, such as spectral measurements, may well not be sufficiently detailed to provide an understanding of observations obtained with quite different techniques, such as thermal measurements. A complete model would ideally contain all the details necessary to explain all possible observations but should, upon suppression of details not important to a particular kind of observation, agree with more restricted models which are good representations of the system for that kind of observation.

The local-structure model qualitatively shows the same essential features as does the molecular-dynamics study, which includes many more molecules, for the vibrational spectrum of liquid water in the 50–1000  $\text{cm}^{-1}$  region. Thus the features of this local-structure model appear to be sufficient to explain the gross appearance of spectral characteristics in the librational and hindered-translational frequency region, such as the number of maxima, their widths and positions; consequently, these spectral features will only yield information concerning local regions of the liquid. For more detailed comparison of model calculations with measured spectra, additional factors such as the effect of the hydrogen bond lattice distortions on the dipole moments and polarizability of the lattice and molecules would need to be included in the calculations. With our present local-structure model, the frequencies of the lowest lattice modes are comparable to the frequency of dielectric relaxation and the widths of the lowest calculated bands are comparable with the band frequencies; thus it seems unlikely that an extension of the size of the local-structure unit would yield additional physically meaningful vibrational frequencies.

## ACKNOWLEDGMENTS

The authors thank the Kansas Agricultural Experiment Station for the support of this research, and Professor Dudley Williams for helpful criticism.

RECEIVED: August 5, 1974

## REFERENCES

1. C. ROBERTSON, B. CURNUTTE, AND D. WILLIAMS, *Mol. Phys.* 26, 183 (1973).
2. M. S. ZAFAR, J. B. HASTED, AND J. CHAMBERLAIN, *Nature Phys. Sci.* 243, 106 (1973); P. S. RAY, *Appl. Opt.*, 11, 1836 (1972).
3. G. E. WALRAFEN, in "Hydrogen-bonded Solvent Systems" (A. K. Covington and P. Jones, Eds.), pp. 9–30, Taylor and Francis, London, 1968.
4. G. E. WALRAFEN, *J. Chem. Phys.* 40, 3249 (1964).
5. G. J. SAFFORD, P. S. LEUNG, A. W. NAUMANN, AND P. C. SCHAPPER, *J. Chem. Phys.* 50, 4444 (1969).
6. R. W. TERHUNE, P. D. MAKER, AND C. M. SAVAGE, *Phys. Rev. Lett.* 14, 681 (1965).
7. P. D. MAKER, private communication.
8. J. B. BRYAN AND B. CURNUTTE, *J. Mol. Spectrosc.* 41, 512 (1972); J. B. BRYAN, A normal coordinate analysis of the local structure of liquid water for interpretation of far infrared spectra, Ph.D. Dissertation, Kansas State University, Manhattan, 1969.
9. E. R. LIPPINCOTT AND R. SCHROEDER, *J. Chem. Phys.* 23, 1099 (1955).
10. R. SCHROEDER AND E. R. LIPPINCOTT, *J. Phys. Chem.* 61, 921 (1955).
11. J. N. BANDEKAR, A Monte-Carlo normal coordinate analysis treatment of intermolecular vibrations in liquid water, Ph.D. Dissertation, Kansas State University, Manhattan, 1973. (Details of coordinate transformations in Appendix.)
12. H. J. PRASK, S. F. TREVINO, J. D. GAULT, AND K. W. LOGAN, *J. Chem. Phys.* 56, 3217 (1972).
13. D. EISENBERG AND W. KAUFMANN, "The Structure and Properties of Water," p. 112, Oxford University Press, New York, 1969.
14. A. H. NARTEN AND H. A. LEVY, *Science* 167, 1520 (1970); M. D. DANFORD AND H. A. LEVY, *J. Amer. Chem. Soc.* 84, 3965 (1962); A. H. NARTEN, M. D. DANFORD, AND H. A. LEVY, *Discuss. Faraday Soc.* 43, 97 (1967).
15. "Random Number Generation and Testing" (IBM Manual GC 20-8011-00).
16. A. RAHMAN AND F. H. STILLINGER, *J. Chem. Phys.* 55, 3336 (1971).

## NOTES

## Incomplete Hydrogen Bonding and the Structure of Liquid Water

Previous calculations (1, 2) of the internal vibration of a water molecule in the liquid have been successful in predicting the bond shift and width as a function of temperature, they were not, however, able to account for shoulders on the high frequency side of the stretching bands. Further, a recent paper by Rahman and Stillinger (3) reported a molecular dynamics calculation of the frequency spectrum. These calculations give a surprisingly large number of hydrogens in such positions that the hydrogen-bond network could not be completed. The failure of our previous attempts to explain the presence of the high frequency shoulders in the OH and OD stretching bands and the incomplete hydrogen-bonding indicated in Rahman and Stillinger's work (3) persuaded us to attempt to include additional "broken" hydrogen bonds in our continuum calculations. Thus, present work is a slight modification of the continuum viewpoint.

The normal coordinate analysis treatment used in this work is similar to our previous treatment (2). Except for a modification of the distribution of O-O distances in the liquid, the O-O distributions for temperatures of interest were constructed from the x-ray pair correlation functions of Narten *et al.* (4) as described in Ref. (2). These distributions were then used for Monte Carlo calculations.

The frequency distribution was obtained as follows: as was done previously (2, 4), the range of O-O distance for a given temperature was divided into one hundred equal parts and a random number sampling technique was adopted. It was assumed, rather arbitrarily, that after the O-O distance reaches 3.5 Å, the hydrogen bond involved "breaks up." This is a distance after which the H-bond force constant remains almost unchanged irrespective of changes in the O-O distance (5, 6). One of the hydrogen bond-lengths was kept at 3.5 Å and the other one was assigned a length at random. This is equivalent to a random configuration except for one "dangling" bond. The corresponding values of  $k$ ,  $r$ , and  $R$  were determined from the Lippincott-Schroeder potential function. The random lengths were chosen by selecting two-digit random numbers generated with the help of a computer. The free bond corresponded to the digit 100. Each two digit number represents a particular O-O distance.

For each configuration the appropriate values of the force constants were substituted into the potential energy function and the secular equation was solved for the normal frequencies. A histogram of the probability of the normal frequency was constructed using the resulting normal frequencies and the relative probability of the corresponding configuration. This histogram was constructed over 15  $\text{cm}^{-1}$  intervals. The calculations were repeated 500 times and with the assumptions regarding the height of the pair correlation functions and the independence of the hydrogen bond-lengths as spelled out in Ref. (2), the resulting histograms are assumed to represent the intensity distribution over each of the fundamental frequency regions.

In the intramolecular case, where we treated HDO, we had the choice of breaking either the OH or OD bond. We did both so that we could get frequencies for a free OH and a free OD in HDO. The bands corresponding to the "free" bonds were quite narrow. In order to get more direct comparison with experimental results, the distribution was smoothed over 75  $\text{cm}^{-1}$  intervals, a value which corresponds to the interruption broadening width expected for systems with relaxation time of the order of  $10^{-12}$  sec. The results are summarized in Table I.

Table I shows that the Monte Carlo calculations of a completely H-bonded system can reproduce peak positions of the main bands only and cannot explain the presence of shoulders. However, if we assume that there exist simultaneously some "broken" hydrogens and some completely bonded deuteriums in the case of HDO, we can see that most of the bands listed in Table I can be accounted for.

TABLE I  
(ALL RESULTS PERTAIN TO 25°C)  
INTRAMOLECULAR VIBRATIONS

		CALCULATED FREQUENCIES			
No.	SPECIMEN	CASE	OD Band Peak Position (cm <sup>-1</sup> )		OH Band Peak Position (cm <sup>-1</sup> )
1	H <sub>2</sub> O	Random	2510		3480
		H free	2510		
		D free		2655	
2	H <sub>2</sub> O	Random			3300 3405 3495
		one H free			3300 3495 3660

		OBSERVED FREQUENCIES			
CASE		OD Band Peak Position (cm <sup>-1</sup> )		OH Band Peak Position (cm <sup>-1</sup> )	
1	Raman HDO in H <sub>2</sub> O	2530	2650		
2	Raman HDO in D <sub>2</sub> O			3435	3628
3	Raman H <sub>2</sub> O Spontaneous Stimulated			3060	3245 3420 3520
		Stimulated in NaClO <sub>4</sub>			3300 3390
4	Raman HDO in (H <sub>2</sub> O:D <sub>2</sub> O) by volume Spontaneous (1:1) Stimulated (1:1) Stimulated (1.5:1)			3280	3460 3550 3605
				3280	3440 3550 3625
				3300	3390 3540 3640
5	Infrared H <sub>2</sub> O			3090	3220 3395 3540 3625

This same procedure, when repeated for the intermolecular vibrations using Bryan's (7) model, by keeping one of the atoms, either H or D, free and assigning the other three O...O lengths at random, yields results given in Table II. Table II shows that  $\nu_1$  increases while  $\nu_2$  and  $\nu_3$  decrease slightly when a hydrogen bond to the hydrogen atom is "broken," but  $\nu_4$ ,  $\nu_5$ , and  $\nu_6$  all decrease appreciably in this process. When we "break" the hydrogen bond to an oxygen atom,  $\nu_1$  and  $\nu_3$  decrease while  $\nu_2$  increases appreciably;  $\nu_4$ ,  $\nu_5$ , and  $\nu_6$  essentially remain unaltered in this process. Thus, breaking a hydrogen bond to the hydrogen atom of a water molecule will cause a shift in the librational frequencies and leave the translational band relatively unchanged while breaking the hydrogen bond to the oxygen atom will cause the translational band to be lowered and will leave the librations unaffected. The decrease of the  $\nu_1$  frequency from 575 cm<sup>-1</sup> to 450 cm<sup>-1</sup> when the hydrogen bond to a hydrogen atom is broken might

TABLE II  
(ALL RESULTS PERTAIN TO 25°C)  
INTERMOLECULAR VIBRATIONS

SPECIMEN	CASE	$\nu_1$	$\delta\nu_1$	$\nu_2$	$\delta\nu_2$	$\nu_3$	$\delta\nu_3$	$\nu_4$	$\delta\nu_4$	$\nu_5$	$\delta\nu_5$	$\nu_6$	$\delta\nu_6$
H <sub>2</sub> O	Random	150	125	150	100	175	100	575	150	725	125	475	125
	H free	200	150	125	75	125	100	450	100	625	125	350	100
	O free	100	50	175	100	100	100	575	100	725	125	475	125
D <sub>2</sub> O	Random	145		145		165		400		510		340	
	D free	175	125	125	100	100	100	300	125	450	125	125	100
	O free	100	75	150	150	100	100	400	175	500	150	150	100

well account for the intensity in this region of the librational band which corresponds to the  $\nu_6$  mode which is infrared inactive in the symmetrical configurations.

These calculations seem to indicate the need for a model which is a blend of the mixture and the continuum models; the breadth of the bands cannot be accounted for by the broken-hydrogen bonds alone while the presence of the bands at 2640 and 3628  $\text{cm}^{-1}$  with appropriate temperature dependence cannot be readily explained by the continuum model. A physically meaningful way of assigning weights to the spectral contribution of the "broken" and "unbroken" hydrogen-bonds which is consistent with the O-O pair correlation function will be necessary before one can discuss the intensity distributions in the stretching bands. We feel these results indicate a weakness in the ansatz we have previously used to get the nearest neighbor distribution function from the x-ray pair correlation functions. There is at present no way to distinguish the hydrogen positions in the O-O pair correlation functions. If the hydrogen atom is far enough out of line with the oxygen atoms, then the bond is so distorted as to be "broken" and should be treated accordingly. At this point one can only say that the positions and breadths of the major bands can be explained with appropriate temperature dependence on the basis of the viewpoint invoked in these calculations.

#### ACKNOWLEDGMENT

The authors wish to thank Kansas State University's Agricultural Experiment Station for the sponsorship of this work.

#### REFERENCES

1. Presented in part at the 27th Symposium on Molecular Spectroscopy and Structure in Columbus, Ohio, June 1972.
2. B. CURNUTTE AND J. BANDEKAR, *J. Mol. Spectrosc.* 41, 500 (1972).
3. A. RAHMAN AND F. H. STILLINGER, *J. Chem. Phys.* 55, 3336 (1971).
4. A. H. NARTEN, M. D. DANFORD, AND H. A. LEVY, X-Ray Diffraction Data on Liquid Water in the Temperature Range 4° to 200°C, private communication.
5. E. R. LIPPINCOTT AND R. SCHROEDER, *J. Chem. Phys.* 23, 1099 (1955).
6. R. SCHROEDER AND E. R. LIPPINCOTT, *J. Phys. Chem.* 61, 921 (1957).
7. J. B. BRYAN AND B. CURNUTTE, *J. Mol. Spectrosc.* 41, 513 (1972).

BASIL CURNUTTE  
JAGDEESH BANDEKAR

*Department of Physics,  
Kansas State University,  
Manhattan, Kansas 66506  
Received April 26, 1973*



### III INFRARED METHODS

#### III.1. THE FAR-INFRARED SPECTRUM OF WATER

Basil Curnutte and Dudley Williams

Physics Department, Kansas State University  
Manhattan, Kansas 66506, U.S.A.

#### ABSTRACT

Studies of the far-infrared spectrum of water provide information concerning the motions of hydrogen-bonded water molecules in the lattice structure of the liquid. A plot of the Lambert absorption coefficient as a function of frequency has one maximum at  $680 \text{ cm}^{-1}$  associated with a broad absorption band attributed to hindered rotations or librations of  $\text{H}_2\text{O}$  molecules in the lattice and a second maximum near  $200 \text{ cm}^{-1}$  associated with a narrower band attributed to hindered translations of  $\text{H}_2\text{O}$  molecules in the lattice; an inflection near  $2 \text{ cm}^{-1}$  in the plot of the Lambert coefficient is attributed to absorption associated with Debye relaxation phenomena. In the present paper we present the values of the indices of refraction and absorption based on recent experimental work and attempt to interpret the results in terms of two recent theories of the structure of water.

The infrared spectrum of the water vapor molecule in its ground electronic state is fairly well understood. In the far-infrared the absorption spectrum is that of an asymmetric rotor and is characterized by irregularly spaced pure rotational lines in the entire spectral range between  $800\text{ cm}^{-1}$  and the microwave region. The vibration-rotation spectrum is characterized by fundamentals  $\nu_1$  and  $\nu_3$  centered at  $3651\text{ cm}^{-1}$  and  $3756\text{ cm}^{-1}$ , respectively, in the spectral region where molecules containing OH groups have strong absorption bands. The third fundamental  $\nu_2$ , associated with the bending motion of the molecule, appears at  $1595\text{ cm}^{-1}$ . Overtone and combination bands are less intense and appear at higher frequencies. In addition to rotational and vibrational energies, the water vapor molecule has translational energy; at atmospheric pressure and below no observable absorption is associated with changes in translational energy.

### III.1.1. THE OBSERVED SPECTRUM

Liquid water is strongly absorbing throughout most of the infrared; the Lambert absorption coefficient  $\alpha(\nu)$  in the  $3400\text{ cm}^{-1}$  region is nearly  $10^8$  times  $\alpha(\nu)$  in the center of the visible region, where water is most transparent. Because of the strong spectral absorption of water in the infrared, it is difficult to obtain quantitative values of absorption by simple transmission measurements; special techniques must usually be employed (1-6). The general appearance of the water spectrum in the infrared is illustrated by Fig. 1, which gives the spectral transmittance  $T(\nu) = \exp[-\alpha(\nu)x]$  as computed for a layer of thickness  $x = 10\mu\text{m}$  on the basis of Lambert coefficients obtained from a combination of transmission and reflection measurements. A layer of this thickness is essentially opaque in the  $3400\text{ cm}^{-1}$  region; the upper curve in the  $3400\text{ cm}^{-1}$  region gives the spectral transmittance of a water layer with a thickness of  $1.125\mu\text{m}$ , much smaller than the wavelength of the radiation in this spectral region. In preparing the curves in Fig. 1 and in most of the subsequent figures, we have used values of  $\alpha(\nu)$  based on our own measurements (6) in the  $5000\text{-}100\text{ cm}^{-1}$  range, on those of Davies *et al.* (7) in the  $100\text{-}20\text{ cm}^{-1}$  range, and on those listed by Ray (8) for the  $20\text{-}1\text{ cm}^{-1}$  range.

Because of its proximity to the corresponding bands of water vapor, the strong absorption in the  $3400\text{ cm}^{-1}$  region is attributed primarily to the  $\nu_1$  and  $\nu_3$  fundamentals of the hydrogen-bonded  $\text{H}_2\text{O}$  molecule but also includes some contribution from the overtone  $2\nu_2$ ; the general contours of this composite band are strongly influenced by temperature changes (9). Similarly, the sharp absorption band near  $1650\text{ cm}^{-1}$  is attributed to the fundamental  $\nu_2$ ; the  $\nu_2$  band shows little change with temperature. In addition to the fundamental bands there are two weaker associational bands in the near infrared portion of the spectrum shown in Fig. 1; these associational bands near  $2120$  and  $4000\text{ cm}^{-1}$  are attributed to combinations of far-infrared bands with fundamentals and have no counterparts in the water vapor spectrum.

The far-infrared region of the liquid-water spectrum shown in Fig. 1 is dominated by two major bands. The first of these is an extremely broad, intense band with

minimum transmittance near  $680\text{ cm}^{-1}$ ; this band shifts to  $505\text{ cm}^{-1}$  in the spectrum of liquid  $\text{D}_2\text{O}$  (10). Because of this large isotopic shift, this broad band has been attributed to the hindered-rotation or librational motion of the  $\text{H}_2\text{O}$  molecule in the field of its neighbors. The second far-infrared band is much narrower and appears as a shoulder near  $200\text{ cm}^{-1}$  on the strong librational band; in  $\text{D}_2\text{O}$  the shoulder band shifts only slightly to lower frequencies (10). This small isotopic shift is consistent with an interpretation of the weaker band in terms of the hindered translational motion of the entire  $\text{H}_2\text{O}$  molecule in the field of its neighbors.

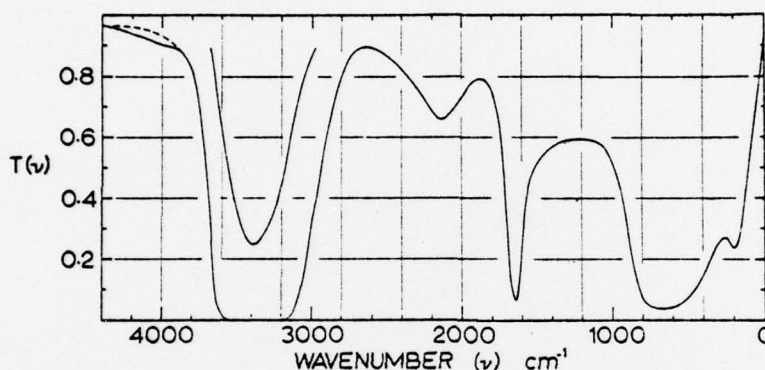


Fig. 1 The spectral transmission of a thin layer of liquid water in the infrared at  $25^\circ\text{C}$ .

More detailed information regarding the absorption of water in the far-infrared is presented in Fig. 2, in which we give a plot of the Lambert absorption coefficient as a function of frequency. Absorption in most of this region is associated with the strong librational band with a maximum near  $680\text{ cm}^{-1}$ ; the general contours of this broad band indicate that it is not a simple band but consists of several overlapping unresolved components. As noted earlier, the librational band has its maximum at  $505\text{ cm}^{-1}$  in  $\text{D}_2\text{O}$ ; it also has a somewhat smaller half width in  $\text{D}_2\text{O}$ . In an attempt to locate the position of the hindered-translation band, Draeger *et al.* (10) have arrived at the value of  $170\text{ cm}^{-1}$  by attempting to construct a contour of the overlapping librational band; their corresponding value for the hindered-translational band in  $\text{D}_2\text{O}$  is  $165\text{ cm}^{-1}$ .

The librational band shifts to lower frequencies and becomes broader with increasing temperature (9,10,11); the peak value of  $\alpha(\nu)$  shows little change with temperature. In ice slightly below the melting point the peak of the librational band appears at  $830\text{ cm}^{-1}$  and is narrower than the corresponding band in water (11); Zimmerman and Pimentel (12) have located the hindered-translational band at  $225\text{ cm}^{-1}$  in the spectrum of ice. In a study of ice at liquid-nitrogen temperatures Bertie, Labbe' and Whalley (13) have shown that the libration and hindered-translation bands have several components.

The value of  $\alpha(\nu)$  is not small anywhere in the entire range between the  $\nu_2$

fundamental and the librational band; as indicated in Fig. 2, the value of  $\alpha(\nu)$  at  $1200 \text{ cm}^{-1}$  is nearly 20 percent of that of  $\alpha(\nu)$  at the librational peak. Absorption of water in this interband region varies with temperature (9). The value of  $\alpha(\nu)$  decreases rapidly with decreasing frequency for frequencies lower than that of the hindered-translation band; there are no indications of additional absorption peaks. Our own studies (6,10) and the recent study of Zafar *et al.* (14) in the submillimeter range have given no evidence of an observable infrared peak near  $60 \text{ cm}^{-1}$ , where Raman (15) and inelastic neutron-scattering studies (16) have revealed a maximum. There is an inflection in the curve in Fig. 2 in the region between  $10 \text{ cm}^{-1}$  and  $1 \text{ cm}^{-1}$ ; this is associated with the so-called Debye absorption associated with a low-frequency relaxation process (8).

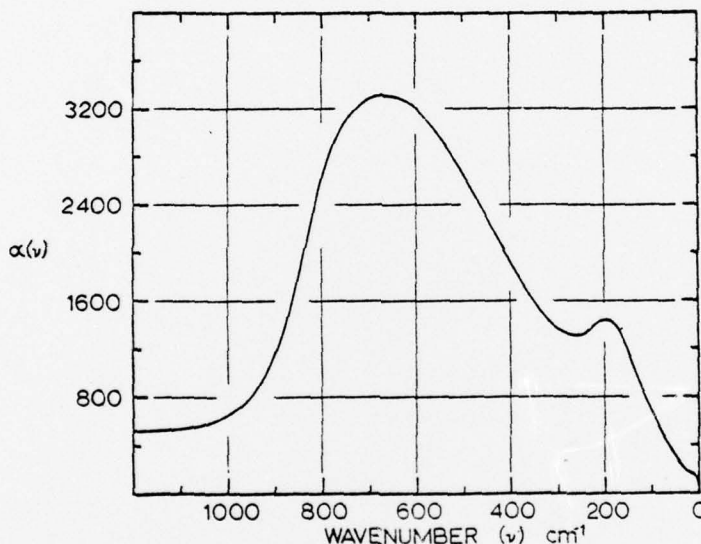


Fig. 2 The Lambert absorption coefficient  $\alpha(\nu)$  as a function of frequency in the intermediate and far infrared at  $25^\circ\text{C}$ .

Although infrared spectroscopists usually content themselves with a plot of  $\alpha(\nu)$  - vs -  $\nu$ , a complete description of the optical properties of a medium like water actually requires a knowledge of its complex refractive index. The imaginary part of the refractive index  $k(\nu) = \lambda \alpha(\nu)/4\pi = \alpha(\nu)/4\pi\nu$  gives a measure of absorption per wavelength; thus, even though  $\alpha(\nu)$  becomes small in the far-infrared,  $k(\nu)$  can remain large. By combining the results of measurements of reflection and absorption, the real part  $n(\nu)$  of the refractive index can be determined. In the remote infrared, known as the submillimeter region, both  $k(\nu)$  and  $n(\nu)$  for water become large and join smoothly with values of these quantities based on dielectric-constant measurements in the microwave and radio frequency regions (8,14). Although for many purposes it is more convenient to give values of optical constants as a function of frequency or wavelength in a log-log plot, we find it desirable for present purposes to give a linear plot

of these quantities in the far infrared.

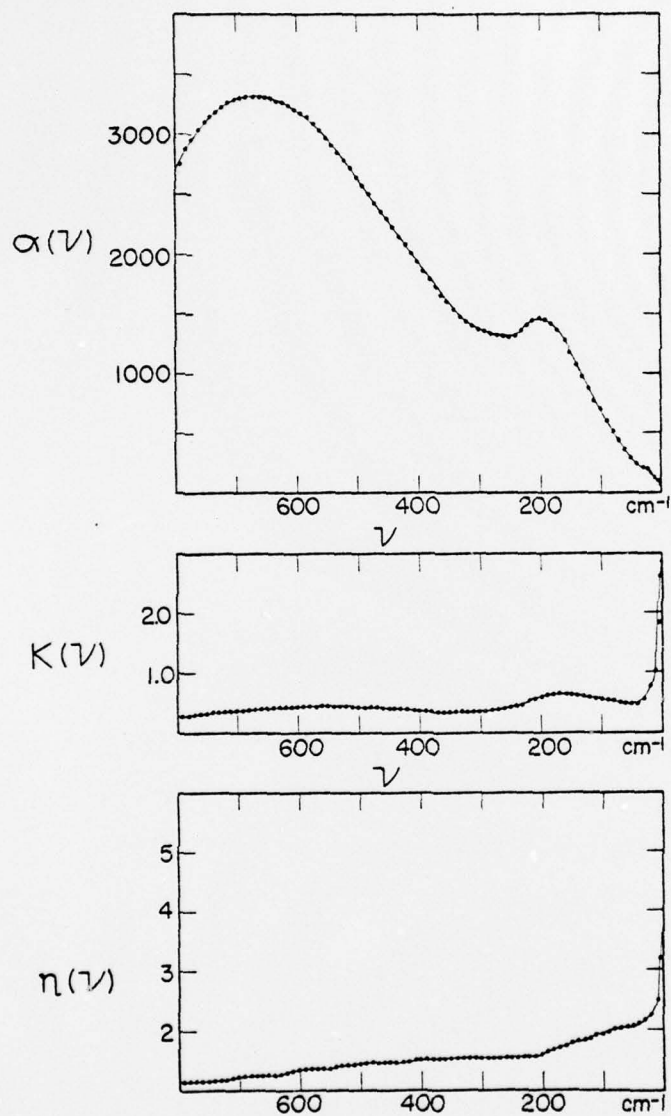


Fig. 3 The Lambert absorption coefficient  $\alpha(\nu)$ , the imaginary part  $k(\nu)$  of the refractive index, and the real part  $n(\nu)$  of the refractive index in the far-infrared for liquid water at 25°C.

In Fig. 3 we give plots of  $\alpha(\nu)$ ,  $k(\nu)$ , and  $n(\nu)$  as functions of frequency in the region between 800  $\text{cm}^{-1}$  and 1  $\text{cm}^{-1}$ . The maximum value of  $k(\nu)$  for the broad librational band appears at 570  $\text{cm}^{-1}$ , and the corresponding maximum for the narrow

hindered translation band is at  $170 \text{ cm}^{-1}$ ; the peak value of  $k(\nu)$  for the hindered-translation band is nearly 50 percent larger than the peak value of  $k(\nu)$  for the libration band (6). At frequencies below  $170 \text{ cm}^{-1}$ ,  $k(\nu)$  remains large and reaches a peak in the vicinity of  $1 \text{ cm}^{-1}$ ; this peak is associated with Debye relaxation phenomena (8). The curve for  $n(\nu)$  exhibits dispersion features in the vicinities of the libration and hindered-translation bands (6) and extrapolates to a value of approximately 9 at very low frequencies (8).

Although the libration and hindered-translation bands are strong in ice (11), values of  $k(\nu)$  for ice in the region  $100 - 1 \text{ cm}^{-1}$  are only  $10^{-2}$  to  $10^{-3}$  times the corresponding values for water (8). A detailed knowledge of  $k(\nu)$  and  $n(\nu)$  in the submillimeter region may therefore be extremely important to an understanding of the differences of the properties of water and ice on a molecular scale.

### III.1.2. THEORETICAL INTERPRETATION OF THE SPECTRUM

Liquid water consists of a hydrogen-bonded network of  $\text{H}_2\text{O}$  molecule units that remain hydrogen bonded to the same neighbors in the local lattice for appreciable times compared with librational periods. Any calculation of the spectroscopic properties of water involves not only the difficulties of the calculation for a disordered crystal lattice but also the additional difficulties imposed by a constantly changing lattice structure. The presence of strong bands with frequencies close to those of the water-vapor fundamentals indicates that individual  $\text{H}_2\text{O}$  molecules making up the water structure maintain their identities for times that are long compared with their fundamental periods of vibration. All absorption at lower frequencies must be associated with lattice vibrations of a system containing these units bound together in various ways.

We shall attempt to interpret the observed far-infrared spectrum in terms of two quite different theories. The first of these, developed by Curnutte and his students (17,18), attempts to interpret the spectrum by means of a model involving parameters fitted to the observed major spectral features of water at  $25^\circ\text{C}$ ; the theory is then tested by applying it without changes in parameters to water at other temperatures and to ice. The second theory, developed by Rahman and Stillinger (19), involves a molecular-dynamics study of a set of rigid  $\text{H}_2\text{O}$  molecular models subject to interaction potentials consistent with measured macroscopic thermodynamic properties of water. By a computer study of the motions of a set of these  $\text{H}_2\text{O}$  units, these authors were able to obtain auto-correlation functions of various physical quantities and to interpret these functions in terms of lattice frequencies; since infrared absorption involves a change of the electric dipole moment of the absorber, all characteristic lattice motions do not necessarily produce features in the far-infrared spectrum. Fortunately, the two quite different theories to be discussed do not lead to basically conflicting conclusions.

A. THE LOCAL LATTICE MODEL THEORY

In their initial study Bryan and Curnutte (17) considered a single  $H_2O$  molecule held in position in a rigid tetrahedral cage of neighboring molecules by forces given by the Lippincott-Schroeder potential, which had been developed (20,21) to describe intermolecular hydrogen bonding, and by an electrostatic interaction between the  $H_2O$  molecule's dipole moment and the electric intensity at the site of the molecule. Such a hydrogen-bonded molecule has three fundamental librational modes and three fundamental hindered-translational modes of oscillation in addition to its internal vibrational modes. Starting with the most probable O-O distance as determined by x-ray studies (22) and with the peak librational and hindered-translational frequencies listed by Walrafen (15), Bryan and Curnutte adopted four empirical parameters needed to give their tetrahedrally hydrogen-bonded molecule the observed peak frequencies. After selection of the parameters they then used Monte Carlo calculations to determine the spectral effects produced by the distribution of O-O distances as determined by x-ray diffraction; they found that variation of the distance between the oxygen atom of the central molecule and the oxygen atoms in the rigid cage over the observed range established in x-ray studies resulted in a broadening of each of the librational bands by approximately  $220\text{ cm}^{-1}$  and each of the hindered-translational bands by approximately  $120\text{ cm}^{-1}$ . In view of the relaxation time  $\tau \approx 10^{-12}$  seconds given by dielectric-constant studies (23), the lifetime of a molecular cage is limited, and this leads to a superposed uncertainty broadening  $\Delta\nu \approx 1/c\tau$  of the order of  $35\text{ cm}^{-1}$ .

A plot of the results of the Monte Carlo calculations gave a frequency spectrum that compared favorably in certain respects with the profiles of the observed Raman and infrared spectra. However, the introduction of random O-O distances destroys the original tetrahedral symmetry at the site of the central molecule so that little can be said regarding definite selection rules or spectral intensities. After the final selection of parameters for water at  $25^\circ\text{C}$ , the Bryan model was then employed to produce spectra of water at other temperatures, the spectrum of liquid  $D_2O$ , and the spectrum of ice with generally satisfactory results in the vicinity of the observed librational and hindered-translational bands from O-O spacings given by x-ray studies. The frequencies of the lattice modes given by the model for water at  $25^\circ\text{C}$  are listed in the first column of Table I; the frequencies listed represent peak values in the spectrum of a single molecule connected by four tetrahedral hydrogen bonds to neighbors in a rigid cage; the O-O distances are randomly spaced over the range established by x-ray studies.

Not all  $H_2O$  molecules in liquid water have complete tetrahedral hydrogen bonding; thus it becomes necessary to estimate the spectral effects of incomplete bonding. The effects of incomplete bonding calculated for a central  $H_2O$  molecule in a rigid cage of neighbors on the basis of most probable O-O distances are listed in the second and third columns of Table I. The second column lists the frequencies to be expected from a molecule with one hydrogen bond to its oxygen atom broken; the third column lists the frequencies to be expected for a molecule with a single

unbonded hydrogen. The additional effects introduced by breaking a single hydrogen bond include new hindered-translational modes at  $100\text{ cm}^{-1}$  and new librational modes at  $350$  and  $400\text{ cm}^{-1}$  as indicated in the table. Incomplete intermolecular bonding thus results in the general lowering of lattice frequencies.

TABLE I

Calculated Frequencies in the Lattice Spectrum of Water at  $25^\circ\text{C}$

<u>Single Molecule in a Rigid Cage</u>		<u>Five-Molecule Unit in a Rigid Cage</u>	
Tetrahedral Bonding	Free O	Free H	(Tetrahedral Bonding)
<u>Librational Frequencies (<math>\text{cm}^{-1}</math>)</u>			
450	475	350	450,450,450,452,452
551	575	450	553,553,553,554,554
722	725	625	722,722,722,723,723
<u>Translational Frequencies (<math>\text{cm}^{-1}</math>)</u>			
165	100	200	77,217,164,164,164
165	175	125	71,219,160,163,165
166	100	125	75,219,162,165,165

Recognizing that the assumption of a completely rigid cage of nearest neighbors was somewhat unrealistic, Bandekar and Curnutte (18) extended the general method to include a central molecule in a non-rigid cage of nearest neighbors -- i.e., a hydrogen bonded five-molecule unit -- connected by hydrogen bonds to a rigid cage of next-nearest neighbors. A normal-coordinate analysis of the five-molecule unit yielded a set of frequencies associated with its own fundamental vibrational modes plus additional frequencies associated with hindered rotational and translational motions of the entire five-molecule unit in the rigid cage of surrounding molecules. With little change in the Bryan parameters, Bandekar obtained the sets of frequencies listed in the final column of Table I. His treatment yielded a set of 5 frequencies close to  $450\text{ cm}^{-1}$  that can be associated with the original  $450\text{ cm}^{-1}$  librational frequency of the single  $\text{H}_2\text{O}$  molecule in the Bryan study; a set of 5 frequencies near  $555\text{ cm}^{-1}$  associated with the original  $551\text{ cm}^{-1}$  libration; and a set of 5 frequencies near  $720\text{ cm}^{-1}$  associated with the original  $722\text{ cm}^{-1}$  libration. In the  $150\text{--}175\text{ cm}^{-1}$  frequency range of hindered translation for the single  $\text{H}_2\text{O}$  unit in the Bryan study, the Bandekar treatment gives 9 frequencies in the narrow range  $160\text{--}165\text{ cm}^{-1}$ ; in addition, there are 3 frequencies between  $71$  and  $77\text{ cm}^{-1}$  that are associated with hindered translation of the entire five-molecule unit in its rigid cage; finally, there are 3 new frequencies in the range  $217\text{--}219\text{ cm}^{-1}$  that can be classified as out-of-phase translatory motions of parts of the five-molecule unit within its



rigid cage. Absorption bands centered at the listed frequencies are broadened by amounts comparable with those listed for the earlier single-molecule model.

This general type of analysis could be extended to include a larger non-rigid group of molecules consisting of the central  $H_2O$  molecule with its nearest and next-nearest neighbors inside a still larger rigid cage. However, even with the five-molecule model, the computed lowest frequencies are comparable with the frequency of dielectric relaxation; furthermore, the widths of the resulting absorption bands are comparable with the band frequencies themselves. Thus, particularly in view of the amounts of computer time involved in taking account of random O-O spacings, the wisdom of extending calculations of this type is questionable.

In summary: The calculations based on this model, which was parameterized to account for the major libration and hindered-translation bands observed in the Raman spectrum of water at  $25^\circ C$ , also accounts satisfactorily for the variation of these bands with temperature, for the corresponding bands observed in ice, and for the corresponding bands appearing in the spectrum of liquid  $D_2O$ . The calculations further predict absorption at frequencies lower than that of the observed hindered-translation peak and at frequencies in the region between the libration and hindered-translation peaks; infrared absorption is indeed observed in these regions. In order to account for the observed general absorption in the interband region between the  $\nu_2$  fundamental and the libration bands, it would probably be necessary to invoke overtones and combinations of the major lattice bands; the possibility of difference bands involving the  $\nu_2$  fundamental and certain lattice modes might also be considered.

### B. THE MOLECULAR-DYNAMICS STUDY OF RAHMAN AND STILLINGER

Turning now to the molecular dynamics study of Rahman and Stillinger (RS), we must first emphasize the basic difference between their treatment and the spectroscopic treatment of Curnutte and his colleagues, who introduced certain parameters to account for major spectral features previously observed; RS introduced no fitted parameters to account for known spectral features in the far infrared or in the low-frequency Raman spectrum. Thus, in considering the results of their theory we should not expect quantitative reproduction of the observed spectrum but should look for qualitative general agreement between predicted and observed spectral features. Closer quantitative agreement could probably be accomplished by the introduction of fitted parameters.

The RS procedure involved a computer study of the dynamical behavior of 216 rigid  $H_2O$  molecular models having a number density corresponding to that of water and subject to a rather simple intermolecular potential proposed by Ben-Naim and Stillinger (24). The temporal evolution of this system of rigid molecular units was studied by the examination and analysis of successive molecular arrangements generated by the computer. By analysis of these computed molecular arrangements it was possible to obtain auto-correlation functions for various properties of the system; Fourier transforms of the auto-correlation function yield the prediction of the frequency

spectrum associated with the properties involved. The Fourier transform plots present a quantity related to the square of the amplitude of oscillation per unit frequency interval as a function of frequency; for want of a better term we shall refer to the ordinates of these plots as spectral density. If electromagnetic radiation were involved, the Fourier transform plot would represent what the electrical engineer calls a power spectrum.

In an analysis of the diffusive motions of the molecular centers of mass, RS have obtained a center-of-mass velocity auto-correlation function; the Fourier transform gives a spectrum that can be compared in a general way with what we have called the hindered-translation spectrum. The plot of spectral density is essentially flat from very low frequencies to approximately  $212\text{ cm}^{-1}$ ; beyond  $212\text{ cm}^{-1}$  spectral density decreases rapidly with increasing frequency. Superposed on the flat portion of the spectral curve is an additional fairly sharp peak at  $50\text{ cm}^{-1}$ ; the peak height is 40 percent higher than that of the flat portion of the spectrum. The sharp peak at  $50\text{ cm}^{-1}$  may well be related to the peak observed near  $60\text{ cm}^{-1}$  in Raman (15) and inelastic neutron scattering studies (16). By itself the Fourier transform of the center-of-mass velocity auto-correlation function does not predict the absorption peak observed near  $200\text{ cm}^{-1}$ .

A more favorable direct comparison with experimental results exists in the librational region, where there is experimental evidence of three bands. The spectrum obtained from the angular-velocity correlation functions for angular velocity about the three principal axes of inertia of the monomer has well separated peaks in spectral density at  $395$ ,  $420$ , and  $847\text{ cm}^{-1}$ . The corresponding spectrum for total angular momentum covers a broad spectral region extending from near zero to  $1400\text{ cm}^{-1}$  with evidence of component peaks at  $424$ ,  $636$ , and  $850\text{ cm}^{-1}$ . The really important results given by these spectra are that the spectral density involved in the rotational motion of the molecular units covers an extremely broad range of frequencies and that three separate peaks are predicted.

The RS result most directly related to the absorption spectrum is given by a plot of spectral density as a function of frequency that is based on the proton total velocity auto-correlation function. This composite spectrum combines features of the center-of-mass velocity spectrum with a spectrum obtained from the velocity auto-correlation function for proton motion relative to the centers of mass of the  $\text{H}_2\text{O}$  monomers. The plot of spectral density is dominated by a broad band with a maximum at  $425\text{ cm}^{-1}$  and with inflection points at  $636$ ,  $850$ , and  $1110\text{ cm}^{-1}$  in the high frequency wing, which exhibits appreciable spectral density for frequencies as high as  $1300\text{ cm}^{-1}$ . A peak at  $212\text{ cm}^{-1}$  appears as a low-frequency shoulder of the main band; a smaller additional sharp peak appears at  $53\text{ cm}^{-1}$ ; and the spectral density is non-zero at very low frequencies. Although the characteristic peak and inflection frequencies are different from the frequencies observed experimentally, the major portion of the broad band coincides with the broad librational band observed in infrared absorption; the low-frequency shoulder band at  $212\text{ cm}^{-1}$  corresponds to the hindered-translation band appearing as a shoulder near  $200\text{ cm}^{-1}$  in the plot

of observed  $\alpha(\nu)$  - vs -  $\nu$  given in Fig. 2. The peak at  $53 \text{ cm}^{-1}$  may well correspond to the  $60 \text{ cm}^{-1}$  peak observed by Raman and neutron-scattering techniques.

### III.1.3. DISCUSSION OF RESULTS

The theoretical plots of Curnutte and his students, which were based initially on Raman results, and those of RS based on a more general study of the molecular dynamics of rigid  $\text{H}_2\text{O}$  units subject to a particular form of intermolecular potential show relative spectral density as a function of frequency. It is not necessarily true that all features in these plots will appear in the infrared absorption spectrum, since absorption occurs only when changes in dipole moment are produced by radiation of the appropriate frequency. For example, rotational motion of an isolated  $\text{H}_2\text{O}$  molecule about its symmetry axis would not be infrared active since no dipole moment changes occur in the course of the motion. However, such a rotational motion of a molecule surrounded by neighbors could become infrared active as a result of dipole moments induced, primarily as a result of changes in hydrogen bonding, in the polarizable neighboring molecules. Any detailed theory of the absorption of infrared radiation should take account of these and similar processes. Such processes are not considered in detail in the formulation of the Curnutte theory and are prohibited in the RS treatment by the assumption of unpolarizable rigid molecules.

A related phenomenon known as translational absorption has been suggested by Litovitz (25) to account for a portion of the observed infrared absorption in the extreme infrared. This type of absorption, which was discovered by Welsh and his collaborators (26), can occur when two colliding polarizable molecules produce a collision pair with a resultant dipole moment capable of interacting with incident radiation; such a collision pair can absorb a quantum of radiant energy. When such an absorption occurs, the members of the collision pair separate with greater translational energy than they had prior to collision; since the energy absorbed in this non-periodic process goes immediately into translational energy, the process is termed translational absorption. Typical translational absorption bands are broad and nearly structureless. Since translational absorption bands for colliding  $\text{H}_2\text{O}$  molecules in liquid water may occur in the remote infrared, they could well account in part for the almost continuous absorption observed in the  $100\text{-}20 \text{ cm}^{-1}$  range by Davies *et al.* (7).

It is interesting to speculate on the nature of the absorption processes involved in the rapid rise of the  $k(\nu)$  curve in Fig. 3 at frequencies below  $10 \text{ cm}^{-1}$ . Little detailed information on the subject is given by the RS curves because of the long total observation times that would be required to give valid estimates of spectral density at extremely low frequencies. The RS molecular-dynamics study does, however, provide some estimates of the logarithmic decay of librational motion that occurs with a time constant comparable with measured time constants for dielectric relaxation. Further detailed experimental and theoretical studies in the millimeter and sub-

millimeter regions should prove to be of importance to an understanding of the liquid structure.

As indicated earlier, the RS spectrum has non-zero spectral density at frequencies considerably higher than those of the main librational peaks. Infrared absorption has been observed (9) in the entire interband region between the librational band and the  $\nu_2$  fundamental. Since the observed absorption extends to frequencies higher than those predicted by the RS plot, it seems likely that for the  $1300\text{ cm}^{-1}$  region the observed absorption may indeed result in part from a difference band involving the  $\nu_2$  fundamental and lattice modes. If the rigid  $\text{H}_2\text{O}$  units in the RS scheme could be replaced with units capable of vibration, this suggestion could be checked. At the expense of greatly increased computation time other intermolecular potentials might be used in the RS scheme to bring the predicted spectrum into closer quantitative agreement with Raman and infrared observations.

The authors should like to express their thanks to the U. S. Office of Naval Research and to the Kansas State Agricultural Experiment Station for support of much of the research reported here.

#### REFERENCES

1. L. Pontier and C. Dechambenoy, *Ann. Geophys.* 21, 462 (1965) *ibid.* 22, 633 (1966).
2. V. M. Zolotarev, B. A. Mikhailov, L. I. Aperovich, and S. I. Popov, *Optika Spectrosk.* 27, 790 (1969). [Translation: *Optics Spectrosc.* 27, 430 (1969).
3. M. R. Querry, B. Curnutte, and D. Williams, *J. Opt. Soc. Am.* 59, 1299 (1969).
4. A. N. Rusk, D. Williams, and M. R. Querry, *J. Opt. Soc. Am.* 61, 895 (1971).
5. C. W. Robertson and D. Williams, *J. Opt. Soc. Am.* 61, 1316 (1971).
6. C. W. Robertson, B. Curnutte, and D. Williams, *Mol. Phys.* 26, 183 (1973).
7. M. Davies, G. W. F. Pardoe, J. Chamberlain, and H. A. Gebbie, *Trans. Faraday Soc.* 66, 273 (1970).
8. P. S. Ray, *Appl. Opt.* 11, 1836 (1972).
9. G. M. Hale, M. R. Querry, A. N. Rusk, and D. Williams, *J. Opt. Soc. Am.* 62, 1103 (1972).
10. D. A. Draegert, N. W. B. Stone, B. Curnutte, and D. Williams, *J. Opt. Soc. Am.* 56, 64 (1966).
11. J. W. Schaaf and D. Williams, *J. Opt. Soc. Am.* 63, 726 (1973).
12. R. Zimmerman and G. C. Pimentel, *Proc. Intern. Meeting Mol. Spectry.*, Bologna, 2, 726 (1962).
13. J. E. Bertie, H. J. Labbe', and E. Whalley, *J. Chem. Phys.* 50, 4501 (1969).
14. M. S. Zafar, J. B. Hasted, and J. Chamberlain, *Nature (Phys. Sci.)* 243, 106 (1973).

15. G. E. Walrafen, *J. Chem. Phys.* 40, 3249 (1964).
16. J. O. Burgman, J. Scienci, and K. Skold, *Phys. Rev.* 170, 808 (1968).
17. J. B. Bryan and B. Curnutte, *J. Mol. Spectry.* 41, 512 (1972), and J. B. Bryan, Doctoral Dissertation, Kansas State University (1969).
18. J. Bandekar, Doctoral Dissertation, Kansas State University (1973).
19. A. Rahman and F. H. Stillinger, *J. Chem. Phys.* 55, 3336 (1971).
20. E. R. Lippincott and R. Schroeder, *J. Chem. Phys.* 23, 1099 (1955).
21. R. Schroeder and E. R. Lippincott, *J. Phys. Chem.* 61, 921 (1957).
22. A. H. Narten, M. D. Danford, and H. A. Levy, ORNL-3997, UC-4 Chemistry, Oak Ridge National Laboratory (1966).
23. D. Eisenberg and W. Kauzmann, The Structure and Properties of Water (Oxford University Press, 1969), pp. 206-208.
24. A. Ben-Naim and F. H. Stillinger, "Aspects of the Statistical-Mechanical Theory of Water" in "Structure and Transport Processes in Water and Aqueous Solutions", edited by R. H. Horne (Wiley-Interscience, New York, In Press.)
25. T. A. Litowitz, Comment at Marburg Symposium (1973).
26. Z. J. Kiss and H. L. Welsh, *Phys. Rev. Letters* 2, 166 (1959).
27. Z. J. Kiss, H. P. Gush, and H. L. Welsh, *Can. J. Phys.* 37, 362 (1959).